AD-A175 236 SILHOUETTE-SLICE THEOREMS(U) MASSACHUSETTS INST OF TECH 1/3
CAMBRIDGE RESEARCH LAB OF ELECTRONICS P L VAN HOVE
SEP 86 TR-522 N00014-81-K-0742

UNCLASSIFIED F/G 12/1 NL

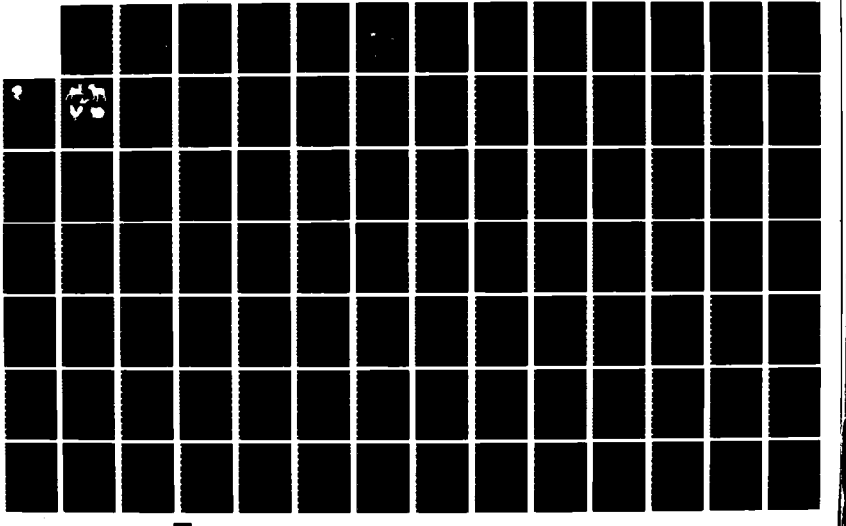

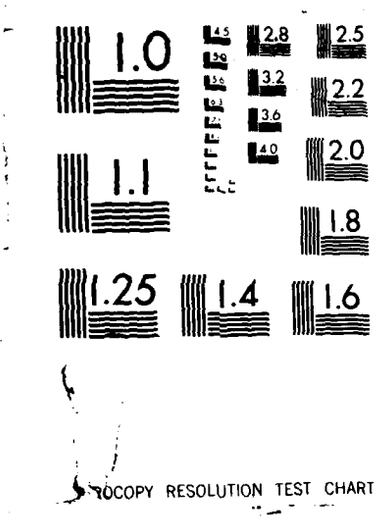
1.0
1.1
1.25
1.4
1.6
2.8
3.2
3.6
4.0
2.5
2.2
2.0
1.8
OCOPY RESOLUTION TEST CHART

Massachusetts Institute of Technology
Department of Electrical Engineering and Computer Science
Research Laboratory of Electronics
Room 36-615
Cambridge, MA 02139

Silhouette-Slice Theorems

Patrick L. Van Hove

Technical Report No. 522

September 1986

This work has been supported in part by the Advanced Research Projects Agency monitored by ONR under Contract No. N00014-81-K-0742, and in part by the National Science Foundation under Grant ECS-8407285.

UNCLASSIFIED

SECURITY CLASSIFICATION OF THIS PAGE

REPORT DOCUMENTATION PAGE

1a. REPORT SECURITY CLASSIFICATION	1b. RESTRICTIVE MARKINGS
2a. SECURITY CLASSIFICATION AUTHORITY	3. DISTRIBUTION/AVAILABILITY OF REPORT
2b. DECLASSIFICATION/DOWNGRADING SCHEDULE	
4. PERFORMING ORGANIZATION REPORT NUMBER(S)	5. MONITORING ORGANIZATION REPORT NUMBER(S)
6a. NAME OF PERFORMING ORGANIZATION: Research Laboratory of Electronics, Massachusetts Institute of Technology	6b. OFFICE SYMBOL (If applicable): Technology
7a. NAME OF MONITORING ORGANIZATION: Office of Naval Research, Mathematical and Information Scien. Div.	
6c. ADDRESS (City, State and ZIP Code): 77 Massachusetts Avenue, Cambridge, MA 02139	7b. ADDRESS (City, State and ZIP Code): 800 North Quincy Street, Arlington, Virginia 22217
8a. NAME OF FUNDING/SPONSORING ORGANIZATION: Advanced Research Projects Agency	8b. OFFICE SYMBOL (If applicable)
9. PROCUREMENT INSTRUMENT IDENTIFICATION NUMBER: N00014-81-K-0742	
8c. ADDRESS (City, State and ZIP Code): 1400 Wilson Boulevard, Arlington, Virginia, 22217	10. SOURCE OF FUNDING NOS.

PROGRAM ELEMENT NO.	PROJECT NO.	TASK NO.	WORK UNIT NO.
		NR 049-506	

11. TITLE (Include Security Classification): Silhouette-Slice Theorems

12. PERSONAL AUTHOR(S): Patrick L. Van Hove

13a. TYPE OF REPORT	13b. TIME COVERED	14. DATE OF REPORT (Yr., Mo., Day)	15. PAGE COUNT
Technical	FROM _____ TO _____	September 1986	266

16. SUPPLEMENTARY NOTATION

17 COSATI CODES			18. SUBJECT TERMS (Continue on reverse if necessary and identify by block number)
FIELD	GROUP	SUB. GR.	

19. ABSTRACT (Continue on reverse if necessary and identify by block number)

In this thesis a new theory analyzing the relations between 3-D convex objects and their silhouettes in orthographic projections ~~is presented~~. The theory is based on three new representations of 3-D surfaces in terms of scalar, vector and tensor functions on the Gaussian sphere, and the matching representations of 2-D curves by functions on the Gaussian circle. The key advantage of these representations is that a slice through the spherical representation of a 3-D object is closely related to the circular representation of the silhouette of the object in a plane parallel to the slice. This relation is formalized in three Silhouette-Slice theorems, which underline the duality between silhouettes in object space and slices in the representation space. These theorems apply to opaque objects and have a conceptual similarity with the Projection-Slice theorem, which applies to absorbing objects.

20. DISTRIBUTION/AVAILABILITY OF ABSTRACT	21. ABSTRACT SECURITY CLASSIFICATION
UNCLASSIFIED/UNLIMITED ☒ SAME AS RPT ☐ DTIC USERS ☐	Unclassified

22a. NAME OF RESPONSIBLE INDIVIDUAL	22b. TELEPHONE NUMBER (Include Area Code)	22c. OFFICE SYMBOL
Kyra M. Hall, RLE Contract Reports	(617) 253-2569	

DD FORM 1473, 83 APR EDITION OF 1 JAN 73 IS OBSOLETE.

UNCLASSIFIED

SECURITY CLASSIFICATION OF THIS PAGE

19.

Silhouette construction with the theorems is demonstrated by examples of silhouettes of complex curved surfaces. Applications to the reconstruction of object shapes from silhouette measurements and to the recognition of objects based on their silhouettes are suggested.

Silhouette-Slice Theorems

by

Patrick Van Hove

Submitted to the Department of Electrical Engineering and Computer Science on
August 1, 1986
in partial fulfillment of the requirements for the degree of
Doctor of Philosophy in Electrical Engineering and Computer Science

Abstract

In this thesis, a new theory analyzing the relations between 3-D convex objects and their silhouettes in orthographic projections is presented. The theory is based on three new representations of 3-D surfaces in terms of scalar, vector and tensor functions on the Gaussian sphere, and the matching representations of 2-D curves by functions on the Gaussian circle. The key advantage of these representations is that a slice through the spherical representation of a 3-D object is closely related to the circular representation of the silhouette of the object in a plane parallel to the slice. This relation is formalized in three Silhouette-Slice theorems, which underline the duality between silhouettes in object space and slices in the representation space. These theorems apply to opaque objects and have a conceptual similarity with the Projection-Slice theorem, which applies to absorbing objects.

Silhouette construction with the theorems is demonstrated by examples of silhouettes of complex curved surfaces. Applications to the reconstruction of object shapes from silhouette measurements and to the recognition of objects based on their silhouettes are suggested.

Thesis Supervisor: Jae S. Lim
Title: Associate Professor of Electrical Engineering

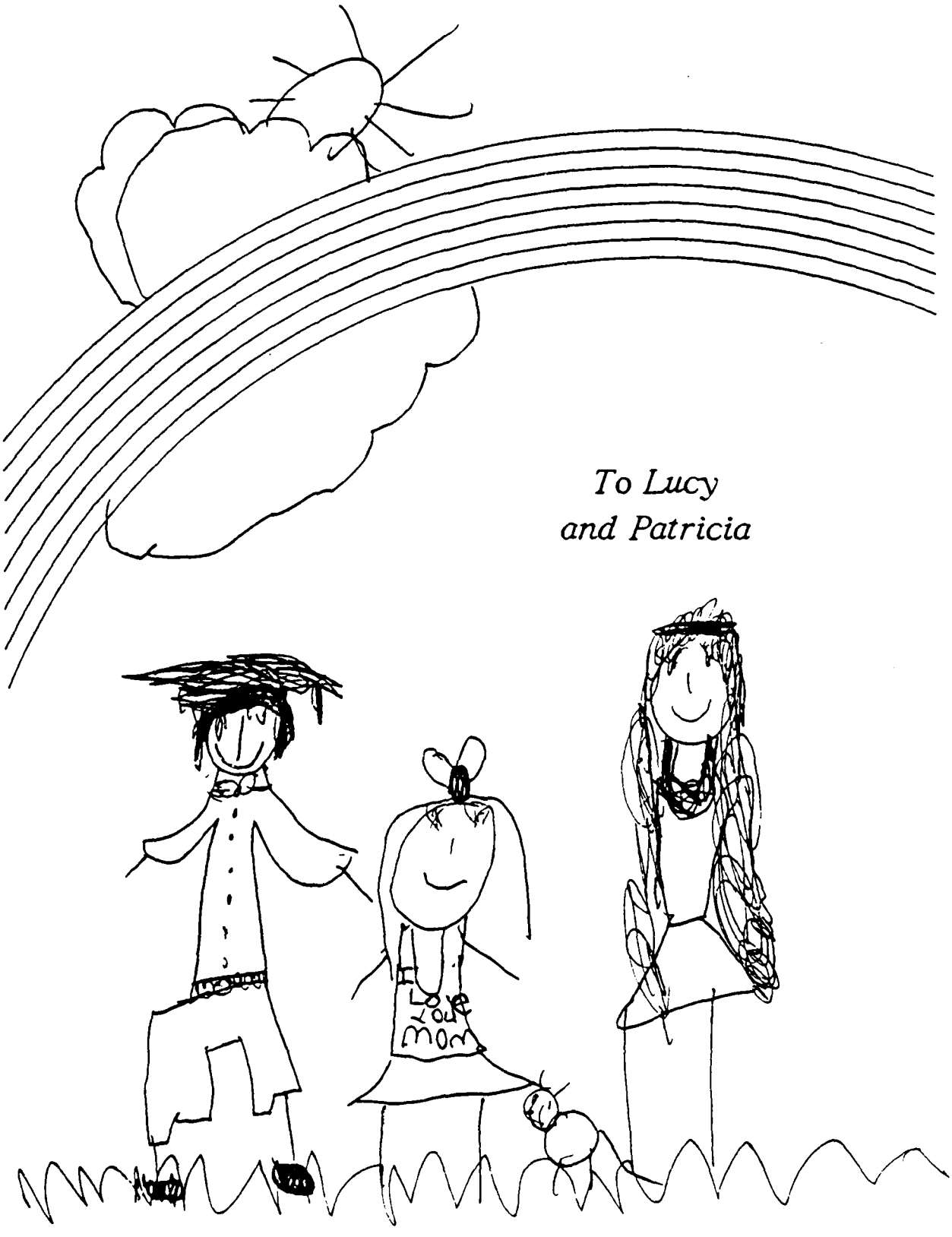

To Lucy
and Patricia

Acknowledgements

I'd like to thank my thesis supervisor, professor Jae S. Lim, for introducing me to the field of image interpretation, and for leaving me substantial freedom in defining my thesis topic. His critical reviews of my work and his constant strive for improvements were extremely helpful. Richard Lacoss and Dan Dudgeon of Lincoln Laboratory interested me in the analysis and understanding of noisy range images, a very rich area which motivated my doctoral research. The support of part of my research by group 21 at Lincoln Laboratory is greatly appreciated, as is the involvement of Dan Dudgeon as a reader of the thesis. The theories developed in this thesis have been strongly influenced by the work of professor Berthold Horn. I owe my regards to Berthold for his inspiring research, his interest in my work, his moral support at appropriate times, and his critics as a reader of the thesis. Jacques Verly of Lincoln Laboratory produced substantial efforts in reading, criticizing and correcting drafts of my proposal and early drafts of the thesis itself. His support has been invaluable. Thanks to Derek, Rick, Fred, Ted and Joann for proofreading the final draft.

I have pursued most of my graduate research within the Digital Signal Processing Group at MIT, a working environment that is hard to beat! Al Oppenheim, Jae Lim and Bruce Musicus have remarkably succeeded in bringing together excellent people, top quality ideas and plentiful hardware. In addition to the technical environment, the companionship of fellow graduate students was extremely enjoyable; thanks to Michele, Susan, Webster, Farid, Meir, Dan, David, Dennis, Evangelos, Cory, Thrasyvoulos and Mike, I had a great time with you in the DSPG! Many thanks also to DSPG's legendary secretary, Monica ('Mom'), and those soon to follow in the legend, Deborah and Phyllis; you contributed a great deal in everyone's good humor. Giovanni's work behind the stages in the computer room was invaluable in keeping the machines running smoothly. Mille Grazie! Although more renown for its knurdy aspects, MIT can also be a great place to practice sports. My jogs with Derek, Bob and Thrasos were great study breaks, as was swimming in the pool and boardsailing on the Charles (thanks Stu).

Patricia and Lucy had some hard times while I was completing my PhD at MIT. For several years, they had to struggle with long separations and an uncertain future. But, when we were together, our feelings were always warm. Thanks a lot for the constant support!

Table of Contents

Chapter 1
Introduction

Visual information is the prime communication medium for humans. Analysis of this visual information and of its processing is important and serves multiple purposes. Visual information generally consists of images of scenes in the three-dimensional world projected on two-dimensional surfaces such as paper, film, video screens or the human retina. Information intrinsically contained in these images is best characterized by regions with intensities, colors and texture, and discontinuities between these regions. On the other hand, scenes are better described by the sets of objects present in the scene, shapes, surface properties and spatial arrangement of these objects and the illumination of the scene. Substantial work has been accomplished in studying the relations between scene properties and image properties. Theories developed so far have permitted for example, the development of systems for synthesizing realistic images, for enhancing images, and for recognizing objects in images.

In most theoretical analyses of the relations between scenes and images, only one or a few image properties are related to their correspondent properties in the scene. In addition, assumptions are made which decouple these relations from other effects. The decoupled problems are amenable to analysis, and their solutions are often found valuable outside the simplified context. The present thesis follows this approach by considering only relations between silhouette shapes in images and object shapes in the scene.

1.1. Silhouettes

The word "silhouette" is generally used in two similar senses. The first corresponds to portrays or scenes depicted as outlines filled in with black, whereas the second corresponds to just the outlines themselves; see Fig.1.1. Clearly, these two concepts are closely related, and it is easy to transform one form into the other. For the sake of clarity, we have decided to use the word "silhouette" for the outline only, and the expression "filled-in silhouette" for the outline filled-in with black. More precisely, the silhouette of an object in an image will refer to the curve which outlines the image region covered by the projection of the object.

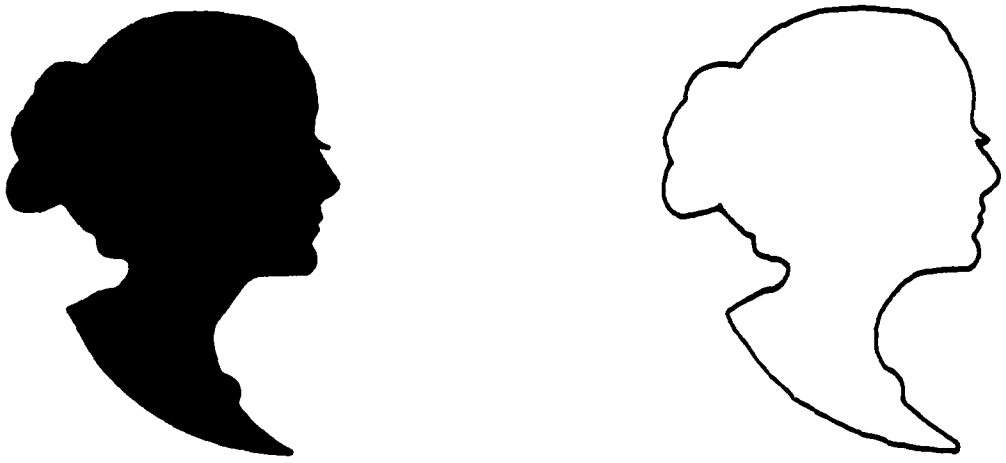

Fig.1.1. Silhouette as a) a filled-in outline, b) an outline. (from [1].)

Among a variety of features which can be identified in an image, silhouettes are known to convey a strong perceptual content for humans [2, 3]. For example, most of us recognize without difficulty the various animals represented by filled-in silhouettes in Fig.1.2. In this thesis, a new theory is developed to relate shapes of silhouettes to shapes of the corresponding 3-D objects.

1.2. Three Basic Problems

Although the initial motivation for our work came from the domain of machine vision, relations between objects and silhouettes can be exploited in a variety of contexts. A majority of the applications are closely tied to one of three basic problems, namely silhouette construction, reconstruction from silhouettes and recognition from silhouettes. These three basic tasks are now outlined as a motivation for the analysis of object-silhouette relations.

The first problem is that of silhouette construction from a description of the 3-D shape of the object and the imaging geometry. This construction is required for example for the synthesis of blueprints from 3-D object models. Presently, most synthetic renditions are in the form of shaded images. For these, silhouette construction is not explicitly required but can be used for anti-aliasing processing or for outlining areas to be covered by surface painting processes.

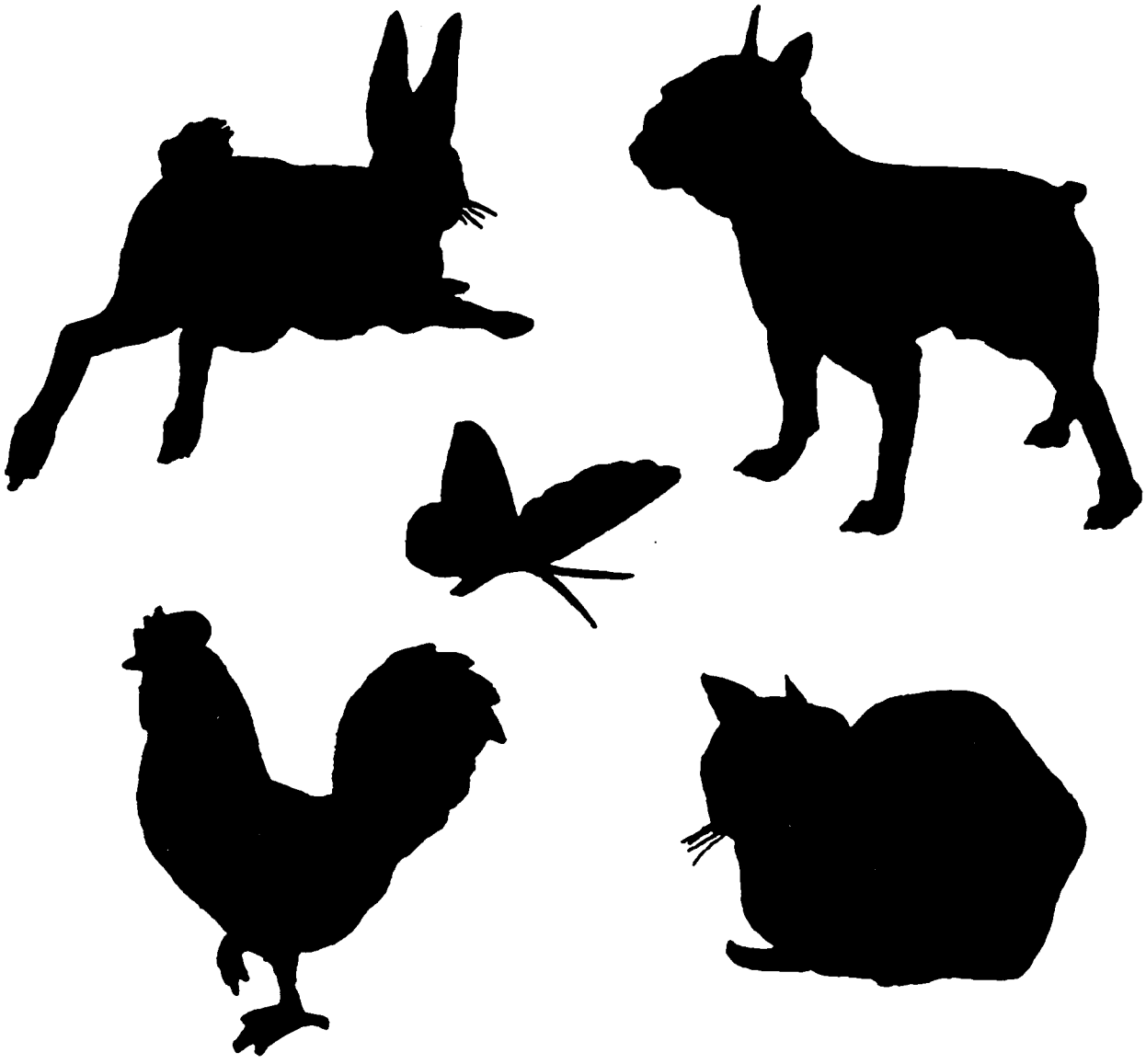

Fig.1.2. Filled-in silhouettes of animals (from [1]).

The second problem is that of reconstructing the shape of a 3-D object from silhouette data. It is easy to see that the reconstruction of the shape of a 3-D object from one silhouette is largely underconstrained. Reconstruction of general shapes is possible only when multiple silhouettes are available for processing; this occurs in some examples of medical imaging and non-destructive testing, and for vision systems where several views of the object are available [4].

The third problem is that of 3-D object recognition from silhouette data. A silhouette recognition system would exploit silhouette data obtained from an image,

and compare this with a description of the 3-D shape of a known object. The system must determine if there is evidence in the silhouettes suggesting the presence of the given object in the imaged scene, and estimate its position and orientation in the scene. A large number of solutions to this problem have been proposed for the case where the viewing direction relative to the object is known a-priori. In that case, the silhouette can be precomputed up to a rotation and a translation in the image plane, so that the matching process is greatly simplified. When there is no a-priori estimate of object orientation relative to the camera, the same object can produce very different silhouette shapes, and the problem is much more complex.

1.3. Previous Work on Silhouettes

Previous approaches to silhouettes are briefly sketched here; they will be discussed in greater detail in Chapter 2. Most algorithms presented in the past for solving the problems mentioned in the previous section have been based on the well-known relation between coordinates of points in the scene and coordinates of their projection in the image [5]. In order to relate object shape and silhouette shape, this relation must be combined with the knowledge of which points of the object in the scene are projected onto the points of the silhouette in the image. Silhouette analysis based on projections of points is satisfactory for the development of many computer graphics algorithms, has helped to develop methods for reconstructing objects from silhouettes and methods for recognizing block objects from their silhouettes. However, there are several drawbacks in the classical formalism. First, the classical method does not explicitly analyze the relation between curved 3-D shapes and their silhouettes. Shapes of generalized cones have been related to the shapes of their silhouettes [6], but these relations are approximate and apply to simple generalized cones only. Second, the classical method does not easily support intuitive reasoning when several object points are related simultanesouly to the corresponding silhouette points. Third, no intermediate representation has been proposed where information from different silhouettes is readily combined. Finally, the relations between silhouette points and object points must be supplemented by various ad hoc arguments to solve different problems.

Deficiencies of the classical silhouette theory are most severe for the problem of recognition, but the other two application areas can also benefit from new results on silhouette analysis.

1.4. Thesis Overview

Solving any of the three basic problems described in section 1.2. requires a good understanding of the relation between the shape of a 3-D object and the shape of its silhouette obtained for any given viewing direction. In this thesis, we present new representations for objects and silhouettes, and the relations between these representations for corresponding object-silhouette pairs. Specifically, silhouette curves will be represented by functions on the Gaussian circle, and object surfaces by functions on the Gaussian sphere. The functions describing these shapes are chosen in such a way that the relation between object functions and silhouette functions is particularly simple. The representation of a given silhouette is simply related to a slice of the representation of the object on the sphere. The new theory hence relates silhouettes of objects to slices of their representations, and the theorems formalizing these relations have been named "Silhouette-Slice" theorems.

The theories presented in this thesis apply to the case of orthographic projection only, and are initially developed for smooth strictly convex objects, such as the superquadric in Fig.1.3. Although the class of smooth convex shapes is somewhat restricted, the theorems will be extended to cover objects with corners, edges and flat components, which include convex polyhedral objects such as in Fig.1.4. As a consequence, the same theories are capable of analyzing silhouettes of curved objects and of

a) b)

Fig.1.3. Superquadric and its Silhouette for the Viewing Direction $\vec{v}$.

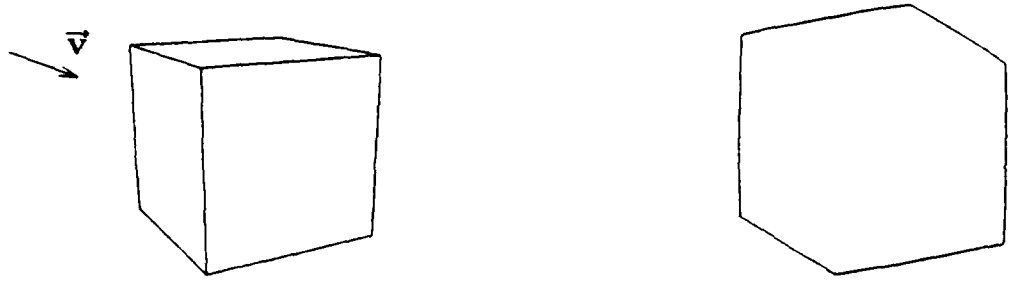

a) b)

Fig.1.4. Cube and its Silhouette for the Viewing Direction $\vec{v}$.

polyhedral objects. Furthermore, some of the results are applicable to non-convex objects such as the torus depicted in Fig.1.5. However, silhouettes of non-convex objects may contain singularities such as inflections and cusps which are not well analyzed with the Silhouette-Slice theorems, but which have been studied in detail in other work [7, 8, 9]. Finally, the scope of the results can be extended considerably when Boolean combinations of objects are considered. Indeed, combinations of simple primitives such as the superquadric in Fig.1.3 have been shown to adequately model complex objects [10].

The new theorems allow the derivation of closed form expressions for the silhouettes of complex 3-D shapes, when these are defined analytically. In addition to these mathematical relations between silhouette and surface shapes for the class of

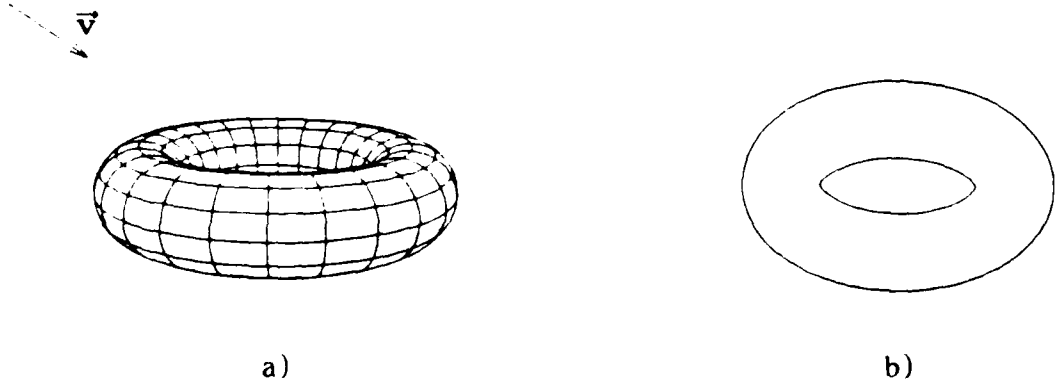

a) b)

Fig.1.5. Torus and its Silhouette for the Viewing Direction $\vec{v}$.

objects of interest, the new theory also provides an elegant qualitative interpretation of these relations. The framework of the Silhouette-Slice theorems is well suited to develop an intuitive understanding of the relations between silhouette shape and object shape. The representations proposed for 3-D shapes can be thought of as intermediate representations in which information from silhouettes corresponding to different viewing angles is readily combined. Finally, the representations of an object by functions on the sphere can be interpreted as a compact representation for the set of all the silhouettes of the object.

1.5. Thesis Organization

The second chapter of the thesis reviews some earlier work on silhouettes in the context of the three basic problems outlined in section 1.2. As object modeling plays an important role in the analysis of relations between object shape and silhouette shape in general, and in the analysis presented in this thesis in particular, previous work on that subject is also reviewed.

Chapter 3 reviews some basic concepts of analytic and differential geometry. In addition to the review of classical concepts, a number of original geometrical concepts are presented. The first is the definition of an invariant measure of surface curvature. The second concept is the definition of local reference directions at each point of the Gaussian sphere, in order to support the discussion of object functions with vector and tensor values. Finally, a relation is proposed between representations of normals with gradients in a Monge parameterization on one side and with coordinates on the Gaussian sphere on the other side.

In Chapter 4, the classical approach to silhouette construction is reviewed. This approach consists of a two-step process, where the first step is the selection of object points which contribute to the silhouette, and the second step is the projection of these points. This approach is illustrated in the case of a simple object, a cone. The equivalent formalism is also presented in the dual space of tangents. For both methods, surface normal orientation is shown to be the key parameter to silhouette construction with orthographic projection. This conclusion motivates representations of objects and silhouettes where normal orientation is explicit.

Chapters 5 and 6 present the major developments in this thesis. A set of representations is developed for 2-D curves and for 3-D surfaces, with the relation between these representations for an object-silhouette pair.

Chapter 5 introduces three different representations for the shapes of 3-D object surfaces and for the shapes of 2-D silhouette curves, as functions on the Gaussian sphere and on the Gaussian circle respectively. All three representations are unique and uniquely invertible for objects in the class of interest, and are explicitly phrased in terms of normal orientations. A close parallel is followed in the discussion of the representations in 2-D and 3-D.

Chapter 6 presents three theorems expressing the relations between corresponding silhouette circular functions and object spherical functions. A unified proof method is presented for the three theorems corresponding to each of the three representations. The spherical transforms of 3-D objects are also interpreted as compact representations of the set of all their silhouettes.

Chapter 7 extends the theories presented in Chapter 5 and 6 to the case of object surfaces with edges, corners and planar faces.

In Chapter 8, examples of silhouette construction with the Silhouette-Slice theorems are provided. Other applications of the method are suggested, such as a strategy for reconstructing objects from silhouette data, and the principles of a recognition scheme for silhouettes.

Finally, Chapter 9 concludes by summarizing the key contributions of this thesis and suggesting directions for future work.

Chapter 2
Literature Review

In this chapter, previous work on silhouette analysis is reviewed. As no general framework previously existed for this analysis, much of the work on silhouettes published in the literature is found in application areas and considers relations between object shape and silhouette shape only in the context of particular tasks. Literature is most abundant for the problem of recognition, but it is also instructive to consider how silhouettes have been handled in other application areas. The first part of this chapter examines existing approaches to the three basic problems outlined in Chapter 1.

In order to relate silhouette shapes and object shapes, it is necessary to base the relations on some description of the shape of the object surfaces. Therefore, surface modeling procedures play a central role in any analysis of the silhouette problem. In addition, one of the key contributions of this thesis is a set of surface representations for which the relations between objects and silhouettes are greatly simplified. The second part of this chapter reviews previous work on surface modeling, with special emphasis on the relations between the proposed representations and the shapes of silhouettes.

2.1. Literature on Silhouettes

2.1.1. Construction of Silhouettes

Most examples of numerical evaluation of silhouettes are found in the synthesis of images in the field of computer graphics. Several references, such as [11, 12], provide a good introduction to the field. The synthesized image can take different forms, such as wireframe diagrams, blueprints, or shaded renditions. In the case of blueprints, the output image consists of lines and curves representing creases in the object surface and silhouettes of the object and of its parts. For this type of output, explicit silhouette construction is necessary. In the case of shaded images however, explicit construction of silhouettes can be avoided, as they are implicitly generated on boundaries of rendered surfaces. Although explicit construction of the silhouettes is not indispensable for the synthesis of shaded images, it can be useful for example in the

elimination of jagged outlines, known as anti-aliasing processing. In the synthesis of both shaded renditions and wireframe drawings, silhouettes can also be used to determine a-priori which regions of the image will be covered by which objects. With this information, the rendition can be divided into several processes without risk of interferences if the processes are run in parallel. Silhouettes can also be useful for the rendition of shadows. The determination of the shadow of an object on a planar surface is equivalent to the determination of a silhouette of the object for an appropriate imaging geometry [13]. Results obtained for silhouettes are hence immediately applicable to shadows. In summary, the construction of silhouettes is used or has a potential for use in several facets of image synthesis.

Computer graphics is a relatively mature field, and some silhouette construction methods are well known. Most of these are based principally on the relation between coordinates of points in the scene and coordinates of their projection in the image plane; these relations are nicely illustrated in the context of graphics in [5]. In addition to the relation between point coordinates, the exact shape of the silhouette depends on which points of the object are projected onto the points of the silhouette; this set of object points is referred to as the *silhouette generator* in this thesis. Methods for determining the silhouette generator depend on the type of representation for the objects. In the case of polyhedral objects, the silhouette generator is the set of all edges touching a face oriented towards the eye position and a face oriented away from the eye position. The selection of this set of edges usually requires a search through all the edges of the polyhedron. Objects with curved surfaces are often described as collections of curved surface patches, such as segments of spheres, cylinders, general quadrics, superquadrics, Bezier patches, B-spline surfaces ... In this case, the silhouette is a 3-D curve containing all the points where the viewing rays are grazing the object surface; this curve is twisted in general. For quadrics and some higher order surfaces, closed-form expressions have been determined for the silhouette generator and for the silhouette itself. For other surfaces, accurate approximations have been proposed.

2.1.2. Reconstruction from Silhouettes

In a significant number of cases, images contain little more information than the silhouettes of the imaged objects. This arises for example in some nondestructive testing x-ray images, in images of backlit objects, and in some range images [14, 15]. It is often desirable to estimate the 3-D shape of the imaged objects in those circumstances. It is intuitively obvious that a large number of different 3-D objects could have generated any given silhouette, so that reconstruction of a 3-D object shape from the shape of one silhouette is ambiguous. Several ways have been proposed to reduce or resolve this ambiguity, e.g. by considering restricted object classes, by using more than a single silhouette, or by applying regularization methods. Previous work on these three facets of reconstruction from silhouettes is now reviewed.

Exact reconstruction of a 3-D shape from one silhouette can be guaranteed only by considering a restricted class of 3-D objects. An interesting class which has been considered is the class of axisymmetric objects. For these objects, the silhouette construction is invertible in the absence of self-occlusions, for known object orientation. However, the orientation of the object axis is usually unknown a-priori and must be estimated from the image data. Methods have been proposed for estimating this orientation from the shape of the silhouette of the object base, or from a self-shadow on the object image [13]. In a recent paper, the author has proposed an alternative method based on the Silhouette-Slice theory, for determining the orientation of the axis [16].

A second approach to the reconstruction of object shape from silhouette data is to consider the problem as improperly posed and to apply regularization techniques [17]. A unique shape estimate is obtained by maximizing some smoothness constraint while matching the observed silhouette. Strong constraints are imposed by the silhouette observations when object surfaces are assumed to be continuous along the silhouette generator, so that the surface must be tangent to the viewing rays corresponding to the silhouette. The object surface orientation is uniquely determined at these points by the silhouette orientation in the image and by these viewing rays. Reconstruction results obtained with this method seem to be in acceptable agreement with the human perception of shape from silhouette images.

Complete and accurate reconstruction of 3-D shapes from silhouette data is possible for a large class of objects, when multiple silhouettes are available. A well-known

solution to this problem consists of first considering, for each projected silhouette, the object outlined by the corresponding viewing rays. This object, referred to as the extruded silhouette by some authors, is a prism for parallel projection, a generalized cone for perspective projection. The orientation of each extruded silhouette in a world reference frame can be determined from the imaging geometry for the corresponding silhouette so that all extruded silhouettes can be combined in the world reference frame. Among all objects with shapes consistent with the measured silhouettes, the intersection of all these extruded silhouettes is the object with the largest volume. This maximal volume object can be considered as an estimate of the object shape. Implementations of this reconstruction procedure are discussed in [4, 18].

2.1.3. Recognition from Silhouettes

Object recognition from image data is a major concern in the field of machine vision. Several books, such as [19, 20, 21], provide a good introduction to the field. Silhouettes are important features in images of objects, so that substantial research has been accomplished in the area of recognition from silhouette data. A summary of some important published research on this topic is sketched below.

Whereas objects in a scene are generally three-dimensional, their silhouettes in images are necessarily two-dimensional. As a result, object shapes can not be directly related to the shape of their silhouettes. Several strategies have been proposed to circumvent this apparent mismatch. The first approach consists of precomputing silhouettes for the known objects and performing the match at the 2-D level. In the second approach, only planar objects or planar object parts are considered, but their plane is not required to be parallel to the image plane. The third approach consists of first processing the observed silhouette to estimate the shape of the corresponding 3-D object, then performing the match at the 3-D level. The fourth approach consists of devising judicious models for both objects and silhouettes so that the match can be performed between features of these models. Most algorithms proposed for recognition from silhouettes can be related to one of the above classes.

Systems which compare the observed silhouette with synthesized silhouettes must perform matches between 2-D outlines differing by only translations and rotations in their plane. Numerous methods have been proposed for performing this

operation on complete silhouettes [22- 30]. However, these methods require the knowledge of the correct 3-D object orientation and work well only when this orientation can be estimated a-priori. Otherwise, a large number of orientations must be tried, requiring matching and either computation or storage of large numbers of silhouettes for each object in the data base. These requirements may easily become excessive for medium to large object data bases.

When only planar objects are considered in the scene, the object outline is related to the observed silhouette by an affine transformation. A method has been proposed to characterize planar objects by features invariant in affine transformations [31]. With this method, general polyhedral objects can be recognized by building a separate model for each planar face and matching each of these to image features.

A different strategy consists of first performing an approximate reconstruction of the 3-D shape of the object using procedures similar to those described in the previous section. The reconstructed shape is then matched with known object models. When a restricted object class can be hypothesized or when a large number of silhouettes is available, accurate reconstruction of the 3-D object shape is possible, and the problem becomes one of 3-D shape matching. When the approach is applied to a single silhouette with no constraints on the 3-D shape, the information is insufficient to accurately reconstruct the 3-D shape so that this strategy is difficult to implement. Work has been done on qualitative estimation of object shape from silhouette data, and on the use of this information for recognition (see for example [32, 33]).

A number of systems have been reported where nontrivial 3-D object features are compared to 2-D silhouette features. Two characteristic examples are described here. The first example is given by the ACRONYM system [34], where object features are a collection of generalized cones which describe the object shape. These features have "ribbons" for silhouettes and the relations between corresponding cone/ribbon parts are readily evaluated. A parsing mechanism converts each measured ribbon into sets of inequality constraints on the parameters of corresponding object cones. These constraints are collected and the matching is converted into a decision procedure for the large resulting set of inequalities. Success of this approach is partially linked to the astute choice of cones and ribbons, a set of corresponding features which judiciously relate silhouette information to object information. The second approach considered

here consists of extracting edge features from both the silhouette and the object and of performing the match based on these edges. Goad proposes a fast implementation of this procedure [35]. In this case too, the choice of features is appropriate since relationships between image edges and object edges are straightforward.

In many of the approaches discussed above, the measured silhouette must be complete. If part of the silhouette is missing, recognition can be much more complex. Missing silhouette parts may be due for example to occlusions in the scene or segmentation errors in early processing of the image data. Although recognition of 2-D objects has been demonstrated in cases of partial occlusion, for example in [36], the problem of 3-D object recognition from partially occluded silhouette data still requires substantial work.

In addition to the work presented above which is intrinsically related to applications, some more general analyses of silhouettes have been presented. Shafer reviews some basic silhouette construction methods, referred to as "classical" in this thesis, and draws a number of conclusions for the analysis of silhouettes of generalized cones [13]. In other work, Koenderink has considered the relation between characteristic events on the silhouette curve and corresponding surface features [7]. His work is the only reference known to the author where relations between shapes of surfaces and shapes of their silhouettes are analyzed in detail. He independently discovered the dual of Euler's theorem [33] presented in Appendix 3.

2.2. Literature on Object models

This section gives a brief overview of modeling methods for 3-D shapes and their consequences for silhouette analysis. Quite different approaches to modeling must be followed, depending on whether the models are used for synthesizing or for recognizing shapes. Modeling methods intended for synthesis are used in CAD/CAM systems, and the theories are covered in texts such as [37, 38]. Modeling for recognition is addressed in texts on computer vision and in a number of articles such as [39, 40]. As models for synthesis pertain to silhouette construction and models for recognition pertain to recognition, both aspects of modeling are addressed here. Since silhouettes depend only on the exterior surfaces of objects, modeling methods specifying the interior of objects such as constructive solid geometry or solid patches are not addressed here.

The synthesis of a complex shape usually starts by breaking up the surface into simpler parts (surface patches), then independently describing each part by some atomic surface element using a limited number of parameters. Basic elements include, in order of increasing complexity, planar facets, segments of spheres, cylinders, cones, quadrics, superquadrics and parametric surfaces such as Bezier patches or B-spline patches. In order to determine silhouettes of the synthetic shapes, closed-form expressions are desirable for the silhouettes of the set of basic element types.

When defining a model for the shape of a given object by the above method, it is generally attractive to position the element boundaries at some meaningful surface boundaries, although this is not necessary. It is usually possible to define or closely approximate the same shape by several different descriptions. In the field of machine vision however, careful attention is paid to the uniqueness of the representation of the objects. Difficult issues arise in recognition when the same shape can be described by different representations. Therefore, representations used for shape synthesis are usually not appropriate as such for recognition applications.

In some early machine vision systems, 3-D objects were represented by 2-D views corresponding to different aspects. The major problem of this method is the large number of different views required for describing each object. Although 3-D representations are now generally preferred, interesting approaches based on 2-D representations are still proposed [41]. Analysis of complex silhouettes such as the ones in

Fig.1.2 is difficult because natural objects such as these animals have extremely complex and variable shapes. Analysis of their silhouettes requires the combination of an understanding of image processing and geometry on one side, and of representation mechanisms for the structure of complex shapes on the other side. Some authors in the computer vision community have adopted a representation of 3-D objects in terms of generalized cones [6, 13, 19, 34, 42]. These models are viewpoint independent and are well adapted to the representation of complex shapes. When applied to silhouette analysis, the proposed method is attractive because silhouettes can be approximately predicted by a simple method for a large class of generalized cylinders. There are however a number of drawbacks to modeling with generalized cones. Generalized cone models are not always unique and, for complex surfaces, the usual approximations involved may lead to incorrect conclusions [43].

A very different modeling approach is taken by Horn with the Extended Gaussian Image [44]. The Extended Gaussian Image represents a complex shape in one step, specifying the shape by a scalar function on the Gaussian sphere. The value of the function on the sphere defines the inverse Gaussian curvature of the surface at the corresponding point of the object. This representation is known to be complete and unique for convex objects. An algorithmic inversion has been proposed and its implementation reported in [45]. The Extended Gaussian Image combines information related to different viewpoints in an elegant way. It has been successfully used in recognizing and positioning 3-D objects [46]. It will be shown in this thesis that the Gaussian mapping greatly simplifies the selection of silhouette generator points. However, the Gaussian curvature of the object is not related to silhouette properties in a straightforward way, a fact that makes the Extended Gaussian Image inappropriate for work on silhouettes.

2.3. Conclusion

To summarize our analysis of the literature on silhouettes, we notice that work published on silhouettes suffers from the lack of a basic theory which would summarize most of the individual results. In addition, a detailed analysis of the relation between complex curved shapes and their silhouettes has not been presented. Finally, our survey of classical modeling techniques reveals that silhouette shapes cannot

usually be related to the 3-D representations. This thesis tries to overcome these deficiencies by contributing a basic theory of silhouettes for objects with curved surfaces. It will be shown that the theory based on curved surfaces can be easily extended to surfaces with edges, corners and planar faces, so that the same theory can be used in many situations.

The new theory is based on a set of three new representations for the shape of 3-D surfaces, and the corresponding representations for planar curves. The new object representations presented in this thesis retain a basic concept of the Extended Gaussian Image, namely the description of object shapes by functions on their Gaussian sphere. The functions used in the representations proposed in this thesis specify points, tangent planes and complete curvature of the object surfaces. These functions are easily related to the corresponding functions for silhouettes corresponding to any viewing direction. Some of the functions on the Gaussian sphere are substantially more complex than the the function represented in Extended Gaussian Image function and require the definition of vectors and tensors at each point of the Gaussian sphere.

Chapter 3
Background

In this chapter, the framework in which the silhouette analysis will be developed, is reviewed. As silhouettes refer to outlines of image projections, the study of silhouette shapes is equivalent to the study of the shape of closed curves. A key issue addressed by this thesis is the relation between silhouette shapes and shapes of the corresponding objects. Opaque objects are completely determined by their bounding surface so that object shapes are equivalent to shapes of closed surfaces. It will hence be possible to phrase the relations between object shapes and silhouette shapes in terms of curves and surfaces. Both curves and surfaces are sets of points which can be specified by expressions for their coordinates in appropriate frames. These sets will be analyzed in this thesis with tools from analytic geometry and differential geometry. Basic concepts from these fields are reviewed here, and notations used throughout the thesis are defined.

In the first section, geometry of points, lines and planes is reviewed. Coordinates are defined for these elements and effects of transformations of axes on these coordinates are studied. Specification of the imaging projection is addressed. Relations between coordinates of points and planes in the scene and the coordinates of their projections in the image are developed.

In the second section, the geometry of curves and surfaces is reviewed. Representations in terms of global parametric equations and in terms of local Monge parameterizations are discussed. Curvature is defined in terms of a Taylor expansion of the Monge parameterization. For curves, the resulting definition is identical to the classical curvature k, which is also the inverse of the radius of curvature $\rho = k^{-1}$. In the case of surfaces however, our method defines curvature by two new invariant tensors which are inverses of each other, and will be denoted here as the tensor of curvature and the tensor of radius of curvature.

In the third section, the Gaussian mapping is reviewed, and definitions of silhouette and object properties in terms of functions on the Gaussian sphere and on the Gaussian circle are proposed. Geographical coordinates on the sphere are

introduced, and representations of vector and tensor valued functions on the sphere are formally addressed. Finally, the global definition of normal orientations on the Gaussian sphere is related to local definitions in terms of Monge parameterizations.

In our review of concepts of geometry, it will often be useful to develop the arguments in the simpler case of two dimensions first, and to use this formulation to introduce the more complicated case of three dimensions. However, for some problems which are essentially meaningful in three dimensions only, the case of three dimensions is analyzed first.

A pragmatic approach is followed through this chapter. More rigorous accounts of differential geometry are provided in textbooks such as [47, 48].

3.1. Geometry of Points

3.1.1. Coordinates of Points and Vectors

Cartesian Coordinates (x, z) and (x, y, z) are used for the representation of points in 2-D and 3-D respectively; see Fig.3.1. Axis orientation corresponds to a counterclockwise rotation from Ox to Oz in 2-D, and to a right-handed trihedron in 3-D. Vectors are denoted as $\mathbf{x} = (x \;\; z)^T$ and $\vec{\mathbf{x}} = (x \;\; y \;\; z)^T$. The notations $\mathbf{n}$ and $\vec{\mathbf{n}}$ are reserved for vectors normal to a curve and to a surface respectively. Unit vectors are denoted as, for example, $\mathbf{l}_x$ for a unit vector along $\mathbf{x}$ in 2-D, and $\vec{\mathbf{l}}_n$ for a unit vector along $\vec{\mathbf{n}}$ in 3-D.

We have chosen the letters x and z to denote the axes in the plane instead of the usual x and y to emphasize the relation between the vertical axis z in 2-D and 3-D.

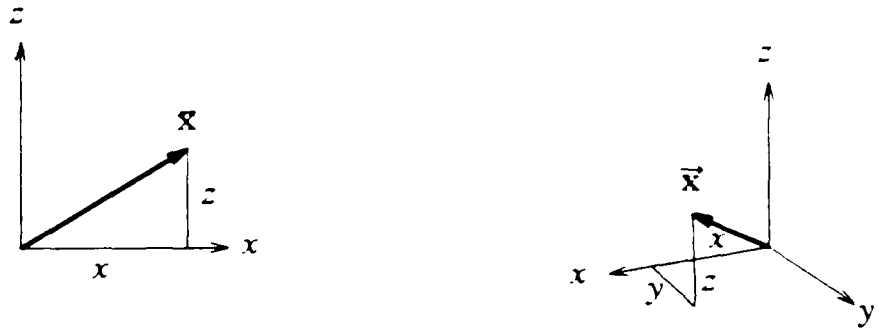

Fig.3.1. Cartesian Coordinates in 2-D and 3-D.

3.1.2. Tangential Coordinates

Tangential coordinates, also referred to as dual coordinates, will be considered for the characterization of lines tangent to a silhouette and planes tangent to an object. These coordinates are discussed in some detail here since no reference consistent with our notation could be found. Additional material and insight can be found in [49].

Curves and surfaces are usually described in terms of their points and the coordinates of these points. However, it is also possible to describe curves and surfaces by the sets of their tangents; these descriptions will be referred to here as tangential representations. Tangential representations require the definition of coordinates for lines and planes. As in the case of points, coordinates for a tangent (a line or a plane) represent the position of this element relative to a system of axes. One set of coordinates used in this text to specify tangents is the set of inverse intercepts with the axes. In 2-D, a line intersecting the axes at $(1/\lambda_x, 0)$ and $(0, 1/\lambda_y)$ will be given coordinates (λ_x, λ_y) and a plane intersecting the axes at $(1/\lambda_x, 0, 0)$, $(0, 1/\lambda_y, 0)$ and $(0, 0, 1/\lambda_z)$ will be given coordinates $(\lambda_x, \lambda_y, \lambda_z)$; see Fig.3.2. These coordinates for lines and planes will be referred to as Cartesian tangential coordinates in this text. They can be viewed as coordinates of elements (lines and planes) represented by points in an other space, which will be referred to here as the tangential space; this space is isomorphic to the dual space. Elements in the tangential space can be referred to by sets of coordinates or also by vectors in the tangential space, $\bar{\lambda} = (\lambda_x \ \lambda_z)^T$ in 2-D and $\vec{\lambda} = (\lambda_x \ \lambda_y \ \lambda_z)^T$ in 3-D.

It is sometimes useful to consider a different set of coordinates for elements in tangential space, which will be referred to as polar tangential coordinates. For both lines in 2-space and planes in 3-space, the polar coordinates specify the distance p to the origin and the normal orientation. Orientations are specified in 2-D by the polar angle ψ and in 3-D by the longitude ξ and latitude η; see Fig.3.2. The conversion from polar coordinates (p, ψ) to Cartesian coordinates (λ_x, λ_y) of a line in 2-D is given by

$$\left| \begin{array}{rcl} \lambda_x & = & \cos\psi / p \\ \lambda_y & = & \sin\psi / p \end{array} \right. \tag{3.1}$$

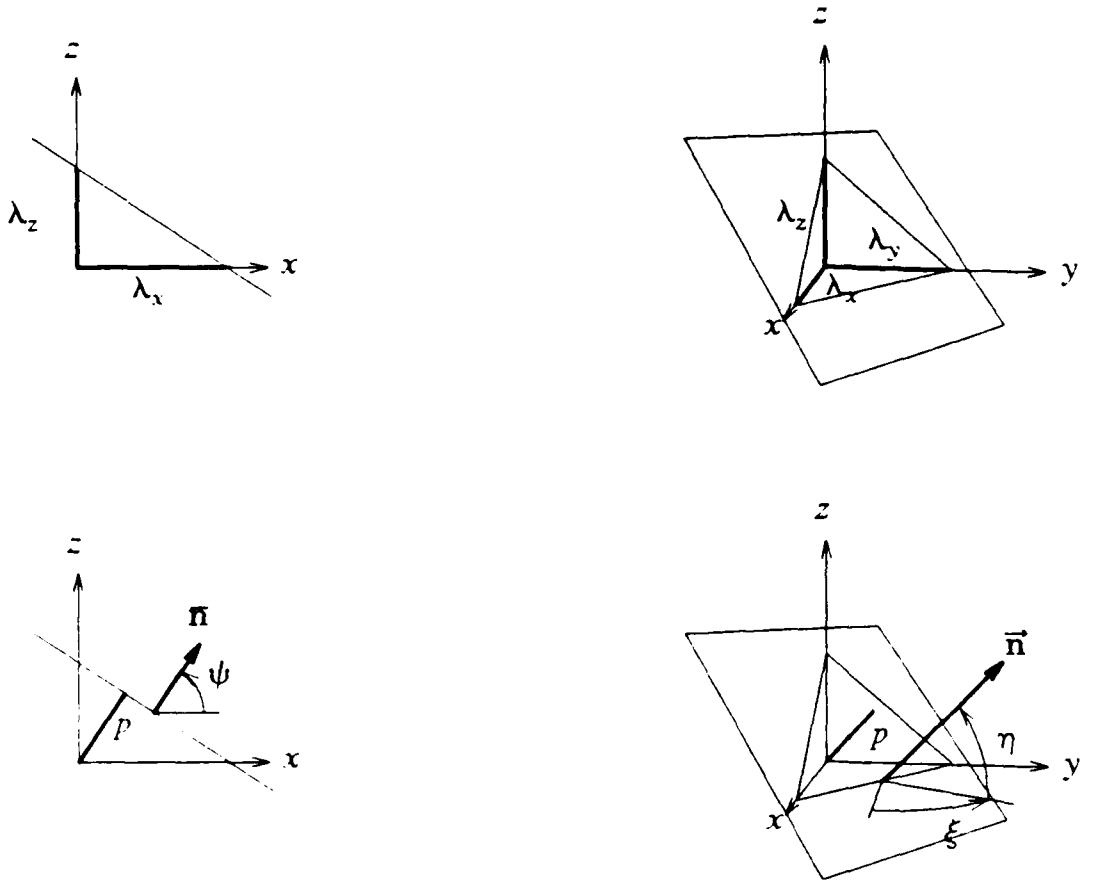

Fig.3.2. Tangential Coordinates.

The corresponding relations between 3-D Cartesian coordinates $(\lambda_x, \lambda_y, \lambda_z)$ and polar coordinates (p, ξ, η) for a plane are given by

$$\left| \begin{array}{rcl} \lambda_x & = & \cos\xi\cos\eta/p \\ \lambda_y & = & \sin\xi\cos\eta/p \\ \lambda_z & = & \sin\eta/p \end{array} \right. \qquad (3.2)$$

Points of a line with tangential coordinate vector $\bar{\lambda}$ have coordinates which satisfy

$$x\ \lambda_x + y\ \lambda_y = 1 \ , \text{also written } \bar{\lambda}^T\ \bar{x} = 1 \qquad (3.3)$$

The vector $\bar{\lambda}$ in tangential space defines a line in point space which is perpendicular to $\bar{\lambda}$ considered as a vector in point space. Similarly, the equation for points of the plane

with coordinate vector $\vec{\lambda} = (\lambda_x \ \lambda_y \ \lambda_z)^T$ is given by

$$x\ \lambda_x + y\ \lambda_y + z\ \lambda_z = 1 \ \text{, also written } \vec{\lambda}^T\ \vec{x} = 1 \tag{3.4}$$

The equation for points on a line with polar tangential coordinates (p, ψ) is given by

$$x\ \cos\psi + y\ \sin\psi = p \tag{3.5}$$

which is sometimes referred to as the normal equation of the line. Points of a plane with polar tangential coordinates (p, ξ, η) satisfy the equation

$$x\ \cos\xi\cos\eta + y\ \sin\xi\cos\eta + z\ \sin\eta = p \tag{3.6}$$

which is referred to as the normal equation of the plane.

3.1.3. Transformations of Axes

Coordinates of points, lines and planes depend on the choice of a system of axes. The same physical point, line or plane is described by different sets of coordinates in two sets of axes. Relations between these coordinates are investigated in this section.

Three systems of axes will be considered in this thesis for the description of curves and surfaces; these systems will be referred to as global, rotated, and local axes. The local axes are rotated and translated with respect to the global axes; they are centered at P_0. The rotated axes are parallel to the local axes but centered at the origin of the global axes. The three systems are sketched in Fig.3.3, for both 2-D and 3-D space.

3.1.3.1. Transformations for Point Coordinates

Denoting coordinates in rotated axes by the subscript R, coordinates in local axes by the subscript l, and coordinates in the global axes by symbols without subscripts, the various coordinates in 2-D are related by

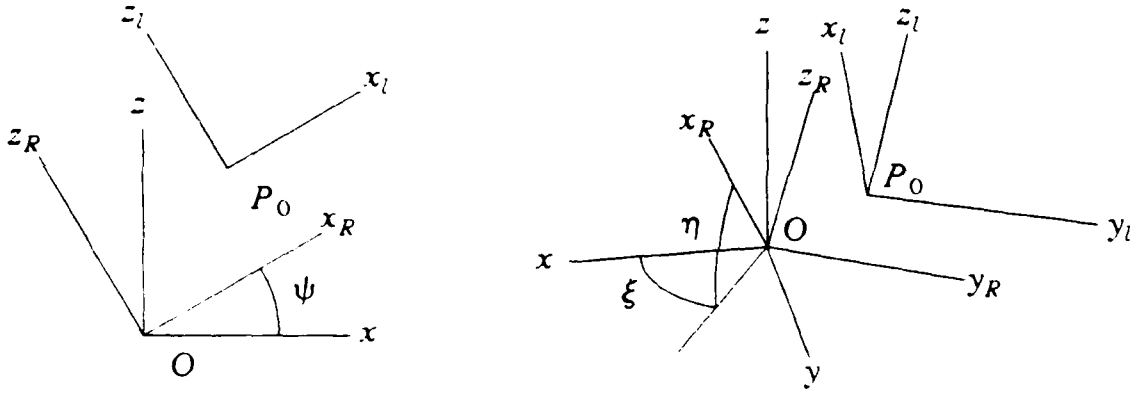

Fig.3.3. Global, Rotated and Local Systems of Axes

$$\begin{bmatrix} x \\ z \end{bmatrix} = \begin{bmatrix} \cos\psi_0 & -\sin\psi_0 \\ \sin\psi_0 & \cos\psi_0 \end{bmatrix} \begin{bmatrix} x_R \\ z_R \end{bmatrix}$$

$$\mathbf{x} = \mathbf{R}_2^{R-G}(\psi_0)\, \mathbf{x}_R \tag{3.7}$$

$$\begin{bmatrix} x \\ z \end{bmatrix} = \begin{bmatrix} x_0 \\ z_0 \end{bmatrix} + \begin{bmatrix} \cos\psi_0 & -\sin\psi_0 \\ \sin\psi_0 & \cos\psi_0 \end{bmatrix} \begin{bmatrix} x_l \\ z_l \end{bmatrix}$$

$$\mathbf{x} = \mathbf{x}_0 + \mathbf{R}_2^{R-G}(\psi_0)\, \mathbf{x}_l \tag{3.8}$$

where the symbol $\mathbf{R}_2^{R-G}$ denotes the matrix of the 2-D rotation from rotated to global axes and $\mathbf{x}_0$ is the coordinate vector of P_0 in global axes. The corresponding relations for coordinates in 3-D are given by

$$\begin{bmatrix} x \\ y \\ z \end{bmatrix} = \begin{bmatrix} \cos\xi_0\cos\eta_0 & -\sin\xi_0 & -\cos\xi_0\sin\eta_0 \\ \sin\xi_0\cos\eta_0 & \cos\xi_0 & -\sin\xi_0\sin\eta_0 \\ \sin\eta_0 & 0 & \cos\eta_0 \end{bmatrix} \begin{bmatrix} x_R \\ y_R \\ z_R \end{bmatrix}$$

$$\vec{\mathbf{x}} = \mathbf{R}_3^{R-G}(\xi_0, \eta_0)\, \vec{\mathbf{x}}_R \tag{3.9}$$

$$\begin{pmatrix} x \\ y \\ z \end{pmatrix} = \begin{pmatrix} x_0 \\ y_0 \\ z_0 \end{pmatrix} + \begin{pmatrix} \cos\xi_0\cos\eta_0 & -\sin\xi_0 & -\cos\xi_0\sin\eta_0 \\ \sin\xi_0\cos\eta_0 & \cos\xi_0 & -\sin\xi_0\sin\eta_0 \\ \sin\eta_0 & 0 & \cos\eta_0 \end{pmatrix} \begin{pmatrix} x_l \\ y_l \\ z_l \end{pmatrix}$$

$$\vec{\mathbf{x}} = \vec{\mathbf{x}}_0 + \mathbf{R}_3^{R-G}(\xi_0,\eta_0)\,\vec{\mathbf{x}}_l \tag{3.10}$$

where the symbol $\mathbf{R}_3^{R-G}$ denotes the matrix of the 3-D rotation between the rotated frame and the global frame, and $\vec{\mathbf{x}}_0$ is the coordinate vector of P_0 in global axes. In the above expressions, ψ_0 is the counterclockwise angle from the global axes to the rotated axes in 2-D and ξ_0, η_0 are the longitude and latitude of the orientation of the rotated Ox_R axis with respect to the global frame in 3-D, a notation consistent with angular coordinates introduced for the Gaussian circle and Gaussian sphere in a later section.

As is done repeatedly in this thesis, both expanded and compressed notations are provided for the same equation. The abridged notation stresses the similarity between relations in 2-D and 3-D, whereas the expanded notation is more explicit.

3.1.3.2. Transformations for Tangential Coordinates

After having considered the transformation of point coordinates between different reference frames, transformations of tangential coordinates are now derived for the case of pure rotations of axes. Coordinates for a plane in rotated axes are obtained by first writing the equation in global axes for the coordinates of the points of the plane. These coordinates are related to the coordinates in the rotated axes using the transformation discussed in the previous section. An equation is obtained for the coordinates of the points of the plane in the rotated axes, from which the tangential coordinates of the plane can be extracted. It will be concluded that the transformations of Cartesian coordinates of planes are identical to the transformations of Cartesian coordinates of points. The same argument and the same conclusions also apply to the coordinates of a line in 2-D.

Consider a plane with global coordinates $\vec{\lambda}$. This plane contains the points $\vec{\mathbf{x}}$ for which; see equ. (3.4)

$$\vec{\lambda}^T\,\vec{\mathbf{x}} = 1 \tag{3.11}$$

The equation of the plane of interest in the new axes has the form

$$\vec{\lambda}_R^T \, \vec{x}_R = 1 \tag{3.12}$$

where $\vec{\lambda}_R^T$ has to be determined. Equation (3.11) is transformed into a form more similar to (3.12) by applying the transformation in equation (3.9) to the point coordinates $\vec{x}$.

$$\vec{\lambda}^T \, \mathbf{R}_3^{R-G} \, \vec{x}_R = 1 \tag{3.13}$$

Identifying this form with equation (3.12) produces

$$\vec{\lambda}_R^T = \vec{\lambda}^T \, \mathbf{R}_3^{R-G} \quad \text{,also written} \quad \vec{\lambda} = \mathbf{R}_3^{R-G} \, \vec{\lambda}_R \tag{3.14}$$

The tangential coordinate vectors for planes hence transform in the same fashion as point coordinate vectors. This is not surprising, since the vector $\vec{\lambda}$ in point space is a normal to the plane at hand. Transformations of tangential coordinates between translated axes is less straightforward and is not discussed here.

3.1.4. Imaging Projections

This section describes how the imaging geometry is specified, and how coordinates of points and lines in the image can be obtained from the coordinates of points and planes in the imaged scene. For a general perspective projection, the imaging geometry is completely defined by the position and orientation of the "camera frame" and by the focal length of the "camera". In this thesis, only orthographic projections are considered; these projections are completely defined by the viewing direction.

It is customary in machine vision to relate the camera frame to the reference frame of a particular object in two steps by considering an intermediate world frame attached to the scene being analyzed. The "camera" is defined by a system of axes $x_C \, y_C \, z_C$; its position and orientation are specified with respect to the world frame $x_W \, y_W \, z_W$ and account for the position and orientation of the imaging device relative to the scene. On the other hand, each object is described in an individual reference frame, say $x_O \, y_O \, z_O$; the relation between this frame and the world frame accounts for the position and orientation of the object in the scene; see Fig.3.4. The geometry of the imaging projection relative to the object is hence determined by the composition of the transformation from $x_O \, y_O \, z_O$ to $x_W \, y_W \, z_W$, then to $x_C \, y_C \, z_C$. In this thesis, only

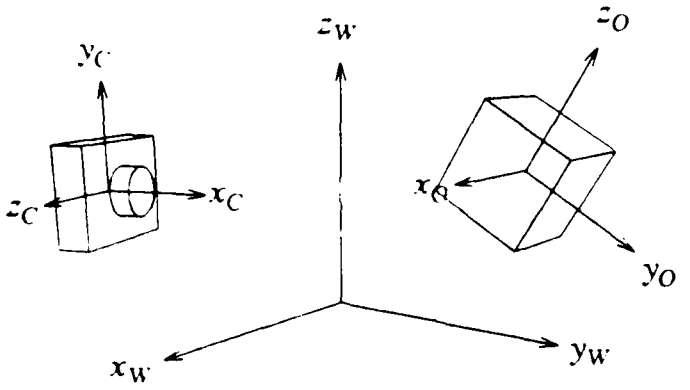

Fig.3.4. Traditional Definition of Positions and Orientations.

---

the combination of these two steps is considered, by describing the imaging geometry directly in the object frame.

For orthographic projections, the imaging geometry is entirely specified by the viewing direction, which is parallel to the vector ∇ pointing away from the scene towards the viewer. The vector ∇ itself is referenced by its longitude ϕ and latitude θ in the object frame; see Fig.3.5.

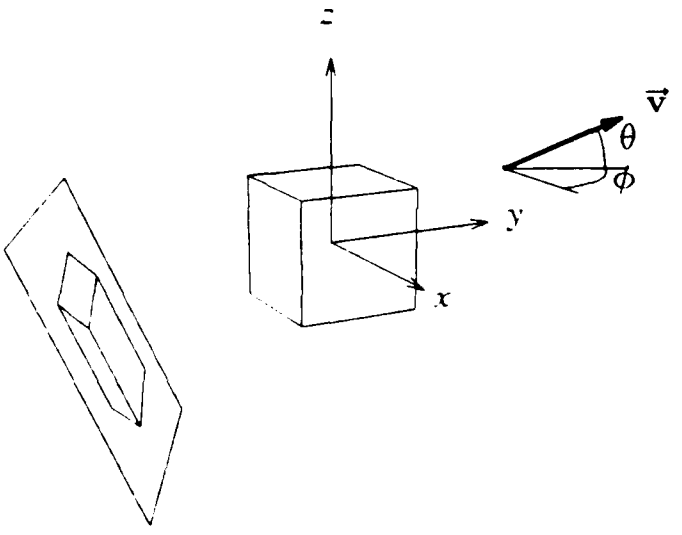

Fig.3.5. Relative Orientation of the Object and the Viewing Direction.

Cartesian coordinates for the unit vector $\vec{1}_v$ are given by

$$\vec{1}_v = (\cos\phi\cos\theta \ \sin\phi\cos\theta \ \sin\theta)^T \qquad (3.15)$$

In the discussions of this thesis, the global frame $Oxyz$ defined in section 3.1.3. denotes a frame in which the object is described, hence a frame similar to $x_O\, y_O\, z_O$. The local frame $P_O x_l\, y_l\, z_l$ defined in section 3.1.3. is not related to the frames introduced here. It is used to locally define the geometry of of the object in the neighborhood of P_O.

Relations between coordinates of points and planes and coordinates of their projections in the image plane are now investigated. Points and planes of 3-D space are referenced to the global object-centered frame $Oxyz$. A cartesian frame $O_\pi x_\pi z_\pi$ is chosen in the image plane Π, where O_π is the projection of the origin O and $O_\pi z_\pi$ is the projection of the Oz axis. Coordinates in these axes of the projection plane will be denoted by a subscript π. In order to simplify the projection operation, it is useful to first consider a rotated system of axes, in which the viewing direction is parallel to one of the axes. This particular rotated frame is referred to as the camera frame here, and coordinates in these axes are denoted by a subscript C. The system $Ox_C\, y_C\, z_C$ is chosen so that Ox_C is parallel to the viewing direction, Oy_C parallel to $O_\pi x_\pi$ and Oz_C parallel to $O_\pi z_\pi$; see Fig.3.6. The coordinates of points in this system of axes are

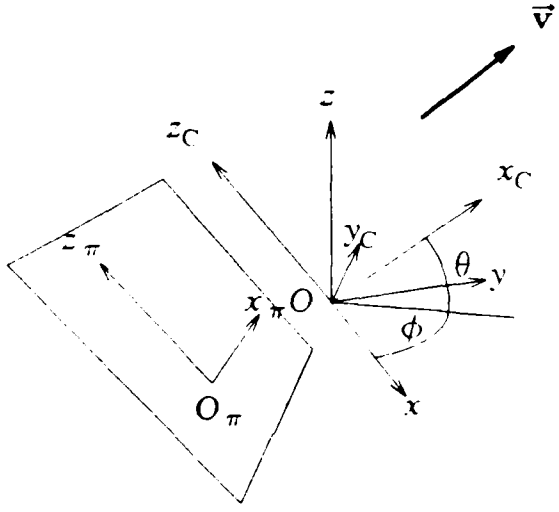

Fig.3.6. Coordinate Frames in 3-D and in the Projection Plane.

related to global coordinates by

$$\begin{pmatrix} x_C \\ y_C \\ z_C \end{pmatrix} = \begin{pmatrix} \cos\phi\cos\theta & \sin\phi\cos\theta & \sin\theta \\ -\sin\phi & \cos\phi & 0 \\ -\cos\phi\sin\theta & -\sin\phi\sin\theta & \cos\theta \end{pmatrix} \begin{pmatrix} x \\ y \\ z \end{pmatrix} \tag{3.16}$$

$$\vec{\mathbf{x}}_C = \mathbf{R}_3^{G-C}\,\vec{\mathbf{x}}$$

Similarly, coordinates of planes in the camera frame are related to global coordinates by

$$\begin{pmatrix} \lambda_{xC} \\ \lambda_{yC} \\ \lambda_{zC} \end{pmatrix} = \begin{pmatrix} \cos\phi\cos\theta & \sin\phi\cos\theta & \sin\theta \\ -\sin\phi & \cos\phi & 0 \\ -\cos\phi\sin\theta & -\sin\phi\sin\theta & \cos\theta \end{pmatrix} \begin{pmatrix} \lambda_x \\ \lambda_y \\ \lambda_z \end{pmatrix} \tag{3.17}$$

$$\vec{\boldsymbol{\lambda}}_C = \mathbf{R}_3^{G-C}\,\vec{\boldsymbol{\lambda}}$$

Projections are meaningful for planes only when they are parallel to the viewing direction, in which case $\lambda_{xC} = 0$. For such planes, the projection in the image plane consists of a line, whereas the projection of all other planes in the scene covers the entire image plane. This property will be useful when considering the projection of surfaces defined in tangential coordinates. Note that a plane is parallel to the viewing direction if

$$\lambda_{xC} = \lambda_x \cos\phi\cos\theta + \lambda_y \sin\phi\cos\theta + \lambda_z \sin\theta = 0 \tag{3.18}$$

In the rotated axes, the viewing direction is parallel to the Ox_C axis. As a consequence, the coordinates in the image plane are related to coordinates in the camera frame by the straightforward expressions

$$\begin{pmatrix} x_\pi \\ z_\pi \end{pmatrix} = \begin{pmatrix} 0 & 1 & 0 \\ 0 & 0 & 1 \end{pmatrix} \begin{pmatrix} x_C \\ y_C \\ z_C \end{pmatrix}$$

$$\mathbf{x}_\pi = \mathbf{I}_{23}\,\vec{\mathbf{x}}_C \tag{3.19}$$

$$\begin{pmatrix} \lambda_{x\pi} \\ \lambda_{z\pi} \end{pmatrix} = \begin{pmatrix} 0 & 1 & 0 \\ 0 & 0 & 1 \end{pmatrix} \begin{pmatrix} \lambda_{xC} \\ \lambda_{yC} \\ \lambda_{zC} \end{pmatrix}$$

$$\vec{\lambda}_{\pi} = \mathbf{I}_{23}\, \vec{\lambda}_{C} \tag{3.20}$$

where $\mathbf{I}_{23}$ denotes the 2x3 matrix including the 2x2 matrix in the above expressions. Note that the last equation relates coordinates of lines in the image to coordinates of planes parallel to the viewing direction in the scene.

Coordinates of the projected points and lines can be obtained directly from coordinates in the global object frame by combining the above projection operations with the rotation from global axes to camera axes in (3.16) and (3.17).

$$\begin{pmatrix} x_{\pi} \\ z_{\pi} \end{pmatrix} = \begin{pmatrix} 0 & 1 & 0 \\ 0 & 0 & 1 \end{pmatrix} \begin{pmatrix} \cos\phi\cos\theta & \sin\phi\cos\theta & \sin\theta \\ -\sin\phi & \cos\phi & 0 \\ -\cos\phi\sin\theta & -\sin\phi\sin\theta & \cos\theta \end{pmatrix} \begin{pmatrix} x \\ y \\ z \end{pmatrix}$$

$$= \begin{pmatrix} -\sin\phi & \cos\phi & 0 \\ -\sin\theta\cos\phi & -\sin\theta\sin\phi & \cos\theta \end{pmatrix} \begin{pmatrix} x \\ y \\ z \end{pmatrix}$$

$$\vec{x}_{\pi} = \mathbf{I}_{23}\, \mathbf{R}_3^{G-C}\, \vec{x} \tag{3.21}$$

$$\begin{pmatrix} \lambda_{x\pi} \\ \lambda_{z\pi} \end{pmatrix} = \begin{pmatrix} 0 & 1 & 0 \\ 0 & 0 & 1 \end{pmatrix} \begin{pmatrix} \cos\phi\cos\theta & \sin\phi\cos\theta & \sin\theta \\ -\sin\phi & \cos\phi & 0 \\ -\cos\phi\sin\theta & -\sin\phi\sin\theta & \cos\theta \end{pmatrix} \begin{pmatrix} \lambda_x \\ \lambda_y \\ \lambda_z \end{pmatrix}$$

$$= \begin{pmatrix} -\sin\phi & \cos\phi & 0 \\ -\sin\theta\cos\phi & -\sin\theta\sin\phi & \cos\theta \end{pmatrix} \begin{pmatrix} \lambda_x \\ \lambda_y \\ \lambda_z \end{pmatrix}$$

$$\vec{\lambda}_{\pi} = \mathbf{I}_{23}\, \mathbf{R}_3^{G-C}\, \vec{\lambda} \tag{3.22}$$

3.2. Curves and Surfaces

In this section, a number of classical results on representations of curves and surfaces are reviewed, and an original definition of curvature is proposed. In the first subsection, definitions of curves and surfaces in point space are presented, followed by

definitions in tangential space and conversions between the two representations. In the second subsection, the Monge parameterization, a particular specification method for curves and surfaces, is presented. In the third subsection, curvature is defined in terms of the coefficients of the second order Taylor expansion of a local Monge parameterization. This definition of curvature is equivalent to commonly used definitions in the case of curves, and provides a new intrinsic definition of curvature in the case of surfaces.

3.2.1. Definitions

Precise definitions of curves and surfaces require careful attention to avoid the possibility of pathological cases. However, refinements will be omitted here for the sake of conciseness. A curve in 2-space is defined as the set of points

$$\{P(x,y) \mid x=x(t),\ y=y(t);\ t \in \mathbf{T}\} \tag{3.23}$$

where $\mathbf{T}$ is some domain for the parameter t. A surface in 3-space is defined as the set of points

$$\{P(x,y,z) \mid x=x(u,v),\ y=y(u,v),\ z=z(u,v);\ (u,v) \in \mathbf{W}\} \tag{3.24}$$

where $\mathbf{W}$ is some 2-D domain for the parameters u, v. Note that in both cases, curves and surfaces are defined as sets of points. Although parametric equations are used to define the sets, the sets themselves exist independently of the parametric equations. Two curves or surfaces are identical if they contain the same points. For example, the curve

$$\{P(x,y) \mid x=x(t(s)),\ y=y(t(s));\ s \in t^{-1}(\mathbf{T})\} \tag{3.25}$$

where $s(.)$ is a monotonic function, is identical to the curve defined in (3.23). The same curves or surfaces may also be specified in different ways, for example the points can be defined by an implicit equation for their coordinates, $F(x,y)=0$ for a curve and $F(x,y,z)=0$ for a surface. The distinction between curve/surface points and curve/surface equations is stressed here. In a later section, a new representation of surface curvature is presented, which depends only on the surface defined as a set of points. In contrast, definitions of surface curvature in most differential geometry textbooks also carry information about the equations used for defining the surface. This difference is investigated in Appendix 4.

Unless otherwise specified, only smooth curves and surfaces are considered in this thesis. Smoothness refers here to the existence and continuity of second order derivatives of parametric equations defining the surface. Other important concepts such as regularity are not discussed here. Partial derivatives will be denoted by subscripts as in $\vec{\mathbf{x}}_u = \partial\vec{\mathbf{x}}/\partial u$, except when confusion is possible. It can be shown that first derivatives of the parametric equations are related to tangent directions. Specifically, $\mathbf{x}_t(t_0)$ is a vector parallel to the tangent to the curve $\mathbf{x}(t)$ at $\mathbf{x}(t_0)$. Similarly, $\vec{\mathbf{x}}_u(u_0,v_0)$ and $\vec{\mathbf{x}}_v(u_0,v_0)$ are tangent to the surface $\vec{\mathbf{x}}(u,v)$ at $\vec{\mathbf{x}}(u_0,v_0)$. The vector $\vec{\mathbf{n}} = \vec{\mathbf{x}}_u \times \vec{\mathbf{x}}_v$ defines a surface normal. First derivatives of parametric equations are hence related to tangent and normal orientations. In a later section, second derivatives will be related to curvatures.

3.2.2. Convexity

As mentioned in the introduction, the silhouette problem is first analyzed in this thesis for convex objects only. For a convex object, the straight segment joining two points of the object is completely included in the object. In order to avoid the presence of straight components in the object surface, a stronger definition of convexity will be required. For a strictly convex object, the open straight segment joining two points of the object must be completely included in the interior of the object, even when the two points are on the boundary of the object. Examples of a non-convex object, a convex object and a strictly convex object are given in Fig.3.7.

Later in the text, curves and surfaces will be described by equations in terms of normal orientations, instead of parametric equations in terms of the generic parameters

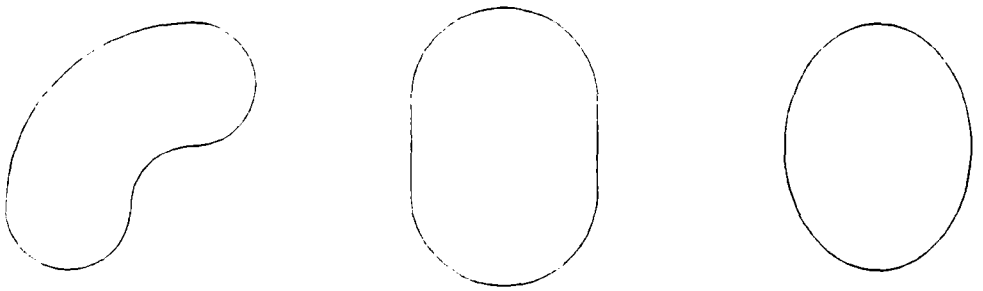

Fig.3.7. Smooth 2-D Objects: a) Non-Convex, b) Convex, c) Strictly Convex.

t , u , v . The parameters chosen for this purpose are the polar angle ψ of the normal for curves and the longitude ξ and latitude η of the normal for surfaces. Representations in terms of angular parameters are unique and regular for the class of strictly convex smooth surfaces considered in this thesis. Relations between this type of parameterization and generic parameterizations are addressed in Appendix 2.

3.2.3. Tangential Space Representations

As indicated in section 3.1.2., it is sometimes useful to define curves and surfaces by their sets of tangents instead of their sets of points. As in the case of point specification, both parametric and implicit equations are possible. For example, a curve can be specified by the set of tangent lines L as

$$\{L(\lambda_x,\lambda_y) \mid F(\lambda_x,\lambda_y)=0\} \tag{3.26}$$

A surface can be specifed by the set of tangent planes P

$$\{P(\lambda_x,\lambda_y,\lambda_z) \mid F(\lambda_x,\lambda_y,\lambda_z)=0\} \tag{3.27}$$

where implicit equations were used in both cases to prescribe coordinates of the tangents. Conversion from a tangent representation to a point representation is now considered. This conversion corresponds to determining curves and surfaces as the envelopes of their sets of tangents. In the general case, the set of lines tangent to a planar curve is a one-parameter family. Points of these lines satisfy equations such as $F(x,y,\alpha)=0$ where α is a parameter for the lines. An equation for the envelope of these is obtained by eliminating the parameter α between

$$\left|\begin{array}{r} F(x,y,\alpha)=0 \\ (\partial/\partial\alpha)F(x,y,\alpha)=0 \end{array}\right. \tag{3.28}$$

Similarly, when all the planes tangent to a surface are given by a two-parameter family with equation $F(x,y,z,\alpha,\beta)=0$, an equation for the envelope is obtained by eliminating the parameters α and β between

$$\left|\begin{array}{r} F(x,y,z,\alpha,\beta)=0 \\ (\partial/\partial\alpha)F(x,y,z,\alpha,\beta)=0 \\ (\partial/\partial\beta)F(x,y,z,\alpha,\beta)=0 \end{array}\right. \tag{3.29}$$

The above formalism will be exploited in Chapter 5, for the discussion of a

representation which explicitly specifies curves and surfaces by the sets of their tangents.

3.2.4. Monge Parameterizations

This section reviews a description of curves and surfaces by explicit equations of the form $x = f(z)$ and $x = f(y,z)$, which are referred to as Monge parameterizations. Several features of these descriptions have prompted their use for describing surfaces in the machine vision literature. These features include a direct relation to image-plane coordinates and straightforward expressions for surface normals. In our work, Monge parameterizations will not be used as general object models because of their strong dependence on the reference frame, but will be used to define surface curvature in local axes. Monge parameterizations in local axes will be related to global descriptions in a later section. Monge parameterizations have been studied mainly for surfaces, which are therefore analyzed first. Subsequently, a simple equivalent is sketched for the case of 2-D curves.

The Monge parameterization for a surface can be considered as a special form of parametric equations, in which the parameters are two of the three Cartesian coordinates, say y and z; see Fig.3.8.

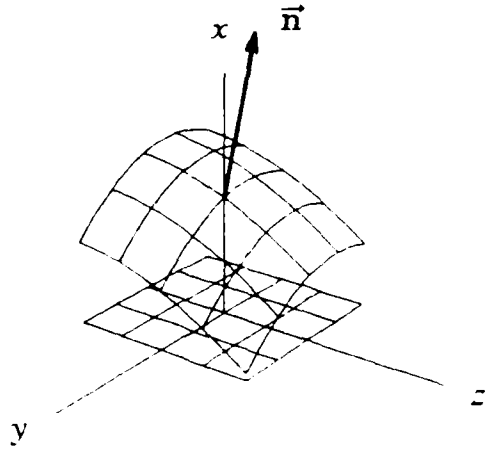

Fig.3.8. Monge parameterization for a Surface.

$$\begin{cases} x = f(y,z) \\ y = y \\ z = z \end{cases} \tag{3.30}$$

Viewing these equations as a parametric form $\vec{\mathbf{x}} = \vec{\mathbf{x}}(y,z)$, a surface normal is easily obtained as

$$\vec{\mathbf{n}} = \vec{\mathbf{x}}_y \times \vec{\mathbf{x}}_z = \begin{pmatrix} 1 \\ -f_y \\ -f_z \end{pmatrix} = \begin{pmatrix} 1 \\ -m_y \\ -m_z \end{pmatrix} \tag{3.31}$$

where $m_y = \partial x / \partial y$ and $m_z = \partial x / \partial z$ are referred to as gradients of the surface. In other work, these gradients are often denoted by the symbols p, q; this notation is not followed here because of possible confusions. The simple expression for surface normals in (3.31) makes Monge parameterizations convenient in surface-reconstruction problems from a single image, such as the shape-from-shading problem [21].

In the equivalent formalism for 2-D curves, the parametric equations in the plane x, z have the form

$$\begin{cases} x = f(z) \\ z = z \end{cases} \tag{3.32}$$

A normal vector for points on the curve is given by

$$\vec{\mathbf{n}} = \begin{pmatrix} 1 \\ -f_z \end{pmatrix} = \begin{pmatrix} 1 \\ -m_z \end{pmatrix} \tag{3.33}$$

3.2.5. Curvature

In this section, definitions for curvature will be proposed and justified. The simpler case of 2-D curves is addressed first, followed by the case of 3-D surfaces.

3.2.5.1. Curvature of 2-D Curves

In the case of a planar curve, curvature corresponds to the intuitive notion of how fast the curve diverges from its tangent. The definition chosen here for curvature is based on this notion, as it is the first non-zero coefficient of a Taylor expansion of the Monge parametric form of the curve in a local coordinate frame. Consider the curve C

around the point P_0, and the local system of axes $P_0x_l\,z_l$ where P_0x_l is along the normal at P_0; see Fig.3.9. The Monge parameterization of the curve in these local axes has the form $x_l = f\,(z_l)$. Since P_0 is on the curve and since P_0z_l is tangent to C at P_0, the Taylor series of $f\,(z_l)$ contains no terms of order zero and one in z_l. The first nontrivial expansion is hence given by

$$x_l = -1/2\; z_l\, k z_l + O(z_l{}^3) \tag{3.34}$$

where the term $kz_l{}^2$ has been decomposed for similarity with the corresponding expression for surfaces. The error term $O(z_l{}^3)$ indicates that the error of the expansion is upper bounded by a third order polynomial in z_l. The curvature of C at P_0 is defined in this thesis as the coefficient k in the above expansion, a choice consistent with the intuitive notion of curvature since large values of k imply a fast divergence of the curve away from its tangent at P_0. Note that the coefficient k in the above Taylor expansion is identical to the second derivative $\partial^2 x_l / \partial z_l{}^2$ at the origin, so that curvature is formally related to second derivatives of the equations of the curve. This definition of curvature is equivalent to the classical definition $k = d\psi/ds$, as is shown in Chapter 5. The inverse of the curvature k is defined as the radius of curvature $\rho = k^{-1}$. A justification of the definition is now presented by showing that the radius of curvature of a circle is equal to the radius of the circle. The equation for a circle of radius R tangent to z_l at the origin is given by

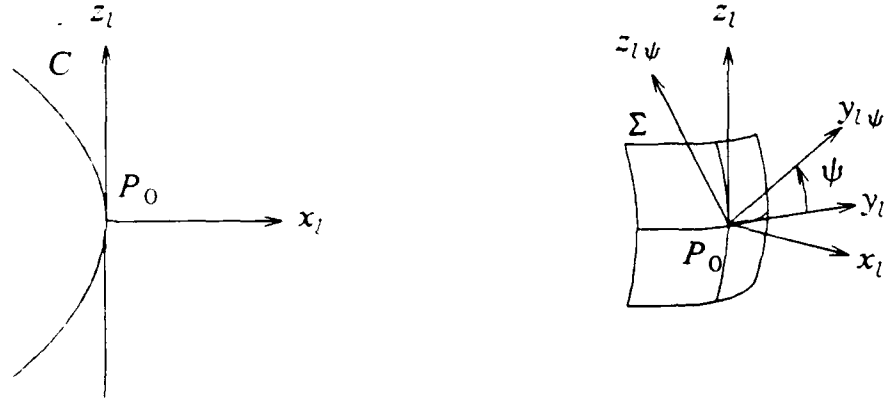

Fig.3.9. Local Axes for the definition of Curvatures in 2-D and 3-D.

$$(x_l + R)^2 + z_l^2 = R^2 \tag{3.35}$$

Considering only the branch through the origin, then expanding to second order in z_l, the following explicit equation is obtained.

$$x_l = -R + \sqrt{R^2 - z_l^2}$$

$$= -R + (R - \frac{z_l^2}{2R}) + O(z_l^3) = -1/2 \frac{z_l^2}{R} + O(z_l^3) \tag{3.36}$$

Comparing this expression with the expression used to define curvature in equation (3.34), it is clear that the curvature for the above circle is given by $k = 1/R$, which is the desired result.

3.2.5.2. Curvature of 3-D Surfaces

In the case of a surface, curvature is also related to the intuitive notion of divergence rate away from the tangent plane. Curvature of a surface will be defined here in the same way as it was defined for a curve, namely as the coefficients of the first non-zero term in the Taylor expansion of a local Monge parameterization of the surface. Specifically, consider the surface Σ in a neighborhood of the point P_0; see Fig.3.9. Consider also the local frame $P_0 x_l y_l z_l$ where x_l is along the normal at P_0. The second order expansion of the surface equation in these axes can be written as

$$x_l = -1/2 \begin{pmatrix} y_l & z_l \end{pmatrix} \begin{pmatrix} k_{11} & k_{12} \\ k_{12} & k_{22} \end{pmatrix} \begin{pmatrix} y_l \\ z_l \end{pmatrix} + O((y_l, z_l)^3) \tag{3.37}$$

where the error term $O((y_l, z_l)^3)$ indicates that the error of the expansion is bounded by a third order polynomial in y_l, z_l. The above equation will also be written in vector form as

$$x_l = -1/2\, \mathbf{z}_l \bar{\bar{\mathbf{K}}} \mathbf{z}_l + O(\mathbf{z}_l^3) \tag{3.38}$$

which stresses the similarity with the 2-D equation (3.34). Characterizing the curvature of a surface is more involved than in the case of a curve, as divergence from the tangent plane may depend on the direction chosen along the tangent plane. In equation (3.37), there are three independent coefficients in the second order term, thus emphasizing the added complexity of surface curvatures over curvatures of curves. Curvature of the surface Σ at P_0 will be taken as the set of second order coefficients of

(3.37), namely as the symmetric 2x2 matrix $\bar{\bar{\mathbf{K}}}$. It is now shown that this matrix is really a tensor by showing that it transforms as a tensor in transformations of axes [47].

Consider a second system of local axes, $P_0 x_{l\psi} y_{l\psi} z_{l\psi}$ related to the original local frame $P_0 x_l y_l z_l$ by a rotation with angle ψ around the $P_0 x_l$ axis; see Fig.3.9. Coordinates in the two frames are related by $x_l = x_{l\psi}$ and

$$\begin{Bmatrix} y_l \\ z_l \end{Bmatrix} = \begin{bmatrix} \cos\psi & -\sin\psi \\ \sin\psi & \cos\psi \end{bmatrix} \begin{Bmatrix} y_{l\psi} \\ z_{l\psi} \end{Bmatrix} \tag{3.39}$$

A Taylor expansion of the Monge parameterization of the surface in the rotated frame is obtained by combining equations (3.37) and (3.39)

$$x_{l\psi} = -\tfrac{1}{2} \begin{Bmatrix} y_{l\psi} & z_{l\psi} \end{Bmatrix} \begin{bmatrix} \cos\psi & \sin\psi \\ -\sin\psi & \cos\psi \end{bmatrix} \begin{bmatrix} k_{11} & k_{12} \\ k_{12} & k_{22} \end{bmatrix} \begin{bmatrix} \cos\psi & -\sin\psi \\ \sin\psi & \cos\psi \end{bmatrix} \begin{Bmatrix} y_{l\psi} \\ z_{l\psi} \end{Bmatrix} \tag{3.40}$$

$$= -\tfrac{1}{2} \begin{Bmatrix} y_{l\psi} & z_{l\psi} \end{Bmatrix} \begin{bmatrix} k_{11\psi} & k_{12\psi} \\ k_{12\psi} & k_{22\psi} \end{bmatrix} \begin{Bmatrix} y_{l\psi} \\ z_{l\psi} \end{Bmatrix}$$

where the 2x2 curvature matrix in the rotated axes is given by

$$\begin{bmatrix} k_{11\psi} & k_{12\psi} \\ k_{12\psi} & k_{22\psi} \end{bmatrix} = \begin{bmatrix} \cos\psi & \sin\psi \\ -\sin\psi & \cos\psi \end{bmatrix} \begin{bmatrix} k_{11} & k_{12} \\ k_{12} & k_{22} \end{bmatrix} \begin{bmatrix} \cos\psi & -\sin\psi \\ \sin\psi & \cos\psi \end{bmatrix} \tag{3.41}$$

The matrix $\bar{\bar{\mathbf{K}}}$ transforms as a covariant tensor in coordinate transformations such as the one studied above, and is therefore a covariant tensor. Therefore, it will be referred to as the tensor of curvature of the surface at P_0. In differential geometry, the name of tensor of curvature is usually reserved for a tensor with 4 indices due to Riemann which is not directly related to $\bar{\bar{\mathbf{K}}}$.

The components of our tensor of curvature are related to second derivatives of the surface equation; for example, $k_{11} = \partial^2 x_l / \partial y_l^2$ at $y_l = z_l = 0$. Preserving the parallelism with the case of curves, the inverse of the tensor of curvature will be defined as the tensor of radius of curvature

$$\bar{\bar{\mathbf{R}}} = \bar{\bar{\mathbf{K}}}^{-1} = \begin{bmatrix} k_{11} & k_{12} \\ k_{12} & k_{22} \end{bmatrix}^{-1} = \begin{bmatrix} r_{11} & r_{12} \\ r_{12} & r_{22} \end{bmatrix} \tag{3.42}$$

The above definition of curvature by a tensor in local axes is original. Its relation with other definitions is discussed in Appendix 4. For a general surface, there exists at each point an orientation ψ of the axes $P_0 y_l{}_\psi z_l{}_\psi$ in the tangent plane for which the 2x2 tensors $\bar{\bar{\mathbf{R}}}$ and $\bar{\bar{\mathbf{K}}}$ are diagonal. In these axes, values on the diagonal of $\bar{\bar{K}}$ are referred to as the principal curvatures k_1 and k_2. The diagonal values of $\bar{\bar{R}}$ are referred to as the principal radii of curvature $\rho_1 = k_1^{-1}$ and $\rho_2 = k_2^{-1}$. The Gaussian curvature of a surface is defined as the product of the two principal curvatures, $k_g = k_1 k_2$; in general axes, $k_g = \det\bar{\bar{\mathbf{K}}}$. The mean curvature of a surface is defined as the mean of the two principal curvatures, $k_m = \frac{1}{2}(k_1 + k_2)$; in general axes, $k_m = \frac{1}{2}\mathrm{tr}\bar{\bar{\mathbf{K}}}$. Note that in the case of a strictly convex surface and an outward normal pointing towards positive x_l, the curvatures k_1, k_2, k_m and k_g are all strictly positive.

To illustrate the above definitions, the tensor of curvature is evaluated for a sphere of radius R through P_0, tangent to the $P_0 y_l z_l$ plane at P_0. The equation of this sphere is given by

$$(x_l + R)^2 + y_l{}^2 + z_l{}^2 = R^2 \tag{3.43}$$

Solving for x_l, considering the branch through the origin, then expanding to second order produces

$$x_l = -R + \sqrt{R^2 - y_l{}^2 - z_l{}^2} = -R + (R - \frac{y_l{}^2}{2R} - \frac{z_l{}^2}{2R}) + O((y_l, z_l)^3) \tag{3.44}$$

$$= -\frac{1}{2}\begin{pmatrix} y_l & z_l \end{pmatrix}\begin{pmatrix} 1/R & 0 \\ 0 & 1/R \end{pmatrix}\begin{pmatrix} y_l \\ z_l \end{pmatrix} + O((y_l, z_l)^3) \tag{3.45}$$

The curvature tensor and the radius of curvature tensor for the sphere are thus respectively given by

$$\bar{\bar{\mathbf{K}}} = \begin{pmatrix} 1/R & 0 \\ 0 & 1/R \end{pmatrix}, \quad \bar{\bar{\mathbf{R}}} = \begin{pmatrix} R & 0 \\ 0 & R \end{pmatrix} \tag{3.46}$$

The form of the tensor of radius of curvature, i.e. a unit tensor scaled by the constant R, expresses the fact that the curvature of the sphere is isotropic and that normal sections all have a radius of curvature equal to R. For the sphere, both principal

curvatures and the mean curvature are equal to $1/R$. Both principal radii of curvature are equal to R. The Gaussian curvature is equal to R^{-2}.

3.3. The Gaussian Mapping

In this section, the theory of the Gaussian mapping is reviewed, together with its application to curve and surface representations. The Gaussian Mapping is presented as a mapping between points on a 3-D surface and points on a unit sphere, and also as a mapping between points on a 2-D curve and points on a unit circle. The images of the mapping are usually referred to as Gaussian circles and Gaussian spheres, and also collectively as Gaussian images. It turns out that the Gaussian images can also represent the normal orientations of curves and surfaces. This construction is then exploited to define representations of curve and surface properties as functions on the Gaussian images, referred to as Property Circles and Property Spheres. Coordinates used in this thesis to parameterize the Gaussian circle and Gaussian sphere are also defined in this section.

Two new concepts are proposed in addition to the classical theory of the Gaussian mapping. First, local reference frames are defined on the Gaussian images and the problem of representing vector and tensor fields on the Gaussian sphere is formally addressed. Second, gradients in local Monge parameterizations of curves and surfaces are related to normal orientations and their specifications by angles on the Gaussian sphere. The advantage of the Gaussian sphere over the Monge gradients for representing normal orientations is two-fold. First, gradients are able to represent only half of the complete set of normal orientations. In contrast, the Gaussian sphere is capable of describing all surface normals [44]. Second, the representation of surface normals with the Gaussian sphere does not favor specific viewing directions as is the case for the Monge gradients.

The Gaussian mapping was initially developed in the context of 3-D surfaces, see for example [50]. We will therefore also start with the case of 3-D surfaces, then show that the equivalent formalism for 2-D curves is trivially obtained.

3.3.1. Definitions

The 3-D Gaussian mapping is a relation between points on a surface and points on a unit sphere, referred to as the Gaussian sphere. To each point P_Σ of the surface corresponds a point P_G on the sphere so that the normals at P_Σ and P_G are parallel and have the same direction; see Fig.3.10.

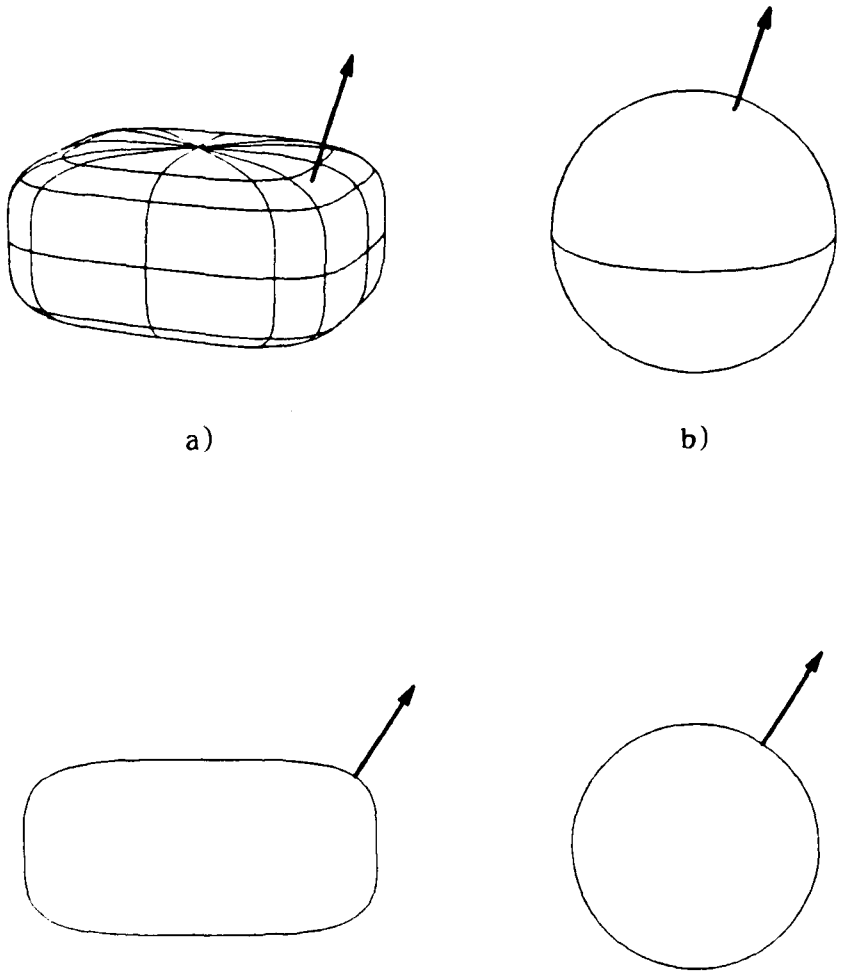

Fig.3.10. Examples of 3-D and 2-D objects, their Gaussian images, and the normal orientations at corresponding points.
a) 3-D object. b) Gaussian sphere of a).
c) 2-D object. d) Gaussian circle of c).

Points on the Gaussian sphere will be referenced by coordinates, namely by the longitude ξ from the x-axis and latitude η from the Oxy equator; see Fig.3.11. Points on the sphere are related to normal orientations in 3-D through the Gaussian mapping. Hence, the coordinates (ξ,η) can also be used to specify directions in 3-D.

The corresponding unit vector is given by

$$\vec{1}_n = \begin{vmatrix} \cos\xi\cos\eta \\ \sin\xi\cos\eta \\ \sin\eta \end{vmatrix} \tag{3.47}$$

The 2-D Gaussian mapping is a relation between points on a curve and points on a unit circle. Corresponding points on the curve and on the circle have parallel normal orientations; see Fig.3.10. Points on the Gaussian circle and the corresponding orientations in the plane are referenced in this text by the polar angle ψ measured counterclockwise from the x-axis; see Fig.3.11. The polar angle ψ can be used as a coordinate for directions in the plane, namely to refer to directions parallel to the unit vector

$$\bar{1}_n = \begin{vmatrix} \cos\psi \\ \sin\psi \end{vmatrix} \tag{3.48}$$

For strictly smooth convex 2-D curves and 3-D surfaces, the Gaussian mapping is one-to-one. Examples of the Gaussian mapping are presented in Appendix 1, when deriving the transforms of various geometrical shapes.

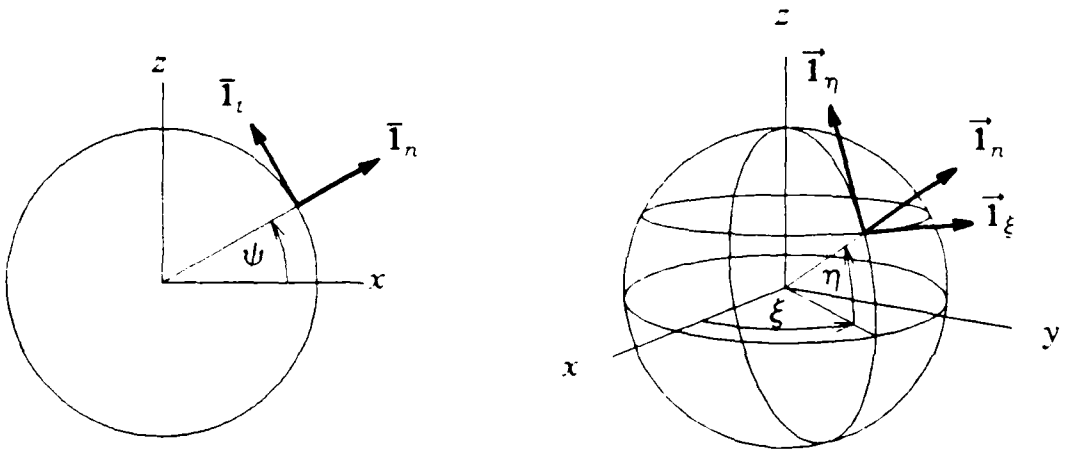

Fig.3.11. Coordinates and local orientations on Gaussian Images.

3.3.2. Property Circles, Property Spheres

In his work on object recognition, Horn defined the extended Gaussian image, a representation of surfaces by scalar functions on the Gaussian sphere [44]. The basic concept of the extended Gaussian image is to represent a function of surface points in terms of normal orientation, then as a function on the sphere, since each point on the sphere is uniquely related to a specific normal orientation; the name of "property spheres" was given to this type of representations in [51]. In this thesis, three new representations of 3-D objects in terms of property spheres will be defined. A major conceptual difference between previously proposed property spheres and two of the new representations stems from the vector and tensor ranges of the new object functions as opposed to a scalar range for the extended Gaussian image. In order to represent vectors and tensors, it is necessary to describe their values in terms of components in a system of axes. We propose to use axes aligned with local orientations on the Gaussian sphere, which are hence different for each point of the sphere and each corresponding object point. The axes chosen in this thesis are oriented in the directions of the unit normal $\vec{1}_n$, the unit tangent $\vec{1}_\xi$ to the parallel and the unit tangent $\vec{1}_\eta$ to the meridian; see Fig.3.11. The components of those unit vectors in global object axes Oxyz are given by

$$\vec{1}_n = \begin{vmatrix} \cos\xi\cos\eta \\ \sin\xi\cos\eta \\ \sin\eta \end{vmatrix} , \quad \vec{1}_\xi = \begin{vmatrix} -\sin\xi \\ \cos\xi \\ 0 \end{vmatrix} , \quad \vec{1}_\eta = \begin{vmatrix} -\cos\xi\sin\eta \\ -\sin\xi\sin\eta \\ \cos\eta \end{vmatrix} \tag{3.49}$$

Note that these vectors are functions of the angles ξ and η. At a later stage, it will be helpful to consider the derivatives

$$\begin{aligned} \frac{\partial\vec{1}_n}{\partial\xi} &= \cos\eta\vec{1}_\xi & \frac{\partial\vec{1}_n}{\partial\eta} &= \vec{1}_\eta \\ \frac{\partial\vec{1}_\xi}{\partial\xi} &= -\cos\eta\vec{1}_n + \sin\eta\vec{1}_\eta & \frac{\partial\vec{1}_\xi}{\partial\eta} &= 0 \\ \frac{\partial\vec{1}_\eta}{\partial\xi} &= -\sin\eta\vec{1}_\xi & \frac{\partial\vec{1}_\eta}{\partial\eta} &= -\vec{1}_n \end{aligned} \tag{3.50}$$

The above system of reference frames is singular at the poles of the sphere. Unfortunately, the topology of the sphere does not permit the definition of a continuous field of axes at each point, without singularities. For our choice of frames, the

singularities correspond to multiply defined frames at the poles. These singularities create some problems, but these can be overcome by requiring special equivalences between the multiple definitions. For $\eta = \pm\pi/2$, all the values of ξ refer to the same point, namely the pole. Compatibility between the potentially different values of a property sphere function for all ξ must hence be ensured. In the case of a scalar function $f(\xi,\eta)$, the consistency conditionbetween the multiple definitions is simply

$$f(\xi,\pm\pi/2) = f(0,\pm\pi/2) \quad \text{for all } \xi \tag{3.51}$$

In the case of vector and tensor fields, the consistency is more complex since the components are referred to different axes for each value of ξ at the poles. The necessary consistencies for a vector function $\bar{v}$ and a tensor function $\bar{\bar{T}}$ are given by

$$\bar{v}(\xi,\pi/2) = \begin{vmatrix} \cos\xi & \sin\xi \\ -\sin\xi & \cos\xi \end{vmatrix} \bar{v}(0,\pi/2) \tag{3.52}$$

$$\bar{\bar{T}}(\xi,\pi/2) = \begin{vmatrix} \cos\xi & \sin\xi \\ -\sin\xi & \cos\xi \end{vmatrix} \bar{\bar{T}}(0,\pi/2) \begin{vmatrix} \cos\xi & -\sin\xi \\ \sin\xi & \cos\xi \end{vmatrix} \tag{3.53}$$

for the north pole. Consistency relations at the south pole are similar, except that the transformation matrices must be transposed.

Representations equivalent to the property spheres are now considered for planar curves. Properties of planar curves expressed in terms of normal orientation can be represented as functions on the Gaussian circle of the curve, these functions being referred to as property circles. Three representations of curves in terms of property circles will be defined in this thesis; they are exactly equivalent to the three new property spheres proposed for surfaces. A key contribution of this thesis will be a set of relations between the 2-D and 3-D representations when these are applied to an object-silhouette pair. As in the case of property spheres, non-scalar property circles rely on the definition of rotated axes for each point on the Gaussian circle. The axes chosen here are oriented along the unit normal $\bar{1}_n$ and the unit tangent $\bar{1}_t$; see Fig.3.11. The components of these vectors in the global axes Oxz of the image plane are given by

$$\bar{\mathbf{I}}_n = \begin{vmatrix} \cos\psi \\ \sin\psi \end{vmatrix} , \quad \bar{\mathbf{I}}_t = \begin{vmatrix} -\sin\psi \\ \cos\psi \end{vmatrix} , \tag{3.54}$$

Derivatives of these vectors with respect to the orientation parameter ψ are given by

$$\frac{\partial \bar{\mathbf{I}}_n}{\partial \psi} = \bar{\mathbf{I}}_t , \quad \frac{\partial \bar{\mathbf{I}}_t}{\partial \psi} = -\bar{\mathbf{I}}_n \tag{3.55}$$

3.3.3. Relations between Monge Gradients and Coordinates of the Gaussian Image

In this section, a relation is obtained between two different specifications of surface normals. Specifically, normal orientations can be defined in terms of gradients in Monge parameterizations, but also by points on the sphere and by angular coordinates for these points in the Gaussian sphere representation. Relations between these two representations are described here, first in the case of 3-D surfaces, where both Monge parameterizations and Gaussian spheres are especially meaningful. A similar formalism is then briefly developed for the case of 2-D curves.

Consider a small surface element $\Delta\Sigma$ in the neighborhood of the point P_0, and a Monge representation of $\Delta\Sigma$ in the local axes $P_0 x_l\, y_l\, z_l$ where x_l is normal to $\Delta\Sigma$. Let the normal orientation $\vec{\mathbf{n}}_0$ at P_0 be defined by the angles ξ_0, η_0 on the Gaussian sphere. The normal $\vec{\mathbf{n}}$ at a points on $\Delta\Sigma$ can be defined by its coordinates ξ, η on the Gaussian sphere, but also by its local gradients m_{yl}, m_{zl} in the local $P_0 x_l\, y_l\, z_l$ axes. Relations will be obtained between the gradients and the differences $\xi - \xi_0$, $\eta - \eta_0$ in angles on the Gaussian sphere, for small values of the gradients; see Fig.3.12. The result is obtained by considering the general form of a normal vector in global axes, transforming this expression to local axes and comparing with the expression in terms of the Monge gradients.

A normal vector is defined in local axes by an expression similar to (3.31).

$$\vec{\mathbf{n}}_l = \begin{vmatrix} 1 \\ -m_{yl} \\ -m_{zl} \end{vmatrix} \tag{3.56}$$

On the other hand, the same normal vector is expressed as a function of angular coordinates on the Gaussian sphere as

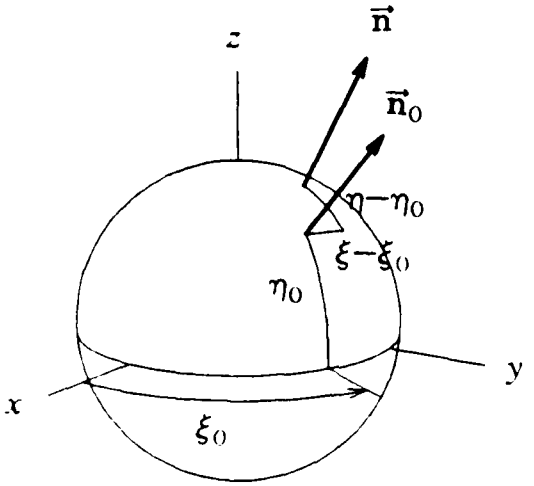

Fig.3.12. Angular Coordinates for Normals on the Gaussian Sphere.

$$\vec{n} = \begin{vmatrix} n\cos\xi\cos\eta \\ n\sin\xi\cos\eta \\ n\sin\eta \end{vmatrix} \tag{3.57}$$

where n is the length of the normal vector. This last expression for normal orientation is now expressed in local axes as

$$\vec{n}_l = \mathbf{R}_3^{G-R}\,\vec{n} = \begin{vmatrix} \cos\xi_0\cos\eta_0 & \sin\xi_0\cos\eta_0 & \sin\eta_0 \\ -\sin\xi_0 & \cos\xi_0 & 0 \\ -\cos\xi_0\sin\eta_0 & -\sin\xi_0\sin\eta_0 & \cos\eta_0 \end{vmatrix} \begin{vmatrix} n\cos\xi\cos\eta \\ n\sin\xi\cos\eta \\ n\sin\eta \end{vmatrix} \tag{3.58}$$

$$= n \begin{vmatrix} \cos\eta\cos\eta_0\cos(\xi-\xi_0) + \sin\eta\sin\eta_0 \\ \cos\eta\sin(\xi-\xi_0) \\ -\cos\eta\sin\eta_0\cos(\xi-\xi_0) + \sin\eta\cos\eta_0 \end{vmatrix}$$

For small values of $(\xi-\xi_0)$ and $(\eta-\eta_0)$, the above form of the normal in local axes is given to first order by

$$\vec{n}_l \approx \begin{vmatrix} 1 \\ \cos\eta\sin(\xi-\xi_0) \\ \sin(\eta-\eta_0) \end{vmatrix} \tag{3.59}$$

Comparing components in the above expression with the corresponding components in

(3.56) produces the following first order relations between Monge gradients and global normal angles

$$\left| \begin{array}{l} m_{yl} \approx -(\xi - \xi_0)\cos\eta_0 \\ m_{zl} \approx -(\eta - \eta_0) \end{array} \right. \tag{3.60}$$

These expressions underline the close relation existing between local gradients and global angular orientation coordinates. Note the $\cos\eta_0$ coefficient which takes into account the shortening of longitude units at higher latitudes.

An argument similar to the one developed above can be developed for the Monge parameterization of curves in 2-D. The relation between the local gradient m_{zl} and the polar angle ψ is obtained as

$$m_{zl} \approx -(\psi - \psi_0) \tag{3.61}$$

3.4. Summary

A number of tools from geometry have been reviewed or presented in this chapter. The combination of these will allow us to develop an elegant theory for the relations between object shapes and silhouette shapes. Chapter 4 reviews the classical analysis of silhouette shapes and motivates some of the directions chosen in our analysis of silhouettes. The main results of this thesis are then presented in Chapters 5 and 6.

Chapter 4
Classical Silhouette Theory

In this chapter, a number of silhouette construction methods are discussed and illustrated by the simple example of the silhouette of a cone. This chapter aims at the double goal of familiarizing the reader with classical silhouette analysis methods, and of discussing some basic concepts which introduce our original formulation of the relation between objects and silhouettes.

First, the well-known silhouette construction based on the silhouette generator is presented; this is the approach primarily used in the literature, and is very similar to the methods presented in [2, 13]. In the second step, silhouette construction is investigated with tangential space representations. Finally, silhouette construction is developed with the Gaussian mapping. These last two approaches are not intrinsically new, but their application to silhouette analysis has not received much attention in the computer graphics and computer vision communities. Through the discussion of these silhouette construction methods, it becomes apparent that normal orientations on the object surface play a prominent role in silhouette construction, and that the representation of surface normals with the Gaussian mapping is particularly convenient for silhouette analysis. This conclusion motivates the development of representations based on the Gaussian mapping and the development of relations between the representations of an object and the representations of its silhouettes.

4.1. Silhouette Construction Based on the Silhouette Generator

In this section, we discuss a classical method for obtaining the shape of a silhouette given the shape of the corresponding object and the viewing direction relative to the object. It is straightforward to see that the silhouette is the projection of a set of points on the surface of the object. This set is a smooth curve for a smooth convex object, and is referred to as the silhouette generator in this thesis; other authors use different terms such as contour generator or boundary rim. The geometry of the projection and the silhouette generator are illustrated in Fig.4.1 for the example of a superquadric. For this example, the silhouette generator is a complex twisted curve. Marr has shown that the silhouette generator is planar for all viewing directions only

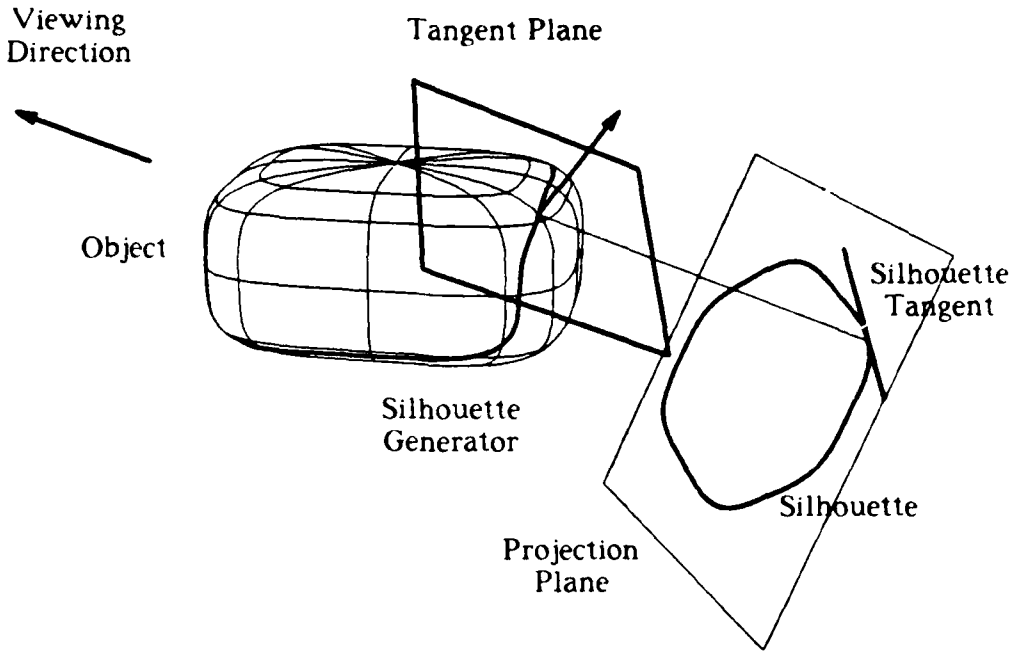

Fig.4.1. Imaging Geometry for Orthographic Projection

when the object surface is quadratic [2]. The silhouette generator is the set of points of the object surface where the projection rays are grazing the surface; for a smooth object, this corresponds to the set of points where the tangent plane is parallel to the viewing direction. An equivalent property of the points on the silhouette generator is that the normal orientation is perpendicular to the viewing direction. The tangent plane and the normal at one point of the silhouette generator are displayed in Fig.4.1.

The silhouette of a smooth convex object in orthographic projection can be determined in two steps. The first step consists of selecting which points of the object surface have a tangent plane parallel to the viewing direction, thereby defining the silhouette generator. The second step consists of projecting the points of the silhouette generator onto the image plane, thereby producing the silhouette itself. This procedure is outlined in the diagram of Fig.4.2.

In order to gain better insight into the relation among object, silhouette and silhouette generator, it may be useful to consider an analogy with shadows. If the projection is replaced by a beam of light parallel to the viewing direction, the object,

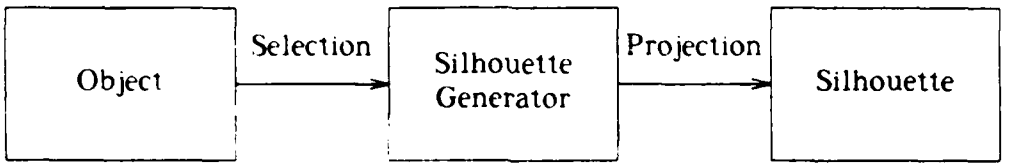

Fig.4.2. Silhouette Construction with Point Representations.

presumed opaque, will cast a shadow on the projection screen. The outline of that shadow is identical to the silhouette in the previous setup. In the shadow setup, only part of the object surface is illuminated by the light beam, as the other part is self-shadowed. The boundary between the illuminated and self-shadowed parts of the object is identical to the silhouette generator. Light rays emanating from the light source graze the object at the points of the self-shadow boundary. Similarly, in the case of silhouettes, rays parallel to the viewing direction graze the object at each point of the silhouette generator.

4.1.1. Example: Silhouette of a Cone

The silhouette construction method described above is now illustrated with the simple example of a circular cone; the geometry of the projection is sketched in Fig.4.3. The geometry of the cone itself and of its silhouette are depicted in Fig.4.4. The strategy for determining the shape of the silhouette consists of first computing the normal orientation at each point of the surface. Then, the surface points with a normal perpendicular to the viewing direction $\vec{1}_v$ are determined; these constitute the silhouette generator. Finally, the silhouette generator points are projected onto the image plane, producing the desired silhouette. In all the developments, the sets of points are defined by parametric equations. Therefore, the final result is a set of parametric equations for the silhouette from which the silhouette shape can be interpreted.

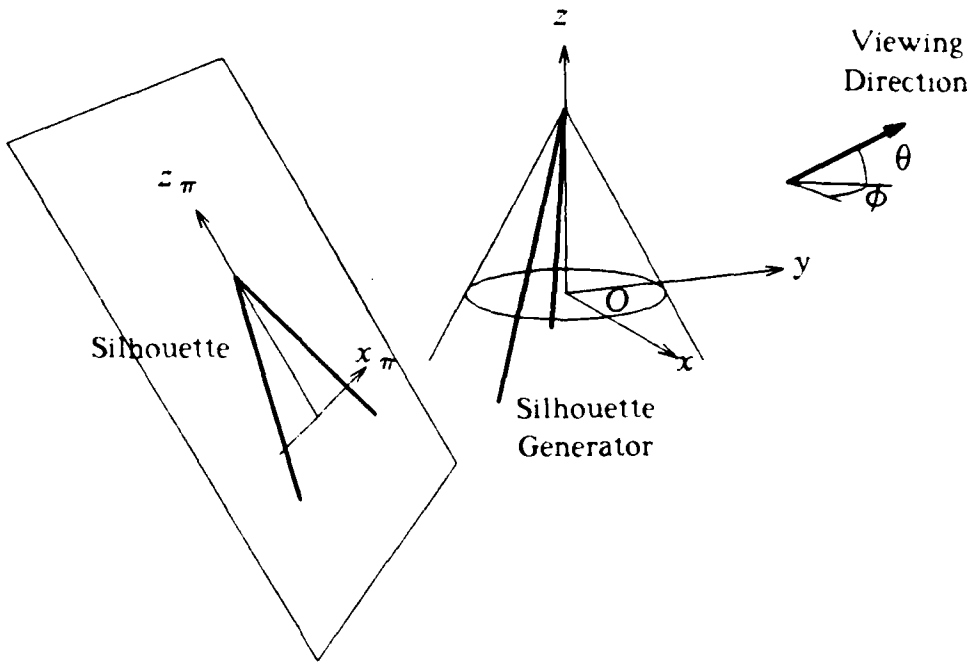

Fig.4.3. Geometry for the Projection of the Cone.

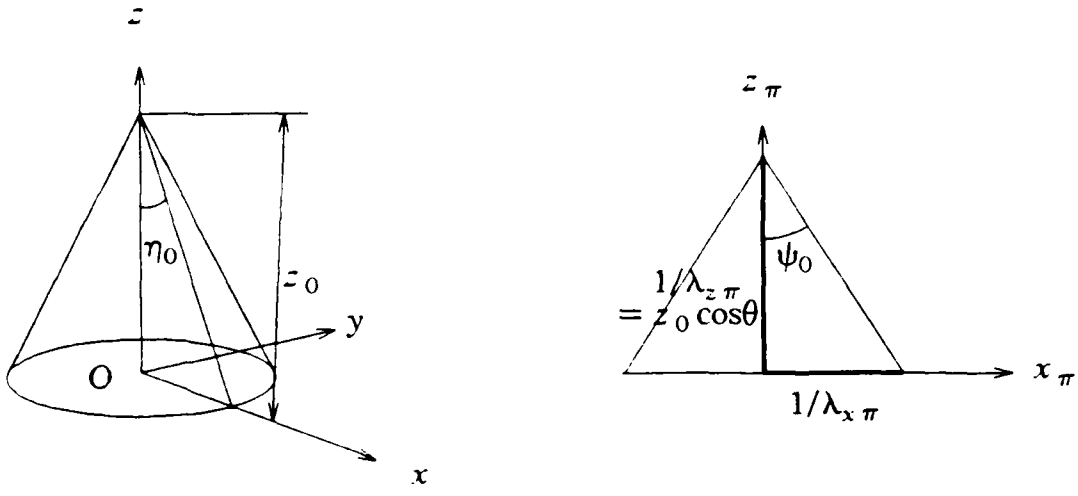

Fig.4.4. a) Circular Cone. b) Silhouette.

In a system of axes centered at a distance z_0 below the vertex of the cone, with the z-axis along the axis of symmetry, the points of the cone can be described by

$$\vec{\mathbf{x}} = \vec{\mathbf{x}}(u, v) = \begin{pmatrix} u \sin\eta_0 \cos v \\ u \sin\eta_0 \sin v \\ z_0 - u \cos\eta_0 \end{pmatrix} \tag{4.1}$$

where $u \in \mathbf{R}^+$, $v \in (0, 2\pi]$ are parameters and η_0 is a constant, equal to the half-angle of opening of the cone. The choice of positive values for u corresponds to the choice of the lower sheet of the cone illustrated in Fig.4.4a).

A vector normal to the surface is obtained by a formula decsribed in section 3.2., by

$$\vec{\mathbf{n}} = \vec{\mathbf{x}}_u \times \vec{\mathbf{x}}_v \tag{4.2}$$

which is proportional to

$$\vec{\mathbf{n}} = \begin{pmatrix} \cos v \cos\eta_0 \\ \sin v \cos\eta_0 \\ \sin\eta_0 \end{pmatrix} \tag{4.3}$$

Comparing this vector with the canonic form of a unit normal vector $\vec{\mathbf{l}}_n$ in terms of the angles (ξ, η) on the Gaussian Sphere,

$$\vec{\mathbf{l}}_n = \begin{pmatrix} \cos\xi \cos\eta \\ \sin\xi \cos\eta \\ \sin\eta \end{pmatrix}$$

it appears that the canonic orientation angles of the normal are related to the parameters of the surface by $\xi = v$, $\eta = \eta_0$ Consider now the orthographic projection with a viewing direction specified by the angles (ϕ, θ) in object-centered axes. The viewing direction unit vector is given by

$$\vec{\mathbf{l}}_v = (\cos\theta\cos\phi \;\; \cos\theta\sin\phi \;\; \sin\theta)^T \tag{4.4}$$

Points of the silhouette generator are the points for which $\vec{1}_n \cdot \vec{1}_v = 0$, i.e.

$$\cos\theta\cos\phi\cos\eta_0\cos\nu + \cos\theta\sin\phi\cos\eta_0\sin\nu + \sin\theta\sin\eta_0 = 0$$

also writtten

$$\cos(\phi - \nu) = -\tan\eta_0\tan\theta \tag{4.5}$$

This equation has two solutions for ν, which will be denoted by

$$\begin{cases} \nu_{SG\,1} = \phi + \operatorname{acos}(-\tan\eta_0\tan\theta) \\ \nu_{SG\,2} = \phi - \operatorname{acos}(-\tan\eta_0\tan\theta) \end{cases} \tag{4.6}$$

The silhouette generator is hence defined by

$$\begin{cases} x = u\sin\eta_0\cos\nu_{SGi} \\ y = u\sin\eta_0\cos\nu_{SGi} \\ z = z_0 - u\cos\eta_0 \end{cases} \tag{4.7}$$

for $u \in \mathbf{R}^+$, $i = 1,2$. These are the equations of two straight lines parameterized in u. The projected silhouette is obtained by applying the projection operation to the coordinates of points of the silhouette generator. The projection transformation for point coordinates was determined to be

$$\begin{pmatrix} x_\pi \\ z_\pi \end{pmatrix} = \begin{pmatrix} -\sin\phi & \cos\phi & 0 \\ -\sin\theta\cos\phi & -\sin\theta\sin\phi & \cos\theta \end{pmatrix} \begin{pmatrix} x \\ y \\ z \end{pmatrix} \tag{4.8}$$

The result of applying this transformation to the parametric equations of the silhouette generator in (4.7) is

$$\begin{cases} x_\pi = u\sin\eta_0\sin(\nu_{SGi} - \phi) \\ z_\pi = -u\sin\eta_0\sin\theta\cos(\nu_{SGi} - \phi) - u\cos\eta_0\cos\theta + z_0\cos\theta \end{cases} \tag{4.9}$$

for i = 1,2. The following equations are obtained after replacing ν_{GSi} by its value in (4.6).

$$\begin{cases} x_\pi = \pm u\sin\eta_0\sqrt{1 - \tan^2\eta_0\tan^2\theta} \\ z_\pi = z_0\cos\theta - u\dfrac{\cos^2\eta_0\cos^2\theta - \sin^2\eta_0\sin^2\theta}{\cos\eta_0\cos\theta} \end{cases} \tag{4.10}$$

These equations for the silhouette define two lines parameterized in u. These lines intersect at the point $(x_\pi, z_\pi) = (0, z_0\cos\theta)$ in the projection plane and are symmetric about the Oz_π axis. The half-angle opening ψ_0 of the two silhouette lines is defined in Fig.4.4b), and can be evaluated as

$$\tan\psi_0 = \frac{x_\pi}{z_0\cos\theta - z_\pi} = \sin\eta_0\cos\eta_0\cos\theta\frac{\sqrt{1-\tan^2\eta_0\tan^2\theta}}{\cos^2\eta_0\cos^2\theta - \sin^2\eta_0\sin^2\theta}$$

$$= \frac{\sin\eta_0}{\sqrt{\cos^2\theta - \sin^2\eta_0}} \tag{4.11}$$

A simpler expression can be obtained for the sine of ψ_0, namely

$$\sin\psi_0 = \frac{\tan\psi_0}{\sqrt{1+\tan^2\psi_0}} = \frac{\sin\eta_0}{\cos\theta} \tag{4.12}$$

The above relation between the opening angle of the cone η_0 and the opening angle ψ_0 of the silhouette is a relation between 3-D object orientation and silhouette slope. It will become clear later on that this type of relation, obtained here in the context of a particular example, is independent of object shape. Furthermore, similar relations will be obtained with much less effort in Chapter 6 using arguments on the Gaussian sphere.

It is worthwhile to note that the simple example of the cone has interesting applications. Indeed, different circular cones can be obtained by choosing different values for the ordinate z_0 and for the opening η_0. A large class of axisymmetric objects can be defined as stacks of sections of such cones, so that a silhouette theory for axisymmetric objects can be developed based solely on this simple analysis for the cone.

4.2. Silhouette Construction in Tangential Space

In this section, silhouette construction is discussed with a method based on tangential representations; these representations were reviewed in section 3.1.2. A tangential representation describes a 3-D object by the set of all its tangent planes. It is easy to see that only the planes tahgent at the points of the silhouette generator effectively contribute to the shape of the silhouette. Since the surface normal is perpendicular to the viewing direction for points on the silhouette generator, the planes tangent to the object on silhouette genrator are all parallel to the viewing direction. This set of planes will be referred to as the silhouette generating planes. The silhouette generating planes are also perpendicular to the image plane, so that their projections are equivalent to their traces in the image plane. These projections are a set of lines tangent to the silhouette, so that this procedure provides a tangential representation of the silhouette. One silhouette generating plane and its projection are illustrated in Fig.4.1. The construction procedure in tangential space is outlined in the block diagram of Fig.4.5.

Silhouette construction in tangential space can be more convenient than in point space. Indeed, the crucial operation of selecting the silhouette generating planes can be much simpler than the corresponding selection of the silhouette generator points. As a consequence, even when the object is initially described in point space, it may be advantageous to evaluate a tangential description of the object from the given point representation first, perform the silhouette construction in tangential space and finally convert the silhouette representation back to a point space representation. The block diagram of Fig.4.6 outlines this scheme.

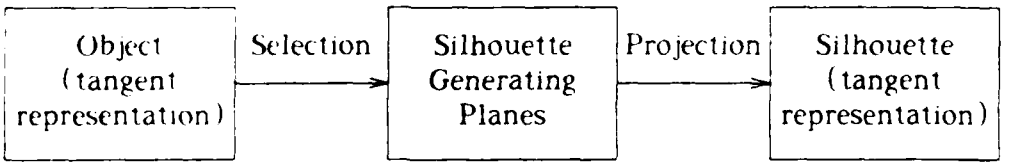

Fig.4.5. Silhouette Construction with Tangential Representations.

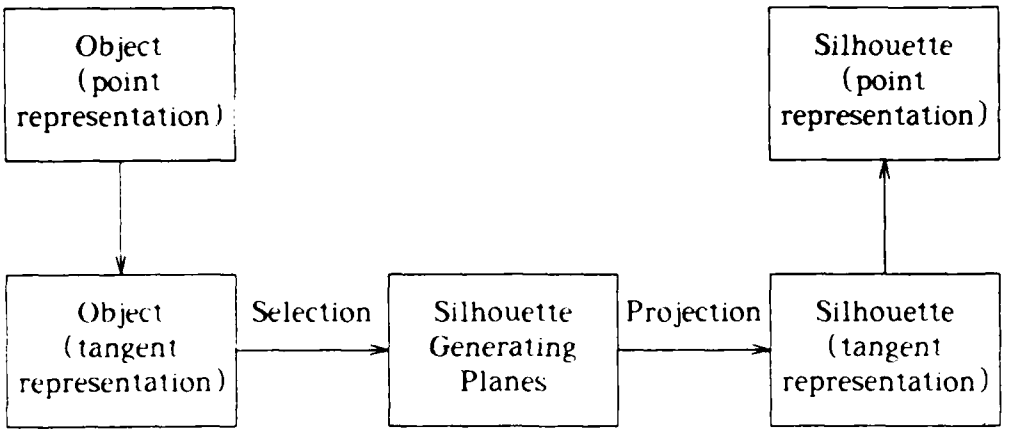

Fig.4.6. Silhouette Construction with Conversion to Tangential Representation.

4.2.1. Example: Silhouette of a Cone

Silhouette construction in tangential space is now illustrated with the same example developed previously in point space. In order to determine the silhouette of the cone, the first step is to determine parametric equations for the tangential coordinates of the cone. The silhouette generating planes are then determined as the tangent planes parallel to the viewing direction. The coordinates of the traces of these planes in the image plane are determined by applying the imaging transformation. This derivation produces parametric equations for the tangential coordinates of the silhouette in the image plane. Finally, the shape of the silhouette is interpreted from these equations.

Equations for the planes tangent to the cone may be obtained by noting that in general, for a point $\vec{x}_0$ with surface normal $\vec{n}_0$, the tangent plane is the set of points with coordinate vector $\vec{x}$ satisfying

$$\vec{n}_0 \cdot (\vec{x} - \vec{x}_0) = 0 \tag{4.13}$$

The plane tangent to the cone at the point with parameter values (u_0, v_0) is obtained by applying the above formula to (4.1) and (4.3), which produces

$$x\ \cos\eta_0\cos v_0 + y\ \cos\eta_0\sin v_0 + z\ \sin\eta_0 - z_0\sin\eta_0 = 0 \qquad (4.14)$$

This equation is compared with the canonic equation of a plane, $x\ \lambda_x + y\ \lambda_y + z\ \lambda_z = 1$, to determine the tangential coordinates $(\lambda_x, \lambda_y, \lambda_z)$ of the tangent planes

$$\left|\begin{array}{l} \lambda_x = \cot\eta_0\cos v\ /\ z_0 \\ \lambda_y = \cot\eta_0\sin v\ /\ z_0 \\ \lambda_z = 1\ /\ z_0 \end{array}\right. \qquad (4.15)$$

Note that these coordinates are undefined for $z_0 = 0$ since in that case, all tangent planes pass through the origin. The case of $z_0 = 0$ can be addressed rigorously using homogeneous tangential coordinates, although this is not done here. The equations obtained above are a set of parametric equations for the tangential coordinates of the circular cone. Note that the parameter u does not appear in the parametric equations. The tangent planes are only a one-parameter family in the case of the cone, as opposed to a two-parameter family in general. This degeneracy stems from the fact that the cone is a special ruled surface, for which each tangent plane is tangent to the surface along a whole line of points.

The silhouette generating planes are now determined by selecting the planes parallel to the viewing direction. The vector $\vec{\lambda}$ determining a plane in tangential space can be considered as a point-space vector normal to the plane defined. The silhouette generating planes have a normal vector perpendicular to the viewing direction and are therefore determined by

$$\vec{\lambda}^T \vec{1}_v = 0 \qquad (4.16)$$

$$\cot\eta_0\cos v\cos\theta\cos\phi + \cot\eta_0\sin v\cos\theta\sin\phi + \sin\theta = 0 \qquad (4.17)$$

$$\cos(v - \phi) = -\tan\theta\tan\eta_0 \qquad (4.18)$$

which produces exactly the same two solutions for v as obtained in section 4.1.1. These solutions are referred to as $v_{SG\,1}$, $v_{SG\,2}$. The silhouette generating planes are characterized by the parametric equations

$$\begin{cases} \lambda_x = \cot\eta_0 \cos v_{SGi} \,/\, z_0 \\ \lambda_y = \cot\eta_0 \sin v_{SGi} \,/\, z_0 \\ \lambda_z = 1 \,/\, z_0 \end{cases} \tag{4.19}$$

for i=1,2, and with v_{SGi} given by equation (4.6). The projection transformation defined in section 3.1.4. is now applied to the tangential coordinates of the planes in (4.19) to obtain the coordinates $\lambda_{x\pi}$, $\lambda_{z\pi}$ of the tangents to the silhouette. The projection transformation for tangents was determined to be

$$\begin{pmatrix} \lambda_{x\pi} \\ \lambda_{z\pi} \end{pmatrix} = \begin{pmatrix} -\sin\phi & \cos\phi & 0 \\ -\sin\theta\cos\phi & -\sin\theta\sin\phi & \cos\theta \end{pmatrix} \begin{pmatrix} \lambda_x \\ \lambda_y \\ \lambda_z \end{pmatrix} \tag{4.20}$$

The result of applying this transformation to the parametric equations fpr the silhouette generating planes in (4.19) is given by

$$\begin{cases} \lambda_{x\pi} = \cot\eta_0 \cos v_{SG} \sin\phi - \cot\eta_0 \sin v_{SG} \cos\phi = \cot\eta_0 \sin(v_{SG} - \phi) \\ \lambda_{z\pi} = -\sin\theta \cot\eta_0 \cos(\phi - v_{SG}) + \cos\theta = 1/\cos\theta \end{cases} . \tag{4.21}$$

The tangential coordinates of the silhouette take on just two values, determined by the above equations for $v_{SG} = v_{SG1}, v_{SG2}$. Therefore, the silhouette is composed of two straight lines. The silhouette is degenerate since, in the general case, a parametric equation for the silhouette tangents would be obtained instead of the fixed values in (4.21).

The two silhouette lines defined in (4.21) are symmetric about the Ox_π axis. The half-angle ψ_0 between the lines is obtained by noting that a line with coordinates $\lambda_{x\pi}$, $\lambda_{z\pi}$ crosses the axes at the points $(1/\lambda_{x\pi},0)$ and $(0,1/\lambda_{z\pi})$; see Fig.4.4b). Note that ψ_0 is also the polar angle of the normal orientation of one of the silhouette lines in the image plane.

It is given by

$$\tan\psi_0 = \frac{1/\lambda_{x\,\pi}}{1/\lambda_{z\,\pi}} = \frac{\tan\eta_0}{\cos\theta\sin(\nu_{SGi} - \phi)} = \frac{\tan\eta_0}{\cos\theta\sqrt{1 - \tan^2\eta_0\tan^2\theta}}$$

$$= \frac{\sin\eta_0}{\sqrt{\cos^2\theta - \sin^2\eta_0}} \tag{4.22}$$

which matches the result obtained previously.

In the above example, it appears that, given an object description in tangential coordinates, the determination of the silhouette equation can be much simpler than with point coordinates. When the object is initially defined by a point coordinate representation, the relative merits of the direct construction method depicted in Fig.4.2 and the indirect method depicted in Fig.4.6 depend on the effort required for converting the representation. For example, if many silhouettes must be computed numerically for the same object, the tangential description must be computed only once, thereby providing a larger potential advantage for the indirect method.

4.3. Silhouette Construction with the Gaussian Mapping

In this section, we will see that the Gaussian mapping suggests a very simple method for selecting the silhouette generator or the silhouette generating planes. Although silhouette construction with the Gaussian mapping can be related directly to silhouette construction in point space, it is instructive to introduce it through the discussion of silhouette construction with polar tangential coordinates, which is presented in the first subsection. Phrasing the construction method developed in the previous section for tangential space representations in terms of polar coordinates provides a relation between normal orientations on the object surface and normal orientations on the silhouette; this relation is independent of object shape. In a second subsection, this relation is re-interpreted by mapping normal orientations on the Gaussian sphere and discovering that the silhouette generator corresponds to a slice of the Gaussian sphere.

4.3.1. Silhouette Construction with Polar Tangential Coordinates

A particular case of silhouette construction in tangential space is considered in this section, where polar coordinates (p,ξ,η) are chosen to represent planes to the 3-D object, and polar coordinates (p,ψ) to describe lines tangent to the 2-D silhouette; these coordinates are defined in section 3.1.2. First, in order to avoid confusion between the perpendicular distance p in 3-D and 3-D, this distance will be represented by the symbol p_π for the silhouette in 2-D.

Consider a description of the surface of a 3-D object by parametric equations for the polar coordinates (p,ξ,η) as a function of two independent parameters, say u and v.

$$\begin{bmatrix} p \\ \xi \\ \eta \end{bmatrix} = \begin{bmatrix} p(u,v) \\ \xi(u,v) \\ \eta(u,v) \end{bmatrix} \tag{4.23}$$

For smooth strictly convex objects and for a regular parameterization in (u,v), the functions defining the angles (ξ,η) in terms of the parameters (u,v) are invertible. The parameters (u,v) in the above expressions can then be replaced by inverse functions in terms of (ξ,η). Examples of this parameter change are presented in Appendix 1. When this change of parameters is performed in equation (4.23), identities are

obtained for ξ and η, and an explicit equation is obtained for p,

$$p = p(\xi,\eta) \tag{4.24}$$

The above representation form is now discussed in some detail, as it will be the basis for new representations of 3-D surfaces. Equation (4.24) represents, for each point P_0 of the object with a normal orientation (ξ,η), the perpendicular distance p between the origin and the tangent plane at P_0. This explicit equation describes the shape of the object surface by expressing the dependence of one polar tangential coordinate on the other two, and can be compared in this respect with the Monge parameterization $z = x(y,z)$ which expresses one Cartesian coordinate as a function of the other two. In both cases, the explicit equations are invariant in transformations involving only the independent variables. The Monge parameterization is therefore invariant in 2-D translations of the Oyz plane, whereas the form in (4.24) is invariant with 3-D rotations around the origin. Hence, this last representation elegantly casts a surface representation in a form invariant with viewing direction. The function $p(\xi,\eta)$ is sometimes referred to as the support function, as it describes the distance from the origin to a potential support plane when the object is oriented with the direction (ξ,η) towards nadir.

Silhouette construction is now investigated for an object shape described by an equation such as (4.24), by first considering the selection of silhouette generating planes, then their projection onto the image plane.

For a plane with polar tangential coordinates (p,ξ,η), the normal orientation is

$$\vec{1}_n = (\cos\xi\cos\eta \ \sin\xi\cos\eta \ \sin\eta)^T \tag{4.25}$$

The silhouette generator equation is $\vec{1}_n^T \vec{1}_v = 0$, more explicitly

$$(\cos\xi\cos\eta \ \sin\xi\cos\eta \ \sin\eta)(\cos\phi\cos\theta \ \sin\phi\cos\theta \ \sin\theta)^T = 0 \tag{4.26}$$

$$\cos(\xi - \phi) = -\tan\eta\tan\theta \tag{4.27}$$

This equation defines a set of values for (ξ,η) which correspond to silhouette generating planes. The following expression for the one-parameter family of solutions will be derived in Chapter 6.

$$\left| \begin{array}{l} \xi_{SG}(t) = \phi + \pi/2 + \operatorname{atan}(\tan t \sin\theta) \\ \eta_{SG}(t) = \operatorname{asin}(\sin t \cos\theta) \end{array} \right. \tag{4.28}$$

where $t \in (0,2\pi]$ is a parameter. The subscript in ξ_{SG}, η_{SG} emphasizes that these expressions apply to the silhouette generating planes. The result in (4.28) can be justified by inserting the proposed solution in equation (4.27), then performing simple trigonometric manipulations to obtain an identity; this justification is omitted here.

Once the silhouette generating planes are determined, the next operation consists of obtaining the coordinates of their traces in the projection plane. The transformation of polar tangential coordinates in the projection can be obtained by exploiting the projection transformation for Cartesian tangential coordinates in (3.22) and by replacing the Cartesian coordinates in terms of the polar tangential coordinates, as given in (3.1) and (3.2). The resulting projection equation for polar tangential coordinates is

$$\begin{bmatrix} \cos\psi/p_\pi \\ \sin\psi/p_\pi \end{bmatrix} = \begin{bmatrix} -\sin\phi & \cos\phi & 0 \\ -\sin\theta\cos\phi & -\sin\theta\sin\phi & \cos\theta \end{bmatrix} \begin{bmatrix} \cos\xi\sin\eta/p \\ \sin\xi\cos\eta/p \\ \sin\eta/p \end{bmatrix} \tag{4.29}$$

The above relation applies only to planes perpendicular to the projection plane, i.e. to planes determined by (4.27) or (4.28). The following expressions for polar tangential coordinates of the silhouette can be obtained after trigonometric manipulations, by replacing ξ and η in the right-hand side of the above projection equation by their values in equation (4.28).

$$\left| \begin{array}{l} \psi = t \\ p_\pi = p \end{array} \right. \tag{4.30}$$

The first equation above provides an interpretation for the generic parameter t in (4.28). The second equation can be combined with (4.28) to obtain an explicit equation for the silhouette in polar tangential coordinates.

$$p_\pi(\psi) = p(\xi_{SG}(\psi), \eta_{SG}(\psi))$$

$$= p(\phi+\pi/2+\operatorname{atan}(\tan\psi \sin\theta), \operatorname{asin}(\sin\psi \cos\theta)) \tag{4.31}$$

The expressions obtained above for silhouette construction in polar tangential coordinates are remarkable in several respects. First, equation (4.28), determines the

silhouette generating planes based on the independent variables (ξ,η) only. This result is hence independent of object shape. Selection of the orientations of silhouette generating planes depends only on viewing orientation and can be precomputed for a set of viewing angles; the resulting selection procedure applies to any object. Second, correspondences between the silhouette orientation coordinate ψ and the object orientation coordinates ξ, η are also independent of object shape, and are given by equations (4.28) after replacing the parameter t by the angle ψ.

$$\left| \begin{array}{l} \xi_{SG} = \phi + \pi/2 + \text{atan}\,(\,\tan\psi\sin\theta\,) \\ \eta_{SG} = \text{asin}\,(\,\sin\psi\cos\theta\,) \end{array} \right. \tag{4.32}$$

Finally, the normal distance p_π for points of the silhouette is related to the normal distance p at the corresponding point of the object by the trivial relation $p_\pi = p$.

4.3.1.1. Example: Silhouette of a Cone

In order to apply the method developed in the previous section to the derivation of the silhouette of the cone, it is necessary first to determine parametric equations for the polar tangential coordinates of the cone, second to convert these into the form of equation (4.24), and third to determine an equation for the silhouette with (4.31).

Polar tangential coordinates for the cone are easily determined by comparing equations (4.15) and (3.2).

$$\left| \begin{array}{lll} \lambda_x = \cot\eta_0 \cos\nu \,/z_0 & = \cos\xi \cos\eta \,/p \\ \lambda_y = \cot\eta_0 \sin\nu \,/z_0 & = \sin\xi \cos\eta \,/p \\ \lambda_z = 1 \,/z_0 & = \sin\eta \,/p \end{array} \right. \tag{4.33}$$

It is clear from the above equations, that

$$\xi=\nu \;,\quad \eta=\eta_0 \;,\quad p=z_0\sin\eta_0 \tag{4.34}$$

This result shows again that the cone is a degenerate case since η=cst, p=cst and only ξ is variable, whereas in general, both ξ and η would be variable and p would be a non-trivial function of (ξ,η). The tangential coordinates of the silhouette are easily determined with (4.31) and (4.32).

$$r_\pi = r_0 \sin\eta_0 , \quad \sin\psi_0 = \frac{\sin\eta_0}{\cos\theta} \tag{4.35}$$

After conversion of these polar coordinates to Cartesian tangential coordinates using (3.1), the above results are found to be identical to those obtained previously in (4.21) and (4.22).

4.3.2. Silhouette Construction with the Gaussian Mapping

In the previous section, relations between normal orientations on the object surface, on the silhouette generator and on the silhouette were obtained by analyzing silhouette construction in polar tangential coordinates. These relations are interpreted in this section by considering normal orientations in the Gaussian sphere and Gaussian circle representations. The resulting interpretation is much more attractive visually than the one obtained in the previous section, although no new equations are derived. Indeed, it is much easier to visualize points on the sphere than orientations in 3-D space. Finally, the relation between silhouette analysis and the Gaussian mapping is extended by introducing property spheres and property circles.

The relation in (4.32) between normal orientations in 3-D and normal orientations in the projection plane has a double interpretation. First, considering ψ as a generic independent parameter, these equations characterize the set of normal orientations of points on the silhouette generator, for a given viewing direction (ϕ,θ). These normal orientations are defined by the polar angles (ξ,η). Second, it relates points on the silhouette parameterized with the normal angle ψ to the corresponding points of the silhouette generator.

It is interesting to interpret these relations in representations particularly suited for normal orientations, namely the Gaussian sphere for the object and the Gaussian circle for the silhouette. The silhouette generator on the object surface is the set of points for which the normal orientation is perpendicular to the viewing direction. As the Gaussian mapping preserves normal orientation, the image of these points on the Gaussian sphere is the set of points for which the normal orientation is perpendicular to the viewing direction or, in other words, the silhouette generator of the sphere for the same viewing direction. It is straightforward to see that this set of points is the great circle perpendicular to the viewing direction. In addition, surface normals at the

points of the silhouette generator are parallel to the projection plane and remain unchanged in the projection operation, so that normal orientations on the silhouette are identical to normal orientations at the corresponding points on the silhouette generator. The consequence is that the great circle of the Gaussian sphere is also a Gaussian circle for the silhouette. The relations discussed above are illustrated in Fig.4.7.

In the above discussion, equation (4.32) has been interpreted in terms of the Gaussian mapping. Although this interpretation indicates a relation between object points and silhouette points, it does not suggest a complete method for inferring the shape of the silhouette from the shape of the object. A complete relation is obtained, however, by combining equation (4.31) with the Gaussian mapping and considering object descriptions by property spheres and silhouette descriptions by property circles. Indeed, the support functions $p(\xi,\eta)$ and $p_\pi(\psi)$ represent perpendicular distances to tangent planes in terms of normal orientations. Mapping normal orientations on Gaussian images produces functions defining p and p_π on the Gaussian sphere and on the Gaussian circle. These can be considered as property spheres and property circles as

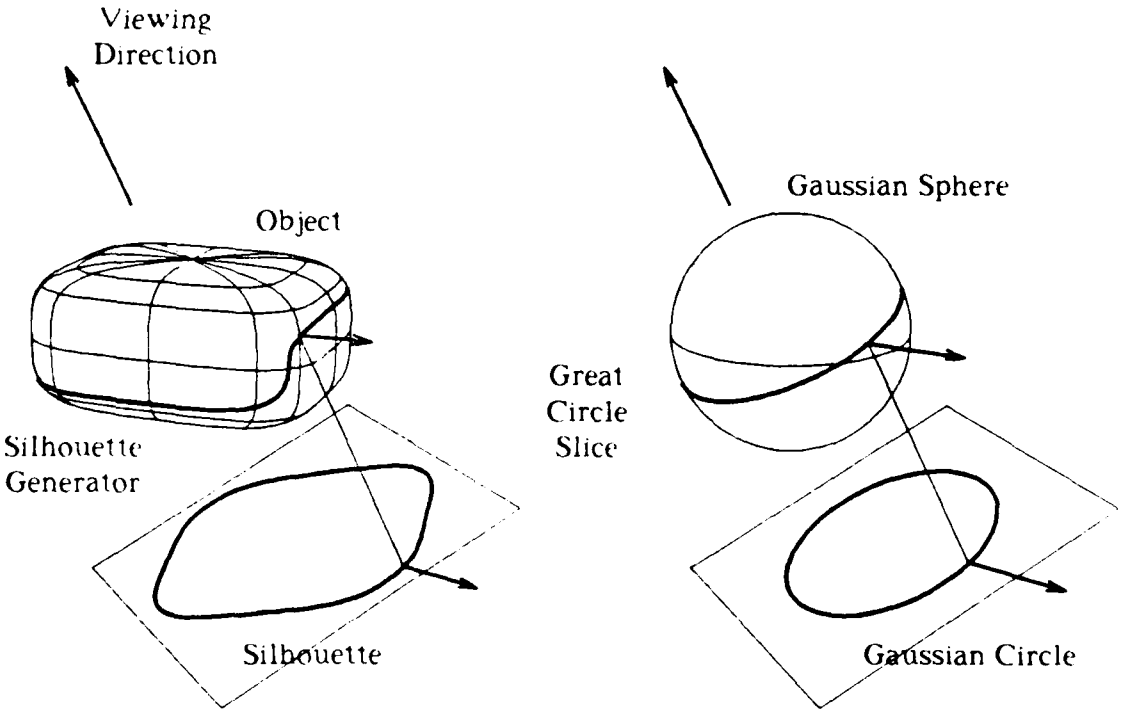

Fig.4.7. Silhouettes and the Gaussian Mapping

defined in section 3.3.2. For these representations, equation (4.31) suggests that the silhouette property circle function values p_π are identical to the property sphere function p on the slice corresponding to the silhouette. Hence, the silhouette property circle can be considered as a slice of the property sphere of the object.

In this section, we have interpreted silhouette analysis with polar tangential coordinates by representing the 3-D object by a property sphere for the distance between origin and tangent planes, and the 2-D silhouette by a property circle for the distance between origin and tangent lines. The silhouette property circle is identical to a slice of the property sphere of the object by a plane perpendicular to the viewing direction, through the center of the sphere.

4.3.2.1. Example: Silhouette of a Cone

Construction of the silhouette with the Gaussian Mapping is now illustrated by the example of the cone. First, the distance p to the tangent is the constant $z_0 \sin\eta_0$ for all points of the cone. As a consequence, the distance p_π to silhouette tangents is simply equal to the same constant everywhere on the silhouette.

The investigation of silhouette normal orientations leads to a more interesting discussion. As derived in previous sections, the normal orientations of points on the surface of the cone are determined by

$$\xi \in (0,2\pi], \quad \eta=\eta_0 \tag{4.36}$$

This set of orientations is represented by the parallel at latitude η_0 on the Gaussian sphere; see Fig.4.8. Considering a projection along the direction (ϕ,θ), the silhouette corresponds to the great circle slice perpendicular to the viewing direction, which is a Gaussian circle for the silhouette. In the case of the cone, this slice intersects the small circle $\eta=\eta_0$ at two points with polar angles ψ_0, $\pi-\psi_0$ in the slice plane. The silhouette is hence characterized by only two distinct normal orientations, so that it is composed of two lines with those normal orientations. The exact position of these lines is determined by the distance p_π to the origin, which was determined previously. The exact value of the orientation ψ_0 in the silhouette plane can be obtained in terms of η_0 and θ by resolving the right-angled spherical triangle in bold lines in Fig.4.8.

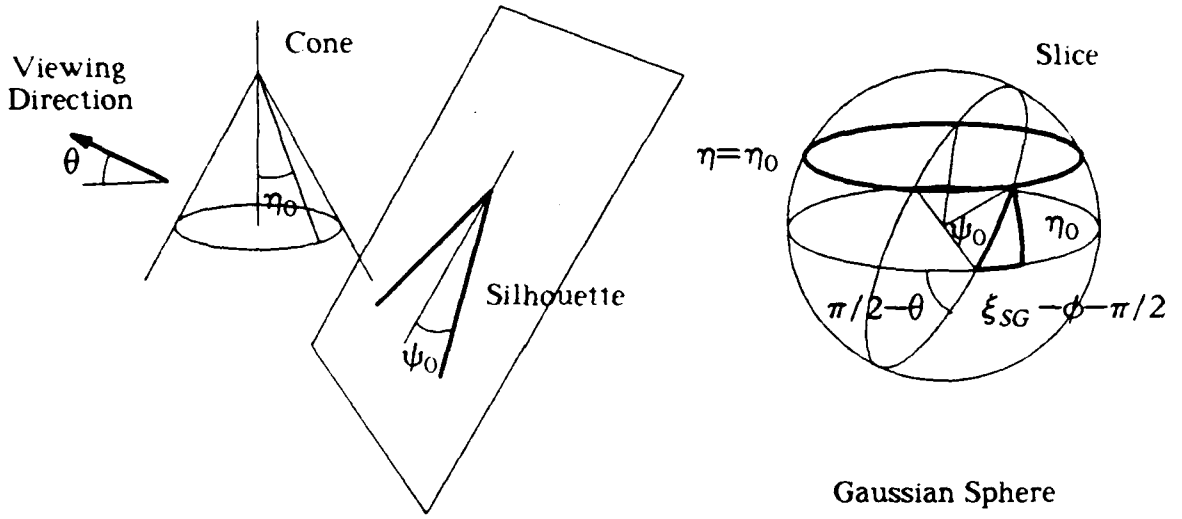

Fig.4.8. Silhouette of the Cone and Gaussian Sphere.

The relation obtained with standard expressions of spherical trigonometry is

$$\sin\eta_0 = \cos\theta \sin\psi_0 \tag{4.37}$$

which is consistent with the results obtained previously with other methods (e.g. equation (4.12)).

Although the Gaussian mapping does not provide new numerical expressions for the relation between silhouette shape and object shape, it is well adapted to conduct qualitative prediction of the results. Indeed, the following conclusions can be drawn by considering the Gaussian sphere of the cone and the silhouette slice in Fig.4.8. First, the intersection points between the parallel of the cone and the great circle slice are on the opposite side from the viewing direction. As a consequence, the silhouette generator on the object is on the same side of the object as the projection plane; this is clearly seen in Fig.4.4. Second, by an appropriate choice of the elevation θ of the viewing direction, it is possible to give the half angle ψ_0 of the silhouette any value between η_0 and $\pi/2$; this is valid for any value of the opening angle η_0 of the cone itself. Hence, if a pair of lines observed in the image plane are presumed to be the silhouette of a cone, nothing can be determined about the shape of the cone without estimating its orientation with respect to the projection plane by some other method.

Finally, for very large elevations θ of the viewing direction, namely for $\theta > \pi/2 - \eta_0$, the great circle does not intersect the parallel $\eta = \eta_0$, and there is no silhouette. It is not hard to see that this corresponds to a case where the viewer is "above" the cone so that its image fills the whole projection plane. Similarly, when $\theta < -\pi/2 + \eta_0$, there is no intersection on the Gaussian sphere, and this corresponds to the case where the viewer is "inside" the cone, so that, once again, no silhouette is obtained in the image plane.

We have shown in this section that interesting qualitative arguments on silhouettes can be developed based on the Gaussian mapping. This advantage of representations with the Gaussian mapping is extremely useful in developing a thorough understanding of the relation between silhouette shape and object shape.

4.4. Conclusion

In this chapter, we have developed a number of silhouette construction methods and their illustration on a simple example. Starting from the method used most frequently in the literature, we have gradually progressed to methods based on tangents, then to methods based on tangent orientations. In the last method, the Gaussian mapping was introduced to interpret first a relation between object points and silhouette points, and second a relation between object properties and silhouette properties. Both relations are independent of object shape, and the first is independent of the choice of object property. The second relation depends on which object property is represented on the Gaussian sphere, and is independent of object shape only for adequate choices of object properties and silhouette properties.

The keys contribution of this thesis are first the formal analysis of the property sphere for the distance to tangents introduced in section 4.3.2., and the demonstration of its relation with corresponding silhouette property circles, and second the development of two additional object properties for which the relation between sphere and circle are independent of object shape.

In Chapter 5, three representations of 3-D objects in terms of property spheres are proposed and analyzed, together with the corresponding representations of silhouettes with property circles. In Chapter 6, the relation between these silhouette property circles and object property spheres is formally developed.

Chapter 5
Representations for Curves and Surfaces Based on the Gaussian Mapping

In this chapter, three property circle representations of 2-D curves and the corresponding property spheres of 3-D surfaces are proposed. The advantages of this type of representation for silhouette analysis were suggested in Chapter 4 and will become more clear in Chapter 6, when simple relations are developed between each of the representations for an object surface and the corresponding representations for its silhouettes.

The three pairs of representations describe three different properties of the objects being described as functions on Gaussian circles and spheres. The first representation describes the normal distance between tangents and a reference point; this scalar property sphere/circle is named the Support Transform (ST). The second representation describes coordinates of object points in rotated axes and is named the Vector Support Transform (VST). The VST has three components for 3-D surfaces, two components for 2-D curves, and it turns out that in each case, one component is identical to the scalar ST. Finally, the third representation describes local curvatures and is named the Curvature Transform (CT). The three representations are collectively referred to by the name of transforms, in part to emphasize that these representations are complete and therefore uniquely invertible, and in part to preserve the similarity between our silhouette theory and the Projection-Slice theorem in computerized tomography.

The particular choice of object properties for these three representations is justified a-posteriori by the existence of simple relations between each transform of an object and the corresponding transforms of its silhouettes; these relations are demonstrated in Chapter 6. The existence of such simple relations was suggested for the ST in Chapter 4. In the case of the VST, it can be expected that simple relations exist between point coordinates in 2-D and 3-D. Finally, in the case of the CT, the dual of Euler's theorem indicates a relation between silhouette curvature and object surface curvature. The dual of Euler's theorem is demonstrated independently of the Gaussian mapping in Appendix 3, and it turns out to be also a corollary of the relations

between the 3-D CT of an object and the 2-D CT of its silhouettes.

The definitions of the transforms presented in this chapter are accompanied by the derivation of conversions to and from Cartesian representations. These relations are useful when evaluating or inverting the transforms for specific object shapes. In addition, the conversion relations are used in Chapter 6 to develop the relations between 3-D transforms of an object and 2-D transforms of its silhouettes.

In this chapter, all arguments are developed for curves and surfaces which are outlines of smooth strictly convex objects. It is possible to describe these curves and surfaces by equations parameterized with the normal orientation angles ψ in 2-D, (ξ,η) in 3-D. Only these parameterizations are considered here for Cartesian coordinates. Relations between these and other parameterizations are briefly discussed in Appendix 2. Extensions of the representations to include object surfaces with edges and their silhouette curves are discussed in Chapter 7.

The concepts of the three transforms are very similar in 2-D and 3-D, a similarity emphasized by the vector notation used in this chapter. As the algebra is more straightforward in the 2-D case, we have chosen to discuss the 2-D transforms in the first section of this chapter and the 3-D transforms in the second section. The algebra supporting the discussion of 3-D surface models is more involved than in the 2-D case, but the parallelism of concepts substantially improves readability. In order to preserve the similarity of notations, some aspects are presented with considerable detail in the case of 2-D curves.

5.1. Representations for Planar Curves

In this section, three property circle representations of 2-D curves are defined, and their transformations to and from Cartesian coordinates are developed. The representations, collectively referred to as transforms, define curve shapes by property functions on the Gaussian circle. The object properties are represented in a different set of rotated axes for each object point, so that the rotations of coordinates defined in equation (3.7) appear in both the direct and inverse transform expressions. Relations among the three transforms of the same curve are developed at the end of this section; these relations are exploited to develop consistency constraints for the ST and the VST.

5.1.1. Support Transform of a Planar Curve

Definition: *The Support Transform of a planar curve is the property circle defining the normal distance between the origin and the tangent at each object point. This distance is denoted by the symbol* p .

The ST is equivalent by definition to a representation of the distance p to the tangent as a function of the normal orientation angle ψ, and is hence a representation of tangents to the curve equivalent to the explicit equation $p(\psi)$ for the polar tangential coordinates. The function $p(\psi)$ is sometimes referred to as the support function, a name which has determined our choice for the name of the Support Transform.

Figure 5.1 illustrates the definition of p_0 for the point P_0 on the curve C. Let ψ_0 be the polar angle of the normal at P_0. The distance p_0 is measured along the normal at P_0, which is parallel to the Ox_R axis of the rotated frame $Ox_R z_R$ for $\psi=\psi_0$. The ST function is hence related to Cartesian coordinates by $p_0 = x_R(P_0)$. This relation is given, for a generic point of the curve, by

$$p(\psi) = x_R(\psi) = \begin{bmatrix} 1 & 0 \end{bmatrix} \begin{bmatrix} x_R(\psi) \\ z_R(\psi) \end{bmatrix} = \begin{bmatrix} 1 & 0 \end{bmatrix} \begin{bmatrix} \cos\psi & \sin\psi \\ -\sin\psi & \cos\psi \end{bmatrix} \begin{bmatrix} x(\psi) \\ z(\psi) \end{bmatrix}$$

$$= \begin{bmatrix} \cos\psi & \sin\psi \end{bmatrix} \begin{bmatrix} x(\psi) \\ z(\psi) \end{bmatrix}$$

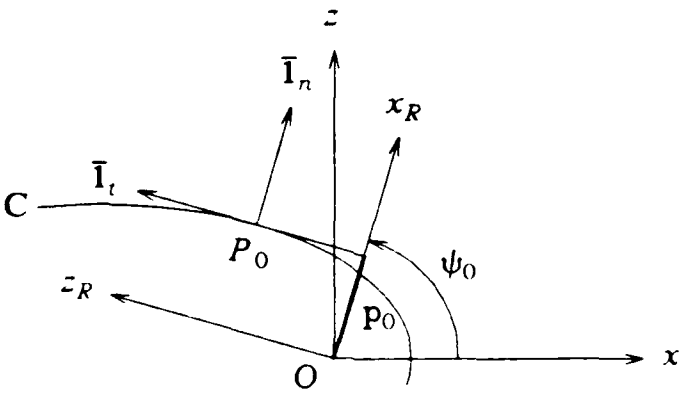

Fig.5.1. Tangent to the curve C at P_0 and normal distance p_0.

$$p(\psi) = \bar{\mathbf{e}}_1^T \mathbf{x}_R(\psi) = \bar{\mathbf{e}}_1^T \mathbf{R}_2^{G-R} \mathbf{x}(\psi) = \bar{\mathbf{l}}_n^T \mathbf{x}(\psi) \tag{5.1}$$

where $\bar{\mathbf{e}}_1$ denotes the canonical unit vector $(1\ 0)^T$. The transformation from ST to Cartesian coordinates is now derived by first considering the equation for the Cartesian coordinates of the points on a tangent line with polar tangential coordinates $p(\psi)$, ψ.

$$x\ \cos\psi + z\ \sin\psi = p(\psi) \tag{5.2}$$

The above equation describes a one-parameter set of tangents to the curve, where ψ is the parameter. The curve itself is the envelope of these lines and its equation can be evaluated by eliminating the parameter ψ between the equation for the tangent and the derivative of this equation with respect to ψ. These two equations are given by

$$\left| \begin{array}{rl} x\ \cos\psi + z\ \sin\psi = & p(\psi) \\ -x\ \sin\psi + z\ \cos\psi = & p_\psi(\psi) \end{array} \right. \tag{5.3}$$

$$\begin{bmatrix} \cos\psi & \sin\psi \\ -\sin\psi & \cos\psi \end{bmatrix} \begin{bmatrix} x \\ z \end{bmatrix} = \begin{bmatrix} p \\ p_\psi \end{bmatrix} \tag{5.4}$$

where $p_\psi = dp/d\psi$. Comparison of these equations with the transformation from global to rotated coordinates, namely

$$\begin{bmatrix} x_R \\ z_R \end{bmatrix} = \begin{bmatrix} \cos\psi & \sin\psi \\ -\sin\psi & \cos\psi \end{bmatrix} \begin{bmatrix} x \\ z \end{bmatrix}$$

$$\mathbf{x}_R = \mathbf{R}_2^{G-R} \mathbf{x} \tag{5.5}$$

reveals that the coordinates of points of the curve in the rotated frame are given by

$$\begin{bmatrix} x_R(\psi) \\ z_R(\psi) \end{bmatrix} = \begin{bmatrix} p(\psi) \\ p_\psi(\psi) \end{bmatrix} \tag{5.6}$$

and that global Cartesian coordinates are related to the ST by

$$\begin{bmatrix} x(\psi) \\ z(\psi) \end{bmatrix} = \begin{bmatrix} \cos\psi & -\sin\psi \\ \sin\psi & \cos\psi \end{bmatrix} \begin{bmatrix} p(\psi) \\ p_\psi(\psi) \end{bmatrix}$$

$$\mathbf{x}(\psi) = \mathbf{R}_2^{R-G}(\psi) \begin{vmatrix} p(\psi) \\ p_\psi(\psi) \end{vmatrix} \tag{5.7}$$

The following alternate vector notation emphasizes the contribution of the ST along each local unit vector on the Gaussian circle.

$$\mathbf{x}(\psi) = p(\psi)\, \bar{\mathbf{I}}_n + p_\psi(\psi)\, \bar{\mathbf{I}}_t \tag{5.8}$$

5.1.2. Vector Support Transform of a Planar Curve

Definition: *The Vector Support Transform of a planar curve is the property circle defining the Cartesian coordinates of each point in a rotated frame oriented along the normal and the tangent at that point. These coordinates are denoted by n and t for the coordinates along the normal and along the tangent respectively. The vector combining these coordinates is denoted by* $\mathbf{s} = [\, n \;\; t \,]^T$.

The above definition emphasizes that the VST describes object point coordinates. However, it is easy to see that the first component of the VST is identical by definition to the scalar ST. Therefore, the VST is a superset of the ST and it explicitly describes tangents to the curve in addition to points of the curve. The presence of two components in the VST and its relation to the ST justify the name of Vector Support Transform.

Figure 5.2 illustrates the definition of the VST for the point P_0 on a curve C described in global axes Oxz. If ψ_0 is the normal orientation angle at P_0, the VST

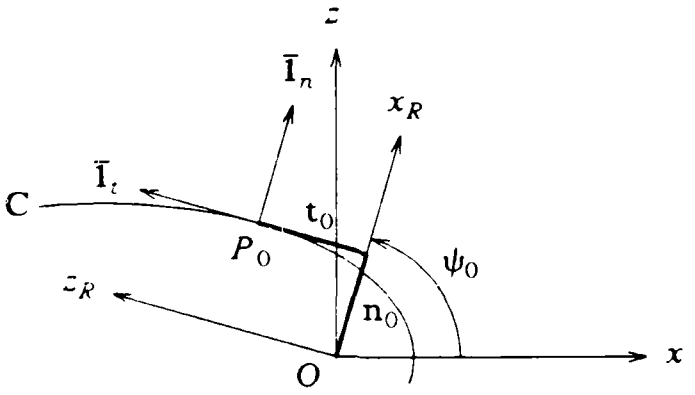

Fig.5.2. VST of P_0 as Coordinates in the Rotated Frame.

defines the coordinates of P_0 in rotated axes $Ox_R z_R$ for $\psi=\psi_0$. The transformation between VST and coordinates in the global axes is given by the transformation of coordinates between rotated and global axes in equation (3.7). The transformation is a rotation with an angle ψ_0 for the point P_0 and, for a general point, the normal angle ψ. This angle has a different value for each point on the curve. The transformation from the VST to equations for Cartesian coordinates in the global frame is given by

$$\begin{bmatrix} x(\psi) \\ z(\psi) \end{bmatrix} = \begin{bmatrix} \cos\psi & -\sin\psi \\ \sin\psi & \cos\psi \end{bmatrix} \begin{bmatrix} n(\psi) \\ t(\psi) \end{bmatrix}$$

$$\mathbf{x}(\psi) = \mathbf{R}_2^{R-G}(\psi)\,\mathbf{s}(\psi) \tag{5.9}$$

The following alternate vector notation emphasizes the contributions of the VST along each local unit vector of the Gaussian circle.

$$\mathbf{x}(\psi) = n(\psi)\,\bar{\mathbf{I}}_n + t(\psi)\,\bar{\mathbf{I}}_t \tag{5.10}$$

The transformation from Cartesian coordinates to the VST is the inverse of the above transformation, namely

$$\begin{bmatrix} n(\psi) \\ t(\psi) \end{bmatrix} = \begin{bmatrix} \cos\psi & \sin\psi \\ -\sin\psi & \cos\psi \end{bmatrix} \begin{bmatrix} x(\psi) \\ z(\psi) \end{bmatrix}$$

$$\mathbf{s}(\psi) = \mathbf{R}_2^{G-R}(\psi)\,\mathbf{x}(\psi) \tag{5.11}$$

5.1.3. Curvature Transform of a Planar Curve

Definition: *The Curvature Transform of a planar curve is the property circle defining the radius of curvature at each corresponding object point. This radius of curvature is denoted by the symbol* ρ.

The CT defines the radius of curvature ρ for each given normal orientation ψ and is hence equivalent to the intrinsic equation $\rho(\psi)$, a representation which is well known in differential geometry [52]. Our motivation for defining curvature by the radius ρ as opposed to the curvature k is the simplicity of object/silhouette relations for this choice of representation for curves and for the corresponding representation for surfaces.

The definition of radius of curvature at the point P_0 of a curve C introduced in section 3.2.5. is based on the Taylor expansion of the Monge parameterization in local axes $P_0 x_l\, y_l\, z_l$ oriented along the tangent and normal at P_0.

$$x_l = -\tfrac{1}{2} z_l\, \rho_0^{-1} z_l + O(z_l^{\,3}) \tag{5.12}$$

where ρ_0 is, by definition, the radius of curvature at P_0. Local axes for the above Monge parameterization are sketched in Fig.5.3. Note that for a convex curve without straight segments, $\rho(\psi) > 0$ for all ψ.

The transformation from the CT function $\rho(\psi)$ to Cartesian coordinates is now determined. In contrast with the ST and the VST, the CT defines the shape of the curve only locally. As a result, it is not possible to determine direct relations between parametric equations $\mathbf{x}(\psi)$ and the CT representation, although a relation will be obtained between the first differential $d\,\mathbf{x}(\psi)$ and the CT. The curve is first considered in a small neighborhood of the point P_0 and analyzed in the fixed local reference frame $P_0 x_l\, z_l$. An expression for the differential $d\,\mathbf{x}_l(\psi)$ in the local axes is obtained by the chain rule

$$d\,\mathbf{x}_l(\psi) = \frac{d\,\mathbf{x}_l(z_l)}{dz_l}\,\frac{dz_l}{dm_{zl}}\,\frac{dm_{zl}}{d\,\psi}\,d\,\psi \tag{5.13}$$

where m_{zl} was defined in section 3.2.4. as the gradient of the local Monge equation. The first two derivatives in the right-hand-side of (5.13) depend on the particular curve shape at P_0 expressed in (5.12). The last derivative in (5.13) depends on the

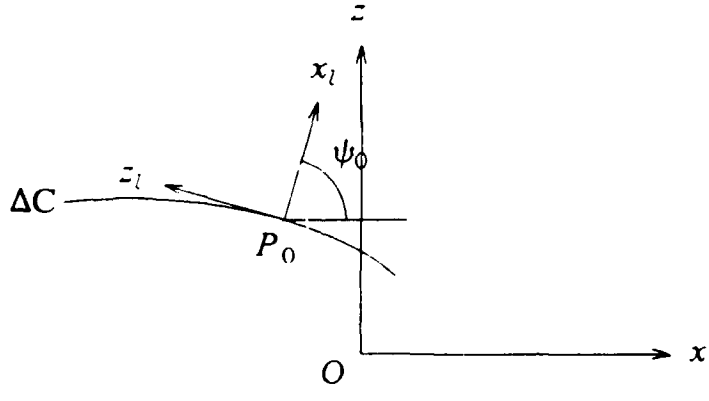

Fig.5.3. Local axes for Defining the Curvature of ΔC at P_0.

relation between the local gradient and the global orientation angle, a relation discussed in section 3.3.3. Each of the factors in (5.13) is evaluated in Appendix 6; the resulting expression for $d\,\mathbf{x}_l$ is given by

$$\begin{bmatrix} dx_l \\ dz_l \end{bmatrix} = \rho_0 \begin{bmatrix} 0 \\ 1 \end{bmatrix} d\psi + O(\psi-\psi_0)\, d\psi$$

$$d\,\mathbf{x}_l = \rho_0\, \bar{\mathbf{I}}_{zl}\, d\psi + O(\psi-\psi_0)\, d\psi \tag{5.14}$$

The above expansion is exact for $\psi = \psi_0$, which corresponds to the point P_0

$$d\,\mathbf{x}_l(\psi_0) = \rho_0\, \bar{\mathbf{I}}_{zl}\, d\psi$$

The differential of global coordinates is obtained by applying the coordinate transformation from $\mathbf{x}_l$ to $\mathbf{x}$, defined in equation (3.8)

$$\begin{bmatrix} dx(\psi_0) \\ dz(\psi_0) \end{bmatrix} = \begin{bmatrix} \cos\psi_0 & -\sin\psi_0 \\ \sin\psi_0 & \cos\psi_0 \end{bmatrix} \begin{bmatrix} 0 \\ 1 \end{bmatrix} \rho_0\, d\psi = \begin{bmatrix} -\sin\psi_0 \\ \cos\psi_0 \end{bmatrix} \rho_0\, d\psi$$

$$d\,\mathbf{x}(\psi_0) = \mathbf{R}_2^{R-G}(\psi_0)\, \bar{\mathbf{e}}_2\, \rho_0\, d\psi = \bar{\mathbf{I}}_{t\,0}\, \rho_0\, d\psi \tag{5.15}$$

As the point P_0 is generic, the above relation is valid for all the points of the curve, so that

$$\begin{bmatrix} dx \\ dz \end{bmatrix} = \begin{bmatrix} -\sin\psi \\ \cos\psi \end{bmatrix} \rho(\psi)\, d\psi$$

$$d\,\mathbf{x}(\psi) = \bar{\mathbf{I}}_t\, \rho(\psi) d\psi = \mathbf{R}_2^{R-G}(\psi)\, \bar{\mathbf{e}}_2\, \rho(\psi)\, d\psi \tag{5.16}$$

The above equation is a first-order differential which can be integrated to produce an expression for Cartesian coordinates of points on the curve

$$\begin{bmatrix} x(\psi) \\ z(\psi) \end{bmatrix} = \begin{bmatrix} x_0 \\ z_0 \end{bmatrix} + \int_{\psi_0}^{\psi} \rho(\psi) \begin{bmatrix} -\sin\psi \\ \cos\psi \end{bmatrix} d\psi$$

$$\mathbf{x}(\psi) = \mathbf{x}_0 + \int_{\psi_0}^{\psi} \rho(\psi) \bar{\mathbf{I}}_t(\psi)\, d\psi \tag{5.17}$$

For a simple closed curve, the vector function $\mathbf{x}(\psi)$ must be periodic in ψ with a period of 2π. Therefore, the CT function $\rho(\psi)$ must satisfy the following constraint

$$\int_0^{2\pi} \rho(\psi) \begin{vmatrix} -\sin\psi \\ \cos\psi \end{vmatrix} d\psi = 0$$

$$\int_0^{2\pi} \rho(\psi)\, \bar{\mathbf{I}}_t(\psi)\, d\psi = 0 \tag{5.18}$$

One interpretation of the above relation is that $\rho(\psi)$, considered on a 2π interval, must have no Fourier series term of order one. The relation in (5.18) has also been interpreted by considering $\rho(\psi)$ as a distribution of mass on the unit circle [53]. The consistency relation is then equivalent to requiring the center of mass of the distribution to be at the center of the unit circle.

Two expressions for the CT in terms of Cartesian parametric equations are now obtained, the first by multiplying both members of equation (5.16) by $\bar{\mathbf{I}}_t$, the second by taking the modulus of (5.16).

$$\rho(\psi) = \frac{d\,\bar{\mathbf{x}}(\psi)}{d\psi} \cdot \bar{\mathbf{I}}_t = \frac{|d\,\bar{\mathbf{x}}(\psi)|}{d\psi} \tag{5.19}$$

Note that the right side of the above expression is identical to a classical definition for the radius of curvature of a convex curve [52].

5.1.4. Relations between the ST, the VST and the CT of a Curve

Relations between the three transforms of a 2-D curve are developed in this section. Based on these relations, a number of consistency criteria are developed for the ST and the VST.

By definition, the first component of the VST is identical to the scalar ST. As a consequence, the VST is a superset of the ST and is therefore redundant, since the ST is complete. Comparing equations (5.8) and (5.10), it is straightforward to determine that

$$\begin{vmatrix} n = p \\ t = p_\psi \\ t = n_\psi \end{vmatrix} \tag{5.20}$$

where the first two equations express the relation between the ST and the VST, and the third equation is a consistency relation for the VST.

In addition to the above relations, a consistency criterion for the ST and for the VST can be obtained by relating these to the CT, then expressing the convexity constraint $\rho > 0$ on the CT. The relation between the ST and the CT is obtained by considering the inverse ST equation

$$\mathbf{x}(\psi) = p(\psi)\,\bar{\mathbf{I}}_n + p_\psi(\psi)\,\bar{\mathbf{I}}_t \tag{5.21}$$

and by comparing the differential of this expression with (5.16). The differential of (5.21) is easily obtained, using the derivatives of unit vectors in (3.55).

$$\mathbf{x}_\psi(\psi) = \left(p(\psi) + p_{\psi\psi}(\psi) \right) \bar{\mathbf{I}}_t \tag{5.22}$$

Comparing this expression with (5.16), the relation between the ST and the CT is determined to be

$$\rho(\psi) = p(\psi) + p_{\psi\psi}(\psi) \tag{5.23}$$

The corresponding relation between the VST and the CT can be obtained by a similar argument.

$$\rho(\psi) = n(\psi) + t_\psi(\psi) \tag{5.24}$$

For a convex curve, $\rho(\psi) > 0$ for all ψ. As a consequence, the following inequalities must apply to the ST and to the VST components:

$$p(\psi) + p_{\psi\psi}(\psi) > 0 \tag{5.25}$$

$$n(\psi) + t_\psi(\psi) > 0 \tag{5.26}$$

It is instructive to consider the relations between each of the three transforms and derivatives of the support function $p(\psi)$.

$$\begin{cases} p(\psi) = p \\ \mathbf{s}(\psi) = [\, p \;\; p_\psi \,]^T \\ \rho(\psi) = p + p_{\psi\psi} \end{cases} \tag{5.27}$$

The above relations emphasize the dependence of the ST, the VST and the CT on derivatives of p up to orders 0, 1 and 2 respectively; similar conclusions will be observed for 3-D surfaces. These relations will be useful in Chapter 7 when analyzing discontinuities of these functions for curves and surfaces with straight edges.

5.1.5. Examples of 2-D Transforms

In Appendix 1, the three 2-D transforms are derived analytically for superconics. Graphs of the transform functions are presented in Fig.5.4 for a superconic with major axis half-lengths $a = 2.0$, $c = 1.0$ and an exponent of $n = 1.2$. The property functions are drawn on polar plots in Fig.5.4, with the origin of the plots offset from the center to allow the representation of negative values in $t(\psi)$.

5.2. Representations for 3-D Surfaces

In this section, three property sphere representations for 3-D surfaces are defined. These representations are extensions to 3-D of the three representations defined for 2-D curves in the previous section. The representations of surfaces will be referred to by the same names as their 2-D counterparts, namely the ST for a property sphere specifying normal distances to tangent planes, the VST for a property sphere of object

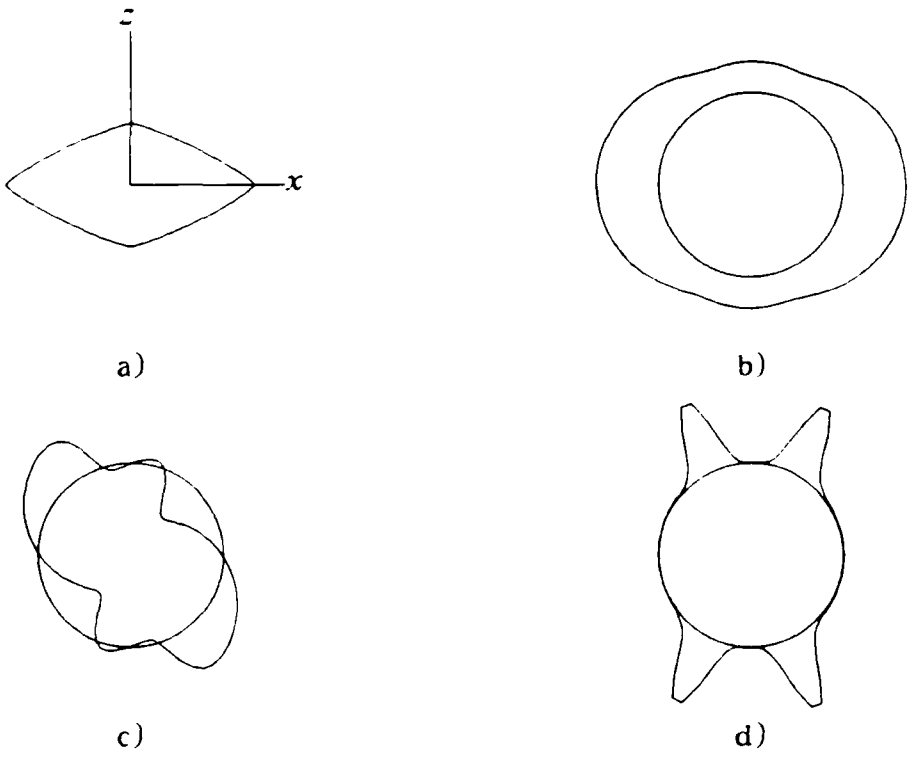

Fig.5.4. 2-D Curve and Polar plots of 2-D Transforms.
a) Superconic with exponent 1.2, b) Support Transform,
c) Tangential Component of Vector Support Transform, d) Curvature Transform.

point coordinates, and the CT for a property sphere of curvatures. Transformations to and from Cartesian coordinates are derived for the three transforms. Relations among the three transforms are developed and exploited to develop consistency constraints for the ST and for the VST. In addition to the above relations, relations between the extended Gaussian image and the three surface transforms are determined. A close parallel has been preserved with the notation used in the case of 2-D silhouettes, as this association improves the readability.

5.2.1. Support Transform of a 3-D Surface

Definition: *The Support Transform of a 3-D surface is the property sphere defining the normal distance from the origin to the tangent plane at each point of the object. This distance is denoted by the symbol* p .

The ST function on the Gaussian sphere specifies the normal distance p to the tangent plane with the given orientation and is hence equivalent to the representation of planes tangent to the surface by the explicit equation $p=p(\xi,\eta)$ for the polar tangential coordinates. In other work, the function $p(\xi,\eta)$ is referred to as the support function for the surface. As illustrated in Fig.5.5, the normal distance p_0 for the point P_0 on the surface element Σ is the distance between the origin and the tangent plane at P_0. This distance is measured along the normal, and is equivalent to the x_R - coordinate of P_0 in rotated axes for $\xi=\xi_0$, $\eta=\eta_0$. The ST function is hence related to Cartesian coordinates for the curve by

$$
\begin{aligned}
p(\xi,\eta) \;&= x_R = \begin{bmatrix} 1 & 0 & 0 \end{bmatrix} \begin{bmatrix} x_R(\xi,\eta) \\ y_R(\xi,\eta) \\ z_R(\xi,\eta) \end{bmatrix} \\
&= \begin{bmatrix} 1 & 0 & 0 \end{bmatrix} \begin{bmatrix} \cos\xi\cos\eta & \sin\xi\cos\eta & \sin\eta \\ -\sin\xi & \cos\xi & 0 \\ -\cos\xi\sin\eta & -\sin\xi\sin\eta & \cos\eta \end{bmatrix} \begin{bmatrix} x(\xi,\eta) \\ y(\xi,\eta) \\ z(\xi,\eta) \end{bmatrix} \\
&= \begin{bmatrix} \cos\xi\cos\eta & \sin\xi\cos\eta & \sin\eta \end{bmatrix} \begin{bmatrix} x(\xi,\eta) \\ y(\xi,\eta) \\ z(\xi,\eta) \end{bmatrix}
\end{aligned}
$$

$$
p(\xi,\eta) = \vec{\mathbf{e}}_1^{\,T}\,\vec{\mathbf{x}}_R(\xi,\eta) = \vec{\mathbf{e}}_1^{\,T}\,\mathbf{R}_3^{G-R}\,\vec{\mathbf{x}}(\xi,\eta) = \vec{\mathbf{1}}_n^{\,T}\vec{\mathbf{x}}(\xi,\eta) \tag{5.28}
$$

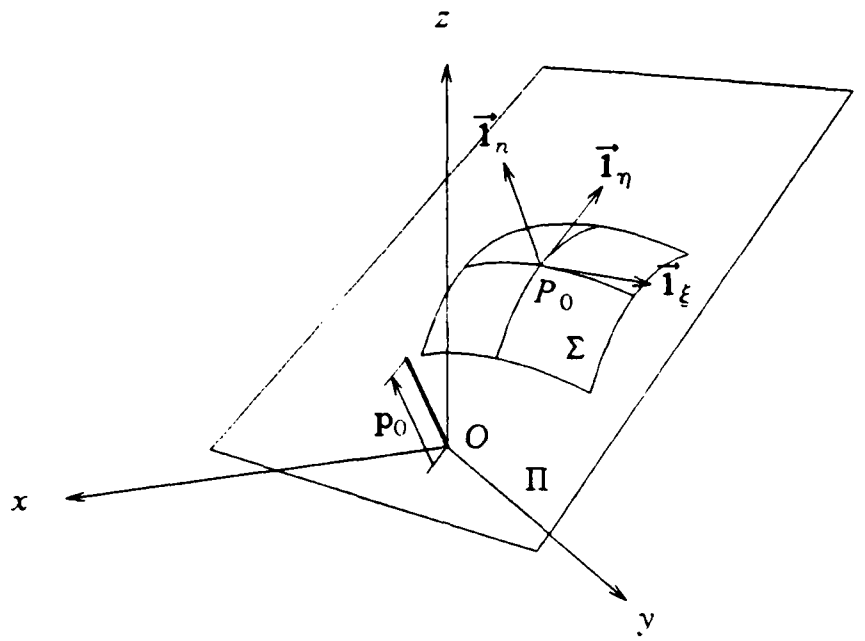

Fig.5.5. Tangent Plane Π to the surface Σ at P_0 and normal distance p_0.

---

where $\vec{e}_1$ denotes the canonical unit vector $(1\,0\,0)^T$. The transformation from ST to Cartesian coordinates is now derived by first considering the equation for the Cartesian coordinates of points on a tangent plane with polar tangential coordinates $\left(p(\xi,\eta), \xi, \eta \right)$.

$$x\ \cos\xi\cos\eta + y\ \sin\xi\cos\eta + z\ \sin\eta = p(\xi,\eta) \tag{5.29}$$

The above equation describes a two-parameter set of planes tangent to the surface. The surface is the envelope of these planes and its equation can be evaluated by eliminating the parameters ξ,η among the equation of the tangent plane and its derivatives with respect to ξ and η. The three equations are given by

$$\left| \begin{array}{rcl} \cos\xi\cos\eta\ x + \sin\xi\cos\eta\ y + \sin\eta\ z &=& p \\ -\sin\xi\cos\eta\ x + \cos\xi\cos\eta\ y &=& p_\xi \\ -\cos\xi\sin\eta\ x - \sin\xi\sin\eta\ y + \cos\eta\ z &=& p_\eta \end{array} \right. \tag{5.30}$$

where the subscripts in p_ξ and p_η denote partial derivatives. After scaling of the second equation by $\cos\eta$,

the above equations can be rewritten in the following matrix form.

$$\begin{bmatrix} \cos\xi\cos\eta & \sin\xi\cos\eta & \sin\eta \\ -\sin\xi & \cos\xi & 0 \\ -\cos\xi\sin\eta & -\sin\xi\sin\eta & \cos\eta \end{bmatrix} \begin{bmatrix} x \\ y \\ z \end{bmatrix} = \begin{bmatrix} p \\ p_\xi/\cos\eta \\ p_\eta \end{bmatrix} \tag{5.31}$$

Comparison of this equation with the transformation from global coordinates to coordinates in rotated axes, namely

$$\begin{bmatrix} x_R \\ y_R \\ z_R \end{bmatrix} = \begin{bmatrix} \cos\xi\cos\eta & \sin\xi\cos\eta & \sin\eta \\ -\sin\xi & \cos\xi & 0 \\ -\cos\xi\sin\eta & -\sin\xi\sin\eta & \cos\eta \end{bmatrix} \begin{bmatrix} x \\ y \\ z \end{bmatrix}$$

$$\vec{\mathbf{x}}_R = \mathbf{R}_3^{G-R}\,\vec{\mathbf{x}} \tag{5.32}$$

reveals that the coordinates of the surface points in the rotated frame are related to the ST by

$$\begin{bmatrix} x_R \\ y_R \\ z_R \end{bmatrix} = \begin{bmatrix} p \\ p_\xi/\cos\eta \\ p_\eta \end{bmatrix} \tag{5.33}$$

and that Cartesian equations for the surface are expressed in terms of the ST by

$$\begin{bmatrix} x(\xi,\eta) \\ y(\xi,\eta) \\ z(\xi,\eta) \end{bmatrix} = \begin{bmatrix} \cos\xi\cos\eta & -\sin\xi & -\cos\xi\sin\eta \\ \sin\xi\cos\eta & \cos\xi & -\sin\xi\sin\eta \\ \sin\eta & 0 & \cos\eta \end{bmatrix} \begin{bmatrix} p(\xi,\eta) \\ p_\xi(\xi,\eta)/\cos\eta \\ p_\eta(\xi,\eta) \end{bmatrix}$$

$$\vec{\mathbf{x}}(\xi,\eta) = R_3^{R-G}(\xi,\eta) \begin{bmatrix} p(\xi,\eta) \\ p_\xi(\xi,\eta)/\cos\eta \\ p_\eta(\xi,\eta) \end{bmatrix} \tag{5.34}$$

The following alternate vector notation emphasizes the contribution of the ST along each local unit vector on the Gaussian sphere.

$$\vec{\mathbf{x}}(\xi,\eta) = p(\xi,\eta)\,\vec{\mathbf{1}}_r + p_\xi(\xi,\eta)/\cos\eta\,\vec{\mathbf{1}}_\xi + p_\eta(\xi,\eta)\,\vec{\mathbf{1}}_\eta \tag{5.35}$$

5.2.2. Vector Support Transform of a 3-D Surface

Definition: *The Vector Support Transform of a 3-D surface is the property sphere defining the three Cartesian coordinates of each surface point in a rotated frame oriented along the local normal, parallel and meridian of the Gaussian Sphere. The components are denoted individually as* n, h *and* v *respectively. The vector combining these components is denoted by* $\vec{\mathbf{s}} = (\, n \;\; h \;\; v \,)^T$.

The above definition emphasizes that the VST specifies point coordinates, but it is easy to see that the first component of the VST is identical to the scalar ST, so that the VST is a superset of the ST and defines tangent planes in addition to points.

Consider on the surface Σ, the point P_0 with normal orientation $\vec{\mathbf{n}}_0(\xi_0,\eta_0)$, as illustrated in Fig.5.6. The VST components n_0, h_0, v_0 for the point P_0 are the Cartesian coordinates of P_0 in the rotated axes $Ox_R y_R z_R$ for P_0. The transformation between this frame and the global object frame is defined in equation (3.9), for $\xi = \xi_0$ and $\eta = \eta_0$. This relation is valid for each point of the surface, when ξ and η

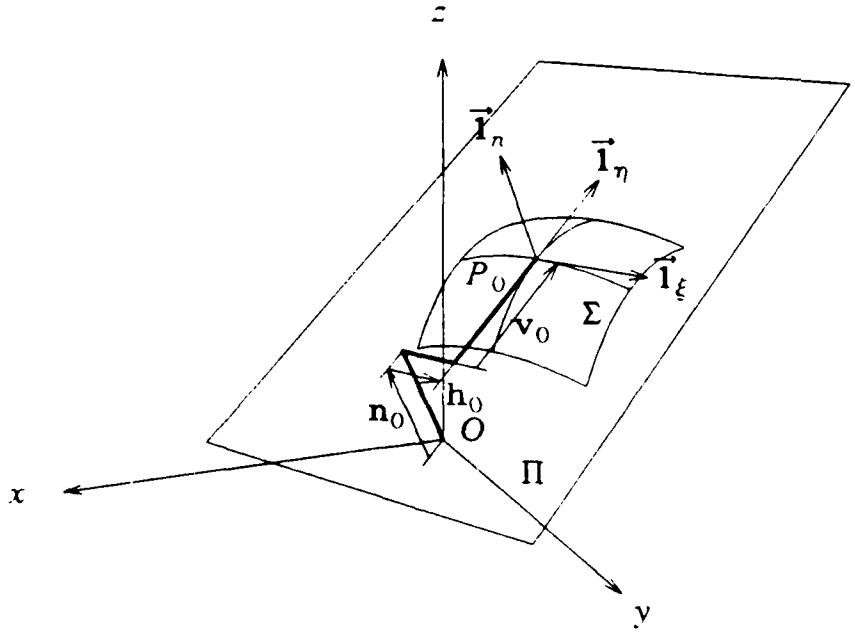

Fig.5.6. Tangent Plane Π to the surface Σ at P_0.
VST $\mathbf{s}_{\vec{0}} = (n_0, h_0, v_0)^T$ and principal orientation vectors.

represent the corresponding normal orientation. The Conversion from Cartesian parametric equations $\vec{\mathbf{x}} = \vec{\mathbf{x}}(\xi,\eta)$ to the VST is hence given by

$$\begin{bmatrix} n(\xi,\eta) \\ h(\xi,\eta) \\ v(\xi,\eta) \end{bmatrix} = \begin{bmatrix} \cos\xi\cos\eta & \sin\xi\cos\eta & \sin\eta \\ -\sin\xi & \cos\xi & 0 \\ -\cos\xi\sin\eta & -\sin\xi\sin\eta & \cos\eta \end{bmatrix} \begin{bmatrix} x(\xi,\eta) \\ y(\xi,\eta) \\ z(\xi,\eta) \end{bmatrix}$$

$$\vec{\mathbf{s}}(\xi,\eta) = \mathbf{R}_3^{G-R}(\xi,\eta)\,\vec{\mathbf{x}}(\xi,\eta) \tag{5.36}$$

The inverse transformation the VST to equations for the Cartesian coordinates is the inverse of the above 3-D rotation, namely

$$\begin{bmatrix} x(\xi,\eta) \\ y(\xi,\eta) \\ z(\xi,\eta) \end{bmatrix} = \begin{bmatrix} \cos\xi\cos\eta & -\sin\xi & -\cos\xi\sin\eta \\ \sin\xi\cos\eta & \cos\xi & -\sin\xi\sin\eta \\ \sin\eta & 0 & \cos\eta \end{bmatrix} \begin{bmatrix} n(\xi,\eta) \\ h(\xi,\eta) \\ v(\xi,\eta) \end{bmatrix}$$

$$\vec{\mathbf{x}}(\xi,\eta) = \mathbf{R}_3^{R-G}(\xi,\eta)\,\vec{\mathbf{s}}(\xi,\eta) \tag{5.37}$$

The following alternate vector notation emphasizes the contribution of the VST along each local unit vector on the Gaussian sphere.

$$\vec{\mathbf{x}}(\xi,\eta) = n(\xi,\eta)\,\vec{\mathbf{1}}_n + h(\xi,\eta)\,\vec{\mathbf{1}}_\xi + v(\xi,\eta)\,\vec{\mathbf{1}}_\eta \tag{5.38}$$

5.2.3. Curvature Transform of a 3-D Surface

Definition: *The Curvature Transform of a 3-D Surface is the property sphere defining the tensor of radius of curvature of the surface expressed in axes oriented along the parallels and meridians of the Gaussian Sphere. The components of the tensor are referred to as* r_{11}, r_{12} *and* r_{22}, *with the index 1 corresponding to the direction of the parallel. The tensor itself is represented by the symbol* $\bar{\bar{\mathbf{R}}}$.

This definition of the CT is a natural extension of the CT defined for 2-D curves in section 5.1.3. Other extensions to three dimensions of the 2-D CT are also possible. For example the 2-D extended Gaussian image is identical to the CT [53], but the 3-D extended Gaussian image represents a scalar property, namely the inverse of the Gaussian curvature of the 3-D surface [44]. Relations between the extended Gaussian image and our 3-D transforms are developed in a later section.

The curvature of a surface Σ at the point P_0 was defined in section 3.2.5., based on the Taylor expansion of the Monge parametric form in local axes at P_0.

$$x_l = -\tfrac{1}{2} \begin{pmatrix} y_l & z_l \end{pmatrix} \begin{pmatrix} r_{11}^0 & r_{12}^0 \\ r_{12}^0 & r_{22}^0 \end{pmatrix}^{-1} \begin{pmatrix} y_l \\ z_l \end{pmatrix} + O((y_l, z_l)^3) \tag{5.39}$$

$$x_l = -\tfrac{1}{2}\, \mathbf{z}_l \bar{\mathbf{R}}_0^{-1} \mathbf{z}_l + O(\mathbf{z}_l^3) \tag{5.40}$$

where x_l is along the normal and y_l, z_l in the tangent plane at P_0. In the above expression, $\bar{\mathbf{R}}_0$ is, by definition, the tensor of radius of curvature at P_0, and $\mathbf{z}_l$ denotes the 2-vector $(y_l \;\; z_l)^T$ in the local tangent plane. The surface and the local axes at P_0 are sketched in Fig.5.7.

The transformation from the CT representation to Cartesian coordinates is now determined. As the CT representation describes only local properties of the object surface, it can not be directly related to Cartesian coordinates, although it will be related to the first differential $d\,\vec{\mathbf{x}}(\xi,\eta)$ of these coordinates. For this purpose, a small surface element $\Delta\Sigma$ in the neighborhood of P_0 is analyzed in the fixed local axes $P_0 x_l\, y_l\, z_l$. An expression for the differential is first obtained in the local axes by the chain rule

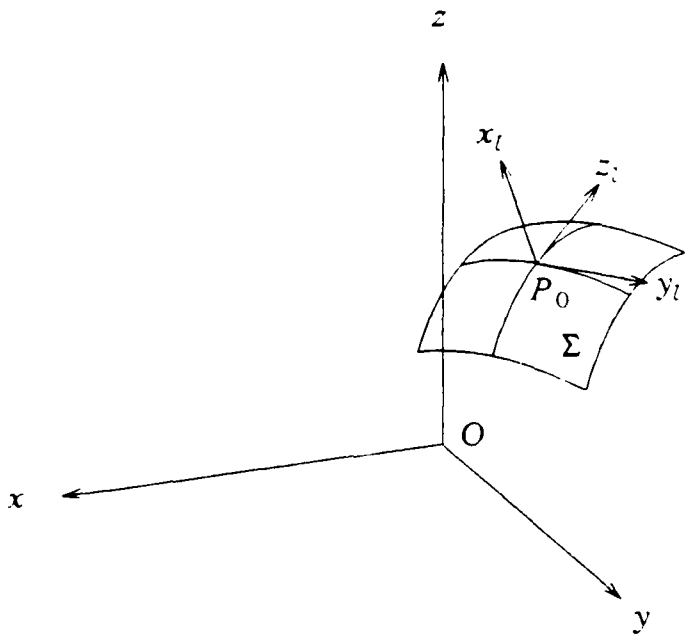

Fig.5.7. Local Axes for the Definition of the Curvature of Σ at P_0.

$$d\vec{x}_l = \frac{D\vec{x}_l(\mathbf{z}_l)}{D\mathbf{z}_l} \frac{D\mathbf{z}_l}{D\vec{m}_{zl}} \frac{D\vec{m}_{zl}}{D\boldsymbol{\xi}} d\boldsymbol{\xi} \tag{5.41}$$

where expressions such as $D\vec{x}_l / D\mathbf{z}_l$ denote Jacobian matrices, $\vec{m}_{zl} = (m_{yl}\ m_{zl})^T$ is the 2-vector of local gradients, and $d\boldsymbol{\xi}$ is the vector of normalized global angle differentials $d\boldsymbol{\xi} = (\cos\eta d\xi\ d\eta)^T$. The first two Jacobian matrices in the right hand side of (5.41) depend on the shape of the particular surface around P_0, defined by (5.39). The last Jacobian matrix in (5.41) depends on the relation between local gradients and global orientation angles, a relation which was discussed in section 3.3.3. Each of the factors in (5.41) are evaluated in Appendix 6. When inserted in equation (5.41), they produce an expression for the differential $d\vec{x}_l$ in local coordinates, valid to first order around P_0. The expression is exact at P_0, and since P_0 is generic, the differential in local axes at a given point is represented by a similar expression.

$$\begin{pmatrix} dx_l \\ dy_l \\ dz_l \end{pmatrix} = \begin{pmatrix} 0 & 0 \\ 1 & 0 \\ 0 & 1 \end{pmatrix} \begin{pmatrix} r_{11} & r_{12} \\ r_{12} & r_{22} \end{pmatrix} \begin{pmatrix} \cos\eta d\xi \\ d\eta \end{pmatrix}$$

$$d\vec{x}_l = \mathbf{I}_{32}\, \bar{\bar{\mathbf{R}}}\, d\boldsymbol{\xi} \tag{5.42}$$

where $\mathbf{I}_{32}$ is a 3x2 matrix consisting of only zeros and ones. A differential for the surface in global coordinates is obtained by applying the coordinate transformation in (3.10).

$$\begin{pmatrix} dx \\ dy \\ dz \end{pmatrix} = \begin{pmatrix} \cos\xi\cos\eta & -\sin\xi & -\cos\xi\sin\eta \\ \sin\xi\cos\eta & \cos\xi & -\sin\xi\sin\eta \\ \sin\eta & 0 & \cos\eta \end{pmatrix} \begin{pmatrix} 0 & 0 \\ 1 & 0 \\ 0 & 1 \end{pmatrix} \begin{pmatrix} r_{11} & r_{12} \\ r_{12} & r_{22} \end{pmatrix} \begin{pmatrix} \cos\eta d\xi \\ d\eta \end{pmatrix}$$

$$d\vec{x} = \mathbf{R}_3^{R-G}\, \mathbf{I}_{32}\, \bar{\bar{\mathbf{R}}}\, d\boldsymbol{\xi} \tag{5.43}$$

In principle, the above differential can be integrated to produce Cartesian equations for the surface. As the integration domain is two-dimensional, an integration path must be prescribed; this question is addressed in the next section.

Transformations from Cartesian equations to the CT are easily developed based on equation (5.43). Indeed, explicit expressions for the partial derivatives of $\vec{x}$ can be obtained from (5.43) as

AD-A175 236 SILHOUETTE-SLICE THEOREMS(U) MASSACHUSETTS INST OF TECH 2/3
CAMBRIDGE RESEARCH LAB OF ELECTRONICS P L VAN HOVE
SEP 86 TR-522 N00014-81-K-0742

UNCLASSIFIED F/G 12/1 NL

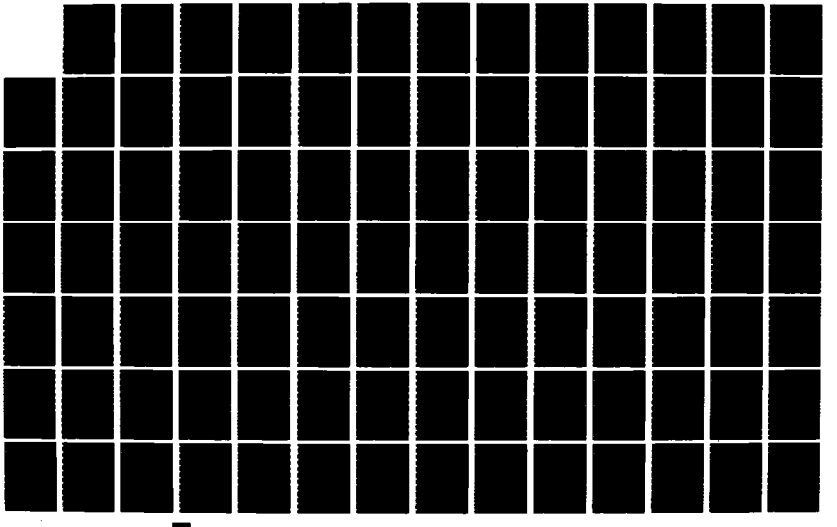

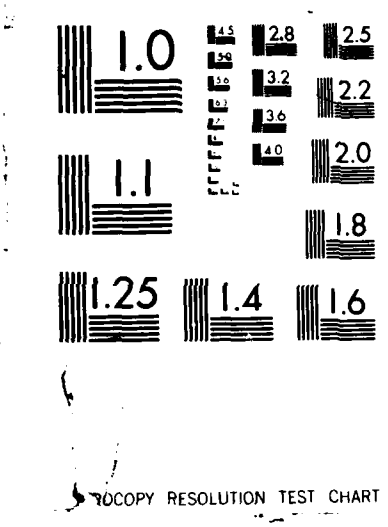
1.0
1.1
1.25
1.4
1.6
2.8
3.2
3.6
4.0
2.5
2.2
2.0
1.8
ROCOPY RESOLUTION TEST CHART

$$\begin{vmatrix} \vec{x}_\xi/\cos\eta \\ \vec{x}_\eta \end{vmatrix} = \begin{pmatrix} r_{11} & r_{12} \\ r_{12} & r_{22} \end{pmatrix} \begin{vmatrix} \vec{1}_\xi \\ \vec{1}_\eta \end{vmatrix} \tag{5.44}$$

An expression for determining the CT of a surface given by parametric equations $\vec{x}(\xi,\eta)$ is hence

$$\begin{pmatrix} r_{11} & r_{12} \\ r_{12} & r_{22} \end{pmatrix} = \begin{vmatrix} \vec{1}_\xi \cdot \vec{x}_\xi/\cos\eta & \vec{1}_\eta \cdot \vec{x}_\xi/\cos\eta \\ \vec{1}_\xi \cdot \vec{x}_\eta & \vec{1}_\eta \cdot \vec{x}_\eta \end{vmatrix} \tag{5.45}$$

5.2.3.1. Consistency Constraints for the 3-D CT

In this section, consistency constraints are determined for the CT function defined on the Gaussian sphere. Equation (5.44) relates first derivatives of Cartesian coordinates to the CT. This expression has a conceptual similarity to the expression for surface reconstruction from needle maps [21]. In both cases, first derivatives of a function are given on a two-dimensional domain. In the case of the needle map, surface reconstruction is possible only if the gradient field corresponding to the needle map is curl-free. The curl-free condition, also referred to as an integrability constraint, corresponds to a zero elevation gain on all closed loops in the image plane, and is equivalent for smooth surfaces to equality of the mixed derivatives. This condition guarantees that integration of the Cartesian coordinates is independent of integration path and is a necessary and sufficient consistency constraint for a needle map. A similar condition is derived here for the CT by requiring equality of the mixed derivatives $\vec{x}_{\xi\eta}$ and $\vec{x}_{\eta\xi}$. These mixed derivatives are first evaluated from (5.44), taking into account the derivatives of local unit vectors given in equation (3.50).

$$\begin{vmatrix} \vec{x}_{\xi\eta} = \dfrac{\partial}{\partial\eta}(r_{11}\cos\eta)\,\vec{1}_\xi + \dfrac{\partial}{\partial\eta}(r_{12}\cos\eta)\,\vec{1}_\eta - r_{12}\cos\eta\,\vec{1}_n \\ \vec{x}_{\eta\xi} = \left(\dfrac{\partial}{\partial\xi} r_{12} - r_{22}\sin\eta\right)\vec{1}_\xi + \left(\dfrac{\partial}{\partial\xi} r_{22} + r_{12}\sin\eta\right)\vec{1}_\eta - r_{12}\cos\eta\,\vec{1}_n \end{vmatrix} \tag{5.46}$$

The consistency constraints are obtained by comparing individual components of the above expressions for the mixed derivatives.

$$\left|\begin{array}{l} \dfrac{\partial}{\partial\eta}(r_{11}\cos\eta) = \dfrac{\partial}{\partial\xi} r_{12} - r_{22}\sin\eta \\ \dfrac{\partial}{\partial\xi} r_{22} = \dfrac{\partial}{\partial\eta}(r_{12}\cos\eta) - r_{12}\sin\eta \end{array}\right. \tag{5.47}$$

When the above consistency relations are verified, the integral of the differential $d\vec{\mathbf{x}}$ is independent of integration path.

A second type of constraint must be satisfied by the components of the CT of a convex object. Specifically, positivity of mean and Gaussian curvatures implies positivity of the trace $(r_{11} + r_{22})$ and of the determinant $(r_{11}r_{22} - r_{12}^2)$

5.2.4. Relations Between the ST, the VST and the CT of a Surface

In this section, relations between the three transforms of a given 3-D surface are developed. From these relations, consistency constraints are determined for the ST and for the VST.

By definition, the first component of the VST is identical to the scalar ST. Since the ST representation is complete, the above relation indicates that the VST is redundant. Comparing equations (5.38) and (5.35), it is straightforward to determine that

$$\left|\begin{array}{l} n = p \\ h = p_\xi/\cos\eta \\ v = p_\eta \end{array}\right. \tag{5.48}$$

$$\left|\begin{array}{l} h = n_\xi/\cos\eta \\ v = n_\eta \\ v_\xi = \partial/\partial\eta(h\cos\eta) \end{array}\right. \tag{5.49}$$

where the first group of equations expresses the relations between the ST and the components of the VST. The equations in the second set are relations among the three VST components.

In addition to the above relations, a set of inequality constraints can be developed for the ST and VST by relating these representations to the CT, then expressing the convexity of the surface in terms of the CT representation. The relation between the ST and CT is derived by considering the inverse ST equation.

$$\vec{\mathbf{x}}(\xi,\eta) = p(\xi,\eta)\,\vec{\mathbf{1}}_n + p_\xi(\xi,\eta)/\cos\eta\,\vec{\mathbf{1}}_\xi + p_\eta(\xi,\eta)\,\vec{\mathbf{1}}_\eta \tag{5.50}$$

and by comparing the derivatives of this expression with (5.44). The derivatives of (5.50) are easily obtained with the derivatives of unit vectors in (3.50).

$$\begin{bmatrix} \vec{\mathbf{x}}_\xi/\cos\eta \\ \vec{\mathbf{x}}_\eta \end{bmatrix} = \begin{bmatrix} p + p_{\xi\xi}/\cos^2\eta - p_\eta\tan\eta & p_{\xi\eta}/\cos\eta + p_\xi\sin\eta/\cos^2\eta \\ p_{\xi\eta}/\cos\eta + p_\xi\sin\eta/\cos^2\eta & p + p_{\eta\eta} \end{bmatrix} \begin{bmatrix} \vec{\mathbf{1}}_\xi \\ \vec{\mathbf{1}}_\eta \end{bmatrix} \tag{5.51}$$

Comparing this expression with (5.44) produces the following expression for the CT tensor in terms of the ST function $p(\xi,\eta)$.

$$\begin{bmatrix} r_{11} & r_{12} \\ r_{12} & r_{22} \end{bmatrix} = \begin{bmatrix} p + p_{\xi\xi}/\cos^2\eta - p_\eta\tan\eta & p_{\xi\eta}/\cos\eta + p_\xi\sin\eta/\cos^2\eta \\ p_{\xi\eta}/\cos\eta + p_\xi\sin\eta/\cos^2\eta & p + p_{\eta\eta} \end{bmatrix} \tag{5.52}$$

For a convex object surface, both the determinant and the trace of $\bar{\mathbf{R}}$ must be positive. The following inequalities must therefore be satisfied by $p(\xi,\eta)$.

$$2p + p_{\xi\xi}/\cos^2\eta + p_{\eta\eta} - p_\eta\tan\eta > 0 \tag{5.53}$$

$$(p + p_{\xi\xi}/\cos^2\eta - p_\eta\tan\eta)(p + p_{\eta\eta}) - (p_{\xi\eta}/\cos\eta + p_\xi\sin\eta/\cos^2\eta)^2 > 0$$

Relations similar to (5.52) can be formulated between the VST and CT; these also allow the development of convexity constraints for the VST. The relation between VST and CT is given by

$$\begin{bmatrix} r_{11} & r_{12} \\ r_{12} & r_{22} \end{bmatrix} = \begin{bmatrix} n + h_\xi/\cos\eta - v\tan\eta & v_\xi/\cos\eta + h\tan\eta \\ h_\eta & n + v_\eta \end{bmatrix} \tag{5.54}$$

The resulting convexity constraints are

$$2n + h_\xi/\cos\eta + v_\eta - v\tan\eta > 0 \tag{5.55}$$

$$(n + h_\xi/\cos\eta - v\tan\eta)(n + v_\eta) - h_\eta(v_\xi/\cos\eta + h\tan\eta) > 0$$

Considering equations (5.48) and (5.52), it can be observed that the ST, VST and CT depend on derivatives of p up to orders 0, 1 and 2 respectively. This conclusion is

identical to the corresponding observation made for the transforms of planar curves.

5.2.5. Relations between the Extended Gaussian Image and the CT, VST, ST

In this section, relations between the extended Gaussian image (EGI) and the three property sphere representations are developed. The EGI is a property sphere for the inverse of the Gaussian curvature. The Gaussian curvature is the determinant of our curvature tensor $\bar{\bar{\mathbf{K}}}$ and is also the inverse of the determinant of the radius of curvature tensor $\bar{\bar{\mathbf{R}}}$; see section 3.2.5. Hence, the EGI is equal to the determinant of the CT.

$$\mathbf{G}(\xi,\eta) = \det\bar{\bar{\mathbf{R}}}(\xi,\eta) \tag{5.56}$$

where $\mathbf{G}$ denotes the EGI function. The CT function is hence a redundant superset of the EGI. In the case of 2-D curves, the CT is identical to the EGI defined in [53]. The 3-D EGI and the 3-D CT can be considered as two different generalizations to 3-D surfaces of the same representation for 2-D curves. The ST can be related to the EGI by combining (5.56) and (5.52).

$$\begin{aligned}\mathbf{G}(\xi,\eta) = \; & (p + p_{\xi\xi}/\cos^2\eta - p_\eta\tan\eta)(p + p_{\eta\eta}) \\ & - (p_{\xi\eta}/\cos\eta + p_\xi\sin\eta/\cos^2\eta)^2\end{aligned} \tag{5.57}$$

The above relation should prove useful in combining EGI and ST representations, such as for the work presented in [45]. Finally, a relation between VST and EGI is obtained by combining (5.56) and (5.54).

$$\begin{aligned}\mathbf{G}(\xi,\eta) = \; & (n + h_\xi/\cos\eta - v\tan\eta)(n + v_\eta) \\ & - h_\eta(v_\xi/\cos\eta + h\tan\eta)\end{aligned} \tag{5.58}$$

5.2.6. Examples of 3-D Transforms

In this section, the three transforms of a simple object are derived. These derivations illustrate the computation of transforms from parametric equations. The object considered here is a sphere of radius R offset from origin, centered at $P_0(x_0,y_0,z_0)$. Transforms of more complicated object shapes are derived in Appendix 1.

Parametric equations for the sphere are given by

$$\begin{cases} x = x_0 + R\cos\xi\cos\eta \\ y = y_0 + R\sin\xi\cos\eta \\ z = z_0 + R\sin\eta \end{cases} \tag{5.59}$$

The ST of this sphere is obtained by applying (5.29) to the above parametric equations

$$p(\xi,\eta) = x_0\cos\xi\cos\eta + y_0\sin\xi\cos\eta + z_0\sin\eta + R \tag{5.60}$$

In the particular case where the center P_0 of the sphere is at the origin, the above expression simplifies to $p(\xi,\eta) = R$.

The VST of the sphere can be derived by applying equation (5.36) to (5.59).

$$\vec{\mathbf{s}}(\xi,\eta) = \begin{bmatrix} x_0\cos\xi\cos\eta + y_0\sin\xi\cos\eta + z_0\sin\eta + R \\ -x_0\sin\xi + y_0\cos\xi \\ -x_0\cos\xi\sin\eta - y_0\sin\xi\sin\eta + z_0\cos\eta \end{bmatrix} \tag{5.61}$$

In the particular case that $\vec{\mathbf{x}}_0 = \vec{\mathbf{0}}$, the VST is given by $\vec{\mathbf{s}}(\xi,\eta) = (R\ 0\ 0)^T$.

It is possible to derive the CT from the parametric equations in (5.59) by different methods. Indeed, the CT can be determined directly from (5.59) with equation (5.45), indirectly from the ST with equation (5.52), or indirectly from the VST with equation (5.54) The indirect derivation via the ST is developed here. Partial derivatives of the ST can be evaluated as

$$\begin{cases} p_\xi = -x_0\sin\xi\cos\eta + y_0\cos\xi\cos\eta \\ p_{\xi\xi} = -x_0\cos\xi\cos\eta - y_0\sin\xi\cos\eta \\ p_{\xi\eta} = x_0\sin\xi\sin\eta - y_0\cos\xi\sin\eta \\ p_\eta = -x_0\cos\xi\sin\eta - y_0\sin\xi\sin\eta + z_0\cos\eta \\ p_{\eta\eta} = -x_0\cos\xi\cos\eta + y_0\sin\xi\cos\eta - z_0\sin\eta \end{cases} \tag{5.62}$$

Using the above derivatives, the 3-D CT function is determined as

$$\begin{bmatrix} r_{11} & r_{12} \\ r_{12} & r_{22} \end{bmatrix} = \begin{bmatrix} p + p_{\xi\xi}/\cos^2\eta - p_\eta\tan\eta & p_{\xi\eta}/\cos\eta + p_\xi\sin\eta/\cos^2\eta \\ p_{\xi\eta}/\cos\eta + p_\xi\sin\eta/\cos^2\eta & p + p_{\eta\eta} \end{bmatrix}$$

$$= \begin{bmatrix} R & 0 \\ 0 & R \end{bmatrix} \tag{5.63}$$

Note that this result is independent of the position of the center of the sphere. The CT function is identical to the curvature tensor of the sphere determined in section 3.2.5..

Each 3-D transform contains large amounts of information, so that it is not easily displayed on one graph. In Chapter 8, some 3-D transforms will be represented by polar plots of their components on meridians of the Gaussian sphere.

5.3. Summary

Three representations for closed curves and the corresponding representations for 3-D surfaces have been defined in this chapter. The motivation behind the study of these representations is the simplification they introduce in the analysis of relations between object shapes and silhouette shapes. In the following chapter, three theorems wil be demonstrated, relating the transforms of a 3-D object to the transforms of its silhouettes. Specifically, it will be shown that the property circle of the silhouette in an orthographic projection can be obtained by slicing the property sphere of the object by a plane perpendicular to the viewing direction and going through the origin, then appropriately projecting the vector or tensor information onto the slice plane. The *specific object properties represented by the three transforms* were carefully chosen to lead to such simple relations.

Aside from their interest in silhouette analysis, the transforms presented in this chapter can also be analyzed simply as representations of 2-D curves and 3-D surfaces. Each of the transforms is now discussed individually in this respect.

In both 2-D and 3-D, the ST is quite similar to the support function, an explicit equation for polar tangential coordinates. Although this form is known, it has not received much attention in the graphics and vision fields.

The 2-D and 3-D VST are simply related to descriptions in terms of Cartesian point coordinates, but their relation with the ST and CT is interesting for at least two reasons. First, the relations between the ST and CT on one side, and the VST on the other side are quite simple, so that the VST may be used as an intermediate step when converting the ST or the CT to a description in terms of Cartesian coordinates. In some applications, when a Cartesian representation is required, the VST itself may be appropriate, thereby eliminating the need for a different Cartesian representation. For example, it should be easy to synthesize a shaded rendition of an object for a general

view-point, based on the VST only. A second interesting feature of the VST is that it forms with the ST and CT, a range of representations depending on derivatives of p up to orders 0, 1, 2. Instead of the VST which combines normal and tangential components of rotated Cartesian coordinates, it is possible to describe property circles and spheres describing only the tangential components. These representations would avoid the trivial redundancy with the ST, but would not be uniquely invertible. For example, the VST of a sphere centered at the origin is zero everywhere and does not depend on the radius of the sphere. We have therefore preferred the definition of the VST proposed in this chapter, and its interpretation as a complete description of point coordinates of the object.

The CT representation of 2-D curves and 3-D surfaces will now be discussed. Forms closely related to the 2-D CT have been proposed by various authors [23, 53, 54]. The 2-D CT is closely related to the intrinsic form relating radius of curvature and normal orientation. Intrinsic descriptions of the shape of curves have been extensively studied in differential geometry and are well known [52]. However, to the best of the author's knowledge, equivalent representations have not been proposed for surfaces. The 3-D CT can be considered as such an intrinsic form for surfaces and should therefore be of interest when analyzing the shapes of 3-D surfaces. Representations of surface shapes presented in textbooks of differential geometry usually rely on two tensors, referred to as the tensor of the first fundamental form and the tensor of the second fundamental form. The two tensors convey information about both the shape of the surface and the parameterization used to define the surface. With this formalism, it is not possible to retain a complete description of surface shape without interfering with the description of the parameterization. The literature on surface representation in machine vision seems strongly influenced by this description of surfaces in terms of fundamental form tensors. Characterizations of surface curvature by local invariants have also been proposed. These invariants combine information from the two fundamental tensors and are independent of parameterization. For example, the extended Gaussian image defines surface shapes by one invariant, the Gaussian curvature; a description of surfaces by two invariants, the Gaussian and mean curvatures, has also been proposed [40]. These representations, although invertible with appropriate boundary conditions, do not carry a complete local

characterization of surface shape. The 3-D CT representation proposed here is an elegant alternative to the classical shape description methods. It combines a new invariant curvature tensor function with the parameterization used to represent normal orientations in the extended Gaussian image. Relations between the CT and classical descriptions of surface curvature are further addressed in Appendix 4.

The framework developed in this chapter for representating shapes stresses the similarities between 2-D and 3-D, and suggests straightforward generalizations to representations of n-dimensional hypersurfaces in (n+1)-dimensional space. These generalizations are not addressed here.

Chapter 6
Silhouette-Slice Theorems

In this chapter, relations between the transforms of 3-D convex object surfaces and the corresponding transforms of their 2-D silhouettes in orthographic projections are determined. It turns out that these relations prescribe pointwise correspondences between property-function values on the Gaussian sphere of the object and property-function values on the Gaussian circle of the silhouette. Hence, there are two aspects to the relation between 2-D and 3-D transforms. The first part of the relation determines which values of the 3-D object property sphere directly contribute to the silhouette, whereas the second part specifies how the values of the 2-D transforms are related to the values of the 3-D transforms at the corresponding points. These two aspects of the relation are closely tied to the selection and projection steps of the classical silhouette construction method reviewed in Chapter 4.

The exact form of the relation between the transforms of the object and the transforms of its silhouettes will be determined by applying the classical silhouette construction method sketched in Fig.4.2 to the surface shape expressed as the inverse transform of each of the three representations. The first step of the classical method will indicate an equivalence of points on the Gaussian circle of the silhouette and points on a slice of the Gaussian sphere of the object. The slice is the intersection of the Gaussian sphere with a plane through the center and perpendicular to the viewing direction. The second step of the classical silhouette construction will indicate how transform values on the slice of the Gaussian sphere of the object are related to transform values on the Gaussian circle of the silhouette. Specifically, it will be shown that the silhouette ST values are identical to the object ST values on the slice, and that the values of the VST and CT of the silhouette can be obtained by projecting onto the slice plane the vector or tensor values of the corresponding 3-D transforms on the slice of the object Gaussian sphere. The relations among 3-D objects, 2-D silhouettes and their transforms have a strong conceptual similarity with the Projection-Slice theorem of computerized tomography. The theorems describing the relations in the case of silhouettes have been named Silhouette-Slice theorems to underline this similarity.

In the first section of this chapter, the relation between Gaussian circles of silhouettes and slices of the Gaussian sphere of the object is demonstrated. Relations among angular coordinates on the sphere, the angular coordinate on the silhouette slice circle and the viewing direction are determined. In the second section, the transformation between local systems of 3-D axes corresponding to the slice of the Gaussian sphere and local systems of axes on the silhouette is derived. It will be shown that this transformation is the composition of two 3-D rotations and a projection, and that its expression can be substantially simplified. In the third section, relations between silhouette property circle functions and object property sphere functions are determined by applying the transformation derived in the second section to coordinates of points of the silhouette generator of the object, expressed in terms of the ST, VST and CT representations. Finally, the results are discussed and compared with the Projection-Slice theorem of computerized tomography.

6.1. Silhouettes, Gaussian Spheres and Gaussian Circles

The first step in determining relations between silhouette properties and object properties is to determine which object points contribute to the silhouette, and which points of the silhouette are affected by which points of the object. It is shown in this section that only the points on the great circle slice of the Gaussian sphere perpendicular to the viewing direction contribute to the silhouette, and that the points of the slice are related to corresponding points of the silhouette by the Gaussian mapping.

The following discussion refers to Fig.6.1 which illustrates a 3-D object and its orthographic silhouette in the image plane. Consider a point P_{SG} on the silhouette generator of the object, its projection P_S in the image plane and its image P_G on the Gaussian sphere. First, by definition of the Gaussian mapping, the normal to the object surface at P_{SG} is parallel to the normal to the sphere at P_G. Second, since P_{SG} is on the silhouette generator, the normal at P_{SG} is parallel to the projection plane, so that its direction is unaffected by the projection operation. Hence, the normals to the silhouette at P_S, to the object at P_{SG} and to the sphere at P_G are all parallel. The image of the silhouette generator on the Gaussian sphere is thus the set of points of the sphere for which the normal orientation is perpendicular to the viewing direction. This set of points is the great circle of the Gaussian sphere perpendicular to the

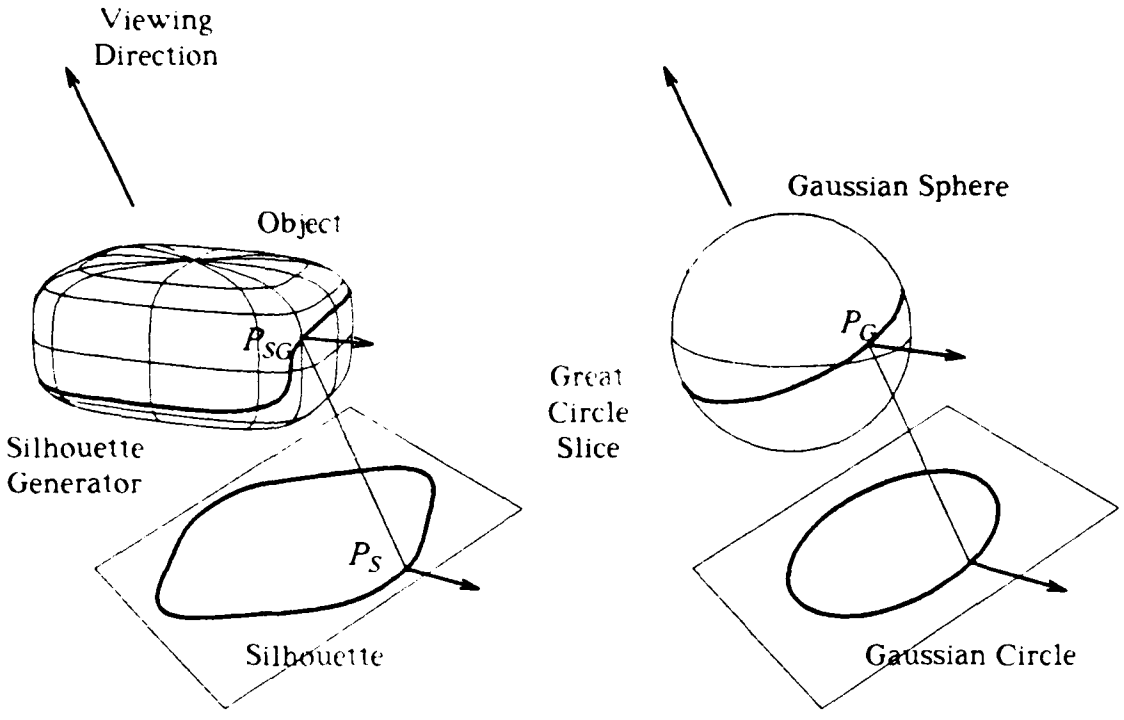

Fig.6.1. Relation between the Silhouette Generator and a Slice of the Gaussian Sphere.

viewing direction. Individual points of the silhouette and of the slice corresponding to the same object point, such as P_S and P_G, are related by the parallelism of their normals. Therefore, the slice of the Gaussian sphere of the object is a Gaussian circle for the silhouette. This conclusion is formalized as follows:

Silhouette-Slice Theorem 0: *Each great circle slice of the Gaussian Sphere of a smooth convex object is the Gaussian Circle of the silhouette of the object in an orthographic projection on a plane parallel to the slice.*

The above theorem is now complemented by trigonometric relations between the angular coordinates (ξ,η) of points on the slice, the angular coordinate ψ on the Gaussian circle of the silhouette, and the angles (ϕ,θ) specifying the orientation of the viewing direction. Consider the point P_G on the slice of the Gaussian sphere corresponding to the viewing direction $\vec{\mathbf{v}}$, as illustrated in Fig.6.2. For this point, the five angles of interest appear in the spherical triangle AP_GC, drawn in bold in the figure. This triangle is also displayed "flattened out" with the values of all its

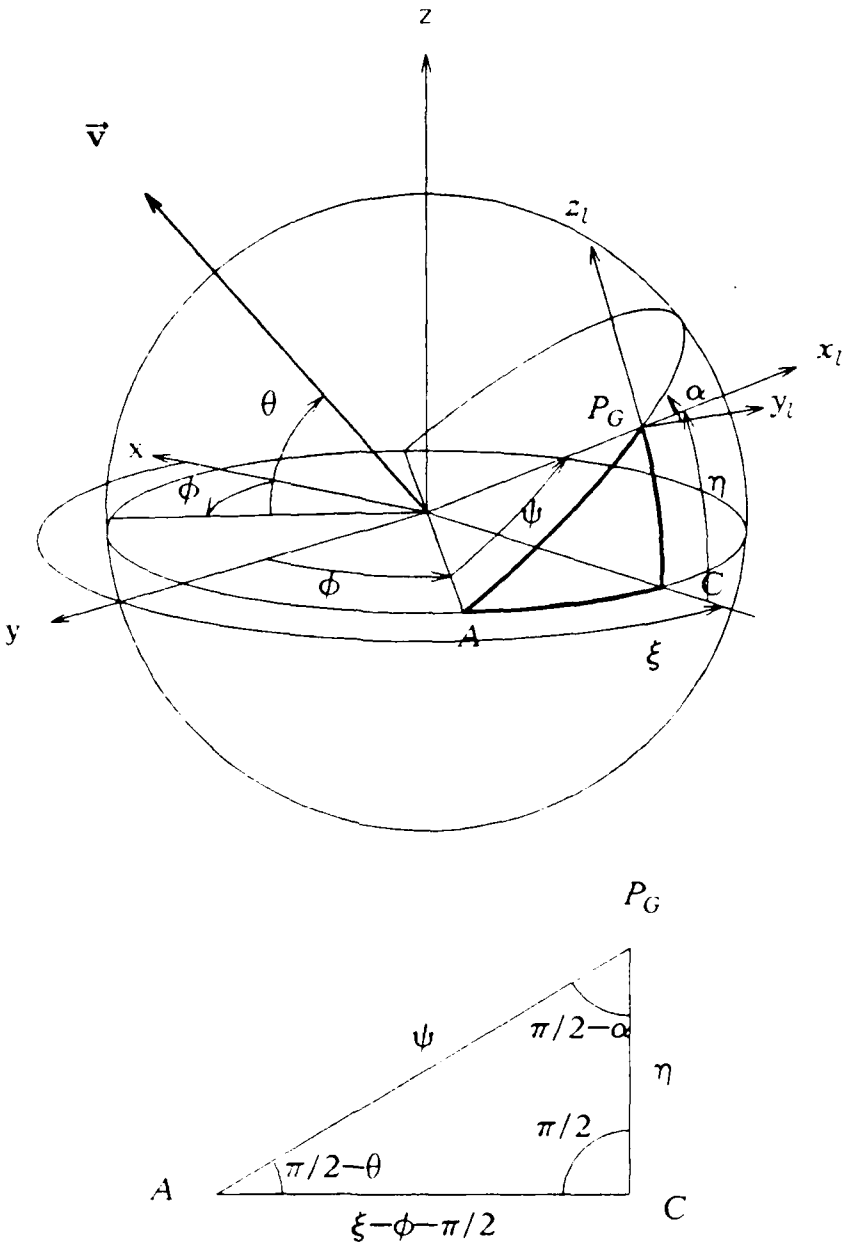

Fig.6.2. Great Circle Slice and Angles on the Gaussian Sphere

---

elements on the same figure. The sixth element of the triangle ABC is related to the angle α characterizing the orientation of the slice plane in local axes $P_G\, x_l\, y_l\, z_l$ at P_G. Applying the standard relations between elements of a right-angled spherical triangle

in[55] to the above triangle produces the following identities

$$\left|\begin{array}{rcll} \sin\eta &=& \tan(\xi-\phi-\tau/2)\ \tan\alpha & (a) \\ -\cos(\xi-\phi) &=& \tan\eta\ \tan\theta & (b) \\ \sin\theta &=& \tan(\xi-\phi-\pi/2)\ \cot\psi & (c) \\ \sin\alpha &=& \tan\eta\ \cot\psi & (d) \\ \cos\psi &=& \tan\theta\ \tan\alpha & (e) \\ \sin\eta &=& \cos\theta\ \sin\psi & (f) \\ -\cos(\xi-\phi) &=& \cos\alpha\ \sin\psi & (g) \\ \sin\theta &=& \cos\eta\ \cos\alpha & (h) \\ \sin\alpha &=& \sin(\xi-\phi)\ \cos\theta & (i) \\ \cos\psi &=& \cos\eta\ \sin(\xi-\phi) & (j) \end{array}\right. \tag{6.1}$$

Note that the angles ξ, ϕ, ψ are defined over the range $[-\pi,+\pi]$ and the angles η, θ over the range $[-\pi/2,\pi/2]$. The full range of these parameters is covered by relating the quadrants of the arguments in the tangent trigonometric functions in expression (6.1)(c).

For a fixed viewing direction (ϕ,θ), the silhouette point with normal orientation ψ in the image plane corresponds to the object point with normal orientation (ξ,η) for the values of these angles satisfying (6.1). Specifically, (6.1)(c) implicitly relates the angles ψ and ξ, whereas (6.1)(f) relates the angles ψ and η. Explicit forms for these relations are given by

$$\left|\begin{array}{l} \xi = \xi_{SG}(\psi) = \phi + \pi/2 + \mathrm{atan}\,(\sin\theta\,\tan\psi) \\ \eta = \eta_{SG}(\psi) = \mathrm{asin}\,(\cos\theta\,\sin\psi) \end{array}\right. \tag{6.2}$$

where the subscripts SG indicate that the angles correspond to points of the slice which are the images of points on the silhouette generator. In the above expression, the range of the arcsine is $(-\pi/2,\pi/2)$ and the quadrant of the arctangent must be the quadrant of ψ when $\theta>0$ and the quadrant symmetric with respect to the x-axis otherwise. The above expressions can be considered as parametric solutions for equation (6.1)(b); this equation is equivalent to the equation of the silhouette generating planes in (4.27). The solutions in (6.2) of this last equation were anticipated in Chapter 4. The angle α is the tilt of the slice at each point relative to the local axes $P_G\,x_l\,y_l\,z_l$. This angle is useful when projecting vectors and tensors defined by their components in local axes, onto the slice plane.

Equations (6.1) and (6.2) can be further exploited to derive expressions for the differentials $d\xi$ and $d\eta$ in terms of $d\psi$ on the slice for a fixed viewing direction. These relations are sketched in Fig.6.3; they will be useful when projecting differentials of Cartesian coordinates expressed in terms of the CT. The differentials of ξ and η along the silhouette generator could be evaluated from derivatives of (6.2), but are evaluated here instead from the corresponding implicit forms (6.1)(c) and (6.1)(f). For a fixed viewing direction, the differential $d\xi_{SG}$ along the silhouette generator is obtained by differentiating a form equivalent to (6.1)(c), namely

$$-\cot\psi = \sin\theta \tan(\xi-\phi)$$

$$\frac{d\psi}{\sin^2\psi} = \sin\theta \frac{d\xi}{\cos^2(\xi-\phi)}$$

which can be simplified, using (6.1)(g) and (6.1)(h).

$$d\xi_{SG} = \frac{\cos\alpha}{\cos\eta} d\psi \tag{6.3}$$

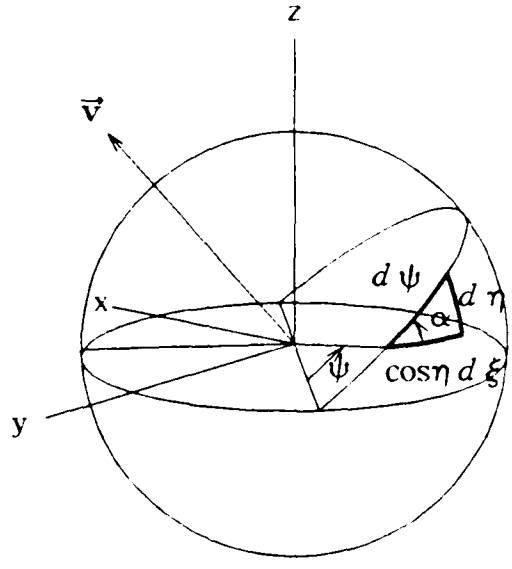

Fig.6.3. Relation between Angle Differentials on the Slice.

The expression for $d\,\eta_{SG}$ is obtained by differentiating (6.1)(f).

$$\sin\eta = \cos\theta\,\sin\psi$$

$$-\cos\eta\,d\,\eta = -\cos\theta\,\cos\psi\,d\,\psi$$

This can be further simplified using (6.1)(d).

$$d\,\eta_{SG} = \sin\alpha\,d\,\alpha \tag{6.4}$$

As a result, the normalized differential $d\,\vec{\xi}_{SG}$ has the following form

$$d\,\vec{\xi}_{SG} = \begin{vmatrix} \cos\eta_{SG}\,d\,\xi_{SG} \\ d\,\eta_{SG} \end{vmatrix} = \begin{vmatrix} \cos\alpha_{SG} \\ \sin\alpha_{SG} \end{vmatrix} d\,\psi \tag{6.5}$$

where α_{SG} refers to the value of α on the silhouette generator. This relation confirms the geometrical intuition suggested by Fig.6.3.

6.2. Projection of the Silhouette Generator

In the previous section, the set of points of the object property sphere which are directly related to the silhouette was determined. In this section, a procedure for relating values of the property functions of the silhouette to the values of the property functions of the object is developed. This procedure consists of formally expressing coordinates of silhouette generator points in terms of the transforms of the object and applying the classical projection operation to these forms. Expressions for the inverse transforms of the property spheres are simplest when object coordinates are expressed in rotated axes at each point; they are given by

$$\vec{x}_R(\xi,\eta) = \begin{vmatrix} p(\xi,\eta) \\ p_\xi(\xi,\eta)/\cos\eta \\ p_\eta(\xi,\eta) \end{vmatrix}$$

$$\vec{x}_R(\xi,\eta) = \begin{vmatrix} n(\xi,\eta) \\ h(\xi,\eta) \\ v(\xi,\eta) \end{vmatrix} = \vec{s}(\xi,\eta) \tag{6.6}$$

$$d\,\vec{x}_R(\xi,\eta) = \begin{vmatrix} 0 & 0 \\ 1 & 0 \\ 0 & 1 \end{vmatrix} \begin{vmatrix} r_{11}(\xi,\eta) & r_{12}(\xi,\eta) \\ r_{12}(\xi,\eta) & r_{22}(\xi,\eta) \end{vmatrix} \begin{vmatrix} d\,\xi/\cos\eta \\ d\,\eta \end{vmatrix} = \mathbf{I}_{32}\,\bar{\mathbf{R}}(\xi,\eta)\,d\,\vec{\xi}$$

The rotated coordinates of points on the silhouette generator are easily obtained from the above expressions by replacing (ξ,η) by their values on the silhouette generator as given in equation (6.2).

$$\left|\begin{array}{rl} \vec{\mathbf{x}}_R(\psi) = & \begin{vmatrix} p(\xi_{SG}(\psi),\eta_{SG}(\psi)) \\ p_\xi(\xi_{SG}(\psi),\eta_{SG}(\psi))/\cos\eta_{SG}(\psi) \\ p_\eta(\xi_{SG}(\psi),\eta_{SG}(\psi)) \end{vmatrix} \\ \vec{\mathbf{x}}_R(\psi) = & \vec{\mathbf{s}}(\xi_{SG}(\psi),\eta_{SG}(\psi)) \\ d\,\vec{\mathbf{x}}_R(\psi) = & \mathbf{I}_{32}\,\bar{\bar{\mathbf{R}}}(\xi_{SG}(\psi),\eta_{SG}(\psi))\,d\,\boldsymbol{\xi}_{SG} \end{array}\right. \tag{6.7}$$

Note that the variables (ξ,η) must be considered as independent when evaluating derivatives p_ξ, p_η for the expression of the ST. However, the differentials $d\,\xi$, $d\,\eta$ in the expression for the CT must be taken along the great circle slice; their relations to $d\,\psi$ are given in (6.5).

The projection of points of the silhouette generator is now addressed. Coordinates of silhouette points can be obtained by first converting the coordinates in rotated frames in (6.7) to coordinates in global object axes by the transformation in (3.9), then applying the projection transformation (3.21). Coordinates of silhouette points in global axes of the projection plane are hence obtained from the rotated coordinates of the object by

$$\mathbf{x}_\pi(\psi) = \mathbf{I}_{23}\,\mathbf{R}_3^{G-C}\,\mathbf{R}_3^{R-G}(\xi_{SG}(\psi),\eta_{SG}(\psi))\,\vec{\mathbf{x}}_R(\psi) \tag{6.8}$$

The operations described in the above equation correspond to the 3-D rotation $\mathbf{R}_3^{R-G}$ from rotated to global coordinates, followed by the 3-D rotation $\mathbf{R}_3^{G-C}$ from global to camera axes, and finally the projection $\mathbf{I}_{23}$ along the first coordinate axis of the camera frame. The composition of the two rotations in the above equation is a third rotation which will be denoted by $\mathbf{R}_3^{R-C}$ and which relates coordinates in the camera axes to coordinates in rotated axes.

This rotation is explicitly written as

$$\mathbf{R}_3^{R-C} = \mathbf{R}_3^{G-C}\,\mathbf{R}_3^{R-G} \tag{6.9}$$

$$= \begin{vmatrix} \cos\phi\cos\theta & \sin\phi\cos\theta & \sin\theta \\ -\sin\phi & \cos\phi & 0 \\ -\cos\phi\sin\theta & -\sin\phi\sin\theta & \cos\theta \end{vmatrix} \begin{vmatrix} \cos\xi\cos\eta & -\sin\xi & -\cos\xi\sin\eta \\ \sin\xi\cos\eta & \cos\xi & -\sin\xi\sin\eta \\ \sin\eta & 0 & \cos\eta \end{vmatrix}$$

$$= \begin{vmatrix} \cos\theta\cos\eta\cos(\xi-\phi) + \sin\theta\sin\eta & -\cos\theta\sin(\xi-\phi) & -\cos\theta\sin\eta\cos(\xi-\phi) + \sin\theta\cos\eta \\ \cos\eta\sin(\xi-\phi) & \cos(\xi-\phi) & -\sin\eta\sin(\xi-\phi) \\ -\cos\eta\sin\theta\cos(\xi-\phi) + \sin\eta\cos\theta & \sin\theta\sin(\xi-\phi) & \sin\eta\sin\theta\cos(\xi-\phi) + \cos\theta\cos\eta \end{vmatrix}$$

When only rotated axes corresponding to points on the silhouette generator are considered, the angles in the above rotation matrix are related by the expressions in (6.1). The expression of $\mathbf{R}_3^{R-C}$ can then be simplified substantially. After tedious but straightforward trigonometric manipulations, it can be shown that

$$\mathbf{R}_3^{R-C}(\xi_{SG}, \eta_{SG}) = \begin{vmatrix} 0 & -\sin\alpha_{SG} & \cos\alpha_{SG} \\ \cos\psi & -\cos\alpha_{SG}\sin\psi & -\sin\alpha_{SG}\sin\psi \\ \sin\psi & \cos\alpha_{SG}\cos\psi & \sin\alpha_{SG}\cos\psi \end{vmatrix}$$

$$= \begin{vmatrix} 0 & 0 & 1 \\ \cos\psi & -\sin\psi & 0 \\ \sin\psi & \cos\psi & 0 \end{vmatrix} \begin{vmatrix} 1 & 0 & 0 \\ 0 & \cos\alpha_{SG} & \sin\alpha_{SG} \\ 0 & -\sin\alpha_{SG} & \cos\alpha_{SG} \end{vmatrix} \tag{6.10}$$

This result can also be derived derived through geometrical reasoning on the composition of the two rotations in equation (6.9). Referring to Fig.6.4, the rotation from rotated to camera axes links coordinates in axes parallel to the local orientations $\vec{\mathbf{i}}_n$, $\vec{\mathbf{i}}_\xi$, $\vec{\mathbf{i}}_\eta$, with coordinates in the global silhouette axes x_π, z_π, which are parallel to $\vec{\mathbf{i}}_{n0}$, $\vec{\mathbf{i}}_{t0}$. It is clear that these two axes can be aligned with $\vec{\mathbf{i}}_n$, $\vec{\mathbf{i}}_\xi$ by a rotation around $\vec{\mathbf{i}}_n$ with an angle α, followed by a rotation with an angle ψ around the rotated $\vec{\mathbf{i}}_\eta$ axis.

The transformation from rotated object coordinates $\vec{\mathbf{x}}_R$ to global silhouette coordinates $\mathbf{x}_\pi$ in the image plane is obtained by combining the above rotations with the projection operator $\mathbf{I}_{23}$, producing

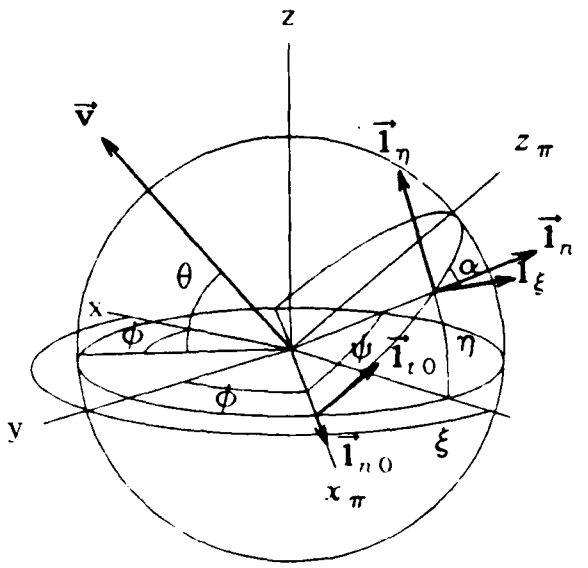

Fig.6.4. Illustration of the Composition of Rotations.

$$\mathbf{x}_\pi = \mathbf{I}_{23}\, \mathbf{R}_3^{G-C}\, \vec{\mathbf{x}}_R$$

$$\begin{pmatrix} x_\pi \\ z_\pi \end{pmatrix} = \begin{pmatrix} 0 & 1 & 0 \\ 0 & 0 & 1 \end{pmatrix} \begin{pmatrix} 0 & -\sin\alpha_{SG} & \cos\alpha_{SG} \\ \cos\psi & -\cos\alpha_{SG}\sin\psi & -\sin\alpha_{SG}\sin\psi \\ \sin\psi & \cos\alpha_{SG}\cos\psi & \sin\alpha_{SG}\cos\psi \end{pmatrix} \begin{pmatrix} x_R \\ y_R \\ z_R \end{pmatrix}$$

$$= \begin{pmatrix} \cos\psi & -\cos\alpha_{SG}\sin\psi & -\sin\alpha_{SG}\sin\psi \\ \sin\psi & \cos\alpha_{SG}\cos\psi & \sin\alpha_{SG}\cos\psi \end{pmatrix} \begin{pmatrix} x_R \\ y_R \\ z_R \end{pmatrix} \tag{6.11}$$

$$= \begin{pmatrix} \cos\psi & -\sin\psi \\ \sin\psi & \cos\psi \end{pmatrix} \begin{pmatrix} 1 & 0 & 0 \\ 0 & \cos\alpha_{SG} & \sin\alpha_{SG} \end{pmatrix} \begin{pmatrix} x_R \\ y_R \\ z_R \end{pmatrix}$$

where the last form was obtained using the factorization of $\mathbf{R}_3^{G-C}$ in (6.10). Comparison of this form with (3.7) suggests that a simpler expression for the imaging transformation is obtained by expressing silhouette coordinates in rotated 2-D frames.

$$\mathbf{x}_{\pi R} = \mathbf{R}_2^{G-R}(\psi)\,\mathbf{x}_{\pi} = \begin{bmatrix} 1 & 0 & 0 \\ 0 & \cos\alpha_{SG} & \sin\alpha_{SG} \end{bmatrix} \begin{bmatrix} x_R \\ y_R \\ z_R \end{bmatrix} \tag{6.12}$$

This expression is now rewritten for the individual components of the silhouette coordinate vector in the rotated frame.

$$\begin{cases} x_{\pi R} &= x_R \\ z_{\pi R} &= y_R \cos\alpha_{SG} + z_R \sin\alpha_{SG} \end{cases} \tag{6.13}$$

This simple expression is a key element in the derivation of the three Silhouette-Slice theorems described in the next section. It formally expresses that for points on the silhouette generator represented by coordinates in rotated axes, normal components are unaffected by the projection operation. Components along the tangent plane are projected as a 2-vector in the tangent plane to produce the corresponding silhouette coordinate along the tangent in the projection plane. This relation between rotated coordinates on the silhouette generator of the object and on the silhouette is illustrated in Fig.6.5. The orientation involved in the above projection is the angle α_{SG} characterizing the orientation of the slice in local axes of the Gaussian sphere. Note the equivalence of the first equation with the relation derived for the normal distance to tangents in Chapter 4, specifically in equation (4.31).

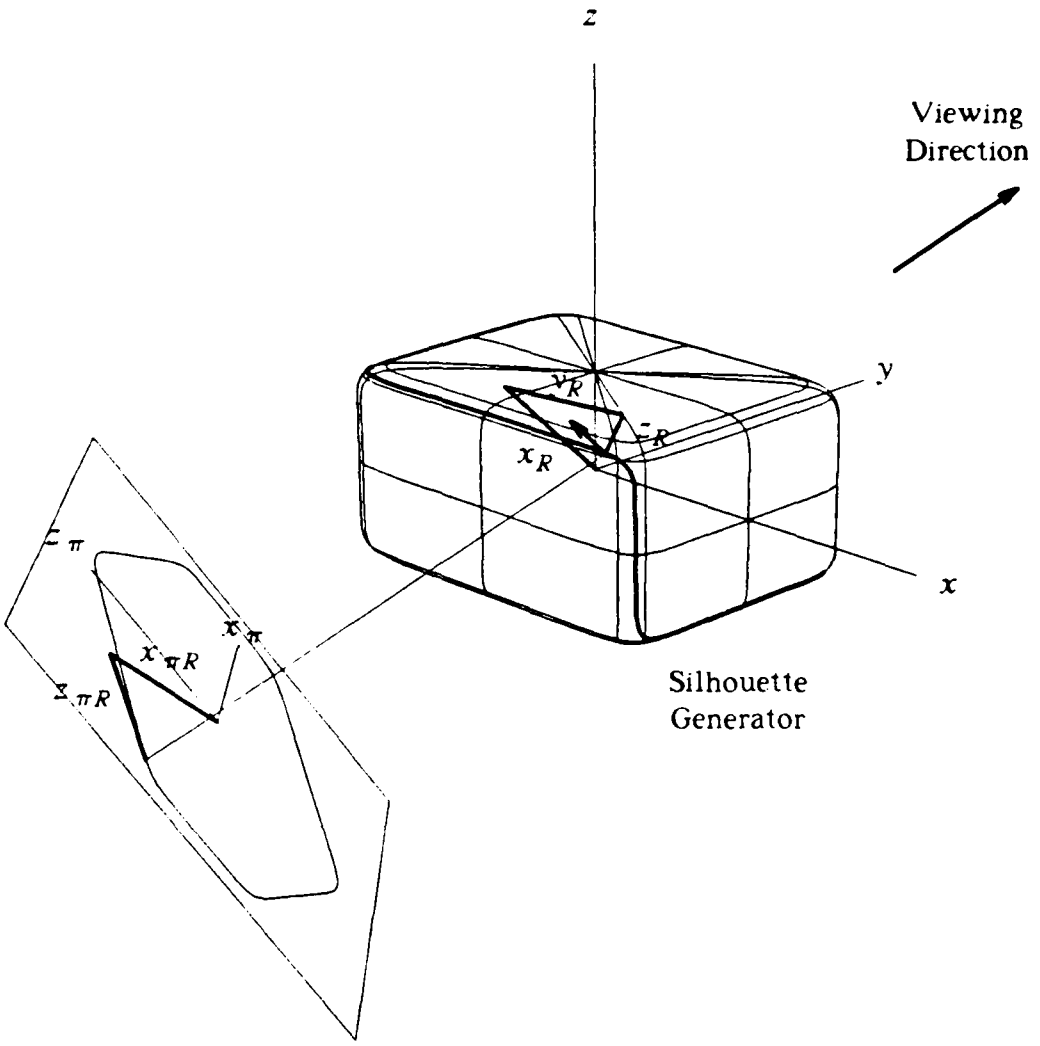

Fig.6.5. Projection of Rotated Coordinates.

6.3. Property Circles of Silhouettes

In this section, formal expressions for silhouettes in terms of the 3-D transforms of the object are obtained by applying the projection transformation in (6.13) to the coordinates of points on the silhouette generator in terms of the 3-D object transforms in equation (6.2). The resulting expressions are then related to the corresponding 2-D transforms of the silhouettes to obtain a direct relation between 3-D transforms of the object and 2-D transforms of its silhouettes. These relations will be formalized as three Silhouette-Slice theorems.

6.3.1. Silhouette-Slice Theorem for the Support Transform

When the imaging transformation for rotated coordinates in (6.13) is applied to the rotated coordinates of silhouette generator points expressed in terms of the ST in (6.6), the following equation is obtained for the silhouette coordinates in rotated local axes.

$$\begin{bmatrix} x_{\pi R} \\ z_{\pi R} \end{bmatrix} = \begin{bmatrix} p \\ p_{\xi} \cos\alpha_{SG} \,/\, \cos\eta_{SG} + p_{\eta} \sin\alpha_{SG} \end{bmatrix} \tag{6.14}$$

where p and its derivatives in the right hand side must be evaluated at $\xi=\xi_{SG}$, $\eta=\eta_{SG}$, so that the right hand side is implicitly parameterized in ψ through ξ_{SG}, η_{SG} and α_{SG}. This expression can be compared with the expression for rotated coordinates in terms of the 2-D ST, namely

$$\begin{bmatrix} x_{\pi R} \\ z_{\pi R} \end{bmatrix} = \begin{bmatrix} p_{\pi} \\ \partial p_{\pi}/\partial\psi \end{bmatrix} \tag{6.15}$$

where the index in p_{π} indicates that this normal distance is relative to the silhouette in the image plane. The equality between the first components in (6.15) reveals that the ST function of the silhouette, $p_{\pi}(\psi)$, is identical to the 3-D ST on the slice of the Gaussian sphere of the object.

$$p_{\pi}(\psi) = p(\xi_{SG}(\psi), \eta_{SG}(\psi)) \tag{6.16}$$

The identity between the second components of (6.15), and (6.14) is consistent with the following evaluation of the partial derivative $\partial p_\pi / \partial \psi$.

$$\frac{\partial p_\pi}{\partial \psi} = \frac{\partial p}{\partial \psi} = \frac{\partial p}{\partial \xi} \frac{d\,\xi_{SG}}{d\,\psi} + \frac{\partial p}{\partial \eta} \frac{d\,\eta_{SG}}{d\,\psi} = p_\xi \frac{\cos\alpha_{SG}}{\cos\eta_{SG}} + p_\eta \sin\alpha_{SG} \tag{6.17}$$

where (6.5) was used to determine $d\,\xi/d\,\psi$ and $d\,\eta/d\,\psi$. The relation between the ST of the silhouette and the ST of the object is formalized as follows:

Silhouette-Slice Theorem 1: *The 2-D Support Transform of an orthographic silhouette of a smooth convex object is the restriction of the 3-D Support Transform of the object surface to the great-circle slice parallel to the projection plane.*

This theorem indicates a silhouette construction method identical to the last method presented in Chapter 4.

6.3.2. Silhouette-Slice Theorem for the Vector Support Transform

When the imaging transformation for rotated coordinates in (6.13) is applied to the rotated coordinates of silhouette generator points expressed in terms of the VST in (6.6), the following expression is obtained for the silhouette coordinates in rotated axes.

$$\begin{pmatrix} x_{\pi R} \\ z_{\pi R} \end{pmatrix} = \begin{pmatrix} n \\ h\cos\alpha_{SG} + v\sin\alpha_{SG} \end{pmatrix} \tag{6.18}$$

where the components (n, h, v) must be evaluated for $\xi = \xi_{SG}$, $\eta = \eta_{SG}$, so that the right hand side implicitly depends on ψ through ξ_{SG}, η_{SG} and α_{SG}. This expression can be compared with the expression of coordinates in rotated axes in terms of the VST, namely

$$\begin{pmatrix} x_{\pi R} \\ z_{\pi R} \end{pmatrix} = \begin{pmatrix} n_\pi \\ t_\pi \end{pmatrix}$$

where the indices in the components n_π, t_π indicate that these correspond to the silhouette in the image plane.

This comparison implies that the relation between the 3-D VST of the object and the 2-D VST of the silhouette is given by

$$\begin{cases} n_{\pi}(\psi) = & n(\xi_{SG}(\psi),\eta_{SG}(\psi)) \\ t_{\pi}(\psi) = & h(\xi_{SG}(\psi),\eta_{SG}(\psi))\cos\alpha_{SG}(\psi) + v(\xi_{SG}(\psi),\eta_{SG}(\psi))\sin\alpha_{SG}(\psi) \end{cases} \tag{6.19}$$

The above equation for the projection of the VST components has the same geometrical interpretation as the projection of rotated coordinates illustrated in Fig.6.5. The relation between the 3-D VST and the 2-D VST is formalized in the following theorem:

Silhouette-Slice Theorem 2: *The 2-D Vector Support Transform of an orthographic silhouette of a smooth convex object is obtained by considering the restriction of the 3-D Vector Support Transform of the object surface to the great-circle slice parallel to the projection plane. The normal component of the 2-D VST is identical to its 3-D counterpart on the slice, and the tangential component of the 2-D VST is obtained by projecting the tangential part of the 3-D VST as a 2-vector onto the projection plane.*

6.3.3. Silhouette-Slice Theorem for the Curvature Transform

When the imaging transformation (6.13) is applied to the differentials of coordinates of silhouette generator points in rotated coordinates in terms of the CT representation (6.6), then combined with the expression for the differentials of the angular variables on the slice in (6.5), the following differentials are obtained for the silhouette coordinates in rotated axes

$$\begin{pmatrix} dx_{\pi R} \\ dz_{\pi R} \end{pmatrix} = \begin{pmatrix} 1 & 0 & 0 \\ 0 & \cos\alpha_{SG} & \sin\alpha_{SG} \end{pmatrix} \begin{pmatrix} 0 & 0 \\ 1 & 0 \\ 0 & 1 \end{pmatrix} \begin{pmatrix} r_{11} & r_{12} \\ r_{12} & r_{22} \end{pmatrix} \begin{pmatrix} \cos\alpha_{SG} \\ \sin\alpha_{SG} \end{pmatrix} d\psi \tag{6.20}$$

Combining the first two matrices on the right-hand side reveals that $dx_{\pi R} = 0$ and that

$$dz_{\pi R} = \begin{pmatrix} \cos\alpha_{SG} & \sin\alpha_{SG} \end{pmatrix} \begin{pmatrix} r_{11} & r_{12} \\ r_{12} & r_{22} \end{pmatrix} \begin{pmatrix} \cos\alpha_{SG} \\ \sin\alpha_{SG} \end{pmatrix} d\psi$$

Comparison of this equation with the expression of the 2-D differential of silhouette coordinates in terms of the 2-D CT, namely $dz_{\pi R} = \rho(\psi)d\psi$, reveals that the CT function $\rho(\psi)$ of the silhouette is related to the 3-D CT function by

$$\rho(\psi) = \begin{pmatrix} \cos\alpha_{SG} & \sin\alpha_{SG} \end{pmatrix} \begin{pmatrix} r_{11SG} & r_{12SG} \\ r_{12SG} & r_{22SG} \end{pmatrix} \begin{pmatrix} \cos\alpha_{SG} \\ \sin\alpha_{SG} \end{pmatrix} \qquad (6.21)$$

where the dependence of the right-hand side on ψ is implicit through α_{SG} and $r_{ijSG} = r_{ij}(\xi_{SG}, \eta_{SG})$. The right-hand side of (6.21) is the projection of $\bar{\bar{\mathbf{R}}}$ along the direction given by $\cos\alpha_{SG}$, $\sin\alpha_{SG}$. As the tensor of curvature is defined in the tangent plane, (6.21) exactly corresponds to a projection of this tensor onto the trace of the image plane in the tangent plane. This relation between silhouette curve CT and object surface CT is formalized as follows:

Silhouette-Slice Theorem 3: *The 2-D Curvature Transform of an orthographic silhouette of a smooth convex object is obtained by considering only the restriction of the 3-D Curvature Transform of the object surface to the great-circle slice parallel to the projection plane, and projecting the tensor-valued object function on the slice onto the projection plane.*

In addition to relating the property functions for the CT, equation (6.21) indicates a remarkable result relating the radius of curvature of the silhouette to the radius of curvature tensor at the corresponding point of the object surface. Remembering that α_{SG} is the angle between the local y_l-axis and the plane of the slice, the above equation indicates that the radius of curvature of the silhouette is the projection of the tensor of radius of curvature on the plane of the slice. This result is the dual of a well known theorem due to Euler in the geometry of surfaces. Both Euler's theorem and its dual are discussed in more detail in Appendix 3.

6.4. Example: Silhouette of a Sphere

The Silhouette-Slice theorems are illustrated in this section by the simple example of a sphere of radius R centered at $P_0(x_0, y_0, z_0)$, as illustrated in Fig.6.6. The three transforms of this sphere were evaluated in section 5.2.6. Although this particular example could be solved by a number of alternative methods, the approach used here provides insight into the mechanism of analytic silhouette evaluation with the

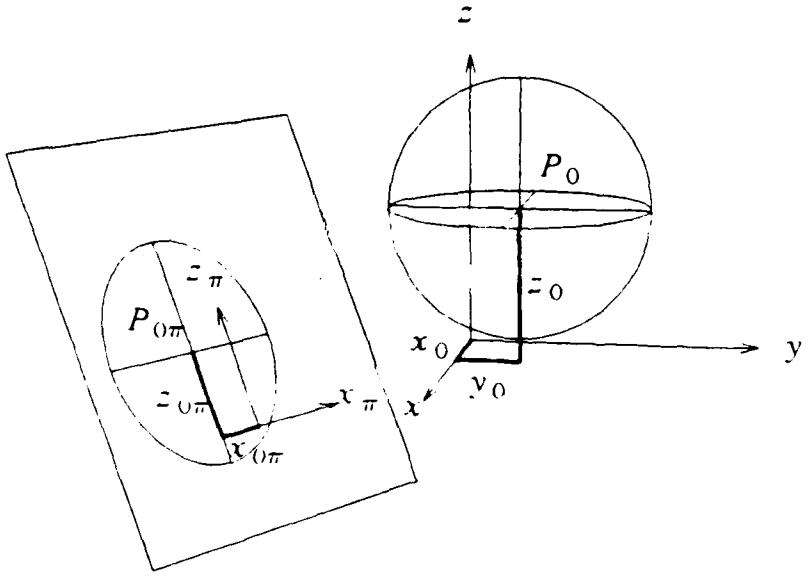

Fig.6.6. Projection of a Sphere

Silhouette-Slice theorems. More complex illustrations of the Silhouette-Slice theorems are provided in Chapter 8.

The 3-D ST of the sphere is given by

$$p(\xi,\eta) = x_0 \cos\xi\cos\eta + y_0 \sin\xi\cos\eta + z_0 \sin\eta + R \tag{6.22}$$

For a viewing direction (ϕ,θ), the 2-D ST of the silhouette is obtained from the above expression with equation (6.16), as

$$p_\pi(\psi) = x_0 \cos\xi_{SG} \cos\eta_{SG} + y_0 \sin\xi_{SG} \cos\eta_{SG} + z_0 \sin\eta_{SG} + R \tag{6.23}$$

where ξ_{SG}, η_{SG} implicitly depend on (ϕ,θ,ψ) by equation (6.2). Replacing ξ_{SG}, η_{SG} by these expressions, performing trigonometric manipulations and rearranging terms produces

$$\begin{aligned} p_\pi &= (-x_0 \sin\phi + y_0 \cos\phi)\cos\psi \\ &\quad + (-x_0 \sin\theta\cos\phi - y_0 \sin\theta\sin\phi + z_0 \cos\phi)\sin\psi + R \end{aligned} \tag{6.24}$$

The coefficients of $\cos\psi$ and $\sin\psi$ in the above expression can be recognized as the coordinates $x_{0\pi}, z_{0\pi}$ of the projection in the image plane of P_0, the center of the sphere.

Indeed, these coordinates are related to the 3-D coordinates (x_0,y_0,z_0) by

$$\begin{pmatrix} x_{0\pi} \\ z_{0\pi} \end{pmatrix} = \begin{pmatrix} 0 & 1 & 0 \\ 0 & 0 & 1 \end{pmatrix} \begin{pmatrix} \cos\phi\cos\theta & \sin\phi\cos\theta & \sin\theta \\ -\sin\phi & \cos\phi & 0 \\ -\cos\phi\sin\theta & -\sin\phi\sin\theta & \cos\theta \end{pmatrix} \begin{pmatrix} x_0 \\ y_0 \\ z_0 \end{pmatrix} \tag{6.25}$$

The 2-D ST of the silhouette is hence given by

$$p_\pi(\psi) = x_{o\,\pi}\cos\psi + z_{0\pi}\sin\psi + R \tag{6.26}$$

This expression is identical to the 2-D ST of a circle of radius R centered at $(x_{0\pi},z_{0\pi})$.

The 3-D VST of the sphere is given by

$$\vec{\mathbf{s}}(\xi,\eta) = \begin{pmatrix} x_0\cos\xi\cos\eta + y_0\sin\xi\cos\eta + z_0\sin\eta + R \\ -x_0\sin\xi + y_0\cos\xi \\ -x_0\cos\xi\sin\eta - y_0\sin\xi\sin\eta + z_0\cos\eta \end{pmatrix} \tag{6.27}$$

The 2-D VST of the silhouette is obtained from the above expression by applying equation (6.19). The resulting normal component of the VST is, by definition, identical to the 2-D ST derived above. The tangential component is given by

$$t_\pi(\psi) = \cos\alpha_{SG}\; h(\xi_{SG},\eta_{SG}) + \sin\alpha_{SG}\; v(\xi_{SG},\eta_{SG}) \tag{6.28}$$

The angles ξ,η,α in the above expression are replaced in terms of ϕ,θ,ψ using (6.1) and (6.2). After trigonometric manipulations, the result is found to be

$$t_\pi(\psi) = -x_{0\pi}\sin\psi + z_{0\pi}\cos\psi \tag{6.29}$$

where $x_{0\pi}$, $z_{0\pi}$ are as defined above. The above result is identical to the tangential component of the VST of a circle centered at $(x_{0\pi},z_{0\pi})$.

The 3-D CT of the sphere was obtained in section 5.2.6. as

$$\bar{\bar{\mathbf{R}}} = \begin{pmatrix} R & 0 \\ 0 & R \end{pmatrix} \tag{6.30}$$

The 2-D CT of the silhouette is obtained from the 3-D CT of the object with equation (5.21) as

$$\rho(\psi) = \begin{vmatrix} \cos\alpha_{SG} & \sin\alpha_{SG} \end{vmatrix} \begin{vmatrix} R & 0 \\ 0 & R \end{vmatrix} \begin{vmatrix} \cos\alpha_{SG} \\ \sin\alpha_{SG} \end{vmatrix} = R \qquad (6.31)$$

which is obviously the 2-D CT of a circle of radius R. Note that the ST is independent of translations so that the position of the silhouette cannot be predicted by the construction with the CT. The independence of the CT on translations is an advantage in some applications, a disadvantage in others. Relative merits of the various transforms and Silhouette-Slice theorems are discussed in Chapter 8 in the context of applications presented there.

6.5. Discussion

In this chapter, theorems have been proposed to relate representations of silhouette curves in terms of functions on their Gaussian circles to the corresponding representations of object surfaces in terms of functions on the Gaussian sphere. Two additional aspects of the Silhouette-Slice theory will be discussed in this section, namely its relation with the Projection-Slice theorem in computerized tomography, and an interpretation of the 3-D transforms as compact representations of the collection of all silhouettes of an object.

6.5.1. Comparison: Silhouette-Slice Theorems and Projection-Slice Theorem

The formal relations among an opaque convex object, its silhouettes, and their representations on Gaussian images are sketched in Fig.6.7. The concept of this diagram bears a strong similarity with that relating an absorbing object, its line-integral projections and their Fourier Transforms, sketched in Fig.6.8. This last set of relations is important in the field of computerized tomography, and is referred to as the Projection-Slice Theorem to stress the duality between projection in object space and slicing in transform space. The similarity between this result and the new relations presented in this thesis has suggested the name of Silhouette-Slice Theorems for the new relations, to stress the duality between silhouette construction in the object domain and slicing in the model domain.

In spite of the formal similarity between the Projection-Slice theory and the Silhouette-Slice theory, there are substantial differences between the two formalisms. First, the Projection-Slice theorem applies to absorbing objects which can be defined by

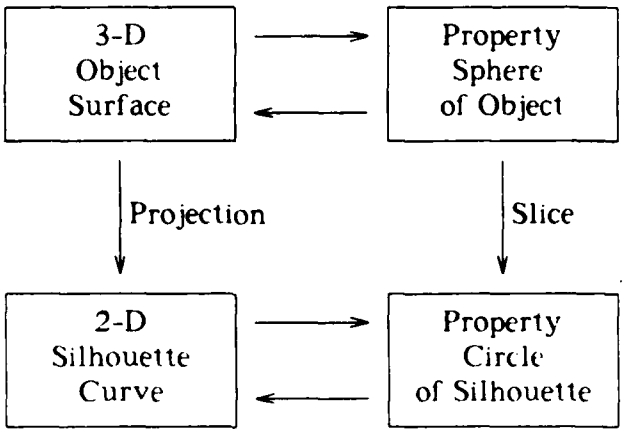

Fig.6.7. Block Diagram for the Silhouette-Slice Concept

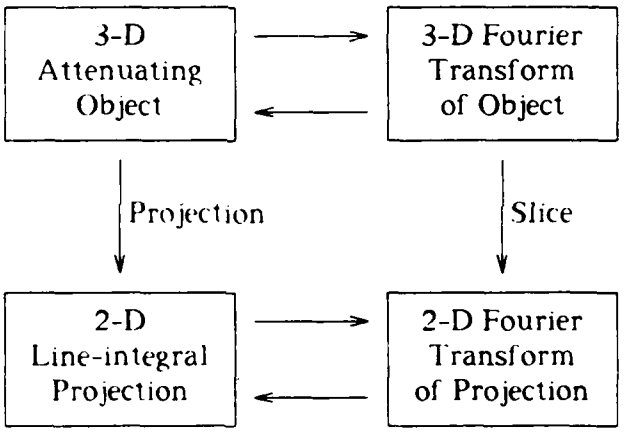

Fig.6.8. Block Diagram for the Projection-Slice Theorem

a real-valued function defined in 3-space, whereas the Silhouette-Slice theorems apply to opaque objects which can be described by functions of two variables, or by functions with binary values defined in 3-space. Second, the Fourier transform used in the Projection-Slice theorem is an integral transform, where each value of the transform depends on all the values of the function specifying the object. On the other hand, the transforms of opaque objects defined in Chapter 5 of this thesis are point transformations where each value of the transform depends only on the value of a function defining the object at one point.

It is possible that a theory of silhouettes comparable to the one presented in this thesis could be obtained by modeling an opaque object as an object with a finite uniform absorption coefficient, to which the Projection-Slice theory applies, then considering the limit of the line-integral projection when the absorption coefficient becomes infinite. This approach to silhouette analysis would provide a nice bridge between theories for absorbing objects and for opaque objects, but we have not been able to find an appropriate formulation for the limiting argument.

6.5.2. 3-D Transforms as Compact Representations of Silhouettes

The relation between slices of 3-D transforms of objects on the Gaussian sphere and 2-D transforms of silhouettes leads to the interpretation of the 3-D transforms as indirect representations of the set of all silhouettes of a convex object. Indeed, for any given orientation of the viewing direction, simple representations of the silhouette, namely the ST, the VST and the CT, are obtained by slicing the corresponding 3-D representation of the object. It is worthwhile to emphasize that this type of construction is possible only for selected representations of the silhouettes. It is tempting to investigate the existence of other 3-D representations of objects, for which a slice would be related to the silhouette by expressions simpler than the inverses of the ST, VST and CT. For example, one could try to construct a "dual" object, such that a silhouette of the original object is identical to a slice of the dual object. A simple counter-example suggests that this construction fails in most cases.

Consider a cube and the silhouettes of this cube obtained for a set of viewing directions covering a 180° arc around the cube; this set of directions and one particular silhouette are represented in Fig.6.9 a). If a "dual" object of the cube exists, it can be constructed by superimposing the set of silhouettes corresponding to the viewing directions in Fig.6.9 around a center, while keeping their respective orientations. The resulting object is shown in Fig.6.9b), where the contribution of the particular silhouette illustrated in Fig.6.9a) is drawn in bold. It is easy to see that this object does not have the desired property by considering a viewing direction outside the set used to synthesize this candidate dual object. One such viewing direction is shown in Fig.6.9a) and the corresponding slice in Fig.6.9b). This slice is quite different from the actual silhouette, which is a perfect square. As each silhouette of a 3-D object is two-

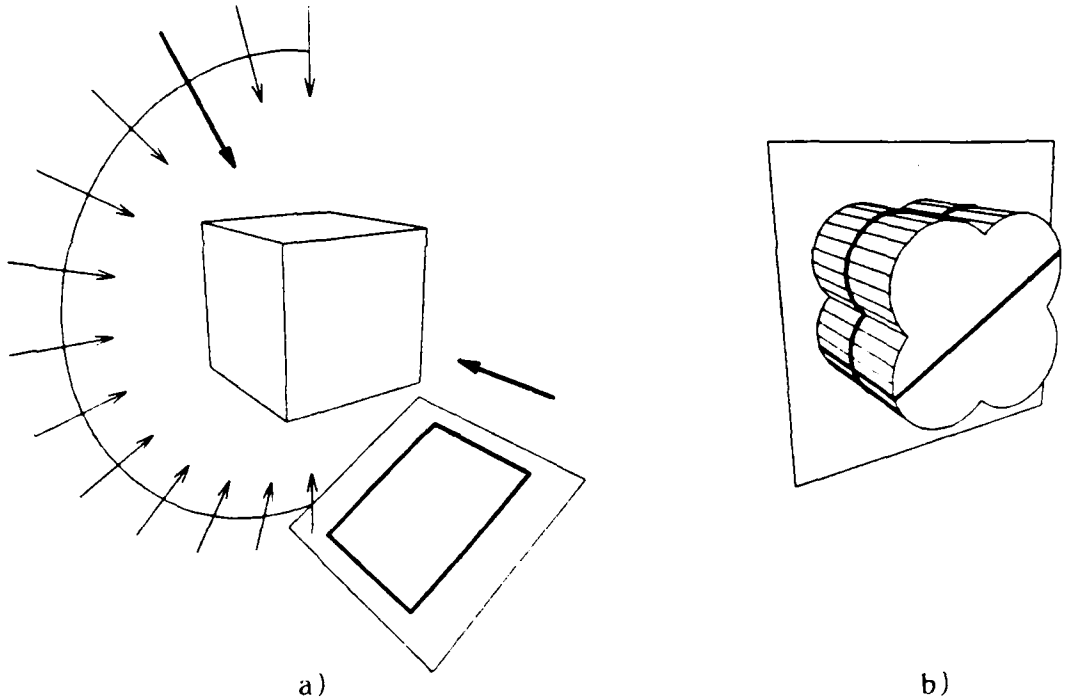

a) b)

Fig.6.9. Counter-Example of a Direct Representation of all Silhouettes.
a) Object, a particular silhouette and the set of viewing directions.
b) Dual object constructed from a set of silhouettes, and a test slice.

dimensional and as the set of viewing directions is two-dimensional also, a "dual" object whose slices are the silhouettes of the original object is necessarily four-dimensional, unless special relations among individual silhouettes are exploited.

The three transforms presented in Chapter 5 are compact representations of the set of all silhouettes of the object, as they are only three-dimensional as is the object itself. In order to obtain this compactness of representations, redundancies among individual silhouettes must be detected and exploited. The existence of redundancies between the set of all silhouettes of a single object are now discussed, together with their impact on the representations of silhouettes and 3-D objects.

Redundancies among silhouettes of an object can be expected in the general case only when relating the contribution of the same surface element in different silhouettes. Consider the set S_i of all silhouettes for which the point P_0 on the object surface is on the silhouette generator. This set of silhouettes corresponds to all the

viewing directions perpendicular to the normal $\vec{n}_0$ at P_0; see Fig.6.10. Let $P_{0\pi i}$ be the projection of P_0 on each silhouette S_i. We have identified three properties of the silhouette curves around the points $P_{0\pi i}$ which have a high degree of redundancy among the different silhouettes S_i. The first two properties are the projections onto the normal and tangent at $P_{0\pi i}$ of the vector from the origin $O_{\pi i}$ to $P_{0\pi i}$. The third property is the radius of curvature, ρ_i, of the silhouette curve at $P_{0\pi i}$. It is straightforward to show that the normal components of the vector $O_\pi \vec{P}_{0\pi i}$ are identical for all silhouettes and that the tangential components of these vectors are the result of the vector projection of a single 2-vector in the tangent plane. Finally, the relation between the curvatures of the S_i's at $P_{0\pi i}$ is given by the dual of Euler's theorem discussed in Appendix 3. This theorem shows that the radii ρ_i depend on the orientation of the viewing direction as a function specified by only three independent parameters, namely the components of the 2x2 tensor of curvature of the surface at P_0.

The above argument clarifies the redundancy between silhouettes corresponding to different viewing directions. This redundancy is now related to property circles and spheres by considering the image P_{0G} of P_0 on the Gaussian sphere, the property sphere value at P_{0G}, and the values of the various silhouette property circles at P_{0G}. It is easy to see that the slices corresponding to the set S_i are all the great circles

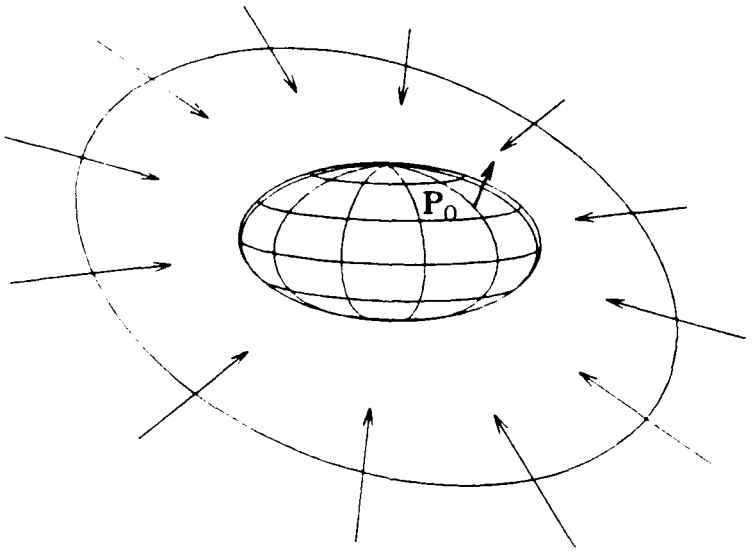

Fig.6.10. Set of Viewing Directions for which P_0 is on the Silhouette Generator.

passing through P_{0G} drawn on Fig.6.11. The relations between property circles defined on these slices at the point P_{0G} correspond to the relations between silhouette properties at $P_{0\pi i}$. For the transforms defined in Chapter 5, the ST property functions have the same value on each slice at P_{0G}, the VST tangential functions are projections of a single 2-vector, and the CT functions are projections of a 2x2 tensor.

We have shown in this section that the Silhouette-Slice theorems provide an interpretation of the 3-D transforms as compact representations of the set of all silhouettes of a convex object. In addition, we have shown which type of constraints must be satisfied by property circles for constructing compact 3-D representations of silhouettes. It is conjectured that, aside from higher order properties corresponding to terms of order 3 and higher of Taylor expansions of curves and surfaces, there are no property spheres and circles representing metric information, other than the ST, VST and CT, for which the Silhouette-Slice theory applies.

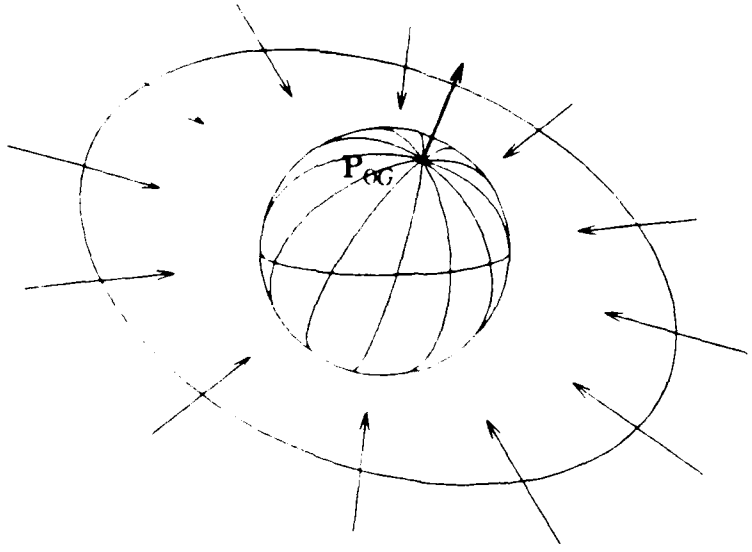

Fig.6.11. Slices of the Gausian Sphere corresponding to Silhouettes including P_0.

6.6. Summary

In this chapter, theorems have been proposed to relate representations of silhouette curves in terms of functions on their Gaussian circles to the corresponding representations of object surfaces in terms of functions on the Gaussian sphere. It was first shown that the silhouette representations are directly related to a great-circle slice of the object representations. In the second step, the silhouette property functions on the Gaussian circle were related to the object property functions on the slice of the Gaussian sphere. The relations are an identity for the ST function and for the normal component of the VST function, a vector projection for the tangential part of the VST function and a tensor projection for the CT function. It is interesting to note the correspondence between the projection operations applied to great circle slices, which are projections of scalars, vectors and tensors, and the observation that the ST, VST and CT depend on derivatives of $p(\psi)$ up to orders 0, 1 and 2 respectively.

The silhouette theory developed in this chapter is applicable to smooth strictly convex objects only. In the following chapter, these results will be extended to objects with corners, edges and planar faces, and to their silhouettes. In Chapter 8, a number of examples of silhouette construction with the three theorems are presented; one of these examples shows that the results are sometimes valid even for non-convex objects. Other potential applications of the Silhouette-Slice theorems are also discussed in Chapter 8.

Chapter 7
Extensions to Surfaces with Edges and Corners and their Silhouettes

In Chapters 5 and 6, a theory relating the shapes of smooth strictly convex object surfaces and the shapes of their silhouettes was developed. In this chapter, extensions of this theory to more general types of objects will be investigated; specifically, object surfaces with abrupt changes of curvature, edges, corners and embedded straight segments will be considered. Using limiting arguments, it will be shown that most of the results developed so far for smooth surfaces can be extended to these types of surfaces. In the first section of this chapter, the basic method for obtaining the extensions is developed. In the subsequent sections, the extensions themselves are analyzed successively for the circular transforms of 2-D curves, for the spherical transforms of 3-D surfaces, and finally for the Silhouette-Slice theorems relating the transforms of the object to the transforms of its silhouettes

7.1. Extensions of Theories developed for Smooth Surfaces

Extensions of the theories developed so far, to include abrupt changes of curvature are trivial. Indeed, continuity of curvatures, which is identical to continuity of second derivatives, was exploited only in the derivation of consistency constraints for the 3-D CT in section 5.2.3.1. Except for these conclusions on consistency, all the theories developed in Chapters 5 and 6 are valid for surfaces with curvature discontinuities and their silhouettes. The other extensions of silhouette analysis will be developed with the following argument. Each convex surface Σ_{NS} ,whether or not smooth and strictly convex, can be considered as the limit of a sequence $\{\Sigma_{Si}\}$ of smooth strictly convex surfaces. In the presence of edges and corners in Σ_{NS}, the sequence $\{\Sigma_{Si}\}$ could be constructed as dilations [56] of the object with balls with radii $1/i$. For each surface Σ_{Si}, the 3-D spherical transform is well defined and can be evaluated by the methods developed in Chapter 5. For a given viewing direction, the Silhouette-Slice theorems apply to these spherical transforms and determine the circular transforms of the silhouettes corresponding to each Σ_{Si}. Finally, these transforms can be inverted to determine the silhouettes S_{Si} of all surfaces Σ_{Si}. If the

initial object surface Σ_{NS} is smooth and strictly convex, the sequence of 3-D transforms of the Σ_{Si} converge to the 3-D transform of Σ_{NS}, the 2-D transforms obtained with the Silhouette-Slice theorem converge to the 2-D transform of the silhouette S_{NS} of Σ_{NS}, and the silhouettes S_i themselves converge to S_{NS}.

Convergence of the above sequences is now investigated in the case where Σ_{NS} does not satisfy the smoothness and/or strict convexity constraints required for the theories developed in Chapters 5 and 6. Although the surface Σ_{NS} is not smooth, its silhouette S_{NS} is well defined, and it is obvious that the sequence of silhouettes $\{S_{Si}\}$ of the surfaces Σ_{Si} converges to the silhouette S_{NS}. However, convergence of the spherical transforms of the Σ_{Si} and of the circular transforms of the S_{Si} is not guaranteed. Since the transforms are defined as functions on the Gaussian images of curves and surfaces, convergence must be analyzed for both the Gaussian mapping itself and for the property functions defined on the Gaussian circle/sphere. Convergence of the mapping is analyzed first. During our analysis of particular discontinuities, it will become apparent that the Gaussian mapping converges to singular mappings in the neighborhood of each discontinuity. Two basic types of singularities will be observed. In the first type, one point of the object is mapped onto many points of the Gaussian image. In the second type of singularity, many points of the object are mapped to the same point of the Gaussian image. For the first type of singularity, each point of the Gaussian image of Σ_{NS} corresponds to a single point of the surface. We will show that in this case, the spherical transforms of Σ_{NS} are well defined and equal to the limits of the transforms of the Σ_{Si}. For the second type of singularity however, only the CT converges in the space of continuous functions. The limits are functions of class C_0 for the VST and generalized functions for the CT.

The extension of the class of surfaces of interest has implications also on the inverse transforms of the circular and spherical functions. The case of the 2-D inverse transforms is considered first. The result of the inverse circular transform is a set of equations parameterized with the normal orientation angle ψ. For a curve with straight segments, a set of equations parameterized with ψ cannot explicitly define all the points of the curve, as is now illustrated by the example of a square with rounded corners.

This curve is sketched in Fig.7.1a) and defined by the parametric equations

$$\begin{vmatrix} x \\ z \end{vmatrix} = \begin{vmatrix} \cos\psi + sign\,(\cos\psi) \\ \sin\psi + sign\,(\sin\psi) \end{vmatrix} \quad 0 \leqslant \psi < 2\pi \tag{7.1}$$

where

$$sign\,(x) = \begin{cases} 1 & \text{for } x > 0 \\ -1 & \text{otherwise} \end{cases}$$

By definition, a curve is the set of points obtained as the image of the domain in parameter space in the transformations specified by the parametric equations. Hence, only the four arcs of circle displayed in Fig.7.1b) are defined by (7.1). In order to define the curve in Fig.7.1a) by parametric equations such as (7.1), it is necessary to consider this representation in a wider sense, namely that the image of the mapping (7.1) from the parameter space to $\mathbf{R}^2$ is a set of arcs such as those in Fig.7.1b), and that these arcs must be implicitly joined by straight segments. Equivalent arguments show that inverse transforms of surfaces for which the Gaussian mapping has singularities of the second type also represent surface patches with gaps corresponding to the straight components. These inverse transforms must also be considered in a wide sense, with straight segments implicitly bridging the gaps.

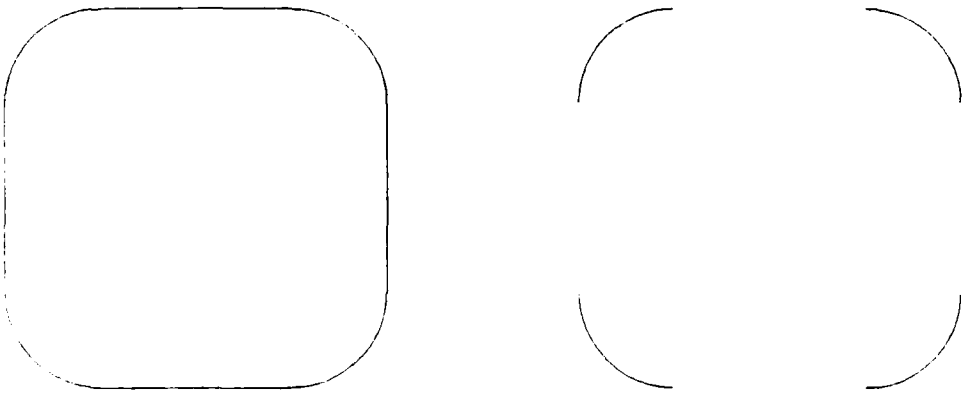

a) b)

Fig.7.1. Curve with Straight Edges. a) Complete Curve.
b) Points explicitly defined by the parametric equations.

In order to make precise conclusions about the limits of the sequences of surfaces, silhouettes and transforms defined above, several issues must be addressed. For example, the type of convergence of the sequences of 2-D curves and 3-D surfaces must be defined and it must be shown that the limits of the sequences depend only on the surface being approximated, not on the particular sequence $\{\Sigma_{Si}\}$. These and other issues are important to develop a mathematical theory, but we have decided instead to rely on intuitive reasoning and to focus on qualitative interpretations of the results.

7.2. Extensions of the Circular Transforms of 2-D Curves

In this section, the circular transforms are extended to curves with corners and edges. In the neighborhood of a corner, a curve is considered as the limit of a sequence of curves with a rounded corner, as the radius of the corner tends to zero. In the neighborhood of a straight edge, the curve is considered as the limit of a sequence of arcs, as the curvature of the arc tends to zero. Finally, the extensions are illustrated by defining a rectangle as the limit of a sequence of superconics of degree n for $n \rightarrow \infty$. The rectangle has both corners and straight edges; its circular transforms obtained with the sequence of superconics are consistent with the results obtained for individual corners and straight edges.

7.2.1. Circular Transforms for a Curve with Corners

The circular transforms are considered here for a corner joining two edges with normals $\bar{n}_1$, $\bar{n}_2$ and corresponding normal orientations ψ_1, ψ_2; see Fig.7.2. The corner

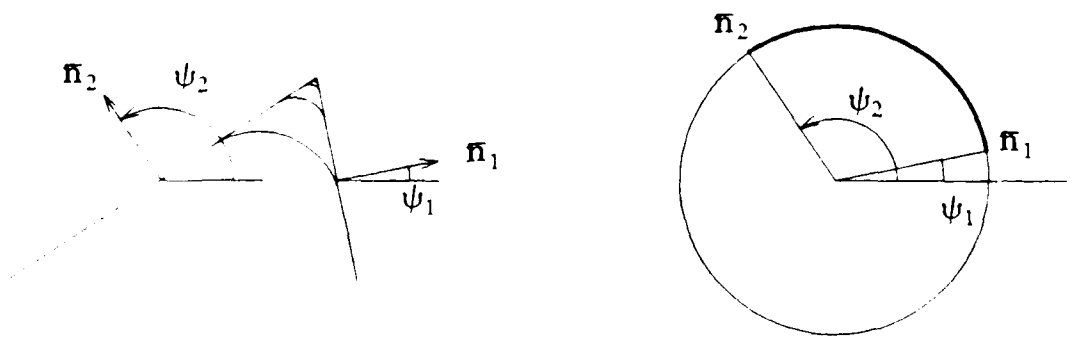

Fig.7.2. Curve with a Corner.
a)Sequence of curves approximating the corner. b) Gaussian circles.

is modeled as the limit of a sequence of arcs joining the two straight edges, as the radius of the arc tends to zero. Each one of these arcs is mapped to the arc $[\psi_1, \psi_2]$ of the Gaussian circle. The image of the corner on the Gaussian circle is hence the arc $[\psi_1, \psi_2]$ joining the images of the sides of the corner. The singularity of the Gaussian mapping is of the first type. Each point of the Gaussian circle represents one point of the object and the sequence of transforms converges to continuous functions. In addition, the values of the three transforms are well defined everywhere in the limit. The inverse transforms correctly reconstruct all the points of the original curve. Among all the transforms, the presence of the corner is conspicuous only in the CT, where the radius of curvature is zero over the image of the corner on the Gaussian circle. The length of the null arc representing the corner in the CT is equal to the exterior angle $\psi_2 - \psi_1$ of the silhouette corner.

7.2.2. Circular Transforms for a Curve with Edges

In this section, the circular transforms are considered for a straight edge of length l and normal orientation ψ_0, from A to B; this edge is considered as the limit of a sequence of arcs joining A and B, when the radius of curvature of the arcs increases without bound; see Fig.7.3. The image of each arc AB on the Gaussian circle is a small segment of the circle around ψ_0 as for example, the bold arc in Fig.7.3b). In the limit, all points of the edge AB map to the single point $\psi = \psi_0$ of the Gaussian circle. As the normal orientation is identical for all points on a straight edge, it is natural that the limiting process defines the Gaussian image of the segment as the single point

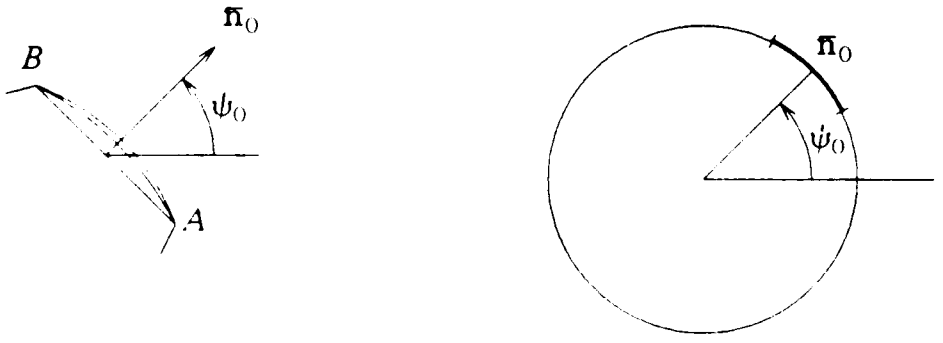

Fig.7.3. Curve with a Straight Edge.
a) Sequence of curves approximating the straight edge. b) Gaussian images.

$\psi=\psi_0$ corresponding to this orientation. For an edge then, the Gaussian mapping has a singularity of the second type. One consequence is that parametric equations defining a curve with edges in terms of normal orientation must be considered in the wide sense defined in section 7.1.

The effect of the singularity of the mapping is now investigated for each of the three circular transforms. In the simple case of a straight edge, it is possible to obtain the resulting transforms without applying the limiting argument. In the case of the ST, the normal distance to the tangent is, by definition, identical for all points on a straight edge. As a consequence, this unique value unambiguously determines the value of the ST for $\psi=\psi_0$. Examining the tangential component t of the VST next, it can be observed that t, by definition the distance between the contact point and the projection of the origin on the tangent, varies continuously along the edge, with a total variation equal to the length l of the edge. The t-component of the VST has hence a step discontinuity of height l at ψ_0. Finally, the effect of the edge on the CT can be predicted with equation (5.20), $\rho(\psi) = p(\psi) + t_{\psi}(\psi)$. As $p(\psi)$ is continuous and $t(\psi)$ has a step discontinuity of height l, it can be predicted that t_{ψ} and therefore ρ have an impulse of height l. This conjecture can be verified by noting that, if s represents the arc length along the curve,

$$s(\psi_2) - s(\psi_1) = \int_{\psi_1}^{\psi_2} \rho(\psi) d\psi \tag{7.2}$$

so that

$$l = \lim_{\epsilon \to 0} \left| s(\psi_0+\epsilon) - s(\psi_0-\epsilon) \right| = \lim_{\epsilon \to 0} \int_{\psi_0-\epsilon}^{\psi_0+\epsilon} \rho(\psi) d\psi \tag{7.3}$$

Therefore, $s(\psi)$ must have an impulse with height l at ψ_0.

$$\rho(\psi) \approx l\ \delta(\psi-\psi_0) \tag{7.4}$$

7.2.3. Example: Transforms of a Rectangle

The extensions of the circular transforms obtained in the previous sections are illustrated here by the example of a rectangle, considered as the limit of a sequence of superconics.

A superconic can be defined by the implicit equation

$$\left|\frac{x}{a}\right|^n + \left|\frac{z}{b}\right|^n = 1 \qquad (7.5)$$

This curve is smooth and strictly convex for $1 < n < \infty$, and tends for $n \to \infty$ to a rectangle with sides $2a$, $2b$ centered at the origin: see Fig.7.4.

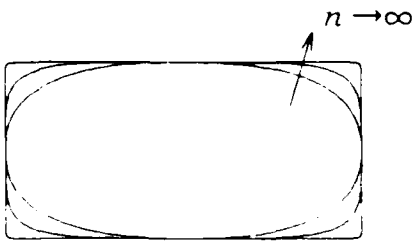

Curves

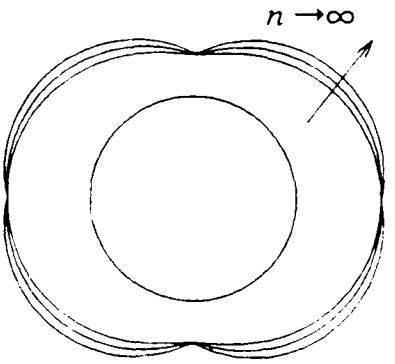

Support Transforms

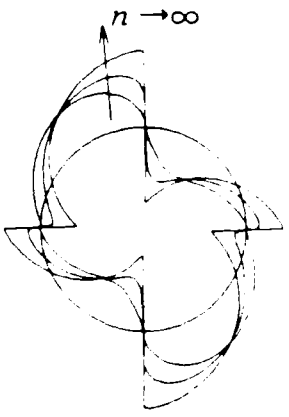

t-component of VST's

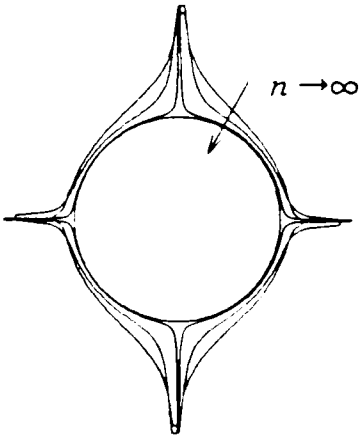

Curvature Transforms

Fig.7.4. Circular Transforms of a Rectangle and of a Sequence of Superconics.

The circular transforms of the superconic are derived in Appendix 1; the property functions are given by

$$p = \left| \, |a\cos\psi|^{k+1} + |b\sin\psi|^{k+1} \, \right|^{1/k+1} \tag{7.6}$$

$$\mathbf{s} = \begin{bmatrix} n \\ t \end{bmatrix} = p^{-k} \begin{bmatrix} p^{k+1} \\ \sin\psi\cos\psi(-a^{k+1}|\cos\psi|^{k-1} + b^{k+1}|\sin\psi|^{k-1}) \end{bmatrix} \tag{7.7}$$

$$\rho(\psi) = \frac{k\,(ab)^{k+1}\,|\cos\psi\sin\psi|^{k-1}}{\left| \, |a\cos\psi|^{k+1} + |b\sin\psi|^{k+1} \, \right|^{\frac{2k+1}{k+1}}} \tag{7.8}$$

where $k = 1/(n-1)$. The limits of the above transforms are now considered for $n \to \infty$, so that $k \to 0$.

$$\lim_{k\to 0} p(\psi) = |a\cos\psi| + |b\sin\psi| \tag{7.9}$$

$$\lim_{k\to 0} t(\psi) = -a\,\sin\psi\, sign(\cos\psi) + b\,\cos\psi\, sign(\sin\psi) \tag{7.10}$$

$$\lim_{k\to 0} \rho(\psi) = \begin{cases} \infty & \text{for } \psi = 0, \pi/2, \pi, 3\pi/2 \\ 0 & \text{otherwise} \end{cases} \tag{7.11}$$

It is clear from the above expressions that the ST is continuous, although it has slope discontinuities at $\psi = 0, \pi/2, \pi, 3\pi/2$. The expression for t reveals discontinuities with alternating heights $2b$ and $2a$ for the same values of ψ. Finally, the CT function contains impulses at these four values of ψ. The strengths of the impulses in the limit for $k \to 0$ can be determined by integration. For example, the height h of the impulse at $\psi = 0$ is determined as

$$h = \lim_{\epsilon\to 0}\lim_{k\to 0} \int_{-\epsilon}^{+\epsilon} \rho(\psi)\,d\psi$$

$$= \lim_{\epsilon\to 0}\lim_{k\to 0} k\,(ab)^{k+1} \int_{-\epsilon}^{+\epsilon} \frac{|\cos\psi\sin\psi|^{k-1}\,d\psi}{\left| \, |a\cos\psi|^{k+1} + |b\sin\psi|^{k+1} \, \right|^{\frac{2k+1}{k+1}}}$$

$$= \lim_{\epsilon \to 0} \lim_{k \to 0} 2bk \int_0^{\epsilon} \psi^{k-1} \, d\psi = 2b$$

The height of the remaining impulses can be determined by symmetry, so that

$$\lim_{k \to 0} \rho(\psi) = 2a \left| \delta(\psi - \pi/2) + \delta(\psi - 3\pi/2) \right| + 2b \left| \delta(\psi) + \delta(\psi - \pi) \right| \qquad (7.12)$$

The above result confirms that the value of the CT is zero for the segments of the Gaussian circle corresponding to the corners of the rectangle. The impulses are located at the images of the sides on the Gaussian circle and have strengths equal to the lengths of the edges. Parametric equations for the rectangle can be obtained by inverting any of the circular transforms determined above; the result is given by

$$\left| \begin{array}{l} x = a \; sign(\cos\psi) \\ y = b \; sign(\sin\psi) \end{array} \right. \qquad (7.13)$$

Note that these equations explicitly represent only the four corners of the rectangle. The limits of the transforms for the rectangle are displayed together with transforms of the superconics in the limiting sequence, in Fig.7.4. The various discontinuities of the circular transforms of the rectangle are consistent with the relations $t = p_{\psi}$, $\rho = p + p_{\psi\psi}$.

Summarizing the extensions of the 2-D transforms, curves with corners are readily accomodated by the formalism developed for the ST, VST and CT in terms of smooth curves. The direct and inverse transforms also apply to curves with straight edges, when generalized functions are considered for the CT, and when the parametric functions in terms of normal orientation are considered in an extended sense.

7.3. Extensions of the Spherical Transforms of 3-D Surfaces

Extensions of the spherical transforms are considered in this section successively for surfaces with curved edges, developable surfaces, surfaces with straight edges, corners, and planar faces.

Each non-smooth surface is considered as the limit of a sequence of smooth surfaces, and its transforms are defined as the limit of the transforms of the surfaces in the sequence. It can be shown by arguments similar to the ones exploited for curves,

that the extension of the forward and inverse transforms is straightforward when the Gaussian mapping has only singularities of the first type, which is the case for surfaces with curved edges and corners. Furthermore, it turns out that the extensions are also straightforward for the ST of surfaces with any of the discontinuities listed above. Extension of the VST to all these surfaces requires only to allow step discontinuities in the tangential components of the spherical function. The discussion of this section will therefore emphasize the two remaining aspects, namely the definition of the Gaussian mapping for non-smooth surfaces, and the singularities introduced in the CT tensor when representing straight surface components.

7.3.1. Curved Edges

The first singularity considered here is a curved edge, such as the edge joining two segments of sphere in the object illustrated in Fig.7.5a). This type of edge can be considered as the limiting case of a torus patch which smoothly joins the two faces of the edge, when the section radius of the torus tends to zero. A sample of the limiting sequence is illustrated in Fig.7.5c). In this example, the torus patch smoothly "fills" the gap between the surfaces on each side of the edge, which have normals with latitudes η_1, η_2. As the section radius goes to zero, the image of the smooth edge on the Gaussian sphere is unchanged. In the limit then, each point on the curved edge is mapped to an arc of points on the Gaussian sphere, namely the great circle arc joining the limits of the normals on both sides of the edge. For example, the point P_0 at longitude ξ_0 on the curved edge in Fig.7.5a) is mapped to the arc between $\vec{n}_1(\xi_0,\eta_1)$ and $\vec{n}_2(\xi_0,\eta_2)$ on the Gaussian sphere, see Fig.7.5b). The Gaussian mapping has a singularity of type 1, so that the three transforms and their inverses are well defined. The presence of the curved edge is not clearly apparent in the ST and the VST of the surface, but the limiting argument can be used to determine that the CT has special values on the Gaussian image of the corner. In Appendix 1, the CT of a torus patch with cross-section radius r and principal radius R is determined to be

$$\bar{\mathbf{R}}_{torus} = \begin{vmatrix} \dfrac{R + r\cos\eta}{\cos\eta} & 0 \\ 0 & r \end{vmatrix} \qquad \eta_1 < \eta < \eta_2 \tag{7.14}$$

The CT value corresponding to the curved edge is obtained as the limit of the above

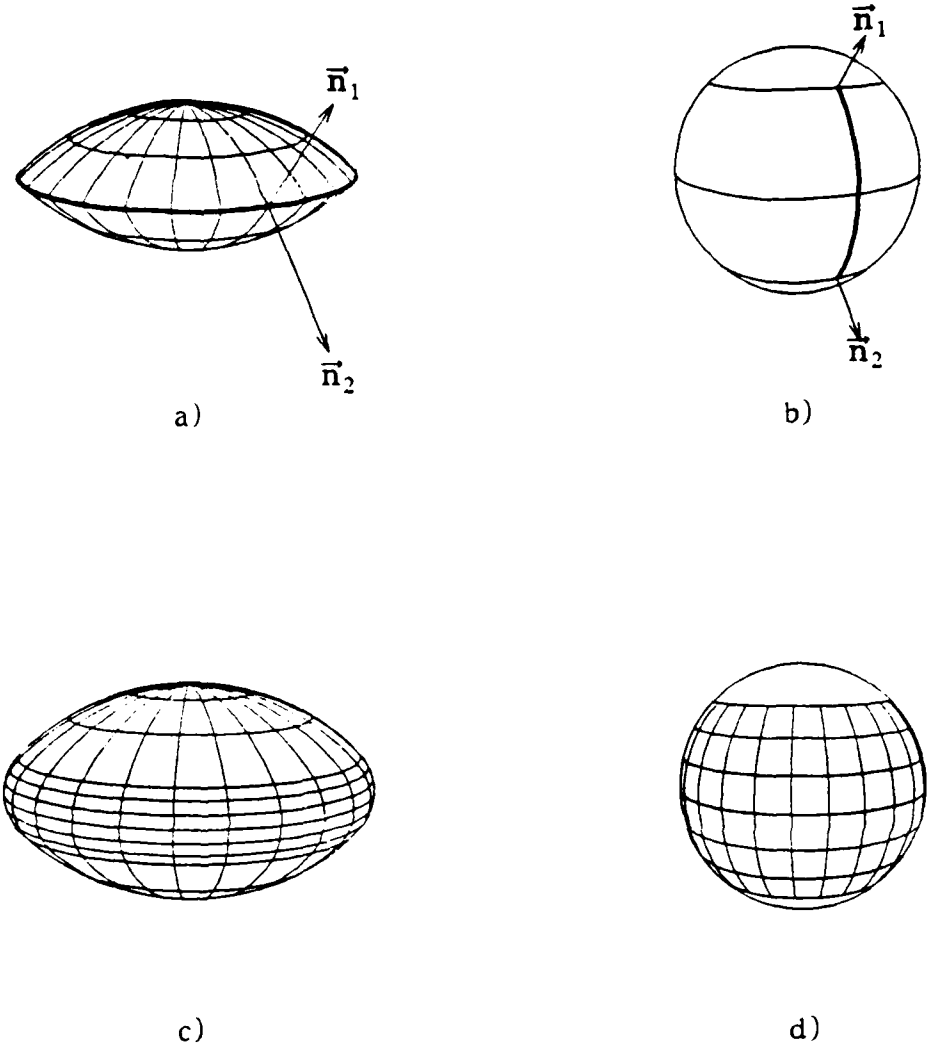

Fig.7.5. Surface with a Curved Edge
a) Surface with sharp edge. b) Gaussian image of a point on the edge.
c) Surface with smooth edge. d) Gaussian image of smooth edge.

---

expression as $r \rightarrow 0$, namely

$$\bar{\mathbf{R}} = \begin{vmatrix} R/\cos\eta & 0 \\ 0 & 0 \end{vmatrix} \quad \eta_1 < \eta_2 \tag{7.15}$$

In our example, the edge is oriented along the local axis $\vec{1}_\xi$. More generally, the CT tensor on a curved edge is singular, i.e. its determinant is zero. The principal values in our example are zero and $R/\cos\eta$, the second of which is related to but not equal to

the radius of curvature of the edge. In addition to being curved, a general edge may also be twisted. However, torsion of a curve is related to third order derivatives of the equations of the curve [47, 52]. Therefore, the expression of the CT for a twisted edge is similar to that for a planar curved edge.

7.3.2. Developable Surfaces

The case of a developable surface is considered in this section, and illustrated by the example of a section of cylinder with radius r and length l ; see Fig.7.6a). This section of cylinder will be considered as the limit of sections of torus with constant section radius r , increasing principal radius R and constant length $l = R(\xi_2 - \xi_1)$ along the principal axis. One of these torus sections is illustrated in Fig.7.6c). The image of the section of torus on the Gaussian sphere is the area between the two meridians with longitudes ξ_1, ξ_2, shown on Fig.7.6d). As the radius R increases to ∞, the longitude interval $\xi_2 - \xi_1 = l/R$ decreases to zero. In the limit, all points on each generatrix of the cylinder are mapped onto a single point of the Gaussian sphere, and the cylinder surface is mapped to a single meridian $\xi = \xi_0$, sketched in Fig.7.6b). The Gaussian mapping has a singularity of the second type .

The CT values corresponding to the torus patch are obtained by the limiting process

$$\bar{\mathbf{R}}_{cyl} = \lim_{R \to \infty,\, R(\xi_2 - \xi_1) = l} \bar{\mathbf{R}}_{torus}$$

$$= \lim_{R \to \infty,\, R(\xi_2 - \xi_1) = l} \begin{vmatrix} \dfrac{R + r\cos\eta}{\cos\eta} & 0 \\ 0 & r \end{vmatrix} [u(\xi - \xi_1) - u(\xi - \xi_2)]$$

where

$$u(x) = \begin{cases} 1 & x \geq 0 \\ 0 & x < 0 \end{cases}$$

$$\bar{\mathbf{R}}_{cyl} = \begin{vmatrix} \dfrac{l\,\delta(\xi - \xi_0)}{\cos\eta} & 0 \\ 0 & r \end{vmatrix} \tag{7.16}$$

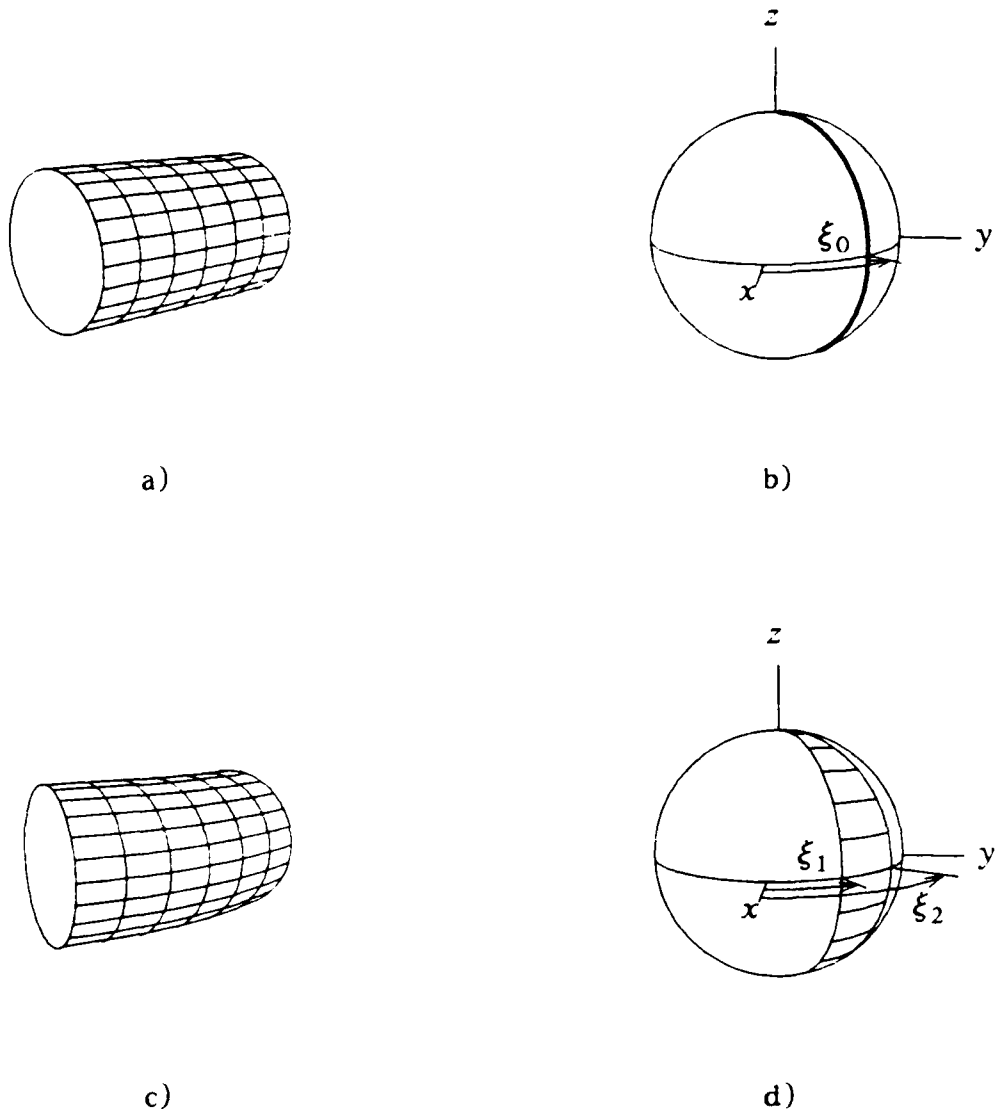

Fig.7.6. Developable Surfaces.
a) Section of a Cylinder. b) Gaussian Image of Cylinder.
c) Section of a Torus. d) Gaussian Image of Torus.

7.3.3. Straight Edges

A straight edge E with length l joining two faces with normals $\vec{n}_1$, $\vec{n}_2$ is now considered, and defined as the limit of a cylinder patch joining the two faces when the radius of the cylinder goes to zero. The edge is depicted in Fig.7.7a), and a rounded surface in the limiting sequence in Fig.7.7c). The image on the Gaussian sphere of the cylinders in the limiting sequence is the great circle arc $\vec{n}_1$, $\vec{n}_2$ sketched in Fig.7.7d).

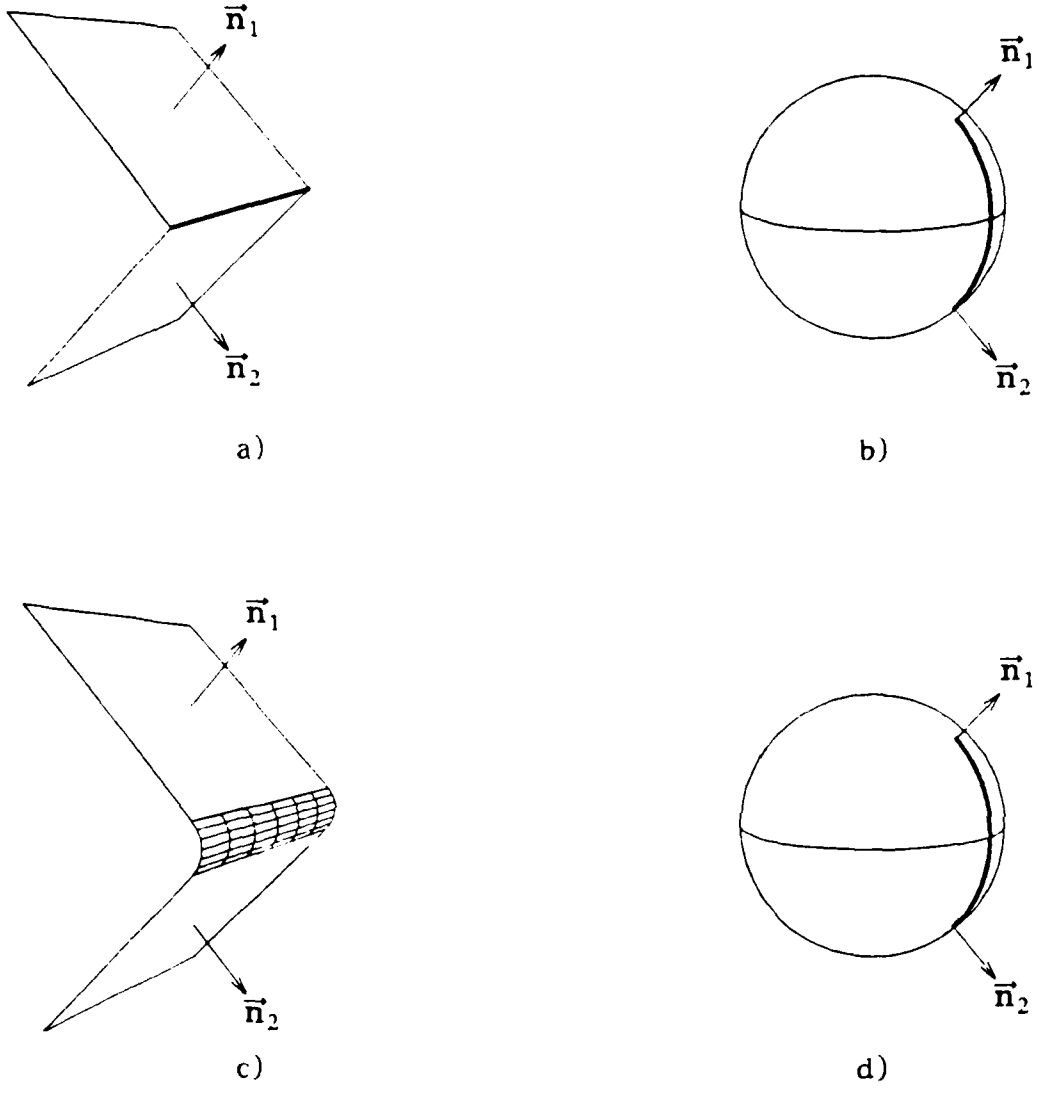

Fig.7.7. Surface with a Straight Edge.
a) Sharp straight edge. b) Gaussian image of edge.
c) Smooth straight edge. d) Gaussian image of smooth edge.

---

and is defined in the limit as the image of the edge E: see Fig.7.7b). The singularity of the Gaussian mapping for this edge is complex, as each point and all points on the edge are mapped to the arc $\vec{n}_1\,\vec{n}_2$.

The behavior of the CT corresponding to this edge is now investigated. The CT of the edge is determined as the limit of the CT's of cylinders in (7.16), as $r \rightarrow 0$. As a consequence, impulses with strength $l/\cos\eta$ are introduced in the tensor component

parallel to the edge, at all points of the Gaussian image of the edge. For example, for a horizontal edge with longitude ξ_0 joining faces with normal latitudes η_1, η_2, the contribution of the edge to the CT tensor is the impulse ridge

$$\bar{\mathbf{R}}_{edge} = \frac{l\ \delta(\xi-\xi_0)}{\cos\eta} \begin{vmatrix} 1 & 0 \\ 0 & 0 \end{vmatrix} (u(\eta-\eta_1)-u(\eta-\eta_2)) \qquad (7.17)$$

Note that the CT value at the points of the Gaussian sphere corresponding to the straight edge has one zero eigenvalue while the other eigenvalue has an impulse.

7.3.4. Corners

The Gaussian mapping and the transform values are now considered for surface corners. A corner is defined as the limit of a rounded corner when the size of the rounding becomes arbitrarily small. A polyhedral corner P_0 is considered first, at the intersection of three faces with normal orientations $\vec{n}_1$, $\vec{n}_2$, $\vec{n}_3$, as illustrated in Fig.7.8a). The image on the Gaussian sphere of a rounded corner approximating the corner at P_0 covers the area between the three great circle arcs $\vec{n}_1\vec{n}_2$, $\vec{n}_2\vec{n}_3$, $\vec{n}_3\vec{n}_1$ illustrated in Fig.7.8b). The limiting process defines the Gaussian image of the sharp corner to be the same area. The Gaussian mapping has a singularity of the first type, so that the spherical functions and their transforms are well defined.

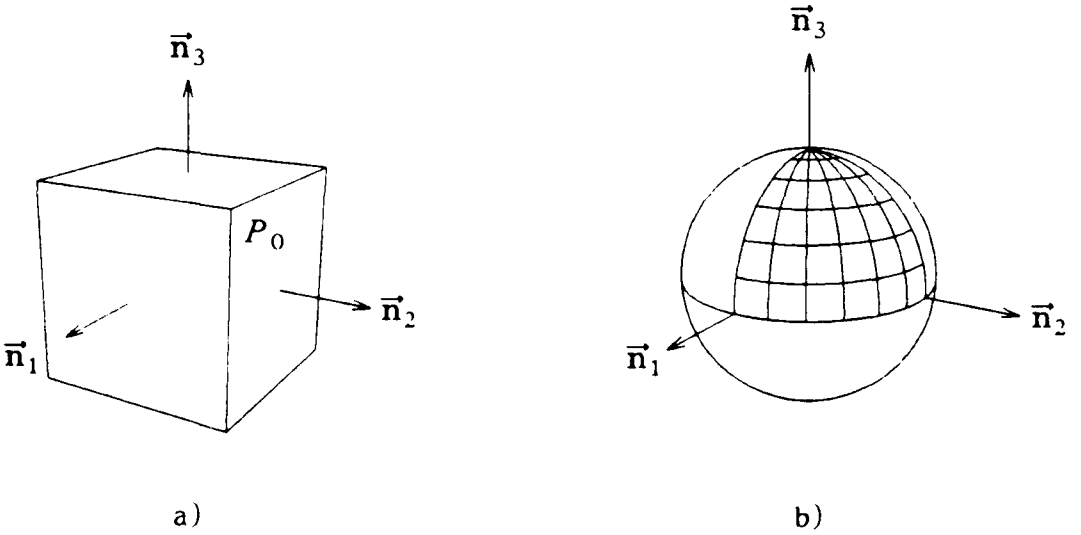

Fig.7.8. Surface Corner.
a) Polyhedral Corner. b) Gaussian Image of the Corner.

Among the three transform functions, only the CT has a special value at a corner, namely the null tensor

$$\bar{\mathbf{R}}_{corner} = \begin{vmatrix} 0 & 0 \\ 0 & 0 \end{vmatrix} \tag{7.18}$$

Polyhedral corners with three or more faces are mapped to spherical polygons on the Gaussian sphere. In general, the image of convex corners is a convex area on the Gaussian sphere. An example of a corner surrounded by a smooth curved surface is given by the tip of an object similar in shape to a football; the image of the corner on the Gaussian sphere is an area limited by a small circle. The surface and the Gaussian image of the corner are displayed in Fig.7.9.

7.3.5. Planar Faces

The discontinuity corresponding to a planar face with normal orientation $\vec{\mathbf{n}}_0$ is now addressed. The image of this face in the Gaussian mapping is first considered. All points of the face have the same normal orientation $\vec{\mathbf{n}}_0$, and are therefore mapped to the corresponding point of the Gaussian sphere: see Fig.7.10. The Gaussian mapping has a singularity of the second type on a neighborhood containing the face. The representation in terms of normal orientations is hence defined only in the extended sense, as are the inverse spherical transforms.

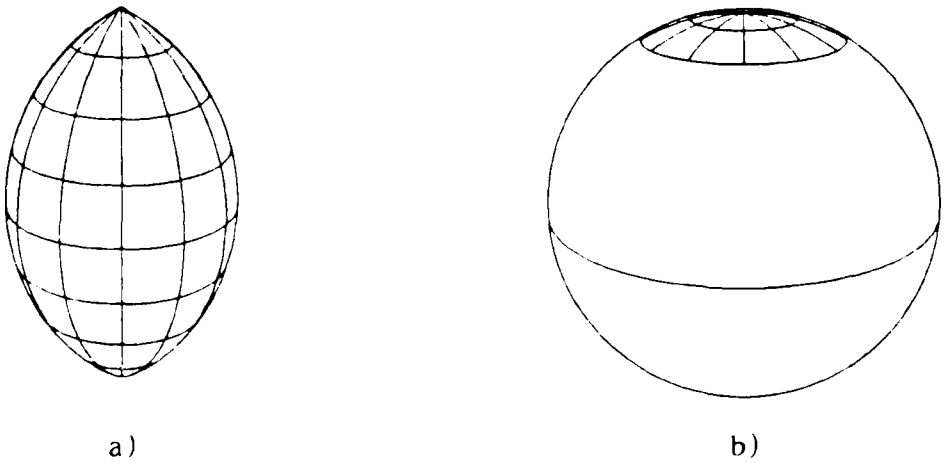

a) b)

Fig.7.9. Surface Corner.
a) Corner on a single curved surface. b) Gaussian image of the corner.

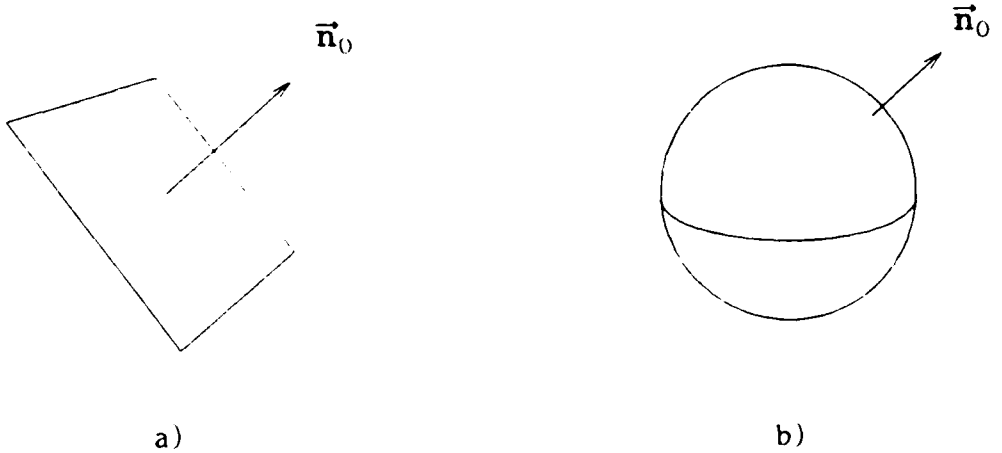

Fig.7.10. Planar Face. a) Surface element. b) Gaussian Image.

The values of the spherical transforms are now considered. First, the normal distance between the origin and the tangents is identical for all points on a planar face. The ST value is hence well defined for the point corresponding to $\vec{n}_0$ on the Gaussian sphere. However, the tangential components of the VST are measured in the plane of the face and have therefore a different value at each point of the face. The tangential VST components are hence undefined at $\vec{n}_0$ and the VST function has step discontinuities at this point of the Gaussian sphere. Considering the behavior of the CT around $\vec{n}_0$, the correspondence with the case of an edge for a planar curve suggests describing the planar face by a tensor impulse in the CT. This conjecture happens to be false however, as it is not possible to explicitly define the shape of any face boundary by only three numbers, the three CT components. It is not possible in general to adequately describe a planar face locally by the CT function on the Gaussian sphere.

The results obtained in this section for the description of non-smooth convex 3-D surfaces by the three spherical transforms are now summarized. At corners and edges of a surface, one point of the surface is mapped to many points on the Gaussian sphere. The values of the spherical transform functions are well defined, and special values are obtained only for the CT, where the tensor is null on a corner, and has a zero eigenvalue on an edge. When a straight component is present in the surface, all points of the segment are mapped to the same point on the Gaussian sphere. This is the case for developable surfaces, straight edges and planar faces. The ST is well defined at the

corresponding points of the sphere, but tangential components of the VST have step discontinuities. In the case of the CT, impulses must be introduced in one eigenvalue of the CT tensor at points corresponding to a straight edge or a developable surface. The other eigenvalue is finite in the case of a developable surface and null for a straight edge. Finally, the shape of a planar face cannot be modeled adequately by the CT.

7.4. Silhouette-Slice Theorems

In this section, extensions of the three Silhouette-Slice theorems presented in Chapter 5 for smooth surfaces are discussed. The appropriate extensions are obtained in most cases by the limiting process described in section 7.1. Specifically, the extended theorems describe the relations between the limit of the spherical transforms of the Σ_{Si} and the limit of the circular transforms of the S_{Si}. When the spherical transform of Σ_{XS} is a function in the strict sense, the limiting process defines the circular transform of the silhouette as the appropriate projection of the great circle slice of the corresponding spherical transform, exactly as in the case of smooth objects. This argument shows that the Silhouette-Slice theorems for the ST and VST can be extended without modifications to cover surfaces with corners, edges and faces, and also developable surfaces. By the same argument, the Silhouette-Slice theorem for the CT can be extended to surfaces with corners and curved edges.

The extension of the Silhouette-Slice theorem for the CT to surfaces with straight edges and to developable surfaces cannot be obtained only by the formal argument used for the other cases, since the corresponding sequences of spherical and circular transforms do not converge in the space of strict-sense functions. This remaining issue concerning the extensions is investigated in a first subsection. The second subsection considers some corollaries of the extended Silhouette-Slice theorems.

7.4.1. Silhouette-Slice Theorem for CT's with Impulses

In the two cases to be analyzed here, namely straight edges and developable surfaces, the 3-D CT was determined in section 7.3. to contain ridges of impulses. The main issue is then to determine how a ridge of impulses intersecting the silhouette slice contributes to the CT on the slice. To simplify the analysis, the issue of slicing a ridge

of impulses is first considered for a scalar function in the Euclidean plane Oxz. Consider a function $f_{xz}(x,z)$ on $\mathbf{R}^2$, and a slice of this function along a line through the origin, with an angle α with the Oz axis; see Fig.7.11. The slice points can be represented by the parametric equations

$$\begin{cases} x = t \sin\alpha \\ z = t \cos\alpha \end{cases} \tag{7.19}$$

where t is a metric parameter along the slice axis. When f_{xz} is a strict-sense function, the values of the function along the slice, $f_t(t)$, are obtained by introducing (7.19) into $f_{xz}(x,z)$, giving

$$f_t(t) = f_{xz}(t \sin\alpha, t \cos\alpha) \tag{7.20}$$

A generalized function is now considered for f_{xz}, namely a ridge of impulses of unit height along the x axis,

$$f_{zx}(x,z) = \delta(z) = \lim_{n\to\infty} \begin{cases} n & 0 \leqslant z < 1/n \\ 0 & \text{otherwise} \end{cases} \tag{7.21}$$

The correct value of the slice is obtained by applying the slicing operation to the sequence of functions in the above definition.

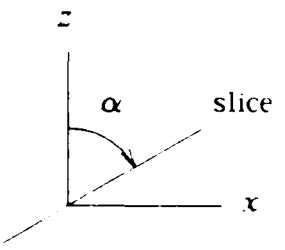

Fig.7.11. Geometry of the Slice in the Oxz plane.

$$f_t(t) = \lim_{n\to\infty} \begin{cases} n & 0 \leq t\cos\alpha < 1/n \\ 0 & \text{otherwise} \end{cases}$$

$$= \lim_{n\to\infty} \begin{cases} n & 0 \leq t < 1/n\cos\alpha \\ 0 & \text{otherwise} \end{cases} \qquad (7.22)$$

$$f_t(t) = \frac{1}{\cos\alpha}\,\delta(t)$$

The same result is also obtained by formally introducing (7.19) directly into (7.21) and carefully considering the scaling of the impulse.

$$f_t(t) = f_{xz}(t\,\sin\alpha, t\,\cos\alpha) = \delta(t\,\cos\alpha)$$

$$= \frac{1}{|\cos\alpha|}\,\delta(t)$$

Hence, the correct result of the slice of an impulse ridge can be formally obtained by simply replacing the two variables of the function being sliced by their expressions in terms of the parameter on the slice, then applying the scaling expression for the $\delta(.)$ distribution.

The analysis of the slicing of impulse ridges in the Euclidean plane suggests that the result of slicing a ridge of impulses in the 3-D CT function on the Gaussian sphere can be evaluated by applying the equation used for predicting the silhouette CT for a smooth surface, equation (6.21)

$$\rho(\psi) = \begin{pmatrix} \cos\alpha_{SG} & \sin\alpha_{SG} \end{pmatrix} \begin{pmatrix} r_{11SG} & r_{12SG} \\ r_{12SG} & r_{22SG} \end{pmatrix} \begin{pmatrix} \cos\alpha_{SG} \\ \sin\alpha_{SG} \end{pmatrix} \qquad (7.23)$$

and considering the change of variables in the impulses present in the components of $\bar{\bar{\mathbf{R}}}$. This procedure leads to the correct silhouette CT function, as is illustrated below for the case of a straight edge with length l. The object axes are chosen so that Oy is parallel to the edge. The contribution of the edge to the 3-D CT is given by (7.17) as

$$\bar{\bar{\mathbf{R}}}_{edge} = \frac{l}{\cos\eta}\,\delta(\xi) \begin{pmatrix} 1 & 0 \\ 0 & 0 \end{pmatrix} \qquad (7.24)$$

For a viewing direction specified by the angles ϕ, θ, the contribution of the edge to the silhouette 2-D CT is given by introducing (7.24) in (7.23).

$$\rho(\psi) = \frac{l}{\cos\eta_{SG}} \delta(\xi_{SG}(\psi)) \cos^2\alpha_{SG}$$

The appropriate scaling of the delta function is accounted for by writing

$$\rho(\psi) = \frac{l}{\cos\eta_{SG}} \frac{1}{\left|\frac{d\,\xi_{SG}}{d\,\psi}\right|_{\psi_0}} \delta(\psi-\psi_0) \cos^2\alpha_{SG}$$

where ψ_0 is determined by $\xi_{SG}(\psi_0) = 0$. The derivative in the above equation was determined in (6.3) as $d\,\xi_{SG}/d\,\psi = \cos\alpha_{SG}/\cos\eta_{SG}$. Therefore,

$$\rho(\psi) = l\ \cos\alpha_{SG}\ \delta(\psi-\psi_0) \tag{7.25}$$

Comparing this result with (7.4) shows that the predicted contribution of the 3-D edge to the silhouette is a 2-D edge with length $l\ \cos\alpha_{SG}$. This result is consistent with the well-known result of the projection of an edge making an angle α_{SG} with the projection plane.

The Silhouette-Slice theorem for the CT is now considered for surfaces with planar faces. As the contribution of planar faces to an object shape cannot be modeled by the 3-D CT, the corresponding contributions to the silhouette shapes cannot be predicted with the CT either. However, planar faces are mapped only to individual points of the Gaussian sphere. Considering a surface with planar faces as the limit of a sequence of smooth convex surfaces, the planar faces will prevent convergence of the sequence of silhouette circular transforms only when the great circle slice passes through some of the points corresponding to the faces. In all other cases, the CT's are well defined on the slice and the Silhouette-Slice theorem applies without modifications. The set of viewing directions for which the slice intersects the image of a face has a measure zero for surfaces with a finite number of faces. As a consequence, the Silhouette-Slice theorem for the CT applies to surfaces with planar faces, for almost all viewing directions.

7.4.2. Corollaries of the Extensions

Two particular consequences of the extended Silhouette-Slice theorems are covered in this section. The first is the relation between the angle of a silhouette corner and the shape of the corresponding corner of the object. The second is an expression for the curvature of the silhouette generated by a flat surface with a curved boundary.

7.4.2.1. Silhouette of a Corner

In section 7.1. and 7.2, it was shown that the presence of a corner on a surface and on its silhouette is apparent mainly in their CT's. Specifically, the 3-D CT of the object surface is the null tensor in the region of the Gaussian sphere corresponding to the object corner, so that the 2-D CT of the silhouette has a zero value for the arc of the slice circle inside the image of the corner. It is clear that whenever the slice corresponding to the viewing direction traverses the image of the 3-D corner on the Gaussian sphere, a corner will appear on the silhouette. The size of the null gap on the 2-D CT of the silhouette is given by the arc length of the slice inside the image of the corner on the Gaussian sphere: see Fig.7.12. As the arc length of the image of the corner on the Gaussian circle is equal to the exterior angle of the silhouette corner, the above discussion provides a qualitative procedure for relating corner angles on the

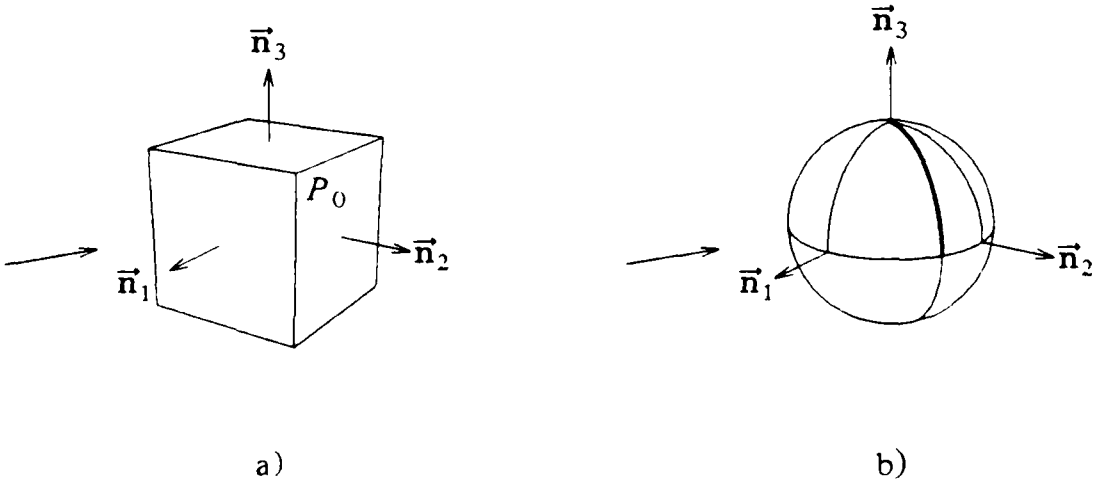

Fig.7.12. Silhouette of a cube corner. a) Corner.
b) Gaussian image, with a slice corresponding to the silhouette with the largest exterior corner angle.

silhouette with the geometry of the 3-D corner of the object. This procedure can be used for example to determine the largest exterior angle of the silhouette corner that can be generated by a given 3-D corner. This angle is given by the largest arc of great circle in the image of the 3-D corner on the Gaussian sphere. This argument shows that a cube corner can generate only right-angled or obtuse silhouette corners: see Fig.7.12.

7.4.2.2. Curvature of the Silhouette of a Planar Object

In this section, the curvature of the silhouette of a planar object with a curved boundary is related to the curvature of the object boundary itself. This result provides an expression for the radius of curvature of the orthographic projection of a 3-D curve, as a function of the radius of the curve and the orientation of the viewing direction.

The problem is first analyzed in a system of axes where Oxy is in the plane of the object and in which $\phi=0$. In the Oxy plane, the object has a 2-D CT $\rho_O(\xi)$ where ξ is chosen to characterize the normal angle in the Oxy plane. In the Gaussian mapping of the object considered as three-dimensional, the two faces of the object are mapped to the poles of the Gaussian sphere, and each point of the boundary to a half meridian with a longitude ξ corresponding to the normal orientation of the curve in the Oxy plane. The 3-D CT of the object can be obtained with equation (7.15)

$$\bar{\bar{\mathbf{R}}} = \begin{vmatrix} \rho_O(\xi)/\cos\eta & 0 \\ 0 & 0 \end{vmatrix} \tag{7.26}$$

The radius of curvature ρ_S of the silhouette is obtained with the Silhouette-Slice theorem for the CT, as

$$\rho_S = \cos^2\alpha_{SG} \frac{\rho_O(\xi_{SG})}{\cos\eta_{SG}} \tag{7.27}$$

It is useful in this case to specify the viewing direction in terms of angles with respect to the Frenet trihedron of the curve at each point. The angles ξ, θ are chosen for this purpose: see Fig.7.13. The angle θ is the angle between the viewing direction and the osculating plane of the curve, whereas ξ is the angle between the projection of the viewing direction in the osculating plane and the principal normal to the curve.

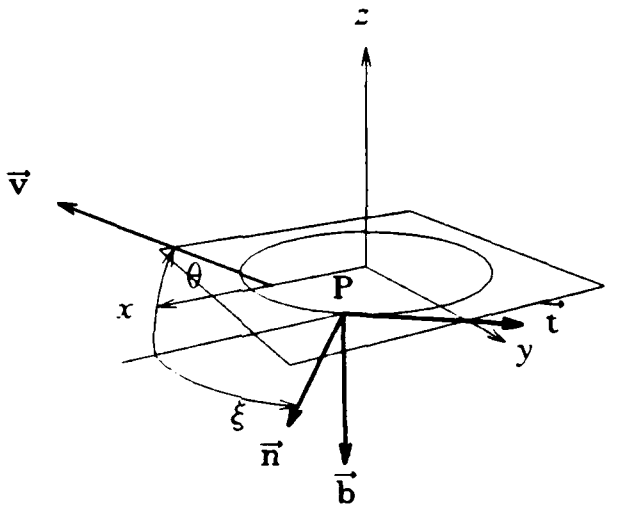

Fig.7.13. Planar Curve and
Angles Specifying the Viewing Direction in the Frenet Trihedron.

Equation (7.27) can be expressed in terms of these angles with (6.1)(h) and (6.1)(i).

$$\rho_S = \frac{(\,1-\sin^2\xi\cos^2\theta\,)^{3/2}}{\sin\theta}\,\rho_O(\xi) \tag{7.28}$$

The above equation expresses the radius of curvature of the orthographic projection of a 3-D curve, in terms of the radius of curvature of the 3-D curve and the orientation of the viewing direction in the Frenet trihedron of the curve. This result can also be obtained by a classical method, as is done in Appendix 5; it is also valid for non-planar curves, since torsion only affects third order derivatives. When $\xi=0$, the viewing direction is in the normal plane of the curve and the relation simplifies to $\rho_S = \rho_O/\sin\theta$.

7.5. Summary

In this chapter, the silhouette theories developed in Chapters 5 and 6 for smooth surfaces have been extended to cover surfaces with discontinuities, edges and planar faces. It is remarkable that theories supported by differential geometry of smooth surfaces provide correct results when extended to surfaces with sharp edges and corners. In addition to the analytic expressions for the silhouette shapes, a number of powerful qualitative relations between silhouettes and 3-D shapes have been derived. These qualitative relations prove to be useful when developing algorithms for object recognition from silhouettes. This is briefly explained in Chapter 8.

Chapter 8
Examples and Applications

This chapter presents a number of examples of silhouette construction with the Silhouette-Slice theorems. In addition, applications of the new theories to the reconstruction of the shapes of 3-D objects from silhouette data are suggested, followed by the principles of a system for recognizing polyhedral objects from their silhouettes. It must be pointed out that the main results of this thesis are theoretical. Applications presented in this chapter prove that these theories are useful for solving practical problems, but they have not been developed in great detail.

It is tempting to develop algorithms for solving each of the three basic silhouette problems by sampling the spherical and circular object functions introduced in Chapter 5, and relating these discrete transforms to Silhouette-Slice theorems for discrete transforms. However, sampling questions introduce difficult obstacles in the development of a discrete theory. First, sampling continuous functions defined on the sphere is a complex problem which has not been adequately solved. In addition, great circle slices corresponding to given viewing directions do not typically intersect the sampling grid on the sphere at sample points. As a result, interpolations between the sample values of the spherical transforms are necessary to generate samples of the silhouette transform in almost all cases. The choice of sample points on the sphere was addressed in [44, 57] for the case of the Extended Gaussian Image. It was shown that the largest number of regularly spaced sample points on the sphere is equal to the largest number of faces on a regular polyhedron, namely 20. For any larger number of samples, an irregular sampling must be considered. In addition to the choice of sample points, both the choice of sample values in terms of the continuous function being represented and the interpolation of sample values to recover the corresponding continuous function must be considered, but these have not been studied in detail. At this point, the unsolved sampling issues make it difficult to apply the new theories directly to the development of numerical algorithms. However, the theories developed in this thesis provide valuable tools for qualitative reasoning which the examples of applications presented in this chapter attempt to illustrate. In addition to the relations between objects and silhouettes, the CT representation for 3-D surfaces presented in

Chapter 5 is a valuable contribution to the understanding of surface shapes, both for geometry and for computer applications. Since this aspect of the theory is not directly related to silhouette analysis, its discussion is relegated to Appendix 4.

8.1. Silhouette Construction

In this section, a number of examples are presented to illustrate silhouette construction with the Silhouette-Slice theorems. These examples demonstrate that numerically correct answers are obtained with the proposed formalism. They further provide insight into the form of the three transforms and the result of the slicing operations. In a number of cases, qualitative reasoning with the Silhouette-Slice theorems is proposed to predict the gross aspect of the silhouette.

As mentioned in the introduction of this chapter, sampling of the spherical and circular functions raises non-trivial issues. To generate the examples presented in this chapter, sampling of the transforms on the Gaussian sphere has been circumvented by using closed-form analytic expressions for the spherical functions. On the other hand, the circular functions and the corresponding silhouettes must be sampled, at least for display purposes. The sampling issues have been largely eliminated by using a large number of samples for the circular transforms of the silhouettes. Our approach to the sampling question is tractable when closed-form expressions are available for the transforms of the surface shapes considered. It will be shown that accurate silhouettes can be determined by this method for many surface shapes. The Silhouette-Slice theorem can provide the shape of silhouettes for surfaces for which no closed-form silhouette expressions are available, for example, for superquadrics. The three spherical transforms for superquadrics are derived analytically in Appendix 1. Although it relies on analytical formulas, our treatment of the sampling problem is compatible with the computation of silhouettes for surface models designed with a CAD system. These surfaces are defined as combinations of a number of surface patches, where each patch is described by a relatively simple analytic equation. The silhouette problem can be solved with the proposed method when spherical transforms can be evaluated analytically for the primitive surface elements.

Although continuous spherical transform functions are used in the examples presented in this section, silhouette shapes have also been obtained by considering

samples of the transform functions on the Gaussian sphere and by relating these to samples of the silhouette transforms on the appropriate slice. This discrete formulation of the Silhouette-Slice theorems requires a large number of interpolations between sample points on the sphere to determine samples of the silhouette circular transforms on the great circle slice. In addition, sampling effects introduce degradations in the shapes of the computed silhouettes. These degradations become negligible for dense samplings, but the number of samples required to ensure a given accuracy cannot be quantified because of the lack of a sampling theory for this problem. The sampling questions are beyond the scope of the thesis, which concentrates on the theories formulated in terms of continuous functions.

Silhouette construction will be illustrated for three different types of objects, namely a cylinder, superquadrics, and a torus. In the context of these examples, a number of qualitative aspects of the theory are discussed. Qualitative aspects of the circular transform graphs such as signs, extrema and zero crossings are related to the silhouette shape. The effect of the choice of a reference frame on the transforms is discussed. A qualitative prediction of the shape of silhouettes of polyhedra with the Silhouette-Slice theorem is presented. This result is then extrapolated to predict the shape of silhouettes of smooth surfaces which are closely approximated by polyhedra, such as some superquadrics. Finally, silhouettes of a torus illustrate the application of the results to a non-convex object and raises issues related to the extension of the results to these objects.

8.1.1. Silhouettes of a Cylinder

The first example is that of a simple axisymmetric object, namely a cylinder of height $2H$ and radius r, sketched in Fig.8.1. The various transforms of the object are also axisymmetric, when the reference point is positioned on the object axis. For a reference point at the center of the cylinder, the 3-D VST of the cylinder is given by

$$\vec{\mathbf{s}} = \begin{cases} \left| (r\cos\eta + H\sin\eta) \;\; 0 \;\; (H\cos\eta - r\sin\eta) \right|^T & 0^o \leqslant \eta \leqslant 90^o \\ \left| (r\cos\eta - H\sin\eta) \;\; 0 \;\; (-H\cos\eta - r\sin\eta) \right|^T & -90^o \leqslant \eta \leqslant 0^o \end{cases} \tag{8.1}$$

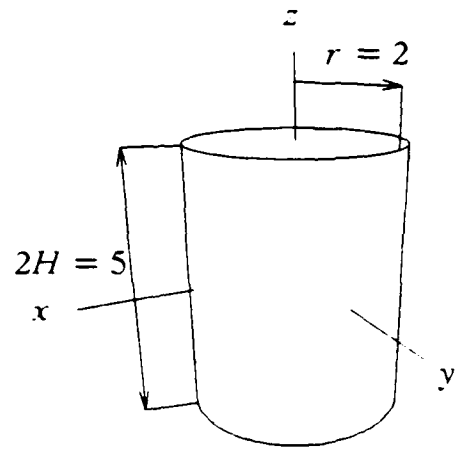

Fig.8.1. Cylinder with radius $r=2$, height $2H=5$.

The CT of the Cylinder is given by

$$\bar{\bar{\mathbf{R}}} = \begin{vmatrix} r/\cos\eta & 0 \\ 0 & 2H\,\delta(\eta) + r\,\delta(\eta-\pi/2) + r\,\delta(\eta+\pi/2) \end{vmatrix} \tag{8.2}$$

Except for h and r_{12} which are identically zero, profiles of the components of the transforms are displayed in Fig.8.2. The profile of an axisymmetric function on the Gaussian sphere is, by definition, a 1-D function representing the values of the axisymmetric function for a fixed value of ξ. The profile is defined for $-90^{o} \leqslant \eta \leqslant 90^{o}$, but the profiles were extended to the range of $-180^{o} \leqslant \eta \leqslant 180^{o}$ for display purposes. In this form, the profiles correspond to a vertical section of the Gaussian sphere. These extended profiles are represented by polar diagrams in Fig.8.2. In these diagrams, the zero value is offset from the center to allow the representation of negative values.

The cylinder does not satisfy smoothness and strict convexity constraints required in the theories of Chapters 5 and 6, because of the presence of edges and embedded straight components. As a result, the ST displays discontinuities in the first derivative, the v-component of the VST displays step discontinuities, and the CT contains impulses. These discontinuities are all related to the length of the corresponding straight surface components, as discussed in Chapter 7. Specifically, the discontinuities in the slopes of the ST, the step discontinuities in v and the lateral impulses in r_{22}

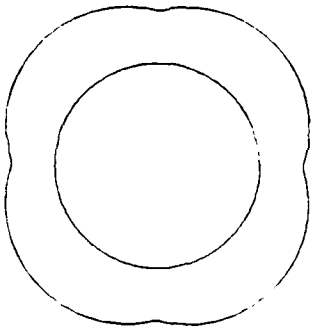

Profile of 3-D ST

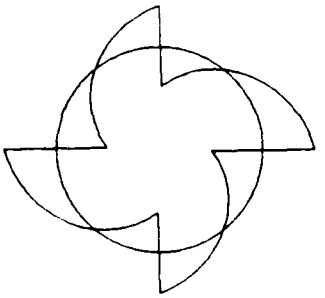

Profile of v-component of 3-D VST

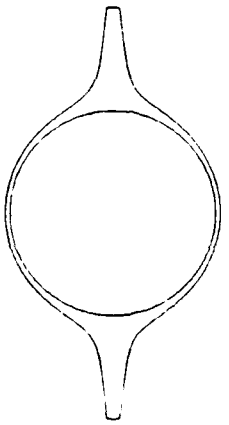

Profile of r_{11}-component of 3-D VST

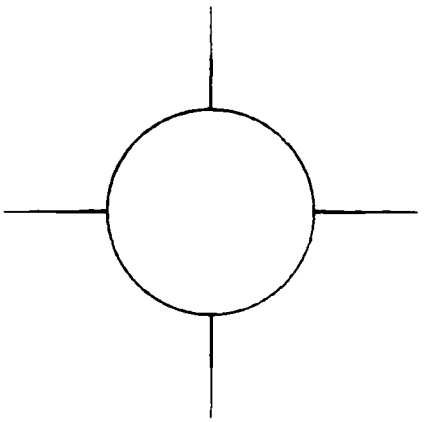

Profile of r_{22}-component of 3-D VST

Fig.8.2. Profiles of the Spherical Transforms of the Cylinder in Fig.8.1.

---

are equal to the height $2H$ of the cylinder.

Circular transform functions for silhouettes of this object are obtained by projecting the spherical function values on the appropriate great circle slice onto the plane of the slice, according to the Silhouette-Slice theorems developed in Chapter 6. Silhouettes and the corresponding circular functions are displayed in Fig.8.3a)-b) for two different orientations of the viewing direction. The circular silhouette functions were computed at 200 equally spaced samples of the appropriate great circle slice; points of the silhouette were generated by inverting the silhouette VST with equation

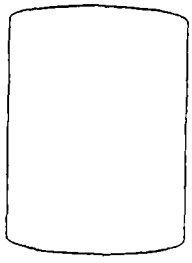

Silhouette for $\theta = 10^o$

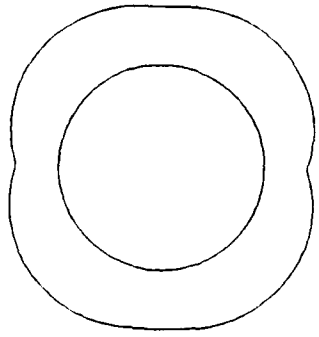

Support Transform

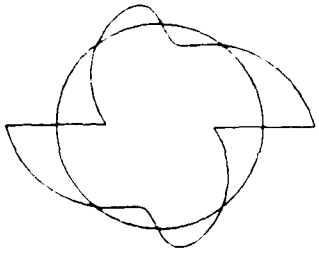

t-component of VST

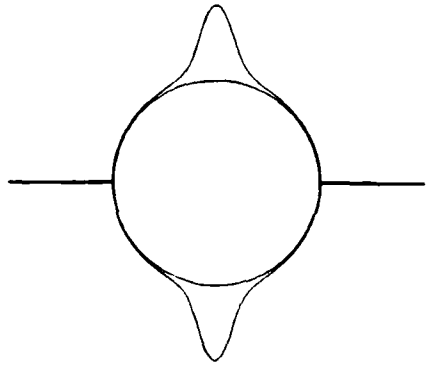

Curvature Transform

Fig.8.3a). Silhouette of the Cylinder for $\theta = 10^o$, and Corresponding Transforms.

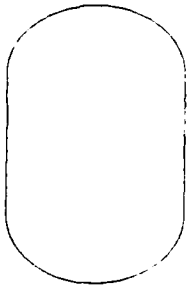

Silhouette for $\theta = 50^{\circ}$

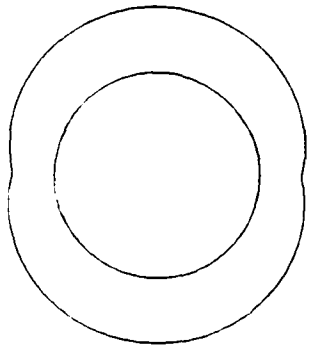

Support Transform

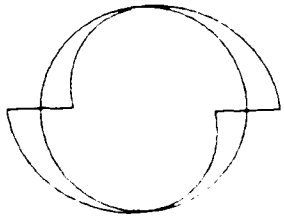

t-component of VST

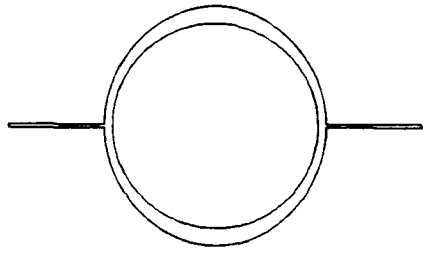

Curvature Transform

Fig.8.3b). Silhouette of the Cylinder for $\theta = 50^{\circ}$, and Corresponding Transforms.

(5.9) applied to the sample values. The following characteristics can be observed on these silhouettes and their circular transforms. The ST is strictly positive everywhere, because of our choice of the origin inside the 3-D object. The angular points in the graph of the ST correspond to the flat sections of the silhouette. The t-component of the VST has values with alternating signs, since it must integrate to 0 over the 2π interval. The zero crossings of t correspond to points for which the normal goes through the reference point. The 2-D CT's of both silhouettes contain two impulses corresponding to the straight sections on the sides of the silhouette, which correspond themselves to the lateral surface of the cylinder. In addition, the 2-D CT of the

silhouette contains two maxima corresponding to the top and bottom parts of the cylinder. Note that the silhouette CT's contain impulses related to the lateral impulses of r_{22} in Fig.8.2, but none related to the top and bottom impulses in r_{22}. This observation can be justified by considering the 3-D graph of r_{22} on the Gaussian Sphere in Fig.8.4. In the 3-D CT of the cylinder, the lateral surface generates an equatorial ridge of impulses. The impulses on the 2-D CT of the silhouette correspond to the intersection of the great circle slice with the equator, as is shown in the figure for a slice corresponding to $\theta=30^{o}$. As all slices cut the equator, the equatorial impulses related to the lateral surface appear on all silhouettes. However, the impulses of the 3-D CT corresponding to the top and bottom parts of the cylinder are located only at the poles of the Gaussian Sphere. Therefore, they affect only great circle slices through the poles, which correspond to silhouettes with $\theta = 0^{o}$.

The effect of translations of the reference point on the various surface spherical transforms and the corresponding silhouette circular functions is now investigated. The effect of origin position on the VST is characterized by the expression

$$\begin{bmatrix} n \\ h \\ v \end{bmatrix} = \begin{bmatrix} \cos\xi\cos\eta & \sin\xi\cos\eta & \sin\eta \\ -\sin\xi & \cos\xi & 0 \\ -\cos\xi\sin\eta & -\sin\xi\sin\eta & \cos\eta \end{bmatrix} \left| \begin{bmatrix} x(\xi,\eta) \\ y(\xi,\eta) \\ z(\xi,\eta) \end{bmatrix} - \begin{bmatrix} x_0 \\ y_0 \\ z_0 \end{bmatrix} \right| \qquad (8.3)$$

where (x_0,y_0,z_0) are the coordinates of the reference point in fixed object-centered coordinates. The ST is identical to the first component of the VST, and the CT is

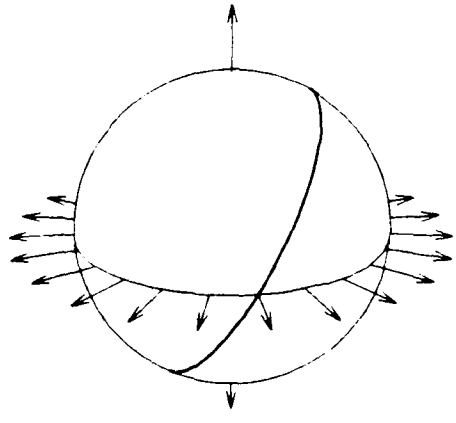

Fig.8.4. Graph of the r_{22} component of the 3-D CT of the cylinder

unaffected by the choice of origin. The effect of the choice of origin on the ST and on the VST components of the silhouette is illustrated in Fig.8.5a)-d) for the silhouette of the cylinder with $\theta = 20^{\circ}$, $\phi = 0^{\circ}$, and for four excentric positions of the reference point. It can be observed in these figures that significant changes of the ST and VST result from the displacement of the origin. Specifically, negative values appear in n_{π} when the reference point is outside the object, the number and locations of zero-crossings of t_{π} and extrema of n_{π}, t_{π} are modified; of course, the numerical values of the transforms are considerably affected.

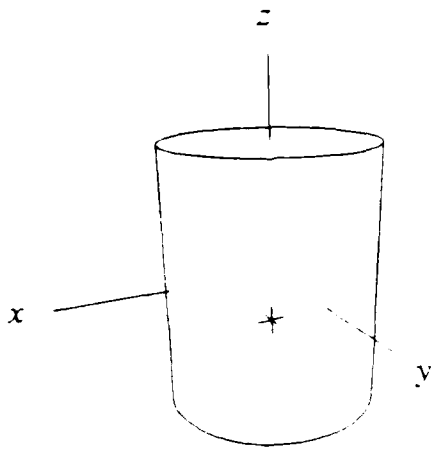

Cylinder and Reference Point

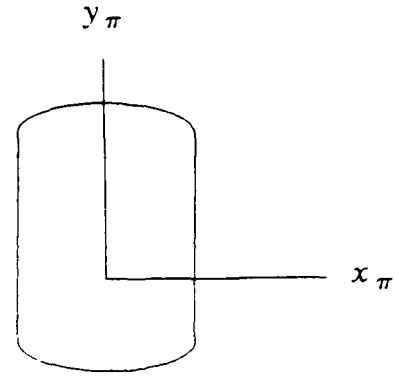

Silhouette

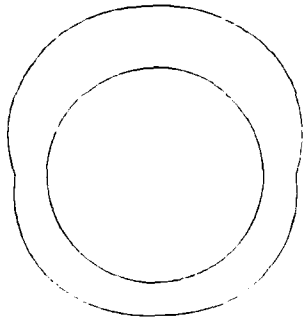

Support Transform

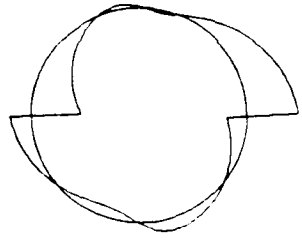

t-component of VST

Fig.8.5a). Normal and Tangential Components of the VST of a Cylinder Silhouette with the Reference Point (0,0,−1).

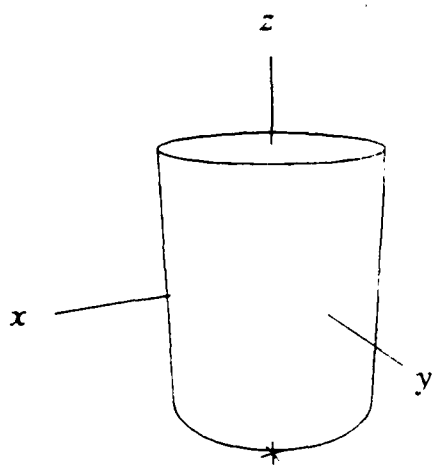

Cylinder and Reference Point

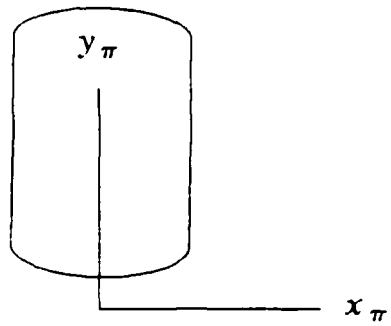

Silhouette

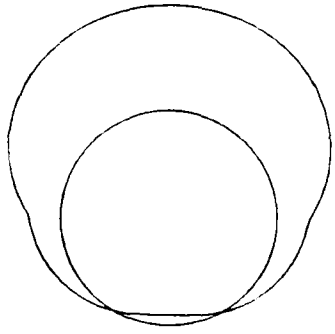

Support Transform

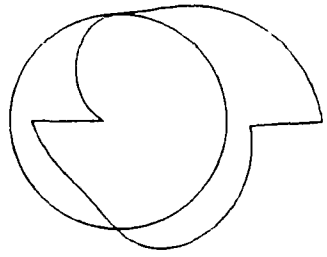

t-component of VST

Fig.8.5b). Normal and Tangential Components of the VST of a Cylinder Silhouette with the Reference Point at (0,0—4).

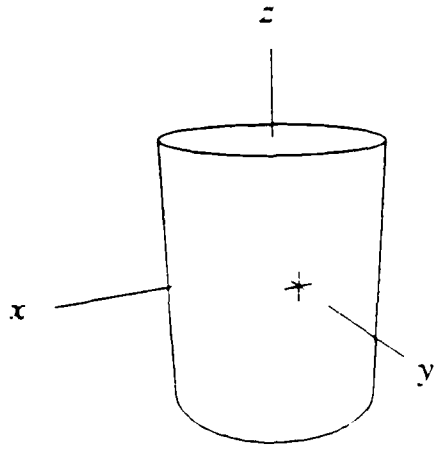

Cylinder and Reference Point

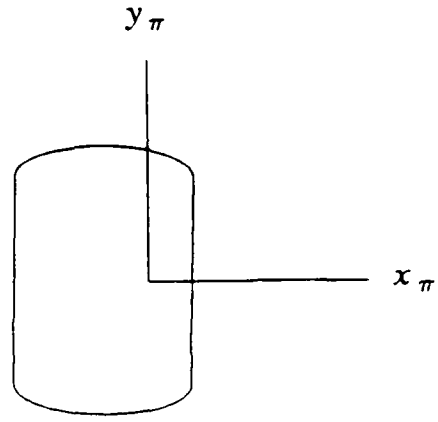

Silhouette

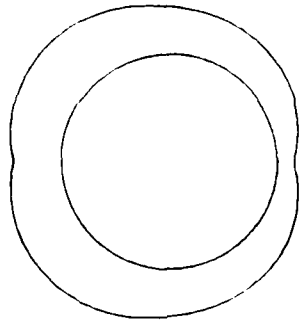

Support Transform

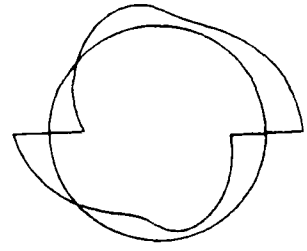

t-component of VST

Fig.8.5c). Normal and Tangential Components of the VST of a Cylinder Silhouette with the Reference Point at (0,1,0).

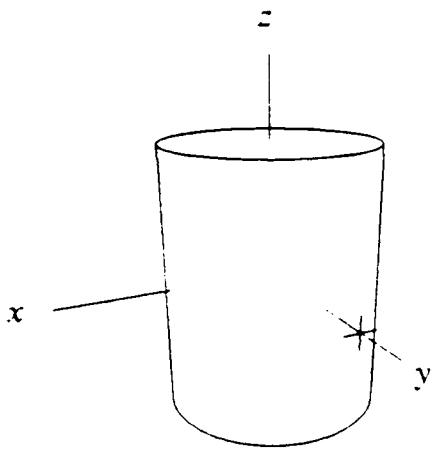

Cylinder and Reference Point

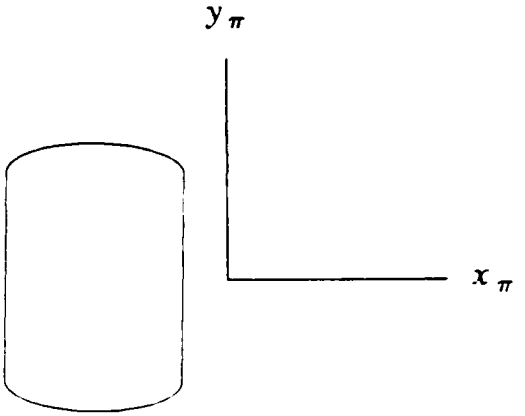

Silhouette

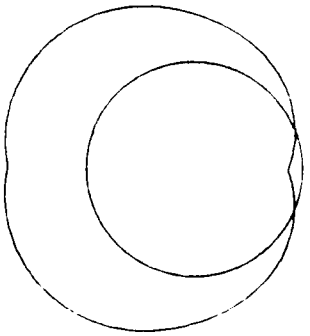

Support Transform

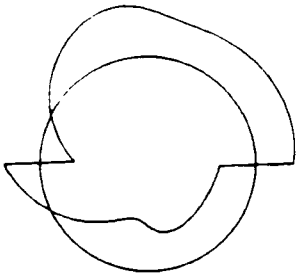

t-component of VST

Fig.8.5d). Normal and Tangential Components of the VST of a Cylinder Silhouette with the Reference Point at (0,3,0).

8.1.2. Silhouettes of Superquadrics

In this section, silhouette construction is demonstrated for a subclass of superquadrics [58]. The subset of superquadrics considered here is defined by the implicit equation

$$\left|\frac{x}{a}\right|^n + \left|\frac{y}{b}\right|^n + \left|\frac{z}{c}\right|^n = 1 \qquad (8.4)$$

The parameters a, b, c correspond to the intersections with the coordinate axes. They hence control the size and elongation of the surface shape. The parameter n, however, controls the smoothness of the surface. For $1<n<\infty$, surfaces defined by (8.4) are smooth and strictly convex. Examples of superquadrics with $a=4$, $b=3$, $c=2$ are displayed in Fig.8.6 for $n = 1, 1.2, 4.5, \infty$. Ellipsoids are a special case of superquadrics for $n=2$. In the limit for $n \rightarrow \infty$, the superquadric becomes a parallelepiped, whereas the limit for $n \rightarrow 1$ corresponds to an octahedron.

It is possible to evaluate the three spherical transforms in closed form for the surfaces specified by (8.4), and therefore to compute the shape of their silhouettes in orthographic projections. The analytic computations of the spherical transforms require relatively tedious algebra and are therefore relegated to Appendix 1. Examples of silhouettes of the two smooth superquadrics in Fig.8.6 are shown in Fig.8.7a)-d). As mentioned in Appendix 1, the CT of superquadrics contain discontinuities when $n>2$. These discontinuities are apparent in Fig.8.7d) for $n=4.5$. They correspond to the six slowly curving parts in the corresponding silhouette. Such discontinuities in the CT of superquadrics with $n>2$ present an additional obstacle to discrete representations of the CT.

An example of qualitative predication of the shape of silhouettes with the Silhouette-Slice theorems is now presented, first for the polyhedra ($n = 1, \infty$), then for the smooth superquadrics ($n = 1.2, 4.5$). The qualitative shape of silhouettes of the octahedron and the parallelepiped can be readily estimated with the Silhouette-Slice theorem for the CT. The CT of the two polyhedra have ridges of impulses on the great circle arcs which are the images of the polyhedron edges on the Gaussian sphere. In Fig.8.8, these arcs have been plotted on the Gaussian sphere for the two polyhedra, for the same values for the diameters as in Fig.8.6. Slices of the 3-D CT of the

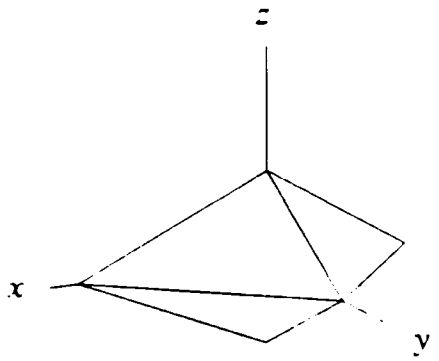

$n = 1$

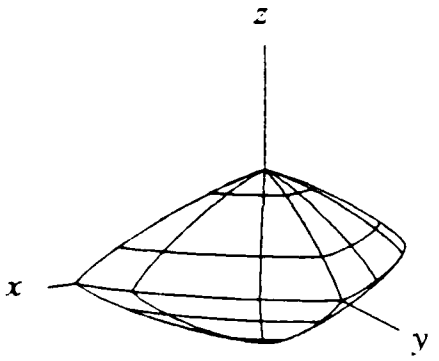

$n = 1.2$

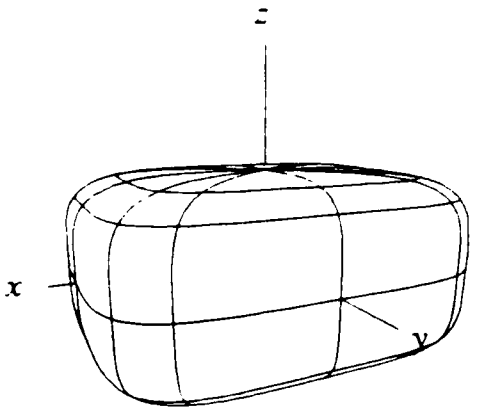

$n = 4.5$

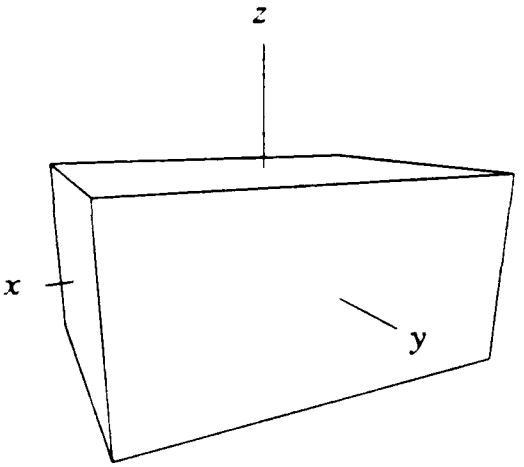

$n = \infty$

Fig.8.6. Superquadrics with $a = 4$, $b = 3$, $c = 2$.

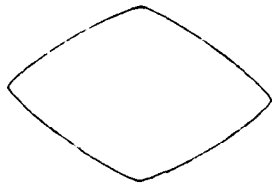

Silhouette

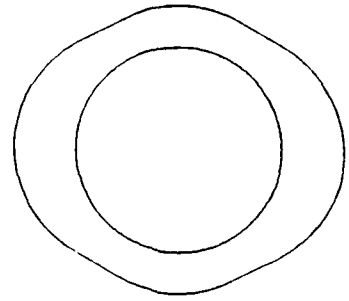

Support Transform

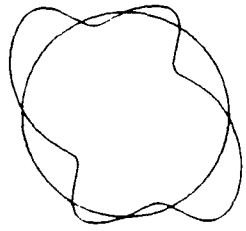

t-component of VST

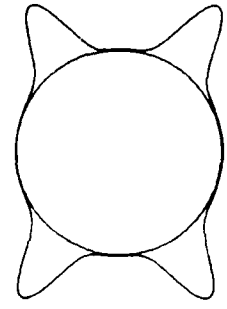

Curvature Transform

Fig.8.7a). Silhouette and corresponding Circular Transforms for the superquadric with $n = 1.2$, for the viewing direction $(\phi,\theta) = (10^{o},10^{o})$

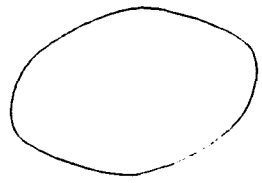

Silhouette

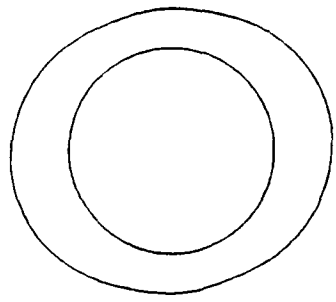

Support Transform

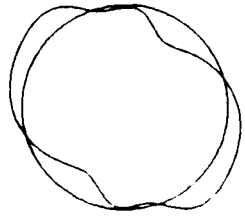

t-component of VST

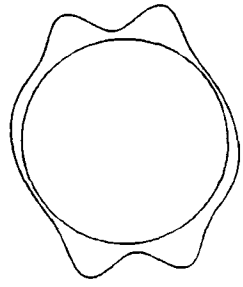

Curvature Transform

Fig.8.7b). Silhouette and corresponding Circular Transforms for the superquadric with $n = 1.2$, for the viewing direction $(\phi,\theta) = (40^{\circ},20^{\circ})$

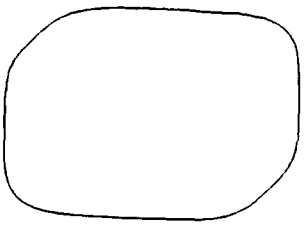

Silhouette

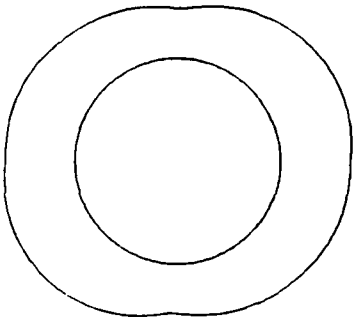

Support Transform

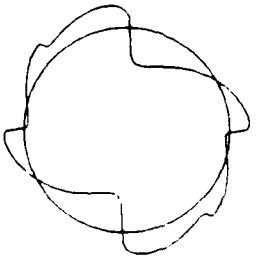

t-component of VST

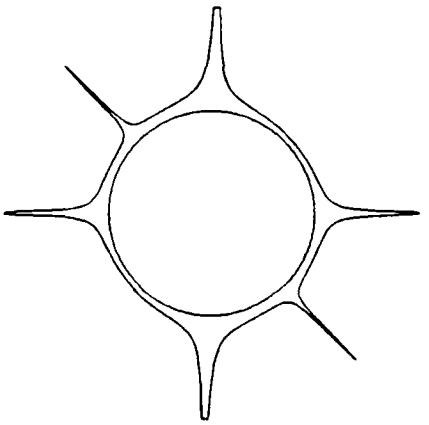

Curvature Transform

Fig.8.7c). Silhouette and corresponding Circular Transforms for the superquadric with $n = 4.5$, for the viewing direction $(\phi,\theta) = (10^{o},10^{o})$

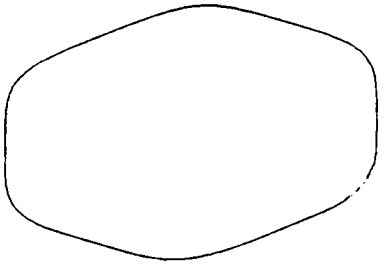

Silhouette

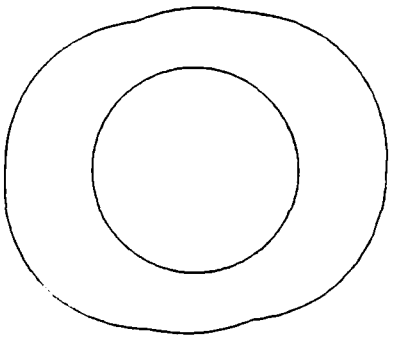

Support Transform

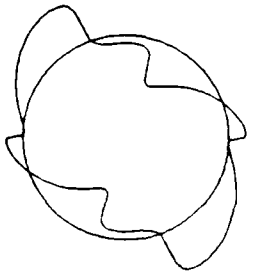

t-component of VST

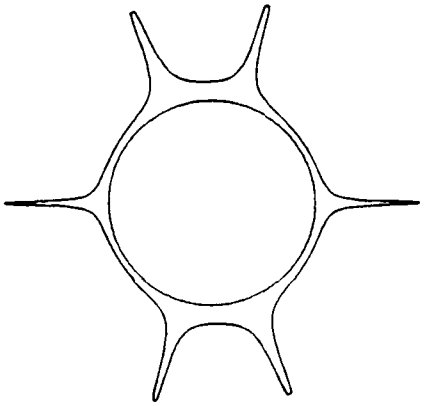

Curvature Transform

Fig.8.7d). Silhouette and corresponding Circular Transforms for the superquadric with $n = 4.5$, for the viewing direction $(\phi,\theta) = (40^{o},20^{o})$

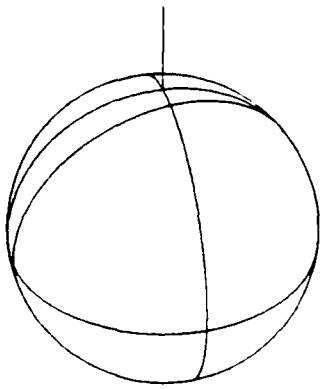

Parallelepiped, $(\phi,\theta) = (10°, 10°)$

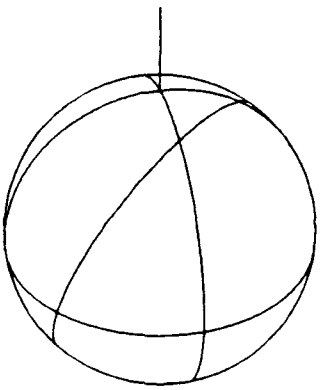

Parallelepiped, $(\phi,\theta) = (40°, 20°)$

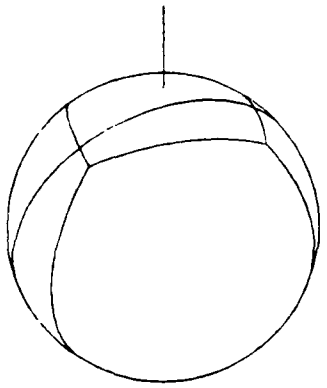

Octahedron, $(\phi,\theta) = (10°, 10°)$

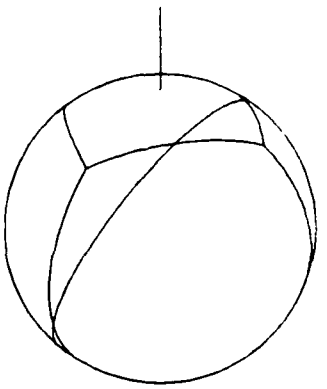

Octahedron, $(\phi,\theta) = (40°, 20°)$

Fig.8.8. 3-D CT of the superquadrics with $n = 1$ (octahedron) and $n = \infty$ (parallelepiped) The CT's have ridges of impulses along the lines drawn on the Gaussian sphere. Also shown are the great circle slices corresponding to two viewing directions.

---

polyhedra are composed of impulses so that the silhouettes are polygons with a number of edges equal to the number of great circle arcs sliced by the silhouette great circle. Except for special coincidences, the number of silhouette edges is 6 for the parallelepiped and can be 4 or 6 for the octahedron. The similarity betwen superquadrics with small values of n and the octahedron ($n = 1$), and between superquadrics with large values of n and the parallelepiped ($n = \infty$) is preserved in the silhouettes.

As a result, the silhouettes of the smooth superquadrics in Fig.8.6 can be predicted to be polygons with bent edges and rounded corners, with a number of edges equal to the numbers for the corresponding polyhedra. It can be observed in Fig.8.7a)-d) that the silhouettes of both superquadrics contain the numbers of bent edges qualitatively predicted by the above argument. The presence of these bent edges in the silhouette is also apparent as maxima in the CT, which are maxima of the radius of curvature.

8.1.3. Silhouettes of Tori

The example of silhouette construction for the torus presented in this section introduces issues arising from the application of the Silhouette-Slice theorems to non-convex objects. It is clear that each point of the Gaussian sphere corresponds to two points of the torus surface (see Fig.8.9) except for the poles of the sphere; each pole corresponds to an infinite number of object surface points. To determine its silhouettes, the torus surface is cut into two parts, which will be called the interior and exterior parts, see Fig.8.10. The set of points along the separation line between the two parts has a zero measure and is not considered here. The Gaussian Mapping is

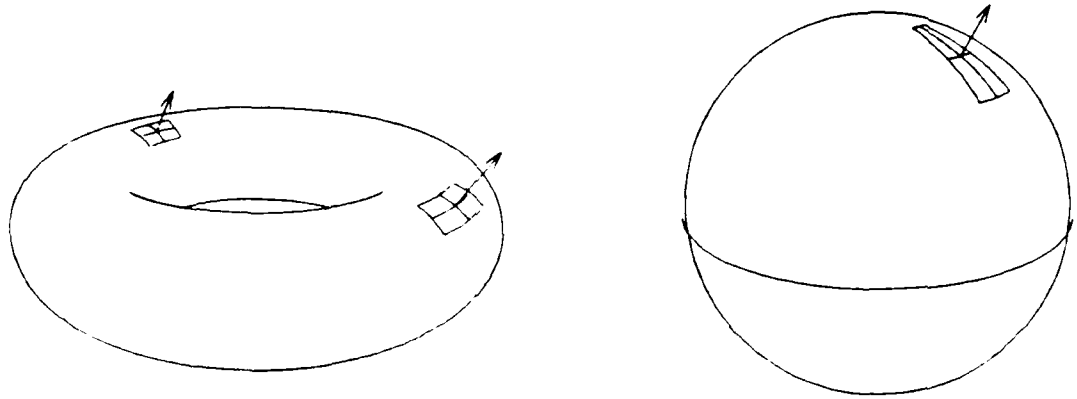

Torus Gaussian sphere

Fig.8.9. Gaussian Mapping of the Torus.
Both points marked on the torus surface map on the same point of the unit sphere.

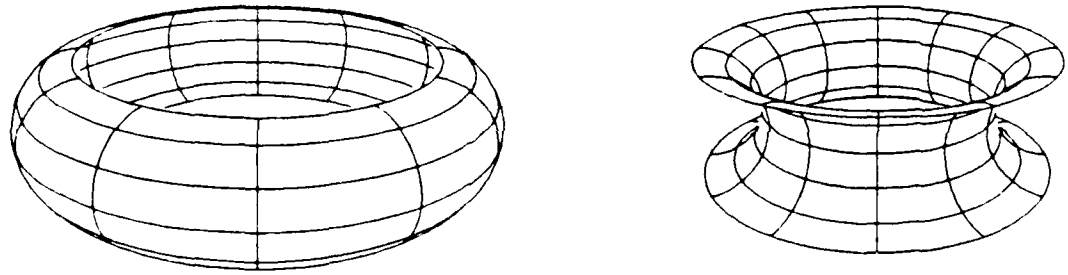

Exterior Surface Interior Surface

Fig.8.10. Interior and Exterior parts of the torus surface.

one-to-one for each of the two parts. The exterior part consists of elliptic surface points only, so that the Silhouette-Slice theory applies without restriction. The interior surface points are all hyperbolic however. As the ST and VST do not specifically depend on surface curvatures, these representations and the related silhouette theory apply without modifications for the interior part. In the case of the CT, the main difference is that the tensor $\bar{\bar{\mathbf{R}}}$ is no longer positive definite. The Spherical transforms of the torus are given by

$$\vec{s} = \begin{bmatrix} n \\ h \\ v \end{bmatrix} = \begin{bmatrix} \pm R\cos\eta + r \\ 0 \\ -(\pm R\sin\eta) \end{bmatrix} \tag{8.5}$$

$$\bar{\bar{\mathbf{R}}} = \begin{bmatrix} (\pm R + r\cos\eta)/\cos\eta & 0 \\ 0 & r \end{bmatrix} \tag{8.6}$$

where r is the radius of the section, R is the radius of the principal axis, and the positive and negative signs in the above equations have to be considered for the exterior and interior parts respectively. These spherical transforms are axisymmetric. Polar plots of the profiles of the non-zero components of these transforms are displayed in Fig.8.11 for both the interior and exterior surfaces. Transforms for the silhouette can be obtained by slicing the above 3-D object transforms. The silhouettes are then obtained by inverse transformation of the silhouette functions. Two examples of silhouettes are developed for a torus with $R=3$, $r=1$, for viewing directions corresponding to $\theta=40^{o}$ and $\theta=25^{o}$. The two silhouette parts corresponding to the interior and exterior parts of the object surface are generated separately, then superimposed in the final figure. For the case of $\theta=40^{o}$, the silhouettes of both parts and their transforms are displayed superimposed in Fig.8.12a). The corresponding diagrams are presented for the case where $\theta=20^{o}$ in Fig.8.12b).

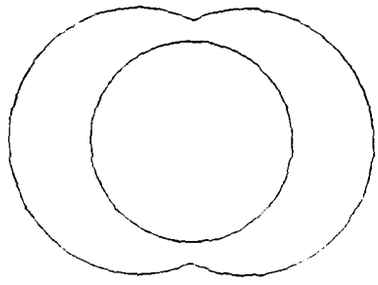

Profile of 3-D ST (*exterior*)

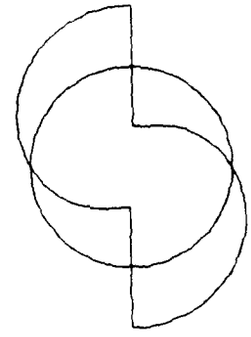

Profile of t-component of 3-D VST (exterior)

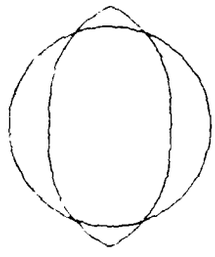

Profile of 3-D ST (interior)

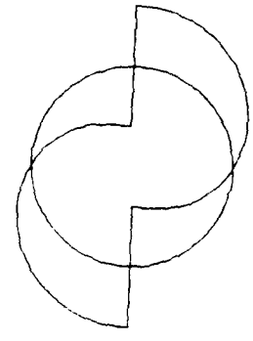

Profile of t-component of 3-D VST (interior)

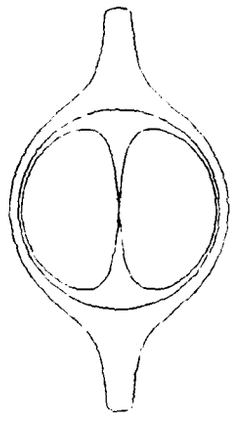

Profile of r_{11}-component of 3-D VST

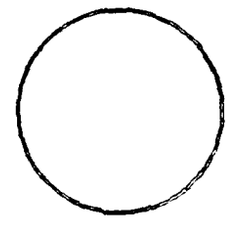

Profile of r_{22}-component of 3-D VST

Fig.8.11. Spherical Transforms of the two parts of the torus

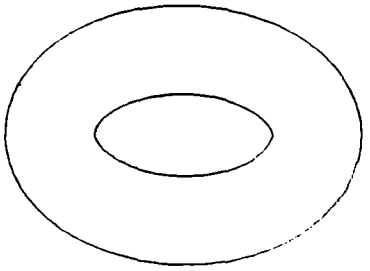

Silhouette

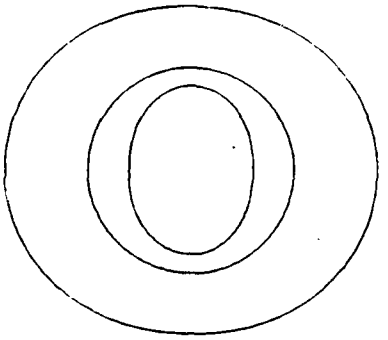

Support Transform

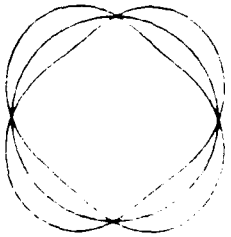

t-component of VST

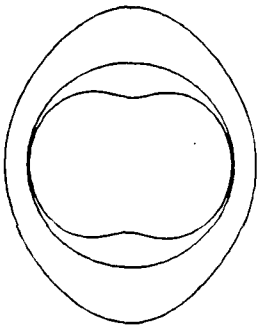

Curvature Transform

Fig.8.12a). Silhouette of the Torus and Circular Transforms.
Viewing Direction: $\theta=40^{o}$.

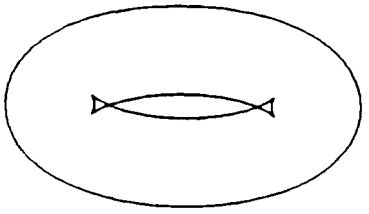

Silhouette

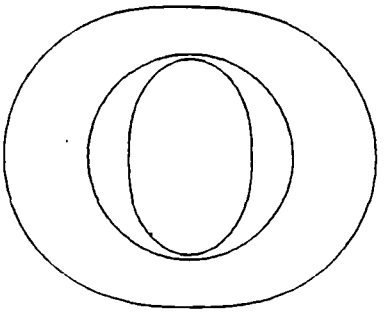

Support Transform

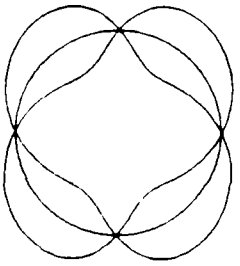

t-component of VST

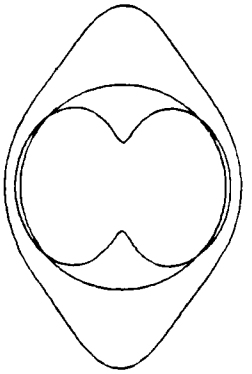

Curvature Transform

Fig.8.12b). Silhouette of the Torus and Circular Transforms.
Viewing Direction: $\theta=25^{o}$.

After the silhouettes are evaluated separately for the interior and exterior parts of the torus, issues of registration may arise when combining the individual silhouette parts. When the silhouettes are obtained with the ST or VST, both parts are referred to the same point in the projection plane and registration is trivial. However, silhouette parts generated with the CT are not related to an origin. In the case of the torus, accurate superposition of the two parts was possible thanks to the symmerty of the surface shape. In the case of a surface in the shape of a distorted torus, the interior and exterior silhouettes could not be accurately registered.

The silhouettes evaluated with the Silhouette-Slice theorems correspond to the projection of all object surface points with a normal perpendicular to the viewing direction. For a non-convex object, some of these points may be occluded by other object parts, so that they do not effectively contribute to the silhouette. The set of silhouette points of a non-convex object determined with the Silhouette-Slice theorems must therefore be considered only as a set of candidate silhouette points. The silhouette itself may be equal to this set, as in the example of Fig.8.12a, or may be a subset of the candidate silhouette, as in the example of Fig.8.12b. Indeed, spurious silhouette parts appear on this figure. They correspond to the projection of points of the object surface for which the normal is perpendicular to the viewing direction, but which are occluded by other parts of the object. When occluded silhouette parts are removed from the interior silhouette, the result displayed in Fig.8.13 is obtained. Note that in this figure, there are two segments of silhouettes in the interior of the object. These must also be eliminated if the silhouette is considered as the set of outline points in the image plane, but are included in the silhouette if it is considered as the set of discontinuity points of a range map in the image plane. Note that, in the example of Fig.8.12a generated for $\theta=40^{\circ}$, the correct silhouette is obtained directly. It can be observed that, for $\theta=40^{\circ}$, the CT of the silhouette part corresponding to the interior surface has a negative radius of curvature while the Gaussian curvature of the surface is negative. In this circumstance, all silhouette points generated with the Silhouette-Slice theorem are true silhouette points. In the case of $\theta=25^{\circ}$, the CT of the silhouette contains alternating signs and zero crossings. The curve of candidate silhouette points has cusps corresponding to the zero crossings. It has been shown by

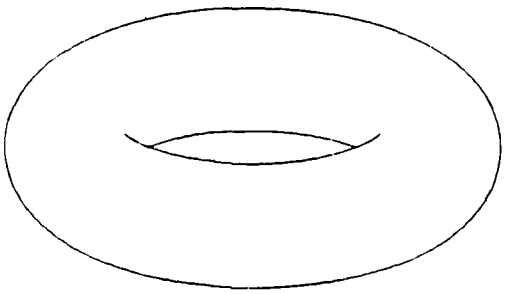

Fig.8.13. Silhouette of the torus for $\theta=25^{\circ}$.
The occluded parts have been removed.

Koenderink[33] that when candidate silhouette points corresponding to a surface with negative Gaussian curvature have a positive curvature, these points are necessarily self-occluded. This property allows us to eliminate the two lateral parts of the interior silhouette in Fig.8.12b. Points on the two remaining longitudinal silhouette parts cannot be tested for visibility by arguments on local surface shapes. On the other hand, the presence of self-occluded silhouette parts suggests the presence of additional silhouette segments for which occlusion occurs due to remote surface elements.

Summarizing our discussion on non-convex objects, each point of the Gaussian sphere may correspond to several points of a non-convex object. The surface can be decomposed into parts so that for each point, the Gaussian mapping is 1:1. When applied to these parts, the Silhouette-Slice theorems provide the correct silhouettes in some cases. More generally, the theorems provide a set of candidate silhouette points in which the silhouette points are included. The actual silhouette points are determined by testing the candidate points for visibility. One necessary visibility condition requires corresponding signs for the curvature of the silhouette and the Gaussian curvature of the surface on the silhouette generator.

8.1.4. Discussion

In this section, silhouette construction has been demonstrated with all three Silhouette-Slice theorems. Through simple experiments, we have observed that construction with the VST is less sensitive to sampling problems than the other two methods, although accurate results are obtained with the three transforms when sufficiently fine samplings are used. We have generated the examples presented in this section with a mixed analytical/numerical method; this strategy can be exploited only when analytical expressions can be determined for the 3-D transforms of the surface shapes of interest. The ST and the VST of a surface can be determined in closed form only for surfaces which can be explicitly parameterized with the normal orientation angles (ξ,η). Although such parameterizations can be derived for several surface shapes, this indicates a limitation of the method. However, it is shown in Appendix 2 that the CT values can be determined analytically for any surface represented by parametric equations. Silhouette construction with the CT is hence applicable to a larger set of surfaces than with the ST and the VST.

In addition to numerical silhouette construction, the Silhouette-Slice theorems can also be exploited to predict qualitatively the shapes of silhouettes. Qualitative shape features of silhouettes include mainly corners, edges and curvatures. These features are best represented by the 2-D CT of the silhouette, and can be easily related to the corresponding features of the object by the Silhouette-Slice theorem for the CT.

We conclude that the CT should be preferred for prediction of qualitative silhouette shape, that the VST is numerically less sensitive than the ST and CT for silhouette construction, but that the CT can be evaluated analytically for a larger set of surfaces than the VST.

8.2. Reconstruction from Silhouettes

The formal problem of reconstructing the shape of a convex object from a set of silhouettes is addressed in this section, and a strategy for solving this problem with the Silhouette-Slice theory is suggested. Due to the lack of a good understanding of sampling issues on the sphere, a practical algorithm for applying the proposed strategy has not been implemented. However, interesting conclusions can be drawn from a formal analysis of the reconstruction problem.

The reconstruction problem addressed in this section can be described as follows. A convex object of unknown shape is projected orthographically onto a number of projection planes Π_i, and the corresponding silhouettes S_i are recorded in each plane. The viewing directions are referred to by their longitude/latitude ϕ_i, θ_i. Given this collection of silhouettes, a method for constructing a description of the 3-D shape of the object is desired. In addition to devising a reconstruction method, it is useful to determine what range of viewing angles ϕ, θ must be covered in order to obtain complete reconstruction.

In the first stage, it is assumed that all silhouette measurements are referred to a global frame $Oxyz$. In each projection plane Π_i, the silhouettes are measured in orthogonal axes $O_\pi x_\pi z_\pi$, where $O_\pi z_\pi$ is the projection of the global Oz axis, see Fig.8.14.

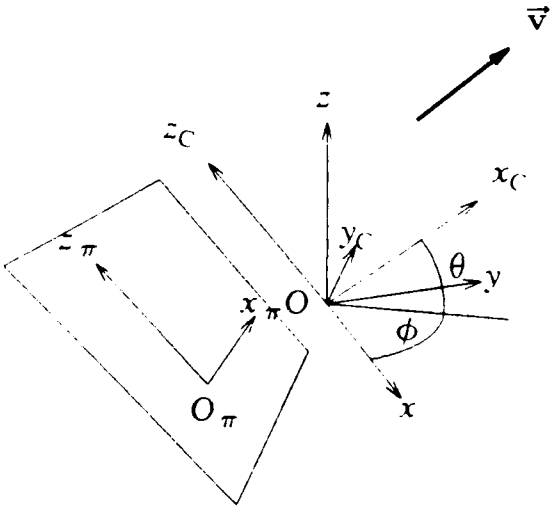

Fig.8.14 Reference frame for the projection plane

The scheme of the reconstruction procedure is to evaluate a circular transform for each measured silhouette, to relate these 2-D transforms to great circle slices of the corresponding 3-D transform of the object, to use this relation to reconstruct the spherical transform, and finally to invert this transform for the object shape.

As reference axes are available in each projection plane, the evaluation of the circular transform of each silhouette is straightforward, and is formally obtained with equations (5.1), (5.11), (5.19). Each circular transform function $p_{\pi i}(\psi)$, $\overline{\mathbf{s}}_i(\psi)$, $\rho_i(\psi)$ is related to the great circle slice of the corresponding spherical transform of the object, which is perpendicular to the viewing direction ϕ_i, θ_i, namely $p(\xi_{SG}, \eta_{SG})$, $\overline{\mathbf{s}}(\xi_{SG}, \eta_{SG})$, $\overline{\overline{\mathbf{R}}}(\xi_{SG}, \eta_{SG})$. The exact relation between the transform value at one point of the silhouette Gaussian circle and the corresponding value of the transform of the object on the slice of the Gaussian sphere depends on the particular transform in question and is given by the appropriate Silhouette-Slice theorem. These relations and their consequences for the reconstruction of 3-D transforms are now investigated in sequence for the ST, the VST, and the CT.

In the case of the ST, the silhouette transform values on the Gaussian circle are exactly equal to the object ST values on the great circle slice of the Gaussian sphere. Therefore, the value of the 3-D ST of the object at one point of the Gaussian sphere is obtained directly as the value of the silhouette ST on a slice passing through that point. In order to recover the complete ST function on the sphere, it is hence necessary to process silhouettes obtained from a range of viewing angles such that the corresponding great circles entirely cover the sphere. One set of such viewing angles is obtained by turning the observer around the object by a 180° arc, see Fig.8.15.

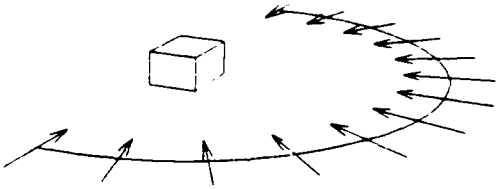

Fig.8.15. A sufficient set of viewing directions for reconstruction with the ST

Reconstruction using the VST is now considered. First, the normal component of the VST is equal to the ST for which reconstruction has been already discussed. The discussion is hence focused on the reconstruction of the horizontal and vertical components h , v of the 3-D VST from the tangential component t of the 2-D VST's of the silhouettes. The Silhouette-Slice theorem for the VST identifies the value of t_{π} on the Gaussian circle of the silhouette to the projection onto the slice plane of the vector $(h \; v)$ at the corresponding point of the great circle slice. Estimating h and v is hence equivalent to estimating a 2-D vector from projections of this vector, and is possible when at least two different projections are known. The vector $(h \; v)^T$ can hence be reconstructed at a point of the Gaussian sphere if and only if its projection t is given on two distinct slices through the point. As a consequence, the set of viewing directions must provide a coverage of the Gaussian sphere by two distinct great circle slices at each point, in order to reconstruct the 3-D VST of the inspected object. A set of viewing directions satisfying this criterion almost everywhere is given by the combination of two different sets of measurements similar to those proposed for the ST. An example of a sufficient set of viewing directions is given in Fig.8.16.

It can be observed that the 2-D VST of each silhouette specifies two values for each point of the Gaussian circle, as opposed to one in the case of the 2-D ST. Although these components are redundant, it is tempting to consider that the VST

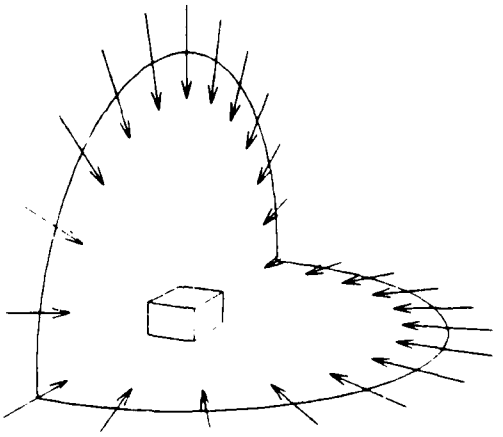

Fig.8.16. A sufficient set of viewing directions for reconstruction with the VST

captures "more information" about the silhouette at each point of the Gaussian circle. Therefore, it seems counterintuitive that the reconstruction using the VST requires a larger set of silhouettes than reconstruction with the ST. This stronger requirement in the case of the VST arises because the redundancy of the 3-D VST was not exploited in the reconstruction method.

Consider now the reconstruction of the object shape through the reconstruction of its 3-D CT. The relation between the 2-D CT of the silhouette at a point of its Gaussian circle and the 3-D CT of the object at the corresponding point on the slice of the Gaussian sphere is that the silhouette 2-D CT, a scalar, is the projection on the slice plane of the object 3-D CT, a 2x2 symmetric tensor. In order to reconstruct a 2x2 symmetric tensor from projections, three projections on different axes are required. In order to reconstruct the value of the 3-D CT of the surface at one point on the Gaussian sphere then, silhouette 2-D CT's on three different great circle slices through the point must be used. The requirement on the minimum set of viewing directions is that the Gaussian sphere must be covered everywhere by three layers of great circle slices. This requirement is satisfied almost everywhere by three orthogonal 180^{o} arcs of viewing directions, such as depicted in Fig.8.17. In this case again, consistency

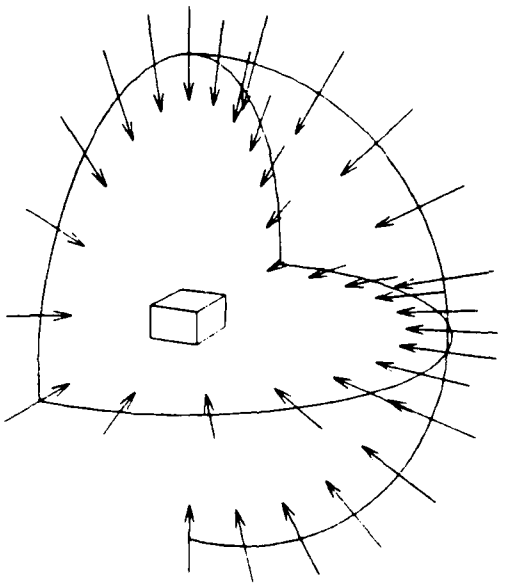

Fig.8.17. A sufficient set of viewing directions for reconstruction with the CT.

constraints on the 3-D CT are not exploited in the above reconstruction strategy. These constraints could be used to relax the requirements on the minimal set of viewing directions.

A substantial difference between 3-D shape reconstruction with the CT on one side and reconstruction with the ST and VST on the other side is that the CT is independent of translations whereas the other two transforms strongly depend on translations of the origin. It was assumed up to now that measurements in each projection plane are referred to axes $O_\pi x_\pi z_\pi$, and that each of these sets of axes is accurately related to the global system of axes $Oxyz$. As silhouette CT's are independent of translations of the origin in their plane, the requirement on registration of the observed silhouettes can be relaxed when reconstruction is performed with the CT. Specifically, only a reference orientation such as the projection of the global Oz direction must be known relative to the global axes in each projection plane, in addition to the orientation of the plane itself. Uncontrolled translations of the reference axes in each projection plane do not affect the reconstruction mechanism. This conclusion can be exploited to determine an interesting difference between the reconstruction of a 3-D object from 2-D silhouettes and the reconstruction of a 2-D object from 1-D silhouettes. Indeed, in the latter case, reconstruction is ambiguous in the absence of an origin for each silhouette. Typical examples of this ambiguity are given by ovals of constant breadth [59]. These 2-D objects have silhouettes of constant length for all orientations, just as circle. These two objects could not be differentiated by unregistered silhouettes.

In the previous paragraphs, reconstruction of 3-D transforms of an object surface from silhouettes has been investigated. Although reconstruction of the object itself merely consists of inverting the reconstructed transform, additional issues may arise in the case of the VST and CT, because of their intrinsic redundancy. It is clear that for a set of silhouettes which actually correspond to the same convex object, consistency of the silhouette circular transforms guarantees consistency of the reconstructed object spherical transform, in the absence of noise and biases. In practical circumstances, however, degradations are inevitable so that the reconstructed 3-D spherical transform is inconsistent in general. When and how to exploit the consistency constraints in the reconstruction is an open question. These constraints could be forced on

the reconstructed spherical transform before reconstruction of the object shape, or they could be exploited earlier, during the construction of the spherical transform, thereby potentially relaxing the requirements on the number of viewing directions.

8.2.1. Discussion

Strategies for reconstructing the shape of a 3-D object from silhouette measurements have been discussed, using the transforms defined in Chapter 5 and the Silhouette-Slice theorems developed in Chapter 6. In order to develop numerical algorithms for implementing these strategies, sampled circular transforms must be considered for representation of the measured silhouettes, and interpolation schemes must be developed for reconstruction of the spherical transforms. As the discrete versions of the Silhouette-Slice theorems have not been formulated yet, the interest of the strategies presented in this section is conceptual at this point.

Reconstruction methods based on the three silhouette-slice theorems are now compared, assuming that satisfactory solutions can be provided for the sampling issues. When consistency constraints of the 3-D transforms are not exploited, the ST seems preferable since it is least redundant and requires the smallest set of viewing directions. For reconstruction using the constraints, the 3-D VST should be preferred, since it incorporates more measurements from the silhouette. In addition, the inversion of the 3-D VST is only a set of 3-D rotations, while derivatives must be estimated for inversion of the 3-D ST. Finally, reconstruction with the CT should be considered when registration of the origins in the various silhouette planes is absent or imprecise.

Incorporating consistency constraints in the reconstruction of a 3-D transform could be implemented as an optimization problem where the solution would have to satisfy the constraints while minimizing the total deviation from the slices corresponding to the measured silhouettes. The solution could be obtained by iterative methods similar to the ones used to solve other surface resontruction problems such as the shape-from-shading problem [21].

8.3. Recognition from Silhouettes

This section suggests an application of the Silhouette-Slice theory to the derivation of constraints for a system performing object recognition from silhouettes. The arguments are based on the extension of the Silhouette-Slice theorem for the CT to polyhedral objects developed in Chapter 7.

It was demonstrated in the previous section that a large number of silhouettes corresponding to different viewing directions are required for accurately reconstructing the shape of a 3-D object. It would seem then that one silhouette contains too little information to discriminate between different objects. Although some different objects may produce exactly the same silhouettes when viewed from selected directions, shapes of objects of interest are sufficiently different in general so that these singularities of the problem are rare. As a result, one silhouette is often sufficient to specify one object in a set of known objects.

The principles of a system for recognizing polyhedral objects from one of their silhouettes are now presented. The system is based on a well-known approach in model-based vision. Primitive features such as points, edges or facets are first extracted from the input data. These features are then matched to corresponding model features, implicitly creating a large matching tree. The tree is explored and pruned by constraints resulting from the pairing of small sets of measured features to sets of model features. Finally, the remaining hypotheses are tested more thoroughly for correspondence with the models. Implementation of this approach has been reported for recognizing 2-D objects from 2-D measurements, and for recognizing 3-D objects from 3-D measurements [60]. In the case of 2-D models and data, powerful constraints arise from the pairing of two object features to two model features, so that the pruning is very effective. When matching 2-D data such as silhouettes to 3-D models, the constraints resulting from the pairing of two primitives are much weaker since there are six degrees of freedom. In the proposed approach, constraints are considered for the pairing of three silhouette features to three model features.

The proposed recognition method is based on primitive features consisting of polyhedral edges. Its scope is restricted to polyhedra or shapes with a sufficient number of straight edges. For a number of objects expected in the input images, it is assumed that geometric models explicitly describing the edges are available. An

unknown silhouette is analyzed by first detecting straight edges and measuring their length and orientation. Pairings are hypothesized between measured edges and edges of the 3-D models. As the number of potential global matches may be astronomical, pairings between sets of only three silhouette edges and three model edges are considered first. Each such set of pairings is tested against a set of constraints, an example of which is derived later in this section. After discarding the pairings that fail these tests, additional edges are added to the remaining hypotheses, and further testing is applied. In a favorable case, a large fraction of the search tree is eliminated by the constraints, leaving only a few potential interpretations of the data. Each of these interpretations is then tested in more detail by an appropriate method.

A number of constraints are now derived for the matching of three silhouette edges to three particular model edges. The derivation of the pruning constraints is substantially simplified by reasoning with the Silhouette-Slice theorems. First, it is worthwhile to note that position and orientation of a detected object are unknown a-priori in recognition problems. The ST and VST strongly depend on the choice of an origin, as was illustrated in section 8.1. Therefore, these transforms are not appropriate for recognition applications. The derivations in this section are based solely on the Silhouette-Slice theorem for the CT.

The contribution of three edges e_1, e_2, e_3 to the 2-D CT of the silhouette is given by three impulses at orientations ψ_1, ψ_2, ψ_3 corresponding to the normals of the edges. The strengths of these impulses are given by the lengths l_1, l_2, l_3 of the silhouette edges, see Fig.8.18. Note that the orientation of the object is unknown a-priori, so that the reference orientation in the silhouette plane cannot be related to the object model. The angles to be considered in the constraints are hence the differences $\psi_{12} = \psi_2 - \psi_1$ and $\psi_{23} = \psi_3 - \psi_2$. These angles can be directly estimated from the image, and can be related to angles in the object model.

Consider now a hypothetical match between the three measured edges e_1, e_2, e_3 and three model edges E_1, E_2, E_3. The three model edges each correspond to an arc of great circle on the Gaussian sphere, as illustrated on Fig.8.19. When the silhouette great circle slice intersects one of these arcs, the image of the corresponding edge is present in the silhouette, and has a normal orientation determined by the orientation of the intersection in the slice plane. The strategy for accepting or rejecting the match

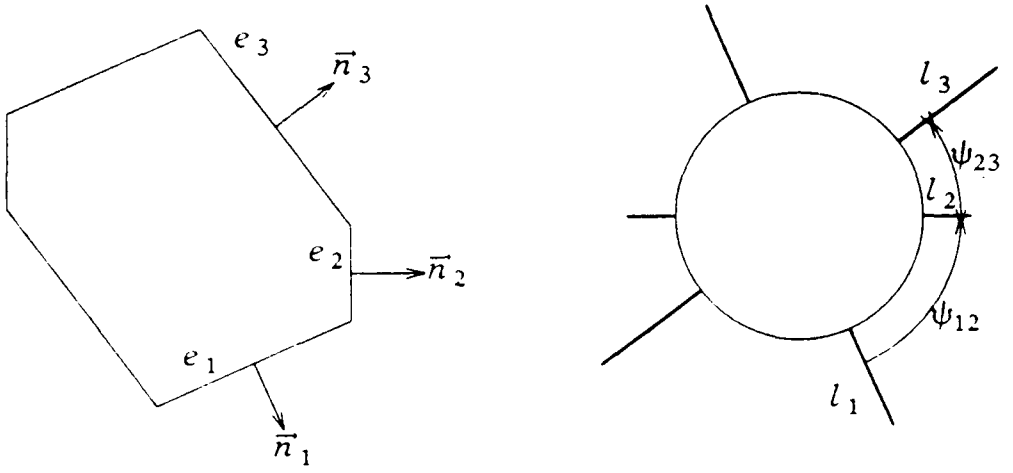

Measured Silhouette 2-D CT

Fig.8.18. Three Silhouette Edges and the corresponding CT

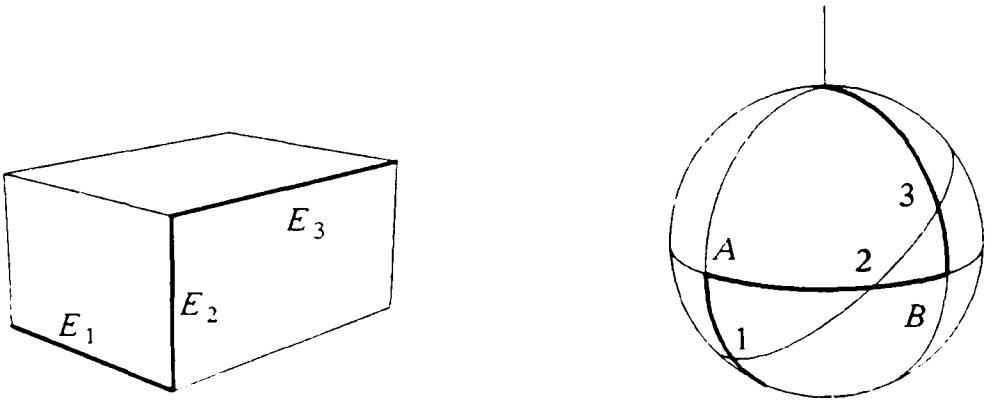

Model Polyhedron 3-D CT

Fig.8.19. Three Model Edges and the corresponding CT arcs

---

consists of first deciding if there is an orientation ϕ, θ of the viewing direction for which the slice cuts the model arcs at points separated by the measured angles ψ_{12}, ψ_{23}. When the hypothesis is accepted on the basis of these orientations, the viewing direction is fixed. For this viewing direction then, the lengths l_{M1}, l_{M2}, l_{M3} of the silhouette edges corresponding to the model edges E_1, E_2, E_3 can be evaluated. For a

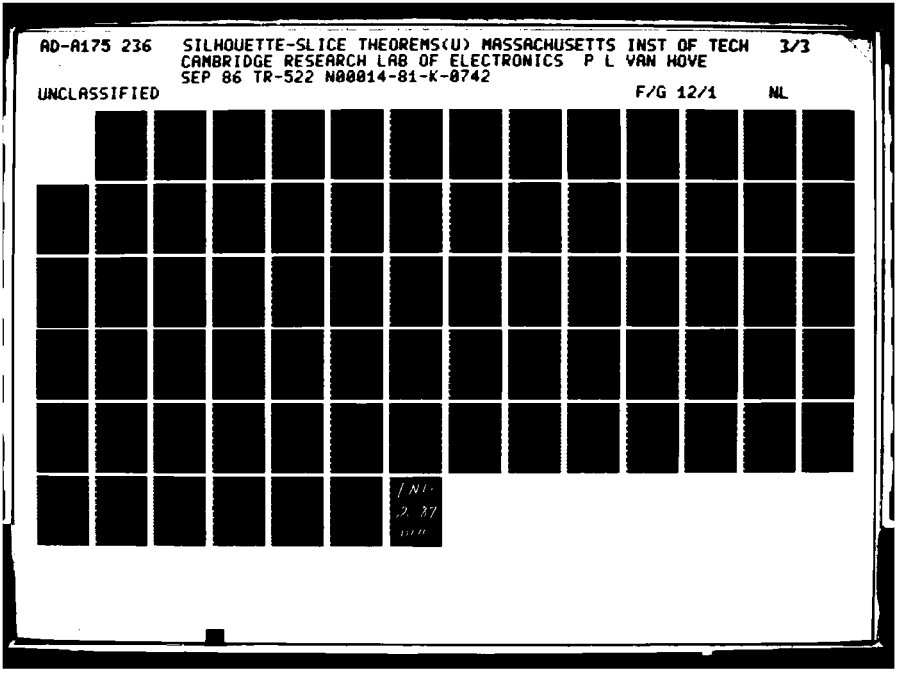
AD-A175 236 SILHOUETTE-SLICE THEOREMS(U) MASSACHUSETTS INST OF TECH 3/3
CAMBRIDGE RESEARCH LAB OF ELECTRONICS P L VAN HOVE
SEP 86 TR-522 N00014-81-K-0742
UNCLASSIFIED F/G 12/1 NL

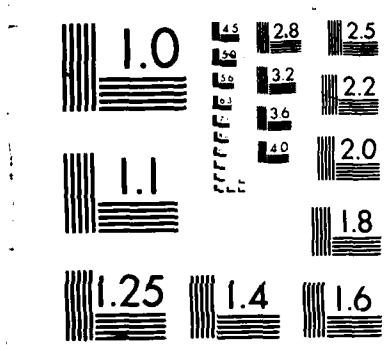

convex object not obscured by other objects, the measured edge lengths l_i must match the estimated lengths l_{Mi} within some tolerance bounds. For non-convex objects, partial self-occlusions may occur, and, more generally, object edges may be partially obscured by other objects. A better test in those cases is to require the measured edges l_i to be smaller than the estimated l_{Mi}, within a tolerance bound.

Expressions for the orientations ϕ, θ and acceptance constraints are now derived for three silhouette edges such as those depicted in Fig.8.18. The derivation is simplified by considering three model edges perpendicular to one another, such as the ones displayed in Fig.8.19. The case of three right angles arises frequently in man-made parts; extensions to include one or two acute or obtuse angles are tractable. Consider hence matching the three silhouette edges e_i depicted in Fig.8.18 with the three model edges depicted in Fig.8.19. The great circle slice corresponding to the match is drawn on Fig.8.19; the angles of interest appear in the two spherical triangles $1A\,2$, $2B\,3$, which are displayed "flattened out" in Fig.8.20. We consider the angles ψ_{12}, ψ_{23} as positive. In order to match the great circle slice, the silhouette edges must be such that $\psi_{12} + \psi_{23} \leq \pi$. The orientation of the corresponding viewing direction is determined by θ and $\phi = \xi_2 - \pi/2$.

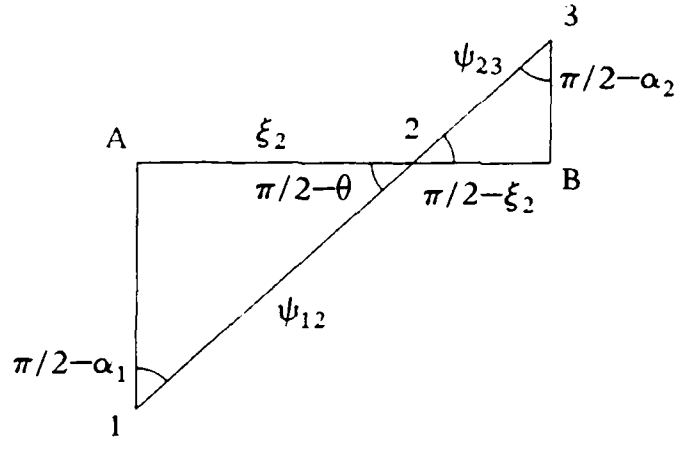

Fig.8.20. Two spherical triangles of interest for deriving the matching constraints.

Standard relations of trigonometry for right-angled spherical triangles[55] are applied to the triangles of figure Fig.8.20 to produce

$$\left|\begin{array}{ll} \tan\xi_2 \cot\psi_{12} & = \cos(\pi/2-\theta) \\ \tan(\pi/2-\xi_2) \cot\psi_{23} & = \cos(\pi/2-\theta) \\ \sin\psi_{12} \cos\alpha_1 & = \sin\xi_2 \\ \sin\psi_{23} \cos\alpha_2 & = \cos\xi_2 \end{array}\right. \tag{8.7}$$

The angles θ and ξ_2 can be extracted from the first two equations above.

$$\left|\begin{array}{ll} \tan\xi_2 & = \sqrt{\tan\psi_{12}\cot\psi_{23}} \\ \sin\theta & = \sqrt{\cot\psi_{12}\cot\psi_{23}} \end{array}\right. \tag{8.8}$$

The above relations imply the necessary constraints that ψ_{12}, $\psi_{23} < \pi/2$; $\psi_{12} + \psi_{23} > \pi/2$. The predicted lengths of the silhouette edges corresponding to E_1, E_2, E_3 are given by

$$\left|\begin{array}{lll} l_{1S} = l_{1M} \cos\alpha_1 & = l_{1M} \dfrac{\sin\xi_2}{\sin\psi_{12}} \\ l_{2S} = l_{2M} \cos\theta & = l_{2M} \left(1 - \cot\psi_{12} \cot\psi_{23}\right)^{1/2} \\ l_{3S} = l_{3M} \cos\alpha_3 & = l_{3M} \dfrac{\cos\xi_2}{\sin\psi_{23}} \end{array}\right. \tag{8.9}$$

These predicted silhouette edge lengths l_{iS} must be tested against the measured silhouette edges l_i.

Although the above system has not been implemented, there are indications that this type of system has a potential for success.

8.3.1. Discussion

A formal application of the Silhouette-Slice theorems to a problem of object recognition was presented in this section, thereby illustrating the use of the transforms and of the theorems in reasoning about silhouettes, and in applying the intuition to practical recognition problems. As object position and orientation are usually unknown a-priori in recognition tasks, the Silhouette-Slice theorem for the CT seems the most useful one for recognition, since the CT is independent of origin

location. In addition, many applications to recognition are based on qualitative relations between silhouette shapes and object shapes. These relations are also obtained most easily with the CT. The theories developed for the CT are hence the most important for applications in object recognition.

8.4. Summary

In this chapter, several applications of the theoretical results of this thesis have been suggested. Examples shown in the section on silhouette construction are close to actual implementations of the Silhouette-Slice theorems to problems in computer graphics. Other examples presented in this chapter are of a more conceptual value. This chapter has suggested the wide applicability of the Silhouette-Slice theorems as reasoning tools in problems of computer graphics and computer vision, and their potential for developing new algorithms in these domains.

Chapter 9
Summary

9.1. Contributions

In this thesis, a new formalism for relating the shapes of objects to the shapes of their silhouettes has been proposed. Three representations of 3-D object surfaces and the equivalent representations of 2-D curves have been defined. It has been shown that the representations of a 2-D silhouette curve are simply related to the representations of the corresponding 3-D object surface. More specifically, object surfaces have been represented by scalar, vector and tensor functions on the Gaussian sphere, and curves by scalar and vector functions on the Gaussian circle. It has been demonstrated that a slice of the Gaussian sphere perpendicular to the viewing direction is a Gaussian circle for the silhouette. Furthermore, the property functions on the Gaussian circle of a silhouette are related by a projection to the property function of the object on the slice corresponding to the silhouette.

The relations between an opaque object, its silhouette and their transforms is conceptually similar to the relations between an absorbing object, its line-integral projection and their Fourier transforms, which are formalized in the Projection-Slice theorem of computerized tomography. These similarities have prompted the use of the name of Silhouette-Slice theorems for the new relations presented in this thesis.

The theory relating property circles of silhouettes to slices of property spheres of objects provides substantial insight into qualitative and quantitative relations between silhouette shapes and object shapes. This insight is useful when reasoning about particular problems involving silhouettes, and provides straightforward explanations of known results. Applications of the theories to three basic problems have been considered, namely silhouette synthesis, reconstruction from silhouettes and recognition from silhouettes. The theories have been demonstrated in this thesis for convex objects and orthographic projections only; in addition, difficult issues remain to be solved before discrete versions of the continuous transforms and Silhouette-Slice theorems can be developed. As a consequence, it has not been possible to develop direct implementations of the theory into general numerical algorithms for solving the

three basic problems. However, methods based on continuous functions have been proposed for applying the results to each of the three problems. Mixed continuous-space / discrete-space algorithms have been proposed and demonstrated for the synthesis of silhouettes of complex curved surfaces such as a torus and superquadrics. A general strategy has been proposed for reconstructing the shape of a convex 3-D object from silhouette observation. The method consists of first constructing the circular transform of each silhouette, then combining these into the spherical transform of the object. Finally, the object shape is obtained by evaluating the inverse 3-D transform. In the context of recognition from silhouettes, several quantitative and qualitative relations between object features and silhouette features have been proposed. These relations are typically exploited in recognition algorithms as constraints on pairings of silhouette features with object features. An example of the use of constraints on edges has been proposed in a strategy for recognizing polyhedral objects from their silhouettes.

The spherical transforms of 3-D surfaces presented in this thesis can be interpreted as compact representations of the set of all silhouettes of the object. In addition, these transforms have potential applications for representing surfaces independently of viewpoint. In particular, the 3-D Curvature Transform is an intrinsic form for surfaces, which specifies surface curvature as a function of normal orientation. Compared to most characterizations of surfaces in computer vision [39] and in differential geometry [47], the originality of the Curvature Transform is two-fold. First, curvature is completely described by an invariant tensor of curvature, as opposed to two tensors in classical differential geometry, and a partial description by one or two scalar invariants in machine vision. Second, the curvature is described with a canonic parameterization, as opposed to generic parameterizations in differential geometry, and to image plane descriptions generally used in machine vision.

The key contribution of this thesis is a new basic theory for analyzing silhouettes. The theory provides useful insight in many questions of relations between silhouette shapes and object shapes, and also in analyzing complex curved surfaces. A number of straightforward applications have been proposed or suggested. It is shown in the next section that there is substantial room for additional work on the theory and on its applications, and that this work is promising.

9.2. Future Research

There are several directions in which the present work can be pursued. Most promising areas are a careful analysis of the sampling questions, and an investigation of extensions to non-convex objects. These two areas are now discussed with more detail.

At this time, to the best knowledge of the author, there is no theory comparable to the Shannon sampling theory for the discrete representation of functions defined on non-Euclidean manifolds such as the sphere. This problem has several facets. First, sets of sample points must be defined on the domain of the function. It has been shown that regular samplings of the sphere are impossible for practical numbers of samples. Irregular samplings have been proposed, but they have a number of disadvantages. The second issue is the definition of sample values; a sample value could be the value of the continuous function at the sample point, or a weighted average of the function values in a neighborhood of the sample point. The third issue is the choice of interpolation algorithms, i.e. algorithms for estimating the value of the continuous function from the sample values, at points other than the sample points. The fourth issue is the characterization of a class of functions for which sampling followed by interpolation leaves the function unchanged. These four issues are tightly coupled, and their solution is likely to involve complex arguments. A precise formulation of the sampling questions would permit the development of algorithms for synthesizing silhouettes, applicable to shapes specified both analytically or numerically. The development of numerical algorithms for shape reconstruction from silhouettes using the circular and spherical transform would also be greatly simplified by solutions of the sampling question.

Extensions of the theory to cover non-convex objects are essential for direct applications of the theories to real-world objects. These extensions include principally the definition of the transforms for non-convex objects in 2-D and in 3-D, and the analysis of the occlusion problem. One method for defining the Gaussian mapping and therefore the spherical transforms for non-convex objects consists of separating the object surface into several patches such that each part has a well-defined Gaussian image. A different method is to consider several Riemann "sheets" on the Gaussian sphere. The same methods are applicable to Gaussian circles of silhouette curves.

When relating Gaussian circles of silhouettes to slices of the Gaussian sphere of the object, different silhouette parts or sheets on the Gaussian circle must be related to their counterparts on the Gaussian sphere of the object. This correspondence is readily preserved in silhouette synthesis, but may raise difficult issues in reconstruction from silhouettes. Indeed, when several sheets are defined on the Gaussian circles of different silhouettes, care must be exercised in preserving a consistent pairing of the sheets when combining the circles as slices on the Gaussian sphere of the object.

In addition to issues involving multiplicity of the Gaussian image, silhouette analysis is more complex for non-convex objects due to the possibility of occlusions. When applying the silhouette construction method with the silhouette generator to non-convex objects, a superset of the silhouette is obtained instead of the silhouette itself. Indeed, some of the points generated by this method may correspond to occluded object surface patches so that they do not appear in the silhouette. The set of points generated by the silhouette construction method for convex objects is hence a set of candidate silhouette points when applied to a non-convex object. This set must then be pruned for occluded points. In the context of reconstruction from silhouettes, the occlusions imply that less information may be obtained from each silhouette. As a consequence, a larger set of viewing directions may be required to reconstruct the complete shape of a non-convex object. The question of which non-convex objects can be reconstructed from the set of all their silhouettes has not been answered yet. These objects have been called "tangible objects"; for each point on the surface of a tangible object, there must be at least one tangent line which does not intersect the surface [61]. Convex objects are a subset of tangible objects, and some non-convex objects are also tangible objects. It is easy to construct non-tangible objects by considering a long flexible cylinder and tying "knots" in this object. A simpler and more striking example is that a torus is not a tangible object, whereas a toroidal object with a square section is.

In addition to the extensions to discrete transforms and to non-convex objects, there is clear potential for extending the theories presented in this thesis in two other directions. One extension would be to consider property spheres of third and higher order terms of Taylor expansions of surface equations, and to relate these to corresponding property circles of silhouettes. A different extension is to define transforms on hyperspheres S_n for n-dimensional hypersurfaces in (n+1)-dimensional

space. These two extensions seem conceptually straightforward, would involve tedious algebra, and may not be very useful.

Aside from extensions of the theories developed in this thesis, there is a large potential for applications. Once sampling issues are resolved, algorithms for numerical synthesis of silhouettes and numerical reconstruction of 3-D shapes from silhouettes can be developed. The mixed analytical/numerical silhouette synthesis method used in this thesis to generate examples could be extended to more surface types by deriving a table of transforms for many known surface patch equations. This project could be implemented on a system for symbolic algebra such as MACSYMA.

The theory presented in this thesis is rich in potential applications in the areas of computer graphics and computer vision. The work presented here provides new insights in the geometry of surfaces which could be useful in understanding differential geometry. This thesis has provided a new basic theory and provides ample room for future research.

Appendix 1
Examples of Transforms

In this appendix, the three transforms are analytically determined for a number of curves and surfaces. Specifically, the Support Transform, Vector Support Transform and Curvature Transform are evaluated for conics, superconics, torus patches, quadrics, and superquadrics.

In each case, the curve or surface is first described by parametric equations for its Cartesian coordinates. With this form, a normal vector is determined at each point, then compared to the unit vector expressed in terms of the canonical normal angles. This comparison provides relations between the generic parameters and the canonical angles, from which canonical parametric equations can be determined, parameterized with the polar angle ψ of the normal orientation for a curve, and with the geographical coordinates (ξ,η) of the normal for a surface. The transformations in (5.1), (5.11), (5.19) are then applied to the equations of a curve to determine its three circular transforms. *Similarly, the three transforms of a surface are obtained using equations* (5.29), (5.36), (5.45).

A1.1. Transforms of Planar Curves

A1.1.1. Conics

Conics are curves described by quadratic implicit equations for the Cartesian coordinates of their points. The general form of this equation in the Oxz plane is

$$A\,x^2 + 2B\,xz + C\,z^2 + 2D\,x + 2E\,z + F = 0 \qquad \text{(A1.1)}$$

When the quadratic form in the left-hand side is not degenerate, the linear terms can be eliminated by a translation of axes, and the mixed second-order term by a rotation of axes. As a result, each non-degenerate quadratic curve can be described by an equation of the type

$$\pm\left(\frac{x}{a}\right)^2 \pm \left(\frac{z}{c}\right)^2 = 1 \qquad \text{(A1.2)}$$

in an appropriate system of axes. When both signs are positive, the above equation

describes an ellipse with half-diameters a and c along the Ox and Oz axes respectively: see Fig.A1.1. A set of parametric equations for the ellipse in (A1.2) is given by

$$\mathbf{x} = \begin{Bmatrix} x \\ z \end{Bmatrix} = \begin{Bmatrix} a\ \cos t \\ c\ \sin t \end{Bmatrix} \tag{A1.3}$$

A1.1.1.1. Normal Vector

A vector $\bar{\mathbf{t}}$ tangent to the ellipse is obtained as the first derivative of the coordinate vector,

$$\bar{\mathbf{t}} = \mathbf{x}_t = \begin{Bmatrix} -a\ \sin t \\ c\ \cos t \end{Bmatrix} \tag{A1.4}$$

A normal vector is then obtained by noting that, in 2-D, $(t_z\ -t_x)^T$ is a vector perpendicular to $(t_x\ t_z)^T$.

$$\mathbf{n}' = \begin{Bmatrix} c\ \cos t \\ a\ \sin t \end{Bmatrix} \tag{A1.5}$$

To preserve the similarity with the case of quadratic surfaces in 3-D, the above normal vector will be scaled by ac.

$$\mathbf{n} = \begin{Bmatrix} (1/a)\cos t \\ (1/c)\sin t \end{Bmatrix} \tag{A1.6}$$

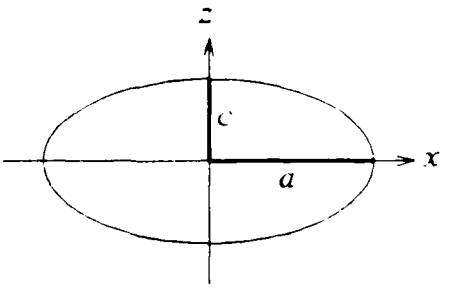

Fig.A1.1. Ellipse with semi-axes $a=4$, $c=2$.

A1.1.1.2. Canonical Parameterization

The normal vector in (A1.6) is compared with the unit vector in terms of the polar normal angle ψ

$$\mathfrak{n} = \begin{vmatrix} (1/a)\cos t \\ (1/c)\sin t \end{vmatrix} = |\mathfrak{n}| \begin{vmatrix} \cos\psi \\ \sin\psi \end{vmatrix} \tag{A1.7}$$

Using the identity $\cos^2 t + \sin^2 t = 1$, it it easy to determine that

$$|\mathfrak{n}| = (a^2\cos^2\psi + c^2\sin^2\psi)^{-1/2} \tag{A1.8}$$

and therefore that the relation between t and ψ is given by

$$\begin{vmatrix} \cos t \\ \sin t \end{vmatrix} = |\mathfrak{n}| \begin{vmatrix} a\cos\psi \\ c\sin\psi \end{vmatrix} \tag{A1.9}$$

The equations of the ellipse in terms of the normal orientation ψ are hence given by

$$\mathfrak{x} = |\mathfrak{n}| \begin{vmatrix} a^2\cos\psi \\ c^2\sin\psi \end{vmatrix} \tag{A1.10}$$

A1.1.1.3. Circular Transforms

The three transforms of the ellipse are determined by applying the transformations in (5.1), (5.11), (5.19) to the canonic equation (A1.10). The ST and VST are given by

$$p = \mathfrak{x}\cdot\bar{1}_n = (a^2\cos^2\psi + c^2\sin^2\psi)^{1/2} = |\mathfrak{n}|^{-1} \tag{A1.11}$$

$$\mathfrak{s} = \mathrm{R}_2^{G-R}\,\mathfrak{x}$$

$$= |\mathfrak{n}| \begin{vmatrix} a^2\cos^2\psi + c^2\sin^2\psi \\ (c^2 - a^2)\sin\psi\cos\psi \end{vmatrix} = p^{-1} \begin{vmatrix} p^2 \\ (c^2 - a^2)\sin\psi\cos\psi \end{vmatrix} \tag{A1.12}$$

In order to determine the CT, the derivative $\mathfrak{x}_\psi$ must be evaluated

$$\mathfrak{x}_\psi = |\mathfrak{n}|\, a^2 c^2 \begin{vmatrix} -\sin\psi \\ \cos\psi \end{vmatrix} \tag{A1.13}$$

The CT function is then obtained as

$$\rho(\psi) = \mathbf{x}_{\psi} \cdot \bar{\mathbf{I}}_t = (ac)^2 |\mathbf{n}|^3 = \frac{(ac)^2}{(a^2\cos^2\psi + c^2\sin^2\psi)^{3/2}} \qquad \text{(A1.14)}$$

A1.1.2. Superconics

Superconics are a class of curves which includes conics, and which are described in centered axes by implicit equations such as

$$\pm \left| \frac{x}{a} \right|^n \pm \left| \frac{z}{b} \right|^n = 1 \qquad \text{(A1.15)}$$

When both signs are positive and n is a real number in $(1,\infty)$, the curve specified by (A1.15) is smooth and strictly convex. It can also be described by the parametric equations

$$\mathbf{x} = \begin{vmatrix} x \\ z \end{vmatrix} = \begin{vmatrix} a\,|\cos t\,|^s\, sign\,(\cos t) \\ b\,|\sin t\,|^s\, sign\,(\sin t) \end{vmatrix} \qquad 0 \leqslant t < 2\pi \qquad \text{(A1.16)}$$

with $s = 2/n$. Special cases include an ellipse for $s = 1$, a rectangle in the limit for $s \to 0$ and a rhombus for $s \to 2$; see Fig.A1.2.

The circular transforms of the superconic are first derived for the first quadrant of the variable t, so that

$$\mathbf{x} = \begin{vmatrix} a\cos^s t \\ b\sin^s t \end{vmatrix} \qquad 0 \leqslant t \leqslant \pi/2 \qquad \text{(A1.17)}$$

A1.1.2.1. Normal Vector

A tangent vector is determined by

$$\bar{\mathbf{t}} = \mathbf{x}_t = \begin{vmatrix} -as\cos^{s-1}t\,\sin t \\ bs\sin^{s-1}t\,\cos t \end{vmatrix} \qquad \text{(A1.18)}$$

The normal vector is then obtained as

$$\mathbf{n}' = \begin{vmatrix} bs\,\sin^{s-1}t\,\cos t \\ as\,\cos^{s-1}t\,\sin t \end{vmatrix} \qquad \text{(A1.19)}$$

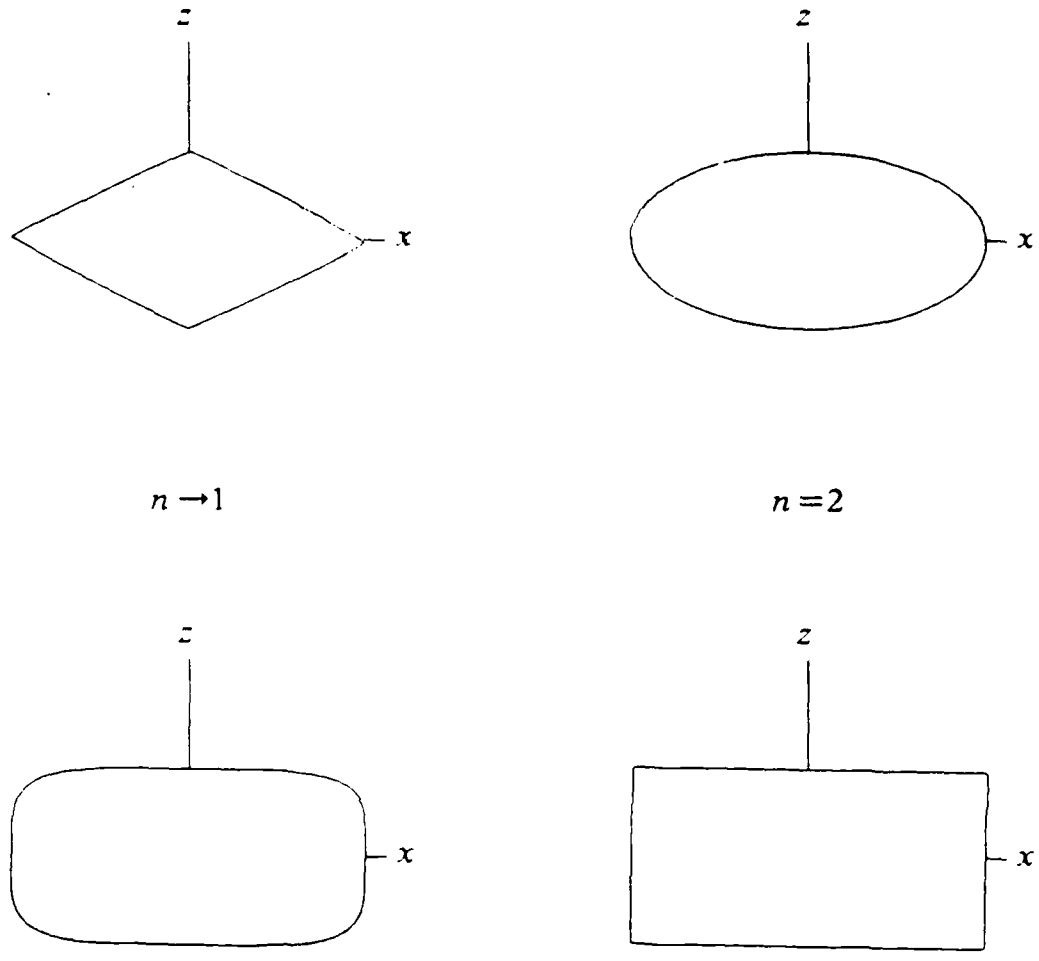

Fig.A1.2. Examples of superconics with half diameters $a=4$, $b=2$.

A simpler form is obtained by scaling the above vector by $ab\ \cos^{s-1}t\ \sin^{s-1}t$

$$\mathbf{n} = \begin{pmatrix} (1/a)\cos^{2-s}t \\ (1/b)\sin^{2-s}t \end{pmatrix} \tag{A1.20}$$

A1.1.2.2. Canonical Parameterization

The normal vector in (A1.20) is compared to the unit normal in terms of the polar angle ψ to determine the relation between t and ψ.

$$\mathbf{n} = \begin{pmatrix} (1/a)\cos^{2-s} t \\ (1/b)\sin^{2-s} t \end{pmatrix} = |\mathbf{n}| \begin{pmatrix} \cos\psi \\ \sin\psi \end{pmatrix} \tag{A1.21}$$

Using the trigonometric identity $\cos^2 t + \sin^2 t = 1$, it is easy to determine $|\mathbf{n}|$ then $\mathbf{x}$ in terms of ψ.

$$|\mathbf{n}| = N^{-1/(k+1)} \tag{A1.22}$$

$$\mathbf{x} = N^{-\frac{k}{k+1}} \begin{pmatrix} a^{k+1}\cos^k \psi \\ b^{k+1}\sin^k \psi \end{pmatrix} \tag{A1.23}$$

with $k = s/(2-s) = 1/(n-1)$ and

$$N = (a\cos\psi)^{k+1} + (b\sin\psi)^{k+1} \tag{A1.24}$$

A1.1.2.3. Circular Transforms

It is straightforward to determine the VST of the superconic by applying the transformation in (5.11) to (A1.23).

$$\mathbf{s} = N^{-\frac{k}{k+1}} \begin{pmatrix} (a\cos\psi)^{k+1} + (b\sin\psi)^{k+1} \\ \sin\psi\cos\psi\,(-a^{k+1}\cos\psi^{k-1} + b^{k+1}\sin\psi^{k-1}) \end{pmatrix} \tag{A1.25}$$

The first component of the above equation is also equal to the ST function

$$p = N^{-\frac{k}{k+1}}[(a\cos\psi)^{k+1} + (b\sin\psi)^{k+1}] = N^{\frac{1}{k+1}} \tag{A1.26}$$

An expression for the ST valid in the four quadrants of the normal angle ψ is given by

$$p = [|a\cos\psi|^{k+1} + |b\sin\psi|^{k+1}]^{\frac{1}{k+1}} = N^{\frac{1}{k+1}} \tag{A1.27}$$

where

$$N = |a\cos\psi|^{k+1} + |b\sin\psi|^{k+1} \tag{A1.28}$$

The corresponding expression for the VST is

$$\mathbf{s} = N^{-\frac{k}{k+1}} \begin{vmatrix} N \\ \sin\psi\cos\psi\,(\,-a^{k+1}\,|\cos\psi|^{k-1} + b^{k+1}\,|\sin\psi|^{k-1}\,) \end{vmatrix} \quad \text{(A1.29)}$$

The CT of the superconic is determined by first evaluating the derivative $\bar{x}_{\psi}$, then evaluating the CT function with (5.19). The derivative is given in the first quadrant by

$$\mathbf{x}_{\psi} = k\,(ab)^{k+1}\,N^{-\frac{2k+1}{k+1}} \begin{vmatrix} -\cos^{k-1}\psi\,\sin^{k}\psi \\ \sin^{k-1}\psi\,\cos^{k}\psi \end{vmatrix} \quad \text{(A1.30)}$$

The CT function, i.e. the radius of curvature, is given by the following expression valid in the four quadrants.

$$\rho(\psi) = \frac{k\,(ab)^{k+1}\,|\cos\psi\,\sin\psi|^{k-1}}{\left|\,|a\cos\psi|^{k+1} + |b\sin\psi|^{k+1}\right|^{\frac{2k+1}{k+1}}} \quad \text{(A1.31)}$$

Polar diagrams of the transform functions are illustrated in Fig.A1.3. for a superconic with $n = 4.5$.

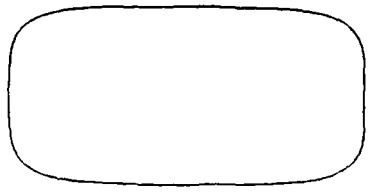

Superconic

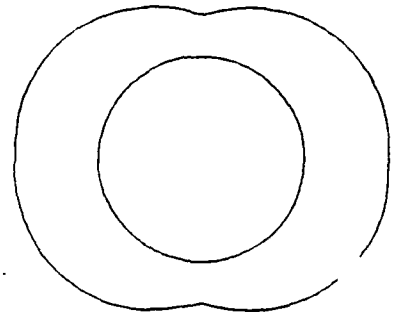

Support Transform

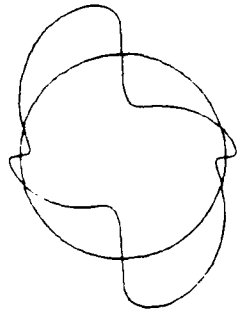

t-component of VST

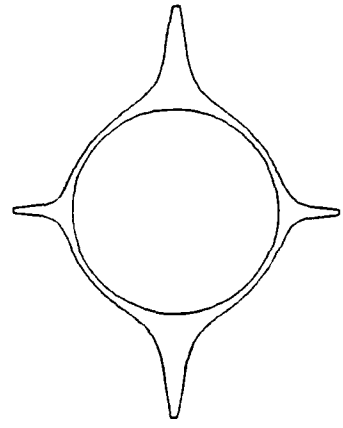

Curvature Transform

Fig.A1.3. Transforms of a superconic with $n = 4.5$

A1.2. Transforms of 3-D Surfaces

A1.2.1. Torus

The torus is an axisymetric surface obtained by rotating a circle of radius r around an axis in its plane. The surface generated by the circle is simple when the distance R from the center of the circle to the axis is larger than r. Consider a system of axes where Oz is along the axis of the cone and Ox is in the plane of the generating cirle and passes through the center of the circle, as illustrated in Fig.A1.4. Parametric equations for the circle are given, in the Oxz plane, by

$$\mathbf{x} = \begin{bmatrix} x \\ z \end{bmatrix} = \begin{bmatrix} R + r\cos\eta \\ r\sin\eta \end{bmatrix} \tag{A1.32}$$

where η is the polar angle of the normal in the Oxz plane. Equations for the torus itself are easily determined as

$$\vec{\mathbf{x}} = \begin{bmatrix} (R + r\cos\eta)\cos\xi \\ (R + r\cos\eta)\sin\xi \\ r\sin\eta \end{bmatrix} \tag{A1.33}$$

where (ξ,η) are the geographical coordinate angles for the normal vector. The identity of the parameters (ξ,η) as canonical angles in the above equations is easily verified by

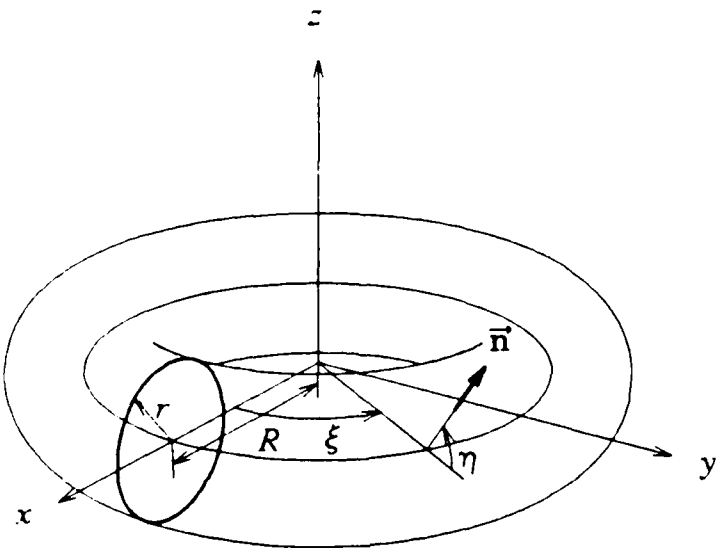

Fig.A1.4. Torus generated by Revolution of a Circle

evaluating a surface normal

$$\vec{\mathbf{n}} = \vec{\mathbf{x}}_u \times \vec{\mathbf{x}}_v = r\,(R + r\cos\eta)\begin{pmatrix}\cos\xi\cos\eta\\ \sin\xi\cos\eta\\ \sin\eta\end{pmatrix} \tag{A1.34}$$

A1.2.1.1. Spherical Transforms

The VST of the torus is easily determined by applying the transformation in (5.36) to the parametric equations of the torus in (A1.33).

$$\vec{\mathbf{s}} = \mathbf{R}_3^{G-R}\vec{\mathbf{x}} = \begin{pmatrix}R\cos\eta + r\\ 0\\ -R\sin\eta\end{pmatrix} \tag{A1.35}$$

The scalar ST is identical to the first component of the above equation, namely

$$p = R\cos\eta + r \tag{A1.36}$$

In order to determine the CT of the torus with (5.45), it is useful to first evaluate the derivatives $\vec{\mathbf{x}}_\xi$ and $\vec{\mathbf{x}}_\eta$

$$\begin{cases}\vec{\mathbf{x}}_\xi = (R + r\cos\eta)\begin{pmatrix}-\sin\xi\\ \cos\xi\\ 0\end{pmatrix}\\ \vec{\mathbf{x}}_\eta = r\begin{pmatrix}-\cos\xi\sin\eta\\ -\sin\xi\sin\eta\\ \cos\eta\end{pmatrix}\end{cases} \tag{A1.37}$$

The components of the CT are then determined to be

$$\begin{cases}r_{11} = \dfrac{\vec{\mathbf{x}}_\xi\cdot\vec{\mathbf{1}}_\xi}{\cos\eta} = \dfrac{R + r\cos\eta}{\cos\eta}\\ r_{12} = \vec{\mathbf{x}}_\eta\cdot\vec{\mathbf{1}}_\xi = 0\\ r_{22} = \vec{\mathbf{x}}_\eta\cdot\vec{\mathbf{1}}_\eta = r\end{cases} \tag{A1.38}$$

Some particular features of the transforms of the torus can be observed in the above equations, and it can be shown that these observations are also valid for all axisymmetric objects. Specifically, the h component of the VST and the r_{12} component of the CT vanish for axisymmetric objects, the n and v components of the VST are identical

to the n , t components of the VST of the generating curve, here the circle of radius r . Finally, the r_{22} component of the 3-D CT is identical to the 2-D CT of the generating curve and the r_{11} component is equal to the distance of the points of the curve to the rotation axis, divided by the cosine of η.

A1.2.2. Quadratic Surfaces

Quadratic surfaces are sets of points in 3-D defined by an quadratic implicit equation in Cartesian coordinates. When the quadratic form is not degenerated, the linear terms in the quadratic equation can be eliminated by a translation of axes and the mixed second degree terms can be eliminated by a rotation of axes. As a result, each generic quadratic surface can be expressed, in an appropriate system of axes, by an equation of the form

$$\pm \left(\frac{x}{a}\right)^2 \pm \left(\frac{y}{b}\right)^2 \pm \left(\frac{z}{c}\right)^2 = 1 \qquad \text{(A1.39)}$$

When the signs in (A1.39) are all positive, the surface is an ellipsoid with semi-axes a , b , c , as illustrated in Fig.A1.5. A set of parametric equations for this ellipsoid is given by

$$\vec{\mathbf{x}} = \begin{pmatrix} a\cos u\cos v \\ b\sin u\cos v \\ c\sin v \end{pmatrix} \qquad \text{(A1.40)}$$

A1.2.2.1. Canonical Parameterization

In order to determine the spherical functions of the ellipsoid, the parametric equations in (A1.40) will be converted into equations in terms of the normal angles (ξ,η). For this purpose, a normal vector to the surface is first evaluated. A scaled normal to the surface determined by (A1.40) is easily obtained as

$$\vec{\mathbf{n}} = \frac{1}{abc\,\cos v}\vec{\mathbf{x}}_u \times \vec{\mathbf{x}}_v = \begin{pmatrix} (1/a)\cos u\cos v \\ (1/b)\sin u\cos v \\ (1/c)\sin v \end{pmatrix} \qquad \text{(A1.41)}$$

where the particular scale factor was chosen to simplify the final expression. This expression is compared with the expression of the normal unit vector as a function of the parameters ξ, η, specifically

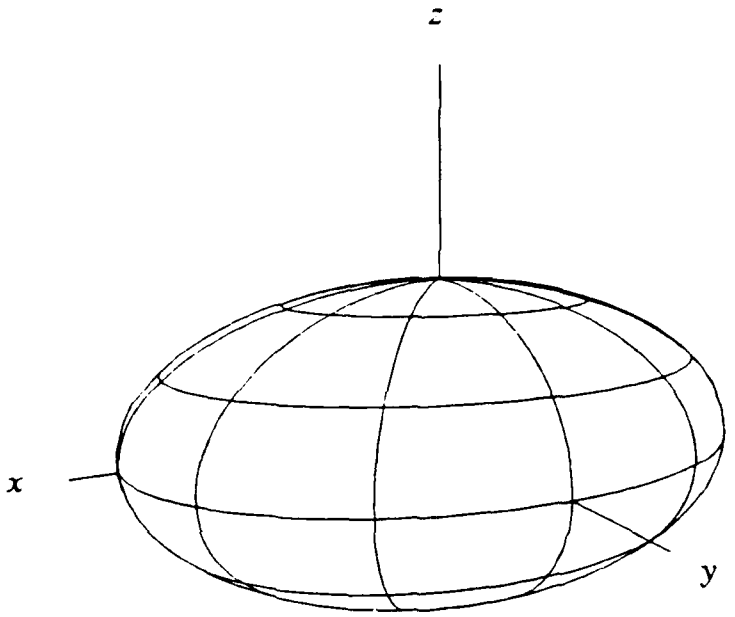

Fig.A1.5. Ellipsoid with semi-axes $a=4$, $b=3$, $c=2$.

$$\begin{pmatrix} (1/a)\cos u\cos v \\ (1/b)\sin u\cos v \\ (1/c)\sin v \end{pmatrix} = |\vec{\mathbf{n}}| \begin{pmatrix} \cos\xi\cos\eta \\ \sin\xi\cos\eta \\ \sin\eta \end{pmatrix} \qquad \text{(A1.42)}$$

Using the identity $\cos^2 u\cos^2 v + \sin^2 u\cos^2 v + \sin^2 v = 1$ and the above equation, it is easy to show that

$$|\vec{\mathbf{n}}| = \left(a^2\cos^2\xi\cos^2\eta + b^2\sin^2\xi\cos^2\eta + c^2\sin^2\eta \right)^{-1/2}$$

and to determine a relation between the parameter sets (u, v) and (ξ,η), namely

$$\begin{pmatrix} \cos u\cos v \\ \sin u\cos v \\ \sin v \end{pmatrix} = |\vec{\mathbf{n}}| \begin{pmatrix} a\cos\xi\cos\eta \\ b\sin\xi\cos\eta \\ c\sin\eta \end{pmatrix} \qquad \text{(A1.43)}$$

The parametric equations can then be expressed in terms of (ξ,η), as

$$\vec{\mathbf{x}} = |\vec{\mathbf{n}}| \begin{pmatrix} a^2\cos\xi\cos\eta \\ b^2\sin\xi\cos\eta \\ c^2\sin\eta \end{pmatrix} \qquad \text{(A1.44)}$$

A1.2.2.2. Spherical Transforms

The VST of the ellipsoid is easily derived by applying the transformation in (5.36) to equation (A1.44), producing

$$\vec{\mathbf{s}} = \mathbf{R}_3^{G-R}\,\vec{\mathbf{x}} = |\vec{\mathbf{n}}| \begin{vmatrix} a^2\cos^2\xi\cos^2\eta + b^2\sin^2\xi\cos^2\eta + c^2\sin^2\eta \\ (b^2 - a^2)\cos\eta\sin\xi\cos\xi \\ (c^2 - a^2\cos^2\xi - b^2\sin^2\xi)\sin\eta\cos\eta \end{vmatrix} \quad \text{(A1.45)}$$

The first component in the above equation is also equal to the scalar ST function $p(\xi,\eta)$. Its expression can be simplified as

$$p = n = \left(a^2\cos^2\xi\cos^2\eta + b^2\sin^2\xi\cos^2\eta + c^2\sin^2\eta \right)^{1/2} = |\vec{\mathbf{n}}|^{-1} \quad \text{(A1.46)}$$

Using the above relationship, the expression of the VST can be rewritten as

$$\vec{\mathbf{s}} = \frac{1}{p} \begin{vmatrix} p^2 \\ (b^2 - a^2)\cos\eta\sin\xi\cos\xi \\ (c^2 - a^2\cos^2\xi - b^2\sin^2\xi)\sin\eta\cos\eta \end{vmatrix} \quad \text{(A1.47)}$$

The CT of the ellipsoid will be determined with equation (5.45). For this purpose, the partial derivatives of $\vec{\mathbf{x}}(\xi,\eta)$ are first evaluated

$$\vec{\mathbf{x}}_\xi = -\frac{(b^2 - a^2)\cos^2\eta\sin\xi\cos\xi}{p^3} \begin{vmatrix} a^2\cos\xi\cos\eta \\ b^2\sin\xi\cos\eta \\ c^2\sin\eta \end{vmatrix} + \frac{1}{p} \begin{vmatrix} -a^2\sin\xi\cos\eta \\ b^2\cos\xi\cos\eta \\ 0 \end{vmatrix}$$

$$= \frac{\cos\eta}{p^3} \begin{vmatrix} -a^2\sin\xi\,(\,b^2\cos^2\eta + c^2\sin^2\eta\,) \\ b^2\cos\xi\,(\,a^2\cos^2\eta + c^2\sin^2\eta\,) \\ (\,a^2 - b^2\,)\,c^2\sin\xi\cos\xi\sin\eta\cos\eta \end{vmatrix} \quad \text{(A1.48)}$$

$$\vec{\mathbf{x}}_\eta = -\sin\eta\cos\eta\,\frac{-a^2\cos^2\xi - b^2\sin^2\xi + c^2}{p^3}\begin{vmatrix} a^2\cos\xi\cos\eta \\ b^2\sin\xi\cos\eta \\ c^2\sin\eta \end{vmatrix} + \frac{1}{p}\begin{vmatrix} -a^2\cos\xi\sin\eta \\ -b^2\sin\xi\sin\eta \\ c^2\cos\eta \end{vmatrix}$$

$$= \frac{c^2}{p^3}\begin{vmatrix} -a^2\cos\xi\sin\eta \\ -b^2\sin\xi\sin\eta \\ (\,a^2\cos^2\xi + b^2\sin^2\xi\,)\cos\eta \end{vmatrix} \qquad \text{(A1.49)}$$

The components r_{11}, r_{12}, r_{22} of the symmetric 2x2 CT tensor $\bar{\bar{\mathbf{R}}}$ are then obtained as

$$r_{11} = \frac{\vec{\mathbf{x}}_\xi \cdot \vec{\mathbf{1}}_\xi}{\cos\eta} = \frac{1}{p^3}\,(\,b^2c^2\cos^2\xi\sin^2\eta + a^2c^2\sin^2\xi\sin^2\eta + a^2b^2\cos^2\eta) \qquad \text{(A1.50)}$$

$$r_{12} = \vec{\mathbf{x}}_\eta \cdot \vec{\mathbf{1}}_\xi = \frac{c^2}{p^3}\,(a^2 - b^2)\sin\xi\cos\xi\sin\eta \qquad \text{(A1.51)}$$

$$r_{22} = \vec{\mathbf{x}}_\eta \cdot \vec{\mathbf{1}}_\eta = \frac{c^2}{p^3}\,(a^2\cos^2\xi + b^2\sin^2\xi) \qquad \text{(A1.52)}$$

A1.2.3. Superquadrics

Superquadrics are generalizations of quadrics to a class of higher order surfaces [58]. A subclass of superquadrics has implicit equations similar to (A1.39), except that the exponents, equal to 2 in the case of a quadric, are replaced by a parameter n in the case of a superquadric. In particular, the superellipsoid generalizes the ellipsoid and is defined by the following explicit equation

$$\left|\frac{x}{a}\right|^n + \left|\frac{y}{b}\right|^n + \left|\frac{z}{c}\right|^n = 1 \qquad \text{(A1.53)}$$

For n fixed to a real value in $(1,\infty)$, the surface described by the above equation is smooth and strictly convex. The limiting cases correspond to an octahedron for $n \to 1$ and a parallelepiped for $n \to \infty$, as illustrated in Fig.A1.6. The ellipsoid displayed in Fig.A1.5 is a particular case of a superellipsoid corresponding to $n = 2$. The part of the superellipsoid surface in the first octant can be parameterized as

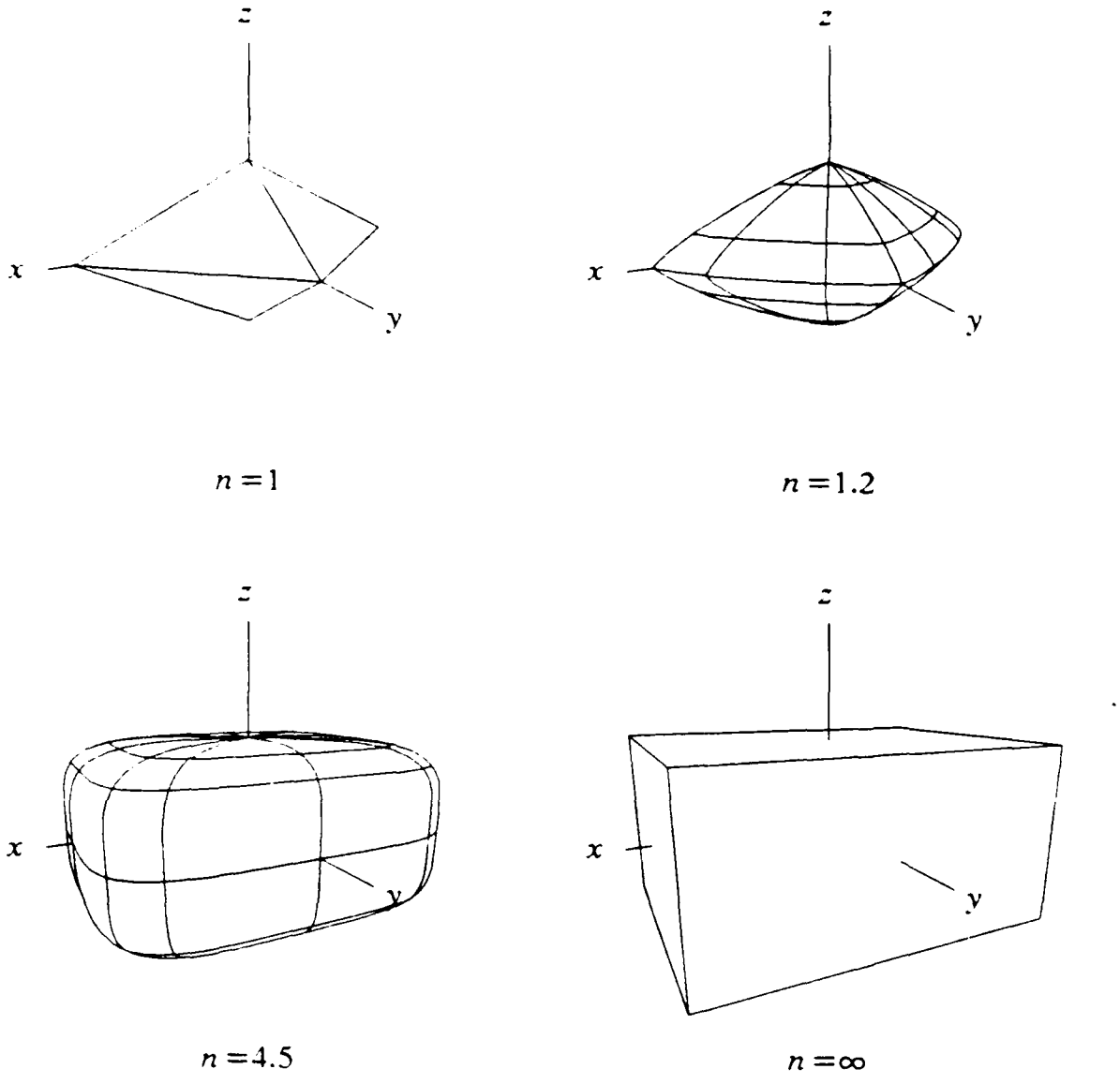

Fig.A1.6. Super-ellipsoids with semi-axes $a=4$, $b=3$, $c=2$, for $n = 1, 1.2, 4.5, \infty$.

$$\begin{pmatrix} x \\ y \\ z \end{pmatrix} = \begin{pmatrix} a \cos^s u \cos^s v \\ b \sin^s u \cos^s v \\ c \sin^s v \end{pmatrix} \tag{A1.54}$$

where $s = 2/n$. The derivation of the transforms of the superellipsoid is relatively tedious. It is helpful to first read the simpler case of the ellipsoid, or the derivation of

the 2-D transforms of superconics.

A1.2.3.1. Canonical Parameterization

The spherical transforms of the superellipsoid are now evaluated. As a first step, the parametric equations in (A1.54) are transformed into a form parameterized with the normal orientation angles. For this purpose, the normal orientation is evaluated.

$$\vec{\mathbf{n}}' = \vec{\mathbf{x}}_u \times \vec{\mathbf{x}}_v = \begin{vmatrix} bc \sin^{s-1}u \cos u \sin^{s-1}v \cos^{s+1}v \\ ac \sin u \cos^{s-1}u \sin^{s-1}v \cos^{s+1}v \\ ab \sin^{s-1}u \cos^{s-1}u \sin v \cos^{2s-1}v \end{vmatrix} \tag{A1.55}$$

A simpler expression of the normal orientation is obtained by scaling the above vector by $abc\,(\sin u \cos u \sin v)^{s-1}\cos^{2s-1}v$. The scaled normal vector is then compared to the unit normal vector expressed in terms of (ξ,η).

$$\vec{\mathbf{n}} = \begin{vmatrix} (1/a)\cos^{2-s}u \cos^{2-s}v \\ (1/b)\sin^{2-s}u \cos^{2-s}v \\ (1/c)\sin^{2-s}v \end{vmatrix} = |\vec{\mathbf{n}}| \begin{vmatrix} \cos\xi \cos\eta \\ \sin\xi \cos\eta \\ \sin\eta \end{vmatrix} \tag{A1.56}$$

Using the identity $\cos^2u \cos^2v + \sin^2u \cos^2v + \sin^2v = 1$ and the above equation, it is easy to show that

$$|\vec{\mathbf{n}}| = \left| (a \cos\xi\cos\eta)^{\frac{2}{2-s}} + (b \sin\xi\cos\eta)^{\frac{2}{2-s}} + (c \sin\eta)^{\frac{2}{2-s}} \right|^{-\frac{2-s}{2}} \tag{A1.57}$$

and

$$\vec{\mathbf{x}} = |\vec{\mathbf{n}}|^{\frac{s}{2-s}} \begin{vmatrix} a^{\frac{2}{2-s}} \cos^{\frac{s}{2-s}}\xi \cos^{\frac{s}{2-s}}\eta \\ b^{\frac{2}{2-s}} \sin^{\frac{s}{2-s}}\xi \cos^{\frac{s}{2-s}}\eta \\ c^{\frac{2}{2-s}} \sin^{\frac{s}{2-s}}\eta \end{vmatrix} \tag{A1.58}$$

As several manipulations of the above equation will be necessary to obtain the spherical functions of the superquadric, it is helpful to simplify it by introducing the parameter $k = s/2-s = 1/(n-1)$ and

$$N = |\vec{\mathbf{n}}|^{-(k+1)} = (a\cos\xi\cos\eta)^{k+1} + (b\sin\xi\cos\eta)^{k+1} + (c\sin\eta)^{k+1} \tag{A1.59}$$

The parametric equations can then be rewritten as

$$\vec{\mathbf{x}} = N^{-\frac{k}{k+1}} \begin{vmatrix} a^{k+1}\cos^k\xi\cos^k\eta \\ b^{k+1}\sin^k\xi\cos^k\eta \\ c^{k+1}\sin^k\eta \end{vmatrix} \tag{A1.60}$$

A1.2.3.2. Spherical Transforms

The expression of the VST of the superellipsoid is easily derived by applying the transformation in (5.36) to the above parametric equation, giving

$$\vec{\mathbf{s}} = \begin{vmatrix} n \\ h \\ v \end{vmatrix} = \begin{vmatrix} \cos\xi\cos\eta & \sin\xi\cos\eta & \sin\eta \\ -\sin\xi & \cos\xi & 0 \\ -\cos\xi\sin\eta & -\sin\xi\sin\eta & \cos\eta \end{vmatrix} \begin{vmatrix} x(\xi,\eta) \\ y(\xi,\eta) \\ z(\xi,\eta) \end{vmatrix} \tag{A1.61}$$

$$= N^{-\frac{k}{k+1}} \begin{vmatrix} (a\cos\xi\cos\eta)^{k+1} + (b\sin\xi\cos\eta)^{k+1} + (c\sin\eta)^{k+1} \\ (b^{k+1}\sin^{k-1}\xi - a^{k+1}\cos^{k-1}\xi)\sin\xi\cos\xi\cos^k\eta \\ (c^{k+1}\sin^{k-1}\eta - a^{k+1}\cos^{k+1}\xi\cos^{k-1}\eta - b^{k+1}\sin^{k+1}\xi\cos^{k-1}\eta)\sin\eta\cos\eta \end{vmatrix}$$

The first component in the above equation also specifies the scalar ST function $p(\xi,\eta)$. Its expression can be simplified as

$$p = n = \left| (a\cos\xi\cos\eta)^{k+1} + (b\sin\xi\cos\eta)^{k+1} + (c\sin\eta)^{k+1} \right|^{\frac{1}{k+1}} \tag{A1.62}$$

Comparing the above expression of p with the expression of N in (A1.59), it is clear that $N = p^{k+1}$, and therefore that

$$\vec{\mathbf{s}} = p^{-k} \begin{vmatrix} p^{k+1} \\ \sin\xi\cos\xi\cos^k\eta\,(b^{k+1}\sin^{k-1}\xi - a^{k+1}\cos^{k-1}\xi) \\ \sin\eta\cos\eta\,(c^{k+1}\sin^{k-1}\eta - a^{k+1}\cos^{k+1}\xi\cos^{k-1}\eta - b^{k+1}\sin^{k+1}\xi\cos^{k-1}\eta) \end{vmatrix} \tag{A1.63}$$

The third spherical function, the CT, is now evaluated for points in the first octant of the superellipsoid. In order to derive the components of the CT tensor with (5.45), it is necessary to evaluate the partial derivatives of $\vec{\mathbf{x}}(\xi,\eta)$. Considering the expression of this vector in (A1.60), it is useful to first evaluate

$$\frac{\partial}{\partial\xi}p^{-k} = \frac{\partial}{\partial\xi}N^{-\frac{k}{k+1}} = \frac{\partial}{\partial\xi}\left|\,(a\cos\xi\cos\eta)^{k+1}+(b\sin\xi\cos\eta)^{k+1}+(c\sin\eta)^{k+1}\right|^{-\frac{k}{k+1}}$$

$$= kN^{-\frac{2k+1}{k+1}}\cos^{k+1}\eta\,(a^{k+1}\sin\xi\cos^{k}\xi - b^{k+1}\sin^{k}\xi\cos\xi) \qquad \text{(A1.64)}$$

$$\frac{\partial}{\partial\eta}p^{-k} = \frac{\partial}{\partial\eta}N^{-\frac{k}{k+1}} = \frac{\partial}{\partial\eta}\left|\,(a\cos\xi\cos\eta)^{k+1}+(b\sin\xi\cos\eta)^{k+1}+(c\sin\eta)^{k+1}\right|^{-\frac{k}{k+1}}$$

$$= kN^{-\frac{2k+1}{k+1}}\cos^{k+1}\eta\,(a^{k+1}\cos^{k+1}\xi\sin\eta\cos^{k}\eta + b^{k+1}\sin^{k+1}\xi\sin\eta\cos^{k}\eta - c^{k+1}\sin^{k}\eta\cos\eta)$$

(A1.65)

The derivatives $\vec{\mathbf{x}}_\xi = \partial\vec{\mathbf{x}}/\partial\xi$ and $\vec{\mathbf{x}}_\eta = \partial\vec{\mathbf{x}}/\partial\eta$ are then evaluated as

$$\vec{\mathbf{x}}_\xi = \frac{\partial}{\partial\xi}\left(\,p^{-k}\,\right)\begin{pmatrix} a^{k+1}\cos^{k}\xi\cos^{k}\eta \\ b^{k+1}\sin^{k}\xi\cos^{k}\eta \\ c^{k+1}\sin^{k}\eta \end{pmatrix} + kp^{-k}\begin{pmatrix} -a^{k+1}\sin\xi\cos^{k-1}\xi\cos^{k}\eta \\ b^{k+1}\sin^{k-1}\xi\cos\xi\cos^{k}\eta \\ 0 \end{pmatrix}$$

$$= \frac{k\cos^{k}\eta}{p^{2k+1}}\begin{pmatrix} -a^{k+1}\sin\xi\cos^{k-1}\xi\,(b^{k+1}\sin^{k-1}\xi\cos^{k+1}\eta + c^{k+1}\sin^{k+1}\eta) \\ b^{k+1}\sin^{k-1}\xi\cos\xi\,(a^{k+1}\cos^{k-1}\xi\cos^{k+1}\eta + c^{k+1}\sin^{k+1}\eta) \\ c^{k+1}\sin\xi\cos\xi\sin^{k}\eta\cos\eta\,(a^{k+1}\cos^{k-1}\xi - b^{k+1}\sin^{k-1}\xi) \end{pmatrix}$$

(A1.66)

$$\vec{\mathbf{x}}_\eta = \frac{\partial}{\partial\eta}\left(\,p^{-k}\,\right)\begin{pmatrix} a^{k+1}\cos^{k}\xi\cos^{k}\eta \\ b^{k+1}\sin^{k}\xi\cos^{k}\eta \\ c^{k+1}\sin^{k}\eta \end{pmatrix} + kp^{-k}\begin{pmatrix} -a^{k+1}\cos^{k}\xi\sin\eta\cos^{k-1}\eta \\ -b^{k+1}\sin^{k}\xi\sin\eta\cos^{k-1}\eta \\ c^{k+1}\sin^{k-1}\eta\cos\eta \end{pmatrix}$$

$$= \frac{kc^{k+1}\sin^{k-1}\eta\cos^{k-1}\eta}{p^{2k+1}}\begin{pmatrix} -a^{k+1}\cos^{k}\xi\sin\eta \\ -b^{k+1}\sin^{k}\xi\sin\eta \\ (a^{k+1}\cos^{k+1}\xi + b^{k+1}\sin^{k+1}\xi)\cos\eta \end{pmatrix} \qquad \text{(A1.67)}$$

From the partial derivatives above, it is easy to determine the components r_{11}, r_{12}, r_{22} of the CT tensor $\bar{\mathbf{R}}$.

$$r_{11} = \frac{\vec{\mathbf{x}}_\xi \cdot \vec{\mathbf{1}}_\xi}{\cos\eta} \tag{A1.68}$$

$$= \frac{k\,(\sin\xi\cos\xi\cos\eta)^{k-1}}{p^{2k+1}} \left| (ab\cos\eta)^{k+1} + (c\sin\eta)^{k+1}(a^{k+1}\sin^{3-k}\xi + b^{k+1}\cos^{3-k}\xi) \right|$$

$$r_{12} = \vec{\mathbf{x}}_\eta \cdot \vec{\mathbf{1}}_\xi \tag{A1.69}$$

$$= \frac{kc^{k+1}\sin\xi\cos\xi\sin^{k}\eta\cos^{k-1}\eta}{p^{2k+1}} \left| a^{k+1}\cos^{k-1}\xi - b^{k+1}\sin^{k-1}\xi \right|$$

$$r_{22} = \vec{\mathbf{x}}_\eta \cdot \vec{\mathbf{1}}_\eta \tag{A1.70}$$

$$= \frac{kc^{k+1}\sin^{k-1}\eta\cos^{k-1}\eta}{p^{2k+1}} \left| a^{k+1}\cos^{k+1}\xi + b^{k+1}\sin^{k+1}\xi \right|$$

Outside the first octant, some of the trigonometric functions take negative values. As fractional powers are undefined for negative numbers, it is necessary to separate the magnitude and sign of the trigonometric functions. The following parametric equations specify the surface points of the superellipsoid in the eight octants.

$$\vec{\mathbf{x}} = N^{-\frac{k}{k+1}} \begin{vmatrix} a^{k+1}\,|\cos\xi\cos\eta|^{k}\,sign\,(\cos\xi\cos\eta) \\ b^{k+1}\,|\sin\xi\cos\eta|^{k}\,sign\,(\sin\xi\cos\eta) \\ c^{k+1}\,|\sin\eta|^{k}\,sign\,(\sin\eta) \end{vmatrix} \tag{A1.71}$$

where

$$N = |a\cos\xi\cos\eta|^{k+1} + |b\sin\xi\cos\eta|^{k+1} + |c\sin\eta|^{k+1} \tag{A1.72}$$

The ST is given by the following expression valid in the eight octants

$$p = \left| |a\cos\xi\cos\eta|^{k+1} + |b\sin\xi\cos\eta|^{k+1} + |c\sin\eta|^{k+1} \right|^{\frac{1}{k+1}} \tag{A1.73}$$

The VST is given by the following vector equation valid in the eight octants.

$$\vec{s} = p^{-\lambda} \begin{vmatrix} p^{\lambda+1} \\ \sin\xi\cos\xi\,|\cos\eta|^{\lambda}\, sign(\cos\eta)\,(b^{\lambda+1}|\sin\xi|^{\lambda-1} - a^{\lambda+1}|\cos\xi|^{\lambda-1}) \\ \sin\eta\cos\eta\left\{ c^{\lambda+1}|\sin\eta|^{\lambda-1} - (a\,|\cos\xi|)^{\lambda+1}|\cos\eta|^{\lambda-1} - (b\,|\sin\xi|)^{\lambda+1}|\cos\eta|^{\lambda-1} \right\} \end{vmatrix}$$

(A1.74)

It can be observed by comparing the previous relations with the corresponding relations in the first octant, that integer powers and k th powers of the trigonometric functions retain their signs, and that trigonometric functions raised to the powers $k-1$ and $k+1$ are taken in absolute value. This conjecture also produces valid answers when applied to the expressions for the CT components in (A1.68), (A1.69), (A1.70).

The spherical functions in (A1.73), (A1.74), (A1.68), (A1.69), (A1.70) can be used to determine the circular functions of silhouettes of superellipsoids in orthographic projections. For example, Fig.A1.7 displays a silhouette of the superquadric with $a=4$, $b=3$, $c=2$, $n=4.5$, and the three corresponding circular functions.

In addition to the three spherical functions presented in the text, it is also possible to determine the EGI function for the superellipsoid with (5.56).

$$G(\xi,\eta) = r_{11}r_{22} - r_{12}^2$$

$$= \frac{k^2\,(abc)^{k+1}\,|\sin\xi\cos\xi\sin\eta\cos^2\eta\,|^{k-1}}{\left|\,|a\cos\xi\cos\eta\,|^{k+1} + |b\sin\xi\cos\eta\,|^{k+1} + |c\sin\eta\,|^{k+1}\right|^{\frac{3k+1}{k+1}}}$$

(A1.75)

For $s \leq 2$ and therefore $k \geq 1$, the EGI is continuous over the whole sphere. For $s > 2$, $k-1 < 0$ and the EGI has discontinuities along the equator $\eta=0$ and along the meridians $\xi=-\pi/2,0,\pi/2,\pi$ on the Gaussian Sphere. These discontinuities account for the fact that the surface expansions around the corresponding points contain only terms of order larger than 2. For $s \to \infty$, $k \to 0$, the EGI vanishes almost everywhere because of the factor k^2 in the numerator of (A1.75); impulses remain at the six discontinuity points $(\xi,\eta) =$ $(.,-\pi/2)$, $(0,-\pi/2)$, $(0,0)$, $(0,\pi/2)$, $(0,\pi)$, $(.,\pi/2)$. The strengths

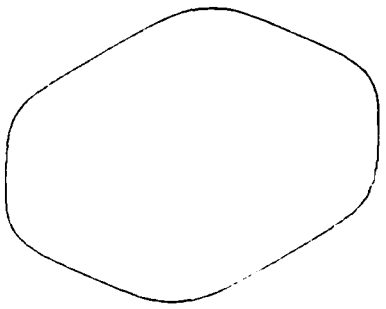

Silhouette

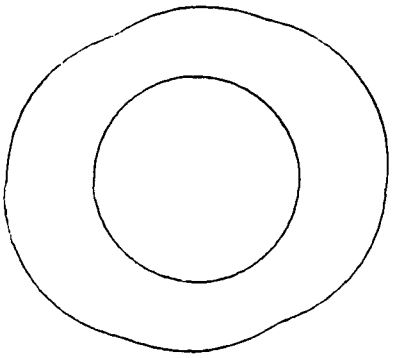

Support Transform

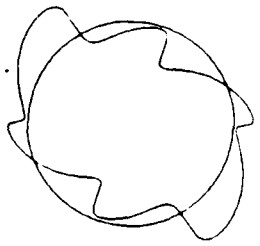

t-component of VST

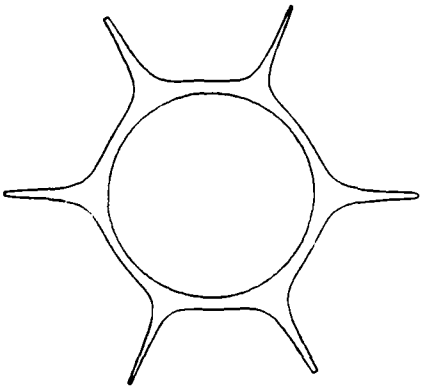

Curvature Transform

Fig.A1.7. Silhouette of Super-ellipsoid and corresponding circular functions for $\theta = 30^{\circ}$, $\phi = 40^{\circ}$.

---

of these impulses can be evaluated as $4ab$ for the poles $(.,-\pi/2)$, $(.,\pi/2)$, $4bc$ for the points $(0,0)$, $(0,\pi)$ and $4ac$ for the points $(0,-\pi/2)$, $(0,\pi/2)$. These values correspond exactly to the areas of the faces of the parallelepiped which is the limiting case of the superellipsoid for $s \rightarrow \infty$, see Fig.A1.6.

$$\frac{dt(\psi)}{dt} = \frac{1}{d\psi(t)/dt} \tag{A2.4}$$

To illustrate the use of derivatives of the formal inverse of $\psi(t)$, an expression for the radius of curvature of a curve is determined in terms of a generic parametric equation such as (A2.1). The radius of curvature can be determined by

$$\rho = \left| \frac{d\mathbf{x}}{d\psi} \right| = \left| \frac{d\mathbf{x}}{dt} \right| \frac{dt}{d\psi} = \left| \frac{d\mathbf{x}}{dt} \right| \frac{1}{d\psi/dt}$$

$$\psi(t) = \operatorname{atan}\left(\frac{\dot{z}}{\dot{x}} \right)$$

$$\frac{d\psi}{dt} = \frac{\ddot{z}\dot{x} - \ddot{x}\dot{z}}{\dot{x}^2 + \dot{z}^2}$$

$$\left| \frac{d\mathbf{x}}{dt} \right| = (\dot{x}^2 + \dot{z}^2)^{1/2}$$

$$\rho = \frac{(\dot{x}^2 + \dot{y}^2)^{3/2}}{\ddot{z}\dot{x} - \ddot{x}\dot{z}} \tag{A2.5}$$

A2.2. 3-D Surfaces

Consider a surface specified by the parametric equations

$$\vec{\mathbf{x}} = \vec{\mathbf{x}}(u,v) = \begin{bmatrix} x(u,v) \\ y(u,v) \\ z(u,v) \end{bmatrix} \tag{A2.6}$$

The problem addressed in this section is the conversion of parametric equations similar to the above form, to a set of equations $\vec{\mathbf{x}}(\xi,\eta)$ for the same surface, where the angles (ξ,η) characterize normal orientation.

First, a relation between the generic parameters (u,v) and the angles (ξ,η) is obtained by comparing the normal vector $\vec{\mathbf{n}} = \vec{\mathbf{x}}_u \times \vec{\mathbf{x}}_v$ with the normal vector expressed in terms of (ξ,η).

Appendix 2
Parameterizing Curves and Surfaces with Normal Orientation

This appendix addresses the issue of converting parametric equations in terms of generic parameters into equations parameterized in terms of normal orientation. The problem is first addressed in the case of planar curves, then in the case of surfaces in 3-D.

A2.1. Planar Curves

Consider a curve specified by parametric equations

$$\mathbf{x} = \mathbf{x}(t) = \begin{bmatrix} x(t) \\ z(t) \end{bmatrix} \tag{A2.1}$$

where t is a generic parameter. The problem addressed here is the conversion of this form into an equation $\mathbf{x}(\psi)$ for the same curve, in terms of the polar angle ψ of the normal orientation. A relation between ψ and t can be obtained by considering the orientation of the tangent vector $\mathbf{x}_t(t)$. The relation is given by

$$\psi = \operatorname{atan}\frac{\dot{z}(t)}{\dot{x}(t)} = \psi(t) \tag{A2.2}$$

where dots indicate derivatives with respect to t. The inverse function of $\psi(t)$ is formally written as $t(\psi)$, and is inserted into (A2.1) to obtain the desired result, namely

$$\mathbf{x} = \mathbf{x}(t(\psi)) = \mathbf{x}(\psi) \tag{A2.3}$$

For a strictly convex planar object, the inverse $t(\psi)$ is well defined and unique everywhere. However, it is possible to explicitly determine the inverse function $t(\psi)$ only in particular cases. In other cases, there is no closed-form inverse of (A2.2) but derivatives of $x(\psi)$ can be determined using the formal inverse $t(\psi)$ and the relation between derivatives of direct and inverse functions.

$$\vec{\mathbf{n}} = \begin{vmatrix} n_x \\ n_y \\ n_z \end{vmatrix} = \begin{vmatrix} y_u z_v - y_v z_u \\ z_u x_v - z_v x_u \\ x_u y_v - x_v y_u \end{vmatrix} = |\vec{\mathbf{n}}| \begin{vmatrix} \cos\xi \cos\eta \\ \sin\xi \cos\eta \\ \sin\eta \end{vmatrix} \tag{A2.7}$$

Explicit expressions for the angles ξ and η can be derived from the above equations as

$$\left| \begin{array}{ll} \xi = & \operatorname{atan}\dfrac{n_y}{n_x} \qquad = \xi(u,v) \\ \eta = & \operatorname{atan}\dfrac{n_z}{(n_x^2 + n_y^2)^{1/2}} \quad = \eta(u,v) \end{array} \right. \tag{A2.8}$$

The formal inverses of the above equations will be denoted by

$$\left| \begin{array}{l} u = u(\xi,\eta) \\ v = v(\xi,\eta) \end{array} \right. \tag{A2.9}$$

For a strictly convex object, the above inverse functions are well defined everywhere, and can be inserted in (A2.6) to obtain the desired parametric equations

$$\vec{\mathbf{x}} = \vec{\mathbf{x}}(u(\xi,\eta), v(\xi,\eta)) = \vec{\mathbf{x}}(\xi,\eta) \tag{A2.10}$$

In many instances, it is not possible to find explicit forms for the inverse equations $u(\xi,\eta)$, $v(\xi,\eta)$, but the expression in terms of the formal inverses can be used to determine derivatives of $\vec{\mathbf{x}}(\xi,\eta)$, using the relation between derivatives of direct and inverse functions.

$$\begin{vmatrix} \dfrac{\partial u}{\partial \xi} & \dfrac{\partial v}{\partial \xi} \\ \dfrac{\partial u}{\partial \eta} & \dfrac{\partial v}{\partial \eta} \end{vmatrix} = \begin{vmatrix} \dfrac{\partial \xi}{\partial u} & \dfrac{\partial \eta}{\partial u} \\ \dfrac{\partial \xi}{\partial v} & \dfrac{\partial \eta}{\partial v} \end{vmatrix}^{-1} \tag{A2.11}$$

The derivatives of $\vec{\mathbf{x}}$ with respect to the angular coordinates are given by

$$\begin{pmatrix} \vec{\mathbf{x}}_\xi \\ \vec{\mathbf{x}}_\eta \end{pmatrix} = \begin{pmatrix} \frac{\partial u}{\partial \xi} & \frac{\partial v}{\partial \xi} \\ \frac{\partial u}{\partial \eta} & \frac{\partial v}{\partial \eta} \end{pmatrix} \begin{pmatrix} \vec{\mathbf{x}}_u \\ \vec{\mathbf{x}}_v \end{pmatrix} = \begin{pmatrix} \frac{\partial \xi}{\partial u} & \frac{\partial \eta}{\partial u} \\ \frac{\partial \xi}{\partial v} & \frac{\partial \eta}{\partial v} \end{pmatrix}^{-1} \begin{pmatrix} \vec{\mathbf{x}}_u \\ \vec{\mathbf{x}}_v \end{pmatrix} \tag{A2.12}$$

The derivatives in the second matrix can be readily evaluated from (A2.8),

$$\left| \begin{aligned} \frac{\partial \xi}{\partial u} &= \frac{ny_u\, nx - ny\, nx_u}{nx^2 + ny^2} \\ \frac{\partial \xi}{\partial v} &= \frac{ny_v\, nx - ny\, nx_v}{nx^2 + ny^2} \\ \frac{\partial \eta}{\partial u} &= \frac{nz_u (nx^2 + ny^2) - nz\,(nx\, nx_u + ny ny_u)}{(nx^2 + ny^2 + nz^2)(nx^2 + ny^2)^{1/2}} \\ \frac{\partial \eta}{\partial v} &= \frac{nz_v (nx^2 + ny^2) - nz\,(nx\, nx_v + ny ny_v)}{(nx^2 + ny^2 + nz^2)(nx^2 + ny^2)^{1/2}} \end{aligned} \right. \tag{A2.13}$$

where subscripts in the components of the normal vector have been replaced by postfixes to avoid confusion with partial derivatives; for example, n_x has been replaced by nx.

An example of the use of the above formulas is the derivation of the radius of curvature tensor $\bar{\bar{\mathbf{R}}}$ from generic parametric equations. The relation between partial derivatives and components of this tensor is given by

$$\begin{pmatrix} \vec{\mathbf{x}}_\xi \\ \vec{\mathbf{x}}_\eta \end{pmatrix} = \begin{pmatrix} r_{11}\cos\eta\, \vec{\mathbf{1}}_\xi + r_{12}\cos\eta \vec{\mathbf{1}}_\eta \\ r_{12}\, \vec{\mathbf{1}}_\xi + r_{22}\vec{\mathbf{1}}_\eta \end{pmatrix} \tag{A2.14}$$

The unit vectors $\mathbf{1}_\xi$, $\mathbf{1}_\eta$ can easily be determined in terms of components of the normal in (A2.7),

$$\vec{\mathbf{1}}_\xi = \begin{pmatrix} -n_y / n_{xy} \\ n_x / n_{xy} \\ 0 \end{pmatrix}, \quad \vec{\mathbf{1}}_\eta = \begin{pmatrix} -n_x n_z / n_{xy} n \\ -n_y n_z / n_{xy} n \\ n_{xy} / n \end{pmatrix} \tag{A2.15}$$

where $n^2 = n_x^2 + n_y^2 + n_z^2$ and $n_{xy}^2 = n_x^2 + n_y^2$.

The components of the tensor can then be determined from the derivatives in (A2.12), as

$$\left| \begin{array}{l} r_{11} = \dfrac{\vec{\mathbf{x}}_\xi \cdot \vec{\mathbf{1}}_\xi}{\cos\eta} \\ r_{12} = \vec{\mathbf{x}}_\eta \cdot \vec{\mathbf{1}}_\xi \\ r_{22} = \vec{\mathbf{x}}_\eta \cdot \vec{\mathbf{1}}_\eta \end{array} \right. \tag{A2.16}$$

It is also possible to evaluate the tensor $\bar{\bar{\mathbf{R}}}$ from generic parametric equations by first evaluating the tensors of the first and second fundamental forms, then applying an appropriate transformation to these tensors. This method was presented in[62] and is briefly reviewed in Appendix 4.

Appendix 3
Duality between Slices and Silhouettes, Euler's Theorem and its Dual.

In this appendix, the duality between slices and silhouettes of quadratic forms is reviewed, and an application of this analysis to curvatures of slices and silhouettes is developed. Silhouettes and slices are first derived for ellipses in 2-D and for quadratic surfaces in 3-D. In both cases, it is shown that silhouettes can be obtained in tangential space (dual space) by exactly the same operation that produces slices in point space. The expressions for slices and silhouettes in the two examples are exploited to formulate two different derivations of Euler's theorem of differential geometry and of its dual.

Throughout this appendix, the vector and matrix notation used in the equations of geometric objects emphasize the duality between equations for curves and surfaces in point space and their correspondents in tangential space. The formulation also clarifies the proposed duality between silhouettes and slices of quadratic forms.

A3.1. Slices and Silhouettes of an Ellipse in 2-D

In this section, the slice of an ellipse by an axis through the center is determined in terms of the polar orientation angle α of the axis; then, the orthographic silhouette of the ellipse on the same axis is also evaluated. The problem is first solved for $\alpha=0$, so that the axis is horizontal, then extended to different values of α by combining the previous result with rotations of the coordinate frame.

An ellipse centered at the origin of the Oyz plane can be defined by the following implicit equation in point space.

$$\begin{bmatrix} y & z \end{bmatrix} \begin{bmatrix} a_{11} & a_{12} \\ a_{12} & a_{22} \end{bmatrix} \begin{bmatrix} y \\ z \end{bmatrix} = 1 \qquad \text{(A3.1)}$$

The equation for the tangents of the ellipse in dual space is derived by first considering the equation of the tangent at the point $P_0(y_0,z_0)$ of the ellipse.

$$\begin{pmatrix} y & z \end{pmatrix} \begin{pmatrix} a_{11} & a_{12} \\ a_{12} & a_{22} \end{pmatrix} \begin{pmatrix} y_0 \\ z_0 \end{pmatrix} = 1 \qquad \text{(A3.2)}$$

The tangential coordinates of a line, also named dual coordinates, are the coefficients λ_x , λ_y of the equation of the line written as $\lambda_x x + \lambda_y y = 1$. The coordinates of the line in (A3.2) are hence given by

$$\begin{pmatrix} \lambda_y \\ \lambda_z \end{pmatrix} = \begin{pmatrix} a_{11} & a_{12} \\ a_{12} & a_{22} \end{pmatrix} \begin{pmatrix} y_0 \\ z_0 \end{pmatrix} \qquad \text{(A3.3)}$$

Conversely, a line with tangential coordinates (λ_y, λ_z) is tangent to the ellipse iff the point P_0 with coordinates

$$\begin{pmatrix} y_0 \\ z_0 \end{pmatrix} = \begin{pmatrix} a_{11} & a_{12} \\ a_{12} & a_{22} \end{pmatrix}^{-1} \begin{pmatrix} \lambda_y \\ \lambda_z \end{pmatrix} \qquad \text{(A3.4)}$$

is on the ellipse. The equation of the ellipse in tangential space, which is the equation specifying all the tangents to the ellipse, is obtained by requiring the coordinates of P_0 in (A3.4) to satisfy the equation of the ellipse in (A3.1).

$$\begin{pmatrix} \lambda_y & \lambda_z \end{pmatrix} \begin{pmatrix} a_{11} & a_{12} \\ a_{12} & a_{22} \end{pmatrix}^{-1} \begin{pmatrix} a_{11} & a_{12} \\ a_{12} & a_{22} \end{pmatrix} \begin{pmatrix} a_{11} & a_{12} \\ a_{12} & a_{22} \end{pmatrix}^{-1} \begin{pmatrix} \lambda_y \\ \lambda_z \end{pmatrix} = 1 \qquad \text{(A3.5)}$$

$$\begin{pmatrix} \lambda_y & \lambda_z \end{pmatrix} \begin{pmatrix} a_{11} & a_{12} \\ a_{12} & a_{22} \end{pmatrix}^{-1} \begin{pmatrix} \lambda_y \\ \lambda_z \end{pmatrix} = 1 \qquad \text{(A3.6)}$$

The explicit tangential equation of an ellipse is hence a quadratic form with a kernel equal to the inverse of the kernel of the quadratic form describing the ellipse in point space.

The slice of the ellipse by the horizontal Oy axis and the silhouette on the same axis are now determined. As seen in Fig.A3.1, both slice and silhouette consist of two points symmetric with the origin, which will be specified by the absolute value of their y-coordinates, y_{slice} and y_{sil}. First, the slice of the ellipse is determined as the points for which $z = 0$, namely

$$\begin{pmatrix} y_{slice} & 0 \end{pmatrix} \begin{pmatrix} a_{11} & a_{12} \\ a_{12} & a_{22} \end{pmatrix} \begin{pmatrix} y_{slice} \\ 0 \end{pmatrix} = 1 \qquad \text{(A3.7)}$$

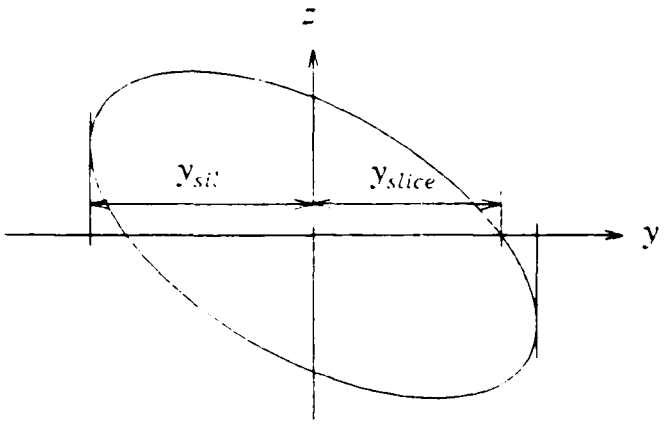

Fig.A3.1. Slice and Silhouette of an Ellipse on the Oy Axis.

An alternative expression for the half-width y_{slice} is given by

$$\frac{1}{y_{slice}^2} = \begin{pmatrix} 1 & 0 \end{pmatrix} \begin{pmatrix} a_{11} & a_{12} \\ a_{12} & a_{22} \end{pmatrix} \begin{pmatrix} 1 \\ 0 \end{pmatrix} \tag{A3.8}$$

The silhouette on the Oy axis is now determined as the intersection of the Oy axis with the vertical tangents to the ellipse, see Fig.A3.1. For these tangents, $\lambda_z = 0$ and $\lambda_y = \lambda_{sil}$ is determined by

$$\begin{pmatrix} \lambda_{ysil} & 0 \end{pmatrix} \begin{pmatrix} a_{11} & a_{12} \\ a_{12} & a_{22} \end{pmatrix}^{-1} \begin{pmatrix} \lambda_{ysil} \\ 0 \end{pmatrix} = 1 \tag{A3.9}$$

$$\frac{1}{\lambda_{ysil}^2} = \begin{pmatrix} 1 & 0 \end{pmatrix} \begin{pmatrix} a_{11} & a_{12} \\ a_{12} & a_{22} \end{pmatrix}^{-1} \begin{pmatrix} 1 \\ 0 \end{pmatrix} \tag{A3.10}$$

The coordinates y_{sil} of the silhouette points are given by $y_{sil} = 1/\lambda_{ysil}$, so that

$$y_{sil}^2 = \begin{pmatrix} 1 & 0 \end{pmatrix} \begin{pmatrix} a_{11} & a_{12} \\ a_{12} & a_{22} \end{pmatrix}^{-1} \begin{pmatrix} 1 \\ 0 \end{pmatrix} \tag{A3.11}$$

The projections and slices on an axis with a polar angle α are now determined by first evaluating the equation of the ellipse in a set of axes $Oy_\alpha z_\alpha$ obtained by rotating the axes Oyz by an angle α; see Fig.A3.2.

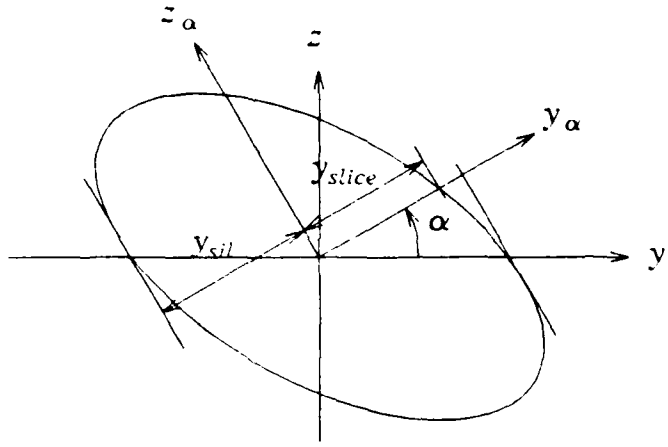

Fig.A3.2. Slice and Silhouette of an Ellipse on a Rotated Axis.

The coordinate transformation between the two systems of axes is given by

$$\begin{pmatrix} y \\ z \end{pmatrix} = \begin{pmatrix} \cos\alpha & -\sin\alpha \\ \sin\alpha & \cos\alpha \end{pmatrix} \begin{pmatrix} y_\alpha \\ z_\alpha \end{pmatrix} \tag{A3.12}$$

An equation for the ellipse in the rotated axes is obtained by inserting (A3.12) into (A3.1), which produces

$$\begin{pmatrix} y_\alpha & z_\alpha \end{pmatrix} \begin{pmatrix} \cos\alpha & \sin\alpha \\ -\sin\alpha & \cos\alpha \end{pmatrix} \begin{pmatrix} a_{11} & a_{12} \\ a_{12} & a_{22} \end{pmatrix} \begin{pmatrix} \cos\alpha & \sin\alpha \\ -\sin\alpha & \cos\alpha \end{pmatrix} \begin{pmatrix} y_\alpha \\ z_\alpha \end{pmatrix} = 1 \tag{A3.13}$$

The equation of the ellipse in the rotated axes has the same form as (A3.1), but the 2x2 matrix is now the product of the three matrices in the above equation. Slices and silhouettes on the Oy_α axis can be obtained by applying equations (A3.8) and (A3.11) in the rotated axes, resulting in

$$\frac{1}{y_{slice}^2} = \begin{pmatrix} \cos\alpha & \sin\alpha \end{pmatrix} \begin{pmatrix} a_{11} & a_{12} \\ a_{12} & a_{22} \end{pmatrix} \begin{pmatrix} \cos\alpha \\ \sin\alpha \end{pmatrix} \tag{A3.14}$$

$$y_{sil}^2 = \begin{pmatrix} \cos\alpha & \sin\alpha \end{pmatrix} \begin{pmatrix} a_{11} & a_{12} \\ a_{12} & a_{22} \end{pmatrix}^{-1} \begin{pmatrix} \cos\alpha \\ \sin\alpha \end{pmatrix} \tag{A3.15}$$

It is useful to consider a particular case where the principal axes of the ellispe are oriented along the coordinate axes. Let d_1 and d_2 be the half diameters along the Oy

and Oz axes respectively. The 2x2 matrix of the ellipse is in this case

$$\begin{vmatrix} a_{11} & a_{12} \\ a_{12} & a_{22} \end{vmatrix} = \begin{vmatrix} 1/d_1^2 & 0 \\ 0 & 1/d_2^2 \end{vmatrix} \tag{A3.16}$$

The expressions for the abscissas of the slice and the silhouette are given in this case by

$$\frac{1}{y_{slice}^2} = \frac{1}{d_1^2}\cos^2\alpha + \frac{1}{d_2^2}\sin^2\alpha \tag{A3.17}$$

$$y_{sil}^2 = d_1^2\cos^2\alpha + d_2^2\sin^2\alpha \tag{A3.18}$$

A3.2. Slices and Silhouettes of 3-D Quadrics

In this section, the slice of a quadric by a plane and its orthographic silhouette are evaluated. The expressions of these curves are derived with the same strategy that was used to determine slices and silhouettes of ellipses. First, the slice and silhouette on a particular plane, here the Oxy plane, are evaluated, then the result for a general plane is obtained by combining the previous result with transformations of axes. Only the first step is discussed here.

In order to show a different facet of quadratic equations in point space and in tangential space, general systems of axes will be considered, as opposed to axes with an origin at the center of the figure used in the discussion of ellipses. In order to describe quadrics in general axes, it is advantageous to use homogeneous coordinates (x, y, z, t) for points in 3-D space. Any quadratic surface can be expressed in point space by an implicit equation of the form

$$\begin{vmatrix} x & y & z & t \end{vmatrix} \begin{vmatrix} a_{11} & a_{12} & a_{13} & a_{14} \\ a_{12} & a_{22} & a_{23} & a_{24} \\ a_{13} & a_{23} & a_{33} & a_{34} \\ a_{14} & a_{24} & a_{34} & a_{44} \end{vmatrix} \begin{vmatrix} x \\ y \\ z \\ t \end{vmatrix} = 0 \tag{A3.19}$$

The equation of the above quadric in tangential space is obtained by first considering the equation of the plane tangent to the quadric at the point $P_0(x_0, y_0, z_0, t_0)$, namely

$$\begin{vmatrix} x & y & z & t \end{vmatrix} \begin{vmatrix} a_{11} & a_{12} & a_{13} & a_{14} \\ a_{12} & a_{22} & a_{23} & a_{24} \\ a_{13} & a_{23} & a_{33} & a_{34} \\ a_{14} & a_{24} & a_{34} & a_{44} \end{vmatrix} \begin{vmatrix} x_0 \\ y_0 \\ z_0 \\ t_0 \end{vmatrix} = 0 \qquad \text{(A3.20)}$$

The tangential coordinates of the tangent plane at P_0 are given by

$$\begin{vmatrix} \lambda_x \\ \lambda_y \\ \lambda_z \\ \lambda_t \end{vmatrix} = \begin{vmatrix} a_{11} & a_{12} & a_{13} & a_{14} \\ a_{12} & a_{22} & a_{23} & a_{24} \\ a_{13} & a_{23} & a_{33} & a_{34} \\ a_{14} & a_{24} & a_{34} & a_{44} \end{vmatrix} \begin{vmatrix} x_0 \\ y_0 \\ z_0 \\ t_0 \end{vmatrix} \qquad \text{(A3.21)}$$

Conversely, a plane with tangential coordinates $(\lambda_x\ \lambda_y\ \lambda_z\ \lambda_t)$ is tangent to the quadric if the coordinates $(x_0 y_0 z_0 t_0)$ obtained by inverting (A3.21) satisfy the equation of the quadric in (A3.19). Therefore, the set of planes tangent to the quadric is characterized by the equation

$$\begin{vmatrix} \lambda_x & \lambda_y & \lambda_z & \lambda_t \end{vmatrix} \begin{vmatrix} a_{11} & a_{12} & a_{13} & a_{14} \\ a_{12} & a_{22} & a_{23} & a_{24} \\ a_{13} & a_{23} & a_{33} & a_{34} \\ a_{14} & a_{24} & a_{34} & a_{44} \end{vmatrix}^{-1} \begin{vmatrix} \lambda_x \\ \lambda_y \\ \lambda_z \\ \lambda_t \end{vmatrix} = 0 \qquad \text{(A3.22)}$$

It will be useful in the sequel to explicitly consider the inverse matrix in the above equation, namely

$$\begin{vmatrix} A_{11} & A_{12} & A_{13} & A_{14} \\ A_{12} & A_{22} & A_{23} & A_{24} \\ A_{13} & A_{23} & A_{33} & A_{34} \\ A_{14} & A_{24} & A_{34} & A_{44} \end{vmatrix} = \begin{vmatrix} a_{11} & a_{12} & a_{13} & a_{14} \\ a_{12} & a_{22} & a_{23} & a_{24} \\ a_{13} & a_{23} & a_{33} & a_{34} \\ a_{14} & a_{24} & a_{34} & a_{44} \end{vmatrix}^{-1} \qquad \text{(A3.23)}$$

The slice of the quadric by the Oxy plane is first considered. Points in this plane are characterized by $z=0$, so that the intersection of the quadric and the plane is the set of points satisfying

$$\begin{bmatrix} x & y & 0 & t \end{bmatrix} \begin{vmatrix} a_{11} & a_{12} & a_{13} & a_{14} \\ a_{12} & a_{22} & a_{23} & a_{24} \\ a_{13} & a_{23} & a_{33} & a_{34} \\ a_{14} & a_{24} & a_{34} & a_{44} \end{vmatrix} \begin{vmatrix} x \\ y \\ 0 \\ t \end{vmatrix} = 0 \qquad \text{(A3.24)}$$

This equation can be rewritten as an equation for homogeneous coordinates (x, y, t) of points in the Oxy plane.

$$\begin{bmatrix} x & y & t \end{bmatrix} \begin{vmatrix} a_{11} & a_{12} & a_{14} \\ a_{12} & a_{22} & a_{24} \\ a_{14} & a_{24} & a_{44} \end{vmatrix} \begin{vmatrix} x \\ y \\ t \end{vmatrix} = 0 \qquad \text{(A3.25)}$$

The above equation shows that the slice is a quadratic curve in 2-D, also called a conic.

The silhouette of the quadric in the Oxy plane is now evaluated. For that matter, it is useful to first consider the silhouette generating planes which are in this case, the planes with $\lambda_z = 0$. For the quadric in (A3.19), the tangential coordinates of these planes satisfy

$$\begin{bmatrix} \lambda_x & \lambda_y & 0 & \lambda_t \end{bmatrix} \begin{vmatrix} A_{11} & A_{12} & A_{13} & A_{14} \\ A_{12} & A_{22} & A_{23} & A_{24} \\ A_{13} & A_{23} & A_{33} & A_{34} \\ A_{14} & A_{24} & A_{34} & A_{44} \end{vmatrix} \begin{vmatrix} \lambda_x \\ \lambda_y \\ 0 \\ \lambda_t \end{vmatrix} = 0 \qquad \text{(A3.26)}$$

It is easy to verify that the trace of a vertical plane $(\lambda_x, \lambda_y, \lambda_z = 0, \lambda_t)$ in the Oxy plane is a line with coordinates $(\lambda_x, \lambda_y, \lambda_t)$. The silhouette of the quadric is hence a curve with tangential equation

$$\begin{bmatrix} \lambda_x & \lambda_y & \lambda_t \end{bmatrix} \begin{vmatrix} A_{11} & A_{12} & A_{14} \\ A_{12} & A_{22} & A_{24} \\ A_{14} & A_{24} & A_{44} \end{vmatrix} \begin{vmatrix} \lambda_x \\ \lambda_y \\ \lambda_t \end{vmatrix} = 0 \qquad \text{(A3.27)}$$

which is the tangential equation of a conic.

The point equation of the conic is then obtained as

$$\begin{vmatrix} x & y & t \end{vmatrix} \begin{vmatrix} A_{11} & A_{12} & A_{14} \\ A_{12} & A_{22} & A_{24} \\ A_{14} & A_{24} & A_{44} \end{vmatrix}^{-1} \begin{vmatrix} x \\ y \\ t \end{vmatrix} = 0 \qquad \text{(A3.28)}$$

In summary, the slice of a quadratic surface by the Oxy plane is a conic: The matrix of its equation in point space is obtained by removing the third column and third row in the matrix of the quadric. The orthographic silhouette of a quadratic surface on the Oxy plane is also a conic; the matrix of its equation in tangential space is obtained by removing the third column and row of the matrix of the tangential equation of the quadric. The matrix of the silhouette in point space is obtained from the matrix of the quadric in point space by first inverting this matrix, then removing the third row and column and finally inverting the resulting matrix.

A particular case is now considered, namely the case of a paraboloid with equation

$$x = -\tfrac{1}{2}(ay^2 + 2byz + cz^2) = \begin{pmatrix} y & z \end{pmatrix} \begin{pmatrix} a & b \\ b & c \end{pmatrix} \begin{pmatrix} y \\ z \end{pmatrix} \qquad \text{(A3.29)}$$

The above equation can be written as a quadratic form similar to (A3.19) for the homogeneous coordinates (x, y, z, t).

$$\begin{vmatrix} x & y & z & t \end{vmatrix} \begin{vmatrix} 0 & 0 & 0 & 1 \\ 0 & a & b & 0 \\ 0 & b & c & 0 \\ 1 & 0 & 0 & 0 \end{vmatrix} \begin{vmatrix} x \\ y \\ z \\ t \end{vmatrix} = 0 \qquad \text{(A3.30)}$$

The tangential equation of the paraboloid is

$$\begin{vmatrix} \lambda_x & \lambda_y & \lambda_z & \lambda_t \end{vmatrix} \begin{vmatrix} 0 & 0 & 0 & 1 \\ 0 & A & B & 0 \\ 0 & B & C & 0 \\ 1 & 0 & 0 & 0 \end{vmatrix} \begin{vmatrix} \lambda_x \\ \lambda_y \\ \lambda_z \\ \lambda_t \end{vmatrix} = 0 \qquad \text{(A3.31)}$$

where

$$\begin{vmatrix} A & B \\ B & C \end{vmatrix} = \begin{vmatrix} a & b \\ b & c \end{vmatrix}^{-1} \tag{A3.32}$$

The slice of this paraboloid by the Oxy plane is given by

$$\begin{vmatrix} x & y & t \end{vmatrix} \begin{vmatrix} 0 & 0 & 1 \\ 0 & a & 0 \\ 1 & 0 & 0 \end{vmatrix} \begin{vmatrix} x \\ y \\ t \end{vmatrix} = 0 \tag{A3.33}$$

which is equivalent to

$$x = -\tfrac{1}{2} \begin{vmatrix} 1 & 0 \end{vmatrix} \begin{vmatrix} a & b \\ b & c \end{vmatrix} \begin{vmatrix} 1 \\ 0 \end{vmatrix} y^2 \tag{A3.34}$$

The silhouette of the paraboloid is now determined. From the discussion on silhouettes of general quadrics, it is known that its equation is quadratic; the matrix of this equation is obtained by suppressing the third row and third column in the matrix of equation (A3.31), then inverting the resulting 3x3 matrix.

$$\begin{vmatrix} x & y & t \end{vmatrix} \begin{vmatrix} 0 & 0 & 1 \\ 0 & A^{-1} & 0 \\ 1 & 0 & 0 \end{vmatrix} \begin{vmatrix} x \\ y \\ t \end{vmatrix} = 0 \tag{A3.35}$$

which is equivalent to

$$x = -\tfrac{1}{2} \frac{y^2}{\begin{vmatrix} 1 & 0 \end{vmatrix} \begin{vmatrix} a & b \\ b & c \end{vmatrix}^{-1} \begin{vmatrix} 1 \\ 0 \end{vmatrix}} \tag{A3.36}$$

When the paraboloid in (A3.29) is sliced by or projected on a plane Oxt making an angle α with the Oxy plane, both the slice and the silhouette are parabolas; see Fig.A3.3. The equations of these parabolas can be obtained by first applying a rotation around Ox, similar to that in (A3.12). The equation of the slice is then

$$x = -\tfrac{1}{2} \begin{vmatrix} \cos\alpha & \sin\alpha \end{vmatrix} \begin{vmatrix} a & b \\ b & c \end{vmatrix} \begin{vmatrix} \cos\alpha \\ \sin\alpha \end{vmatrix} t^2 \tag{A3.37}$$

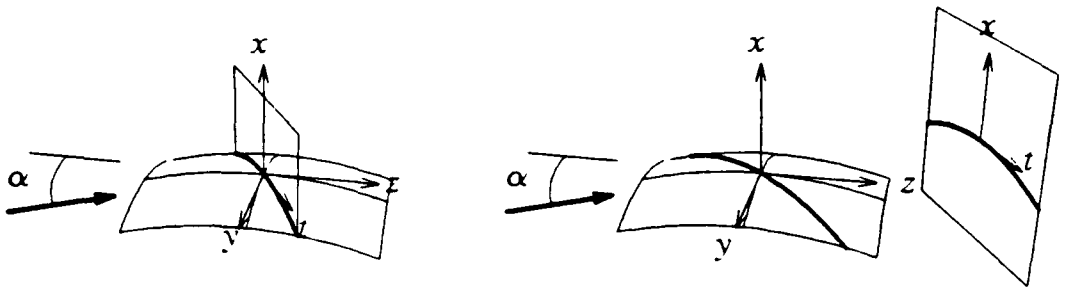

Slice Silhouette

Fig.A3.3. Slice and Silhouette of the Paraboloid

The equation of the silhouette is given by

$$x = -\tfrac{1}{2} \frac{1}{\begin{pmatrix} \cos\alpha & \sin\alpha \end{pmatrix} \begin{pmatrix} a & b \\ b & c \end{pmatrix}^{-1} \begin{pmatrix} \cos\alpha \\ \sin\alpha \end{pmatrix}} t^2 \qquad \text{(A3.38)}$$

A3.3. Euler's Theorem and its Dual

Euler's theorem in differential geometry relates the curvature of normal slices of a surface to the principal curvatures of the surface itself. At a point of the surface with principal curvatures k_1, k_2, the curvature k_{slice} of a normal slice making an angle α with the first principal direction is given by

$$k_{slice} = k_1 \cos^2\alpha + k_2 \sin^2\alpha \qquad \text{(A3.39)}$$

The dual of Euler's theorem relates the curvature of orthographic silhouettes of a surface to the principal curvatures at corresponding points of the surface. When a point of the surface with curvatures k_1, k_2 is on the silhouette generator, the curvature k_{sil} at the corresponding point of the silhouette on a plane making an angle α with the first principal direction is given by

$$\frac{1}{k_{sil}} = \frac{1}{k_1} \cos^2\alpha + \frac{1}{k_2} \sin^2\alpha \qquad \text{(A3.40)}$$

An equivalent formulation of the dual of Euler's theorem in terms of radii of curvature is given by

$$\rho_{sil} = \rho_1 \cos^2\alpha + \rho_2 \sin^2\alpha \qquad \text{(A3.41)}$$

Our proofs of these two theorems will be based on the relation between curvatures and coefficients of quadratic terms in the Taylor expansion of Monge parameterizations. Our analysis is done for one point on the surface, which is chosen as the origin of the system of axes; the Ox axis is chosen along the normal of the surface. Planar curves are also considered in a system of axes centered at the point of interest and with Ox along the normal. The expansion for a curve is given by

$$x = -\tfrac{1}{2} k\ y^2 + O(y^3) \qquad \text{(A3.42)}$$

where k is the curvature at (0,0). The equation for a surface is given by

$$x = -\tfrac{1}{2} \begin{pmatrix} y & z \end{pmatrix} \begin{pmatrix} k_{11} & k_{12} \\ k_{12} & k_{22} \end{pmatrix} \begin{pmatrix} y \\ z \end{pmatrix} + O((y,z)^3) \qquad \text{(A3.43)}$$

where $\bar{\bar{\mathbf{K}}} = k_{ij}$ is defined as the tensor of curvature of the surface at (0,0). Finally, it is easy to see that second order expansions of both slices and silhouettes depend only on the second order expansion of the surface at the corresponding point.

The proposed theorems will be obtained in two different ways. First, the results of section A3.2 are applied to the second order term in (A3.43), then, the curvature of the slice and of the silhouette are obtained with (A3.42). The second proof is obtained by considering the two operations of slicing and projecting in a plane parallel to and close to the tangent plane, say the plane $x = -\epsilon$. The slice of (A3.43) in this plane is an ellipse so that the results derived in section A3.1 can be applied. This last analysis of curvatures in terms of a section by a plane parallel to the tangent plane is well known. The ellipse in question is usually referred to as the Dupin indicatrix.

A3.3.1. Proof by Operations on Quadrics

The second order expansion of the surface at (0,0) in (A3.43) corresponds to a paraboloid to which equations (A3.37), (A3.38) can be applied.

The slice by a plane Oxt at an angle α with Oxy is the curve specified by

$$x = -1/2 \begin{pmatrix} \cos\alpha & \sin\alpha \end{pmatrix} \begin{pmatrix} k_{11} & k_{12} \\ k_{12} & k_{22} \end{pmatrix} \begin{pmatrix} \cos\alpha \\ \sin\alpha \end{pmatrix} t^2 \qquad \text{(A3.44)}$$

Comparing this expression with (A3.42) reveals that the curvature k_{slice} of the slice is

$$k_{slice} = \begin{pmatrix} \cos\alpha & \sin\alpha \end{pmatrix} \begin{pmatrix} k_{11} & k_{12} \\ k_{12} & k_{22} \end{pmatrix} \begin{pmatrix} \cos\alpha \\ \sin\alpha \end{pmatrix} \qquad \text{(A3.45)}$$

This expression reduces to (A3.39) when $k_{12}=0$. The expansion of the orthographic silhouette of the surface on the Oxt plane is obtained with (A3.38),

$$x = -1/2 \frac{1}{\begin{pmatrix} \cos\alpha & \sin\alpha \end{pmatrix} \begin{pmatrix} k_{11} & k_{12} \\ k_{12} & k_{22} \end{pmatrix}^{-1} \begin{pmatrix} \cos\alpha \\ \sin\alpha \end{pmatrix}} t^2 \qquad \text{(A3.46)}$$

The curvature of the silhouette is obtained by comparison with (A3.42),

$$\frac{1}{k_{sil}} = \begin{pmatrix} \cos\alpha & \sin\alpha \end{pmatrix} \begin{pmatrix} k_{11} & k_{12} \\ k_{12} & k_{22} \end{pmatrix}^{-1} \begin{pmatrix} \cos\alpha \\ \sin\alpha \end{pmatrix} \qquad \text{(A3.47)}$$

This expression can be rewritten for $\rho_{sil}=1/k_{sil}$ in terms of the radius of curvature tensor $\bar{\bar{\mathbf{R}}} = \bar{\bar{\mathbf{K}}}^{-1}$

$$\rho_{sil} = \begin{pmatrix} \cos\alpha & \sin\alpha \end{pmatrix} \begin{pmatrix} r_{11} & r_{12} \\ r_{12} & r_{22} \end{pmatrix} \begin{pmatrix} \cos\alpha \\ \sin\alpha \end{pmatrix} \qquad \text{(A3.48)}$$

The above form reduces to (A3.40) when $r_{12}=0$.

A3.3.2. Proof by Operations on Dupin's Indicatrix

The slice of a surface by a plane parallel to the tangent plane at the origin is a quadratic form when the slice plane is close to the tangent plane. A curve with the same shape is also obtained by slicing only the second order of the expansion in (A3.43) at any distance from the tangent plane. Considering the section plane $x = -1/2$, the slice is the Dupin indicatrix

$$\begin{pmatrix} y & z \end{pmatrix} \begin{pmatrix} k_{11} & k_{12} \\ k_{12} & k_{22} \end{pmatrix} \begin{pmatrix} y \\ z \end{pmatrix} = 1 \qquad \text{(A3.49)}$$

The expressions obtained in section A3.1 for slices and silhouettes of an ellipse are now applied to Dupin's indicatrix. The slice by $x = -1/2$ of the second order expansion of a curve such as in (A3.42) is given by $ky^2 = 1$, which indicates that half diameters d in the plane $x = -1/2$ are related to curvatures k by $d^2 = k^{-1}$. This relation between half diameters and curvatures, combined with (A3.14) and (A3.15) produces the same expressions for the curvatures as in (A3.45) and (A3.47).

A number of additional properties of Dupin's indicatrix can be easily shown. First, the surface of the ellipse is given by

$$S = \pi d_1 d_2 = \pi k_1^{-2} k_2^{-2} = \pi K_g^{-2} \tag{A3.50}$$

where K_g is the Gaussian curvature of the surface. It is interesting to note that diameters of the ellipse are related to curvatures of slices, and that the area of the ellipse is related to the Gaussian curvature. A further property of the silhouette curvature can be easily demonstrated by reasoning on Dupin's indicatrix. This property, due to Koenderink [43], relates the silhouette curvature k_{sil}, the curvature k_{rad} of a slice parallel to the viewing direction and the Gaussian curvature k_g. The relation can be obtained by considering the slice y_{rad} of Dupin's indicatrix in the direction with orientation $(\alpha+\pi/2)$ perpendicular to the silhouette axis with orientation α. The expression for y_{rad} is obtained with (A3.17),

$$\frac{1}{d_{rad}^2} = \frac{1}{d_1^2}\sin^2\alpha + \frac{1}{d_2^2}\cos^2\alpha \tag{A3.51}$$

The product $y_{rad}\, y_{sil}$ can readily be evaluated, and the result transposed to curvatures.

$$y_{rad}\ y_{sil} = d_1 d_2 \tag{A3.52}$$

Therefore,

$$k_{rad}\ k_{sil} = K_g \tag{A3.53}$$

A3.4. Summary

In this appendix, we have first shown that silhouettes of quadratic curves and surfaces can be evaluated in tangential space in the same way that slices are evaluated in point space. Second, we have exploited the relations between curvatures and quadratic forms to derive expressions for curvatures of slices and silhouettes of surfaces. These two expressions can be considered as duals of one another. Finally, we have shown that the concept of the Dupin indicatrix, proposed initially for the representation of curvatures of slices of a surface, can also be exploited as a representation of silhouette curvature, radial curvature, Gaussian curvature and of their relations.

Appendix 4
Representations of Surface Curvature

In this appendix, several descriptions of surface curvature are reviewed and compared, including the classical method of differential geometry [47], representations proposed in computer vision [44, 40, 63], and the representation proposed in this thesis. The various representations will be compared by relating them to the classical representation of differential geometry in terms of the two fundamental tensors.

Features of representations of surface curvature investigated in this appendix include expressions for curvatures of slices and silhouettes of the surface, parameterization of the representation, consistency of the representation, and recovery of the global shape of the surface from the description of its local curvature.

A4.1. Representation of Surface Curvature by Two Fundamental Tensors

This section reviews the classical definition of surface curvature; further material is found in any textbook of differential geometry.

Consider a surface Σ and a specification of the points of this surface by parametric equations

$$\vec{\mathbf{x}} = \vec{\mathbf{x}}(u, v) \tag{A4.1}$$

The lines u =cst, v = cst define a coordinate chart on this surface, as pictured on Fig.A4.1. In general, this chart is not orthogonal, its spacing is different in u and v, and its local shape varies along the surface. At each point, the metric implied by this chart defines the expression for the length ds of a small arc specified by its increments (du, dv).

$$ds^2 = d\vec{\mathbf{x}} \cdot d\vec{\mathbf{x}} = \begin{pmatrix} du & dv \end{pmatrix} \begin{vmatrix} \vec{\mathbf{x}}_u \cdot \vec{\mathbf{x}}_u & \vec{\mathbf{x}}_u \cdot \vec{\mathbf{x}}_v \\ \vec{\mathbf{x}}_u \cdot \vec{\mathbf{x}}_v & \vec{\mathbf{x}}_v \cdot \vec{\mathbf{x}}_v \end{vmatrix} \begin{pmatrix} du \\ dv \end{pmatrix} \tag{A4.2}$$

The above expression is referred to as the first fundamental form, and the 2x2 matrix on the right hand side, as the tensor of the first fundamental form. This matrix is

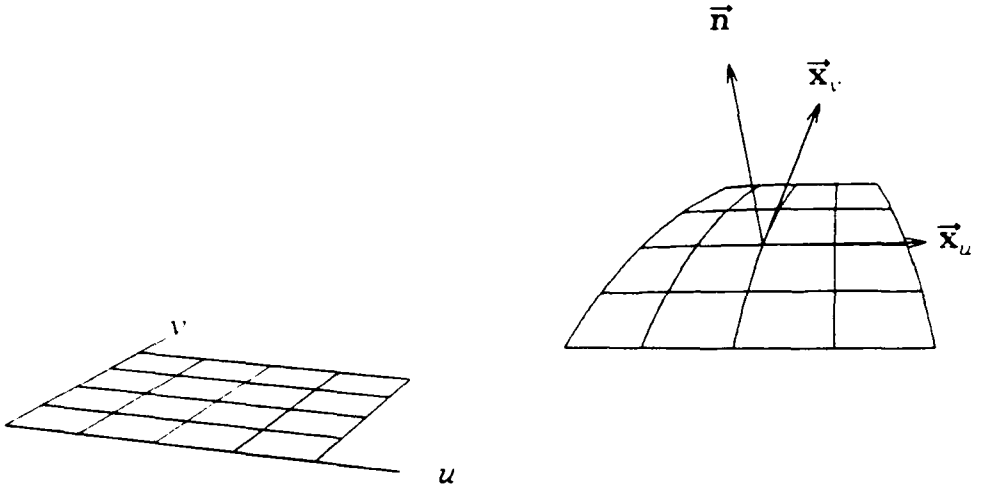

Fig.A4.1. Coordinate Charts Defined by the Parameterization

---

denoted by $\bar{\bar{G}}$ and its components by E, F, G, so that

$$\bar{\bar{G}} = \begin{vmatrix} \vec{x}_u . \vec{x}_u & \vec{x}_u . \vec{x}_v \\ \vec{x}_u . \vec{x}_v & \vec{x}_v . \vec{x}_v \end{vmatrix} = \begin{vmatrix} E & F \\ F & G \end{vmatrix} \tag{A4.3}$$

Denoting the 2-vector of the arc differentials $(du \;\; dv)^T$ by $\bar{ds}$, the first fundamental form can be written in compact notation as

$$ds^2 = \bar{ds}^T \; \bar{\bar{G}} \; \bar{ds} \tag{A4.4}$$

The curvature of the surface is related to the rate of deviation of the surface from its tangent plane, and can be described by the form

$$-d\vec{x} \cdot d\vec{1}_n = \begin{vmatrix} du & dv \end{vmatrix} \begin{vmatrix} -\vec{x}_u . \vec{1}_{n_u} & -\tfrac{1}{2}(\vec{x}_u . \vec{1}_{n_v} + \vec{x}_v . \vec{1}_{n_u}) \\ -\tfrac{1}{2}(\vec{x}_u . \vec{1}_{n_v} + \vec{x}_v . \vec{1}_{n_u}) & -\vec{x}_v . \vec{1}_{n_v} \end{vmatrix} \begin{vmatrix} du \\ dv \end{vmatrix}$$

(A4.5)

where $\vec{1}_n$ is the unit normal vector. The above form is referred to as the second fundamental form, and the 2x2 matrix on the right hand side as the tensor of the second fundamental form. This matrix is denoted by $\bar{\bar{D}}$ and its components by e, f, g, so that the second fundamental form can be written as

$$-d\,\vec{\mathbf{x}}\cdot d\,\vec{\mathbf{1}}_n = \begin{Vmatrix} du & dv \end{Vmatrix} \begin{Vmatrix} e & f \\ f & g \end{Vmatrix} \begin{Vmatrix} du \\ dv \end{Vmatrix} \tag{A4.6}$$

or, in compact form, as

$$-d\,\vec{\mathbf{x}}\cdot d\,\vec{\mathbf{1}}_n = \overline{\mathbf{ds}}^T\ \overline{\overline{\mathbf{D}}}\ \overline{\mathbf{ds}} \tag{A4.7}$$

It can be shown that the tensor $\overline{\overline{\mathbf{D}}}$ is also related to projections of the second derivatives of equations of the surface onto the unit normal

$$\overline{\overline{\mathbf{D}}} = \begin{Vmatrix} e & f \\ f & g \end{Vmatrix} = \begin{Vmatrix} \vec{\mathbf{x}}_{uu}.\vec{\mathbf{1}}_n & \vec{\mathbf{x}}_{uv}.\vec{\mathbf{1}}_n \\ \vec{\mathbf{x}}_{uv}.\vec{\mathbf{1}}_n & \vec{\mathbf{x}}_{vv}.\vec{\mathbf{1}}_n \end{Vmatrix} \tag{A4.8}$$

Transformations of the matrices $\overline{\overline{\mathbf{D}}}$, $\overline{\overline{\mathbf{G}}}$ in changes of parameterization are now investigated. The resulting expressions justify referring to these matrices as tensors, and characterize the types of these tensors.

Consider a different parameterization (u_1, v_1) of the surface Σ discussed above, where the old parameters (u, v) are related to the new parameters (u_1, v_1) by

$$\begin{cases} u = u(u_1, v_1) \\ v = v(u_1, v_1) \end{cases} \tag{A4.9}$$

The fundamental tensor $\overline{\overline{\mathbf{G}}}_1$ is given, in the new parameterization, by

$$\overline{\overline{\mathbf{G}}}_1 = \mathbf{J}^T\ \overline{\overline{\mathbf{G}}}\ \mathbf{J} \tag{A4.10}$$

where $\mathbf{J}$ is the Jacobian matrix of the transformation (A4.9),

$$\mathbf{J} = \frac{\partial \bar{u}}{\partial \overline{u_1}^T} = \begin{Vmatrix} \dfrac{\partial u}{\partial u_1} & \dfrac{\partial u}{\partial v_1} \\ \dfrac{\partial v}{\partial u_1} & \dfrac{\partial v}{\partial v_1} \end{Vmatrix} \tag{A4.11}$$

Similarly, the tensor $\overline{\overline{\mathbf{D}}}$ is modified as

$$\overline{\overline{\mathbf{D}}}_1 = \mathbf{J}^T\ \overline{\overline{\mathbf{D}}}\ \mathbf{J} \tag{A4.12}$$

Matrices which transform as in (A4.10) and (A4.12) in coordinate transformations are twice covariant tensors. This justifies referring to $\overline{\overline{\mathbf{G}}}$ and $\overline{\overline{\mathbf{D}}}$ as tensors.

A4.1.1. Curvatures of Slices and Silhouettes

When the surface is sliced by a plane perpendicular to the surface at some point, a curve for which the principal normal is identical to the normal to the surface is obtained. It is interesting to relate the curvature of these curves to the two tensors of the surface. Curvatures of normal slices and their dependence on orientation of the slice completely characterize the local shape of the surface at a given point. For a curve oriented locally along $\overline{ds}$ and with a principal normal along the normal $\vec{1}_n$ to the surface, the curvature is given by

$$\kappa_{slice} = \frac{\begin{pmatrix} du & dv \end{pmatrix} \begin{pmatrix} e & f \\ f & g \end{pmatrix} \begin{pmatrix} du \\ dv \end{pmatrix}}{\begin{pmatrix} du & dv \end{pmatrix} \begin{pmatrix} E & F \\ F & G \end{pmatrix} \begin{pmatrix} du \\ dv \end{pmatrix}} = \frac{\overline{ds}^T \, \bar{\bar{D}} \, \overline{ds}}{\overline{ds}^T \, \bar{\bar{G}} \, \overline{ds}} \qquad \text{(A4.13)}$$

Both tensors $\bar{\bar{D}}$ and $\bar{\bar{G}}$ contribute to determine the curvature of slices of the surface, and hence of the surface itself. This is due to the fact that $\bar{\bar{D}}$ determines the deviation of the surface from its tangent plane, relative to the parameterization in (u, v). At the same time, the metric implied on the surface by this parameterization is described by $\bar{\bar{G}}$. In order to determine the shape of the surface independently of the parameterization and the curvature κ_{slice} of its slices, it is hence necessary to combine the information contained in both tensors.

The dependence of the curvatures of slices of a surface on characteristics of the surface is formalized in Euler's theorem, which is analyzed in detail in Appendix 3. The theorem states that the expression of the curvature in (A4.13) has a maximum value κ_1 and a minimum value κ_2, and that these extrema correspond to orientations $\overline{ds}$ which are 90° apart. The extrema of (A4.13) are investigated in the next section, during the discussion of curvature invariants.

It will be shown in a later section that the curvature of a silhouette of the surface Σ in a plane parallel to the section plane corresponding to $\overline{ds}$ can be related to the two tensors at the corresponding point of the silhouette generator, by the expression

$$\kappa_{sil} = \frac{\begin{pmatrix} du & dv \end{pmatrix} \begin{pmatrix} E & F \\ F & G \end{pmatrix} \begin{pmatrix} du \\ dv \end{pmatrix}}{\begin{pmatrix} du & dv \end{pmatrix} \begin{pmatrix} E & F \\ F & G \end{pmatrix} \begin{pmatrix} e & f \\ f & g \end{pmatrix}^{-1} \begin{pmatrix} E & F \\ F & G \end{pmatrix} \begin{pmatrix} du \\ dv \end{pmatrix}}$$

$$= \frac{\overline{ds}^T \overline{\overline{G}}\, \overline{ds}}{\overline{ds}^T \overline{\overline{G}}\, \overline{\overline{D}}^{-1} \overline{\overline{G}}\, \overline{ds}} \qquad \text{(A4.14)}$$

In summary, given the two fundamental tensors and an orientation defined in the local parameterization of the surface, it is easy to determine the curvature of the slice or the silhouette of the surface along the given direction. Note however that, when the orientation is specified with respect to a global system of axes, it may be difficult to describe this orientation with the local parameterization.

A4.1.2. Consistency and Inversion of the Representations

It is well known in differential geometry that the six components of the tensors $\overline{\overline{G}}$, $\overline{\overline{D}}$ are not independent; they are related by a series of relations known as the Mainardi-Codazzi relations. Furthermore, it has been shown (Bonnet's theorem) that given any set of six functions (E, F, G, e, f, g) which satisfy the Mainardi-Codazzi relations, it is possible to synthesize a surface for which the two fundamental tensors have the given forms. The reconstructed surface is unique up to a solid translation and rotation. The Mainardi-Codazzi relations are hence necessary and sufficient consistency relations between the components of $\overline{\overline{G}}$ amd $\overline{\overline{D}}$. These relations can be found in any textbook of differential geometry; their form is relatively obscure for the non-expert.

A4.1.3. Parameterization

When the surface shape is defined by the tensors $\overline{\overline{G}}$ and $\overline{\overline{D}}$, these tensors are referenced to the values of the parameters (u, v) at the corresponding surface points. If this representation is used as a model for a known surface in a recognition system, matching with a measured surface may be extremely complicated if the measured surface cannot be defined in the same parameterization. In order to relate parameterizations of the model and of measured surfaces, it is necessary to define "canonical" parameterizations. Examples of proposed parameterizations are Monge

parameterizations [40], parameterizations along lines of curvature [63], and coordinates on the Gaussian sphere [44]. The advantages of each of these description modes is that the Monge descriptions are easily obtained from image measurements, the lines of curvature are intrinsic to the surface itself, and representations with the Gaussian sphere are invariant with viewing direction.

It is possible to use any of the above three parameterizations to define surfaces with the two fundamental tensors. When lines of curvature are used, it turns out that the tensor $\bar{\bar{D}}$ is diagonal. In that case, the shape of the surface is determined by the five functions E, F, G, e, g [63]. The redundancy of the representation is reduced, but not eliminated.

A4.2. Definition of Curvature by the Shape Matrix and its Invariants

Since the intrinsic curvature of a surface is expressed in the combination if the tensors $\bar{\bar{D}}$ and $\bar{\bar{G}}$, it is tempting to develop combinations of these tensors, in order to describe curvature by a single form. An example of this type of combination is given by the "Shape Matrix" $\bar{\bar{\beta}}$ [64]

$$\bar{\bar{\beta}} = \bar{\bar{G}}^{-1}\bar{\bar{D}} \tag{A4.15}$$

It is easy to derive the rule for the transformation of $\bar{\bar{\beta}}$ in changes of parameterization, from the rules for $\bar{\bar{G}}$ and $\bar{\bar{D}}$:

$$\bar{\bar{\beta}}_1 = \bar{\bar{G}}_1^{-1}\bar{\bar{D}}_1 = (\mathbf{J}^T\bar{\bar{G}}\mathbf{J})^{-1}(\mathbf{J}^T\bar{\bar{D}}\mathbf{J}) = \mathbf{J}^{-1}\bar{\bar{G}}^{-1}\bar{\bar{D}}\mathbf{J}$$

$$\bar{\bar{\beta}}_1 = \mathbf{J}^{-1}\bar{\bar{\beta}}\mathbf{J} \tag{A4.16}$$

The above transformation rule determines that $\bar{\bar{\beta}}$ is a once covariant, once contravariant tensor. It is easy to show that for this type of tensor, the determinant and the trace are invariant in coordinate transformations

$$tr(\bar{\bar{\beta}}_1) = tr(\mathbf{J}^{-1}\bar{\bar{\beta}}\mathbf{J}) = tr(\mathbf{J}\mathbf{J}^{-1}\bar{\bar{\beta}}) = tr(\bar{\bar{\beta}})$$

$$\det(\bar{\bar{\beta}}_1) = \det(\mathbf{J}^{-1}\bar{\bar{\beta}}\mathbf{J}) = \det\mathbf{J}^{-1}\det\bar{\bar{\beta}}\det\mathbf{J} = \det\bar{\bar{\beta}} \tag{A4.17}$$

As a result, the eigenvalues of $\bar{\bar{\beta}}$ are also invariant in changes of parameterizations. The relation between the eigenvalues of $\bar{\bar{\beta}}$ and the principal curvatures is now determined. The principal curvatures κ_1, κ_2 are defined as the extrema of normal curvatures

$$\kappa_{1,2} = \begin{matrix} \min \\ \max \end{matrix} \frac{\overline{ds}^T \bar{\bar{D}} \overline{ds}}{\overline{ds}^T \bar{\bar{G}} \overline{ds}} \tag{A4.18}$$

It is clear that the right hand side of the above expression does not depend on scale factors in $\overline{ds}$. Therefore, the extrema are also obtained for vectors $\overline{ds}$ with a fixed scale.

$$\kappa_{1,2} = \begin{matrix} \min \\ \max \end{matrix} \overline{ds}^T \bar{\bar{D}} \overline{ds} \; ; \quad \text{constraint: } \overline{ds}^T \bar{\bar{G}} \overline{ds} = 1 \tag{A4.19}$$

The above constrained optimization can be solved by introducing a Lagrange multiplier for the constraint,

$$\kappa_{1,2} = \begin{matrix} \min \\ \max \end{matrix} \overline{ds}^T \bar{\bar{D}} \overline{ds} - \lambda \left(\overline{ds}^T \bar{\bar{G}} \overline{ds} - 1 \right) \tag{A4.20}$$

The stationary points of the above expression can be evaluated by equating its derivative with respect to $\overline{ds}^T$ to 0.

$$2 \bar{\bar{D}} \overline{ds} - 2 \lambda \bar{\bar{G}} \overline{ds} = 0 \tag{A4.21}$$

The above expression is left-multiplied by the matrix $\bar{\bar{G}}^{-1}$, which is nonsingular, to yield

$$\left(\bar{\bar{G}}^{-1} \bar{\bar{D}} - \lambda \mathbf{I} \right) \overline{ds} = 0 \tag{A4.22}$$

The stationary points of the curvature in (A4.18) are hence obtained when $\overline{ds}$ is an eigenvector of $\bar{\bar{\beta}}$. It can be verified that these points are true extrema. Let the normalized eigenvectors of $\bar{\bar{\beta}}$ be $\bar{d}_1$, $\bar{d}_2$, and the corresponding eigenvalues be λ_1, λ_2. The extrema of the curvature are given by

$$\kappa_{1,2} = \frac{\bar{d}_{1,2}^T \bar{\bar{D}} \bar{d}_{1,2}}{\bar{d}_{1,2}^T \bar{\bar{G}} \bar{d}_{1,2}} = \frac{\bar{d}_{1,2}^T \bar{\bar{G}} \bar{\bar{\beta}} \bar{d}_{1,2}}{\bar{d}_{1,2}^T \bar{\bar{G}} \bar{d}_{1,2}} = \frac{\bar{d}_{1,2}^T \bar{\bar{G}} \lambda_{1,2} \bar{d}_{1,2}}{\bar{d}_{1,2}^T \bar{\bar{G}} \bar{d}_{1,2}} = \lambda_{1,2} \tag{A4.23}$$

The tensor $\bar{\bar{\beta}}$ has hence the remarkable characteristic that its eigenvalues are the principal curvatures. As a consequence, the trace of $\bar{\bar{\beta}}$ is equal to twice the mean

curvature and the determinant of $\bar{\bar{\beta}}$ is equal to the Gaussian curvature of the surface. These properties show that $\bar{\bar{\beta}}$ is closely related to intrinsic curvature properties of the surface. However, it will be shown in the next section that curvatures of slices and silhouettes of the surface with generic orientations cannot easily be determined with only the tensor $\bar{\bar{\beta}}$.

A4.2.1. Curvatures of Slices and Silhouettes

The curvature of a slice of the surface oriented along the vector $\overline{ds}$ on the surface is given by

$$\kappa_{slice} = \frac{\overline{ds}^T \, \bar{\bar{D}} \, \overline{ds}}{\overline{ds}^T \, \bar{\bar{G}} \, \overline{ds}} = \frac{\overline{ds}^T \, \bar{\bar{G}} \, \bar{\bar{\beta}} \, \overline{ds}}{\overline{ds}^T \, \bar{\bar{G}} \, \overline{ds}} \tag{A4.24}$$

It is clear from the above expression, that when a slice is defined by its contravariant vector $\overline{ds}$, both $\bar{\bar{\beta}}$ and $\bar{\bar{G}}$ must be known to determine its curvature.

The curvature of a silhouette of the surface can be obtained by applying to the above expression, the duality between the curvature of a slice and the curvature of a silhouette on a plane parallel to the slice. This duality is demonstrated in Appendix 3, and it is shown that the radius of curvature of the silhouette depends on the principal radii of curvature of the surface by the same expression that determines the curvature of the slice in terms of the principal curvatures. The dependence of the curvature of the slice on the principal curvatures is explicitly obtained by decomposing $\bar{\bar{\beta}}$ in (A4.24) into its diagonal factorization

$$\kappa_{slice} = \frac{\overline{ds}^T \, \bar{\bar{G}} \, \mathbf{L} \begin{bmatrix} \kappa_1 & 0 \\ 0 & \kappa_2 \end{bmatrix} \mathbf{L}^T \, \overline{ds}}{\overline{ds}^T \, \bar{\bar{G}} \, \overline{ds}} \tag{A4.25}$$

where $\mathbf{L}$ is the matrix formed by the two normalized eigenvectors $\bar{d}_1$, $\bar{d}_2$ of $\bar{\bar{\beta}}$. The duality argument determines that the curvature of the silhouette is given by

$$\kappa_{sil} = \frac{\overline{ds}^T \, \bar{\bar{G}} \, \overline{ds}}{\overline{ds}^T \, \bar{\bar{G}} \, \mathbf{L} \begin{bmatrix} 1/\kappa_1 & 0 \\ 0 & 1/\kappa_2 \end{bmatrix} \mathbf{L}^T \, \overline{ds}} \tag{A4.26}$$

The three factors in the denominator of the right hand side are easily recognized as the diagonal factorization of $\bar{\bar{\beta}}^{-1}$ so that

$$\kappa_{sil} = \frac{\overline{ds}^T \, \bar{\bar{G}} \, \overline{ds}}{\overline{ds}^T \, \bar{\bar{G}} \, \bar{\bar{\beta}}^{-1} \overline{ds}} = \frac{\overline{ds}^T \, \bar{\bar{G}} \, \overline{ds}}{\overline{ds}^T \, \bar{\bar{G}} \, \bar{\bar{D}}^{-1} \bar{\bar{G}} \, \overline{ds}} \qquad \text{(A4.27)}$$

A4.2.2. Consistency, Completeness and Reconstruction

A number of representations of surfaces based on the shape matrix $\bar{\bar{\beta}}$ or on its invariants have been proposed in the computer vision literature.

First, the extended Gaussian image[44] represents a surface shape by only one invariant, the Gaussian curvature, parameterized with the normal orientation of the surface. It can be shown that this representation is complete for a closed convex surface, and that its consistency can be expressed globally by three scalar constraints. These constraints are easily formulated when the extended Gaussian image is specified as a distribution on the Gaussian image of the surface, specifying the inverse of the Gaussian curvature of the object. The constraint is then equivalent to requiring the center of mass of the distribution to be at the center of the sphere. The inversion of the extended Gaussian image is laborious [45]. Because of the consistency constraints, it is not possible to modify the value of the extended Gaussian image at one point only and therefore to assess the effect of point values on the global surface shape, but there are strong indications that the global shape of the surface is affected by any local change of the Gaussian curvature function. Whether or not the above conjecture is true, there are no simple relations for determining the local shape of the surface from only the Gaussian curvature function, and as a consequence, no simple relations for evaluating the curvatures of slices and silhouettes of the surface. Aside from the disadvantages discussed above, the extended Gaussian image has a number of desirable characteristics, such as its invariance with rotations and the ease of computation of this representation from experimental range maps or needle maps.

In other work, Besl and Jain have proposed a representation of surface shapes by the two invariants of the tensor $\bar{\bar{\beta}}$, namely the mean curvature $\kappa_m = \frac{1}{2}(\kappa_1 + \kappa_2)$ and the Gaussian curvature $\kappa_g = \kappa_1 \kappa_2$ [40]. The parameterization proposed for indexing the values of the invariants are image plane coordinates, a choice equivalent to a

Monge parameterization of the surface with a base plane perpendicular to the viewing direction. Since this representation specifies more information than the extended Gaussian image does, it is likely that it is complete and redundant, so that consistency constraints must be satisfied by the two invariants. However, the parameterization is different than in the extended Gaussian image, and the uniqueness and consistency issues have not been carefully addressed in this case. Although the mean and Gaussian curvatures determine the local aspect of the surface shape, they do not determine the orientation of this shape with respect to a global reference, so that this representation does not provide simple expressions for the curvatures of slices and silhouettes of the surface. To the best knowledge of the author, there is no algorithm for reconstructing the surface shape, given the two invariants as functions of coordinates in the image plane.

A4.3. Representations Proposed in this Thesis

The Curvature Transform (CT) introduced in this thesis specifies a single tensor representing the local curvature of the surface, as a function of normal orientations. The parameterization of this representation is identical to the one used in the extended Gaussian image, but the function represented is more complex. As defined in Chapters 3 and 5, the characteristic represented by the CT is the inverse of the "tensor of curvature" of the surface, expressed by its components in axes parallel to the local axes on the Gaussian sphere. The curvature tensor $\bar{\bar{\mathbf{K}}}$ can be defined in terms of second derivatives of local Monge parameterizations of the surface

$$\bar{\bar{\mathbf{K}}} = \begin{pmatrix} \partial^2 x_l / \partial y_l^{\,2} & \partial^2 x_l / \partial y_l \, \partial z_l \\ \partial^2 x_l / \partial y_l \, \partial z_l & \partial^2 x_l / \partial z_l^{\,2} \end{pmatrix} \tag{A4.28}$$

where x_l is along the normal, y_l parallel to the corresponding parallel on the Gaussian sphere, and z_l parallel to the meridian of the Gaussian sphere. Comparing this expression with (A4.8), it can be shown that the tensor $\bar{\bar{\mathbf{K}}}$ is equal at each point of the surface to the tensor $\bar{\bar{\mathbf{D}}}$ for a Monge parameterization in local axes at the point. In order to define $\bar{\bar{\mathbf{K}}}$ at a given point P_0, a change of parameters $(u, v) \rightarrow (u^*, v^*)$ must be found such that, at P_0,

$$\bar{\bar{K}} = J^{*T}\,\bar{\bar{D}}J^{*} \tag{A4.29}$$

$$\bar{\bar{G}}^{*} = J^{*T}\,\bar{\bar{G}}J^{*} = I_{22} \tag{A4.30}$$

Indeed, the metric of the local Monge parameterization at P_0 is Euclidean, so that the metric tensor must be the unit matrix I_{22}. It is important to note that the parameterization by (u^*, v^*) applies only to the point P_0 and that, although the tangent vectors $\vec{x}_{u^*}$, $\vec{x}_{v^*}$ are along the local directions $\vec{1}_\xi$, $\vec{1}_\eta$, the parameters (u^*, v^*) are not directly related to the orientation angles ξ, η themselves. Assuming that J^* is regular, equation (A4.30), can be modified to

$$J^{*}\,J^{*T} = \bar{\bar{G}}^{-1} \tag{A4.31}$$

Any matrix J^* satisfying the above equation is the Jacobian of a parameter change which leads to a Euclidean metric around P_0. A solution of this equation will be written formally as

$$J^{*} = \bar{\bar{G}}^{-1/2}$$

The solution of (A4.31) is ambiguous since a product of J^* by any orthonormal 2x2 matrix is also solution of the equation. The ambiguity is resolved by requiring the vector $\vec{x}_u$ to be horizontal. The expression for the tensor of radius of curvature is written formally as

$$\bar{\bar{K}} = \bar{\bar{G}}^{T\,-1/2}\bar{\bar{D}}\,\bar{\bar{G}}^{-1/2} \tag{A4.32}$$

$$\bar{\bar{R}} = \bar{\bar{G}}^{T\,1/2}\bar{\bar{D}}^{-1}\,\bar{\bar{G}}^{1/2} \tag{A4.33}$$

Explicit expressions for obtaining the components of $\bar{\bar{K}}$ in terms of the components of $\bar{\bar{G}}$ and $\bar{\bar{D}}$ were determined in[62]

$$\left|\begin{aligned}
k_{11} &= \frac{[e z_{v^*}^2 - 2f z_{u^*} z_{v^*} + g z_{u^*}^2]}{Z} \\
k_{12} &= \frac{[e z_{v^*}(G z_{u^*} - F z_{v^*}) + f(E z_{v^*}^2 - G z_{u^*}^2) - g z_{u^*}(-F z_{u^*} + E z_{v^*})]}{Z\sqrt{EG - F^2}} \\
k_{22} &= \frac{[e(G z_{u^*} - F z_{v^*})^2 + 2f(G z_{u^*} - F z_{v^*})(-F z_{u^*} + E z_{v^*}) + g(-F z_{u^*} + E z_{v^*})^2]}{Z(EG - F^2)}
\end{aligned}\right. \tag{A4.34}$$

where z_u , z_v denote partial derivatives of z . It turns out that the tensor $\bar{\bar{\mathbf{K}}}$ is invariant in changes of the parameterization (u, v), and that its eigenvalues are identical to the eigenvalues of $\bar{\bar{\beta}}$. It is interesting to note the similarities and differences between the tensors $\bar{\bar{\mathbf{K}}}$ defined in (A4.32) and $\bar{\bar{\beta}}$ defined in (A4.15). Major differences between $\bar{\bar{\mathbf{K}}}$ and $\bar{\bar{\beta}}$ are that $\bar{\bar{\mathbf{K}}}$ is symmetric while $\bar{\bar{\beta}}$ is not, in general; as a consequence, $\bar{\bar{\mathbf{K}}}$ has three independent components while $\bar{\bar{\beta}}$ has four components. Furthermore, $\bar{\bar{\mathbf{R}}}$ is related to local axes on the Gaussian sphere while $\bar{\bar{\beta}}$ is related to local axes determined by the parameterization.

A4.3.1. Curvatures of Slices and Silhouettes

It has been shown during the demonstration of the Silhouette-Slice theorems that the radius of curvature of the silhouette is simlpy related to the radius of curvature tensor $\bar{\bar{\mathbf{R}}}$, which is the inverse of $\bar{\bar{\mathbf{K}}}$, by

$$\rho_{sil} = \begin{pmatrix} \cos\alpha & \sin\alpha \end{pmatrix} \bar{\bar{\mathbf{R}}} \begin{pmatrix} \cos\alpha \\ \sin\alpha \end{pmatrix} \tag{A4.35}$$

where α directly characterizes the orientation of the projection plane in the local axes. Similarly, the curvature of a slice of the surface is given by

$$k_{slice} = \begin{pmatrix} \cos\alpha & \sin\alpha \end{pmatrix} \bar{\bar{\mathbf{K}}} \begin{pmatrix} \cos\alpha \\ \sin\alpha \end{pmatrix} \tag{A4.36}$$

The above expressions emphasize that the shape of slices and silhouettes of the surface are easily determined from only the tensor $\bar{\bar{\mathbf{R}}}$ specified by the CT.

A4.3.2. Consistency, Completeness and Reconstruction

In Chapter 5, simple first order differential equations were determined for parametric equations of a surface, given its CT. The existence of these equations implies the completeness of the CT. In addition, consistency relations for the CT were derived simply by requiring equality of the mixed derivatives of the parametric equations in terms of the CT. These relations are equivalent to the Mainardi-Codazzi equations for the representation with the two fundamental tensors, but they are much simpler.

A4.4. Discussion

When comparing the various representations of surfaces reviewed in this appendix, it appears that the Curvature Transform has a number of advantages for describing surface curvature. The CT has only three independent components, while preserving completeness both locally and globally. It is easy to determine the shape of slices and silhouettes of a surface defined by its CT. Finally, the consistency relations and the reconstruction of the surface shape are straightforward for the CT representation. An additional advantage of the CT is the existence of closed-form relations with the other two representations proposed in this thesis, namely the Support Transform and the Vector Support Transform. The major disadvantage of the CT is its limitation to convex objects.

When choosing a representation for a particular application involving descriptions of surface shapes, several factors must be considered. An aspect which was not discussed in this appendix is the estimation of the representation from experimental measurements and the robustness of these estimates. Experiments with the new representation must be performed before it can be compared with other representations based on this criterion.

Appendix 5
Curvature of the Projection of a 3-D Curve

In this appendix, the radius of curvature of the projection of a 3-D curve is computed in terms of the radius of curvature at the corresponding points of the 3-D curve and the orientation of the viewing direction relative to the local Frenet trihedron.

Consider a point O on the curve C, and the system of axes $Oxyz$ oriented along the principal normal $n=x$, the tangent $t=y$ and the binormal $b=z$ at O; see Fig.A5.1. Including terms up to the second order, the curve can be described around O by the equations

$$\left| \begin{array}{l} x = -\dfrac{1}{2\rho_o} s^2 \\ y = s \\ z = 0 \end{array} \right. \qquad \text{(A5.1)}$$

where ρ_o is the radius of curvature at O. The viewing direction $\vec{v}$ is defined in the axes $Oxyz$ by its latitude θ and longitude $-\xi$. A rotated system of axes $Ox_R y_R z_R$ is also considered, such that Ox_R is along the viewing direction v and Oy_R is on the Oxy plane, see Fig.A5.1. The projection operation is trivial in the rotated axes, as it corresponds to retaining the y_R and z_R coordinates and discarding x_R.

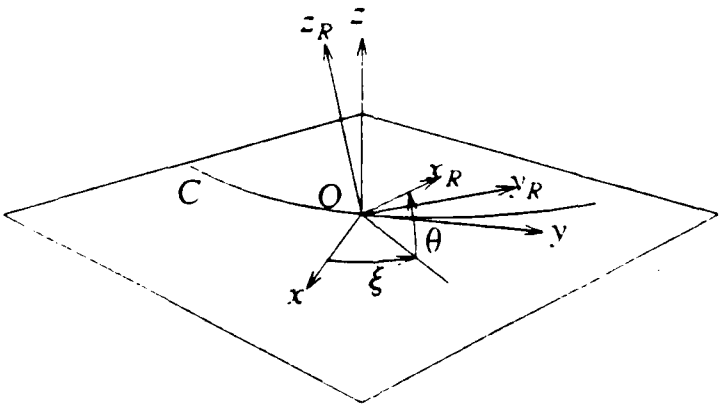

Fig.A5.1. Curve C, local axes $Oxyz$ and rotated axes $Ox_R y_R z_R$.

The transformation between the two systems of axes $Oxyz$, $Ox_R y_R z_R$ is given by

$$\begin{vmatrix} x_R \\ y_R \\ z_R \end{vmatrix} = \begin{vmatrix} \cos\xi\cos\theta & -\sin\xi\cos\theta & \sin\theta \\ \sin\xi & \cos\xi & 0 \\ -\cos\xi\sin\theta & \sin\xi\sin\theta & \cos\theta \end{vmatrix} \begin{vmatrix} x \\ y \\ z \end{vmatrix} \tag{A5.2}$$

For points in the Oxy plane, the projection is obtained by merely applying (A5.2) to the x , y coordinates of each point, then discarding the x_R coordinate in the rotated frame.

$$\begin{vmatrix} y_R \\ z_R \end{vmatrix} = \begin{vmatrix} \sin\xi & \cos\xi \\ -\cos\xi\sin\theta & \sin\xi\sin\theta \end{vmatrix} \begin{vmatrix} x \\ y \end{vmatrix} \tag{A5.3}$$

Applying the above transformation to the parametric equations of the curve in (A5.1), produces parametric equations for the projected curve

$$\begin{vmatrix} y_R = -\sin\xi \dfrac{s^2}{2\rho_o} + \cos\xi\, s \\ z_R = \cos\xi\sin\theta \dfrac{s^2}{2\rho_o} + \sin\xi\sin\theta\, s \end{vmatrix} \tag{A5.4}$$

The radius of curvature is now evaluated at the origin, using the standard expression

$$\rho = \frac{(\dot{y}_R^2 + \dot{z}_R^2)^{3/2}}{\dot{y}_R \ddot{z}_R - \ddot{y}_R \dot{z}_R} \tag{A5.5}$$

where the dots stand for derivatives with respect to the parameter of the curve, here s . The derivatives in the above expression are evaluated at the origin as

$$\dot{y}_R(0) = \cos\xi,\ \dot{z}_R(0) = \sin\xi\sin\theta,\ \ddot{y}_R(0) = -\frac{\sin\xi}{\rho_o},\ \ddot{z}_R(0) = -\frac{\cos\xi\sin\theta}{\rho_o} \tag{A5.6}$$

As a consequence, the radius of curvature of the projection of the curve around O is given by

$$\rho_s = \frac{(\cos^2\xi + \sin^2\xi\,\sin^2\theta)^{3/2}}{\sin\theta}\rho_o = \frac{(1 - \sin^2\xi\,\cos^2\theta)^{3/2}}{\sin\theta}\rho_o \tag{A5.7}$$

This result is consistent with that obtained in section 7.4.2.

Appendix 6
Evaluation of two Differentials in Chapter 5

In this appendix, the differentials of local coordinates of a curve and of a surface are evaluated in terms of global angle differentials, providing the expansions of equations (5.13) and (5.41) in the text.

The case of a curve is addressed first; it is illustrated in Fig.5.3 in the text. In fixed local axes, an expression for the differential $d\,\mathfrak{X}(\psi)$ in the neighborhood of P_0 is obtained by the chain rule

$$d\,\mathfrak{X}_l(\psi) = \frac{d\,\mathfrak{X}_l(z_l)}{dz_l}\,\frac{dz_l}{dm_{zl}}\,\frac{dm_{zl}}{d\,\psi}\,d\,\psi \qquad \text{(A6.1)}$$

where m_{zl} is the gradient of the local Monge equation defined in section 3.2.4. The first two derivatives in the right-hand-side of (5.13) are obtained for the particular curve shape at P_0 from (5.12). The last derivative in (5.13) depends on the relation between the local gradient and the global orientation angle, a relation discussed in section 3.2.4.

Each of the factors in (5.13) is now evaluated.

Parametric equations for the curve C around P_0 are easily obtained from (5.12), namely

$$\begin{aligned}\begin{bmatrix} x_l \\ z_l \end{bmatrix} &= \begin{bmatrix} 0 \\ 1 \end{bmatrix} z_l + \begin{bmatrix} 1 \\ 0 \end{bmatrix} \left(-\tfrac{1}{2} z_l\, \rho_0^{-1} z_l \right) + O(z_l^{\,3}) \\ &= \begin{bmatrix} 0 \\ 1 \end{bmatrix} z_l + O(z_l^{\,2})\end{aligned}$$

$$\mathfrak{X}_l = z_l\, \bar{\mathbf{I}}_{zl} + O(z_l^{\,2}) \qquad \text{(A6.2)}$$

The first derivative of the above equation with respect to the parameter z_l is given by

$$\begin{pmatrix} \dfrac{dx_l}{dz_l} \\ \dfrac{dz_l}{dz_l} \end{pmatrix} = \begin{pmatrix} 0 \\ 1 \end{pmatrix} + O(z_l)$$

$$d\,\mathfrak{X}_l / dz_l = \bar{\mathbf{I}}_{zl} + O(z_l) \tag{A6.3}$$

The derivative dz_l / dm_{zl} is now evaluated. In the neighborhood of P_0, the local gradient m_{zl} on the curve C is given by

$$m_{zl} = \partial x_l / \partial z_l = -\rho_0^{-1} z_l + O(z_l^2) \tag{A6.4}$$

It follows that

$$z_l = -\rho_0 m_{zl} + O(m_{zl}^2) \tag{A6.5}$$

so that

$$\frac{dz_l}{dm_{zl}} = -\rho_0 + O(m_{zl}) \tag{A6.6}$$

Finally, the local gradient is related to the global orientation angle ψ by (3.61)

$$m_{zl} = -(\psi - \psi_0) + O((\psi - \psi_0)^2) \tag{A6.7}$$

so that

$$\frac{dm_{zl}}{d\psi} = -1 + O(\psi - \psi_0) \tag{A6.8}$$

The derivatives obtained above are inserted in equation (5.13) to obtain the differential $d\,\mathfrak{X}_l$ in local axes

$$\begin{pmatrix} dx_l \\ dz_l \end{pmatrix} = \begin{pmatrix} 0 \\ 1 \end{pmatrix} (-\rho_0)(-1)\, d\psi + O(\psi - \psi_0) = \rho_0 \begin{pmatrix} 0 \\ 1 \end{pmatrix} d\psi + O(\psi - \psi_0)$$

$$d\,\mathfrak{X}_l = \rho_0\, \bar{\mathbf{I}}_{zl}\, d\psi + O(\psi - \psi_0) \tag{A6.9}$$

which is the result exploited in the text, in equation (5.14).

Differentials of coordinates of a surface are now investigated in a local reference frame around the point P_0; This frame is illustrated in Fig.5.7 in the text. An expression for the differential in the local axes $P_0 x_l\, y_l\, z_l$ is obtained by the chain rule

$$d\,\vec{\mathbf{x}}_l = \frac{D\vec{\mathbf{x}}_l(\mathbf{z}_l)}{D\mathbf{z}_l}\,\frac{D\mathbf{z}_l}{D\vec{\mathbf{m}}_{zl}}\,\frac{D\vec{\mathbf{m}}_{zl}}{D\boldsymbol{\xi}}\,d\,\boldsymbol{\xi} \qquad \text{(A6.10)}$$

where expressions such as $D\vec{\mathbf{x}}_l / D\mathbf{z}_l$ denote Jacobian matrices, $\vec{\mathbf{m}}_{zl} = (m_{yl}\ m_{zl})^T$ is the 2-vector of local gradients, and $d\,\boldsymbol{\xi}$ is the vector of normalized global angle differentials $d\,\boldsymbol{\xi} = (\cos\eta d\,\xi\ d\,\eta)^T$. The first two Jacobian matrices on the right hand side of (A6.10) are obtained for the particular surface shape around P_0 from (5.39). The last Jacobian matrix in (A6.10) is a relation between local slopes and global orientation angles which can be derived from relations obtained in section 3.2.4. Each of the factors in (A6.10) is now evaluated in sequence.

Parametric equations for the surface around P_0 are given by

$$\begin{pmatrix} x_l \\ y_l \\ z_l \end{pmatrix} = \begin{pmatrix} 0 & 0 \\ 1 & 0 \\ 0 & 1 \end{pmatrix} \begin{pmatrix} y_l \\ z_l \end{pmatrix} - \tfrac{1}{2} \begin{pmatrix} 1 \\ 0 \\ 0 \end{pmatrix} \begin{pmatrix} y_l & z_l \end{pmatrix} \begin{pmatrix} r^0_{11} & r^0_{12} \\ r^0_{12} & r^0_{22} \end{pmatrix}^{-1} \begin{pmatrix} y_l \\ z_l \end{pmatrix} + O((y_l, z_l)^3)$$

$$= \begin{pmatrix} 0 & 0 \\ 1 & 0 \\ 0 & 1 \end{pmatrix} \begin{pmatrix} y_l \\ z_l \end{pmatrix} + O((y_l, z_l)^2)$$

$$\vec{\mathbf{x}}_l = \mathbf{I}_{32}\,\mathbf{z}_l + O(\mathbf{z}_l^2) \qquad \text{(A6.11)}$$

where $\mathbf{I}_{32}$ is a 3x2 matrix whose columns are the canonic vectors $\vec{\mathbf{e}}_2, \vec{\mathbf{e}}_3$. $\mathbf{I}_{32}$ is also the matrix of the injective transformation from the local tangent plane $P_0 y_l\, z_l$ into 3-space referenced by $P_0 x_l\, y_l\, z_l$. The Jacobian matrix of the above expression is given by

$$\begin{pmatrix} \frac{\partial x_l}{\partial y_l} & \frac{\partial x_l}{\partial z_l} \\ \frac{\partial y_l}{\partial y_l} & \frac{\partial y_l}{\partial z_l} \\ \frac{\partial z_l}{\partial y_l} & \frac{\partial z_l}{\partial z_l} \end{pmatrix} = \begin{pmatrix} 0 & 0 \\ 1 & 0 \\ 0 & 1 \end{pmatrix} + O((y_l, z_l)^2)$$

$$\frac{D\vec{\mathbf{x}}_l}{D\mathbf{z}_l} = \mathbf{I}_{32} + O(\mathbf{z}_l^2) \tag{A6.12}$$

The Jacobian matrix $\dfrac{D\mathbf{z}_l}{D\bar{\mathbf{m}}_{zl}}$ is now evaluated. The local gradient $\bar{\mathbf{m}}_{zl}$ on the surface Σ in the neighborhood of P_0 can be obtained from (5.39)

$$\begin{pmatrix} m_{yl} \\ m_{zl} \end{pmatrix} = -\begin{pmatrix} r_{11}^0 & r_{12}^0 \\ r_{12}^0 & r_{22}^0 \end{pmatrix}^{-1} \begin{pmatrix} y_l \\ z_l \end{pmatrix} + O(\mathbf{z}_l^2)$$

$$\bar{\mathbf{m}}_l = -\bar{\bar{\mathbf{R}}}_0^{-1}\, \mathbf{z}_l + O(\mathbf{z}_l^2) \tag{A6.13}$$

This equation is inverted to produce

$$\begin{pmatrix} y_l \\ z_l \end{pmatrix} = -\begin{pmatrix} r_{11}^0 & r_{12}^0 \\ r_{12}^0 & r_{22}^0 \end{pmatrix} \begin{pmatrix} m_{yl} \\ m_{zl} \end{pmatrix} + O(\bar{\mathbf{m}}_{zl}^2)$$

$$\mathbf{z}_l = -\bar{\bar{\mathbf{R}}}_0\, \bar{\mathbf{m}}_l + O(\bar{\mathbf{m}}_{zl}^2) \tag{A6.14}$$

The desired Jacobian matrix is then obtained by differentiation.

$$\begin{pmatrix} \frac{\partial y_l}{\partial m_{yl}} & \frac{\partial y_l}{\partial m_{zl}} \\ \frac{\partial z_l}{\partial m_{yl}} & \frac{\partial z_l}{\partial m_{zl}} \end{pmatrix} = -\begin{pmatrix} r_{11}^0 & r_{12}^0 \\ r_{12}^0 & r_{22}^0 \end{pmatrix} + O(\bar{\mathbf{m}}_{zl}^2)$$

$$\frac{D\mathbf{z}_l}{D\bar{\mathbf{m}}_{zl}} = -\bar{\bar{\mathbf{R}}}_0 + O(\bar{\mathbf{m}}_{zl}^2) \tag{A6.15}$$

Finally, the local gradients are related to the global angles by (3.61) from which the following form is derived for the last Jacobian matrix in equation (A6.10).

$$\begin{vmatrix} \dfrac{\partial m_{yl}}{\cos\eta\,\partial\xi} & \dfrac{\partial m_{yl}}{\partial\eta} \\ \dfrac{\partial m_{zl}}{\cos\eta\,\partial\xi} & \dfrac{\partial m_{zl}}{\partial\eta} \end{vmatrix} = -\begin{vmatrix} 1 & 0 \\ 0 & 1 \end{vmatrix} + O((\xi-\xi_0,\eta-\eta_0)^2)$$

$$\frac{D\vec{m}_{zl}}{D\boldsymbol{\xi}} = -\mathbf{I}_{22} + O((\boldsymbol{\xi}-\boldsymbol{\xi}_0)^2) \qquad \text{(A6.16)}$$

where $\mathbf{I}_{22}$ is the 2x2 unit matrix. The expressions obtained above for the Jacobian matrices are inserted in equation (A6.10) and produce an expression for the differential $d\,\vec{\mathbf{x}}_l$ in local coordinates, valid to first order around P_0. The expression is exact at P_0 and since P_0 is generic, applies to all regular points in appropriate local axes.

$$\begin{pmatrix} dx_l \\ dy_l \\ dz_l \end{pmatrix} = \begin{pmatrix} 0 & 0 \\ 1 & 0 \\ 0 & 1 \end{pmatrix} \begin{pmatrix} r_{11} & r_{12} \\ r_{12} & r_{22} \end{pmatrix} \begin{pmatrix} \cos\eta\, d\,\xi \\ d\,\eta \end{pmatrix}$$

$$d\,\vec{\mathbf{x}}_l = \mathbf{I}_{32}\,\bar{\bar{\mathbf{R}}}\,d\,\boldsymbol{\xi} \qquad \text{(A6.17)}$$

A differential for the surface in global coordinates is obtained by applying the coordinate transformation in (3.10) to the above differentials

$$\begin{pmatrix} dx \\ dy \\ dz \end{pmatrix} = \begin{pmatrix} \cos\xi\cos\eta & -\sin\xi & -\cos\xi\sin\eta \\ \sin\xi\cos\eta & \cos\xi & -\sin\xi\sin\eta \\ \sin\eta & 0 & \cos\eta \end{pmatrix} \begin{pmatrix} 0 & 0 \\ 1 & 0 \\ 0 & 1 \end{pmatrix} \begin{pmatrix} r_{11} & r_{12} \\ r_{12} & r_{22} \end{pmatrix} \begin{pmatrix} \cos\eta\, d\,\xi \\ d\,\eta \end{pmatrix}$$

$$d\,\vec{\mathbf{x}} = \mathbf{R}_3^{R-G}\,\mathbf{I}_{32}\,\bar{\bar{\mathbf{R}}}\,d\,\boldsymbol{\xi}$$

which is the result exploited in the text, in equation (5.42).

References

[1] C. Belanger-Grafton, *Silhouettes, A Pictorial Archive of Varied Illustrations*. New York: Dover, 1979.

[2] D. Marr, "Analysis of Occluding Contour," *Proceedings of the Royal Society of London, Ser. B*, vol. 197, pp. 441-475, 1976.

[3] H.G. Barrow and J.M. Tennenbaum, "Interpreting Line Drawings as Three Dimensional Surfaces," *Artificial Intelligence*, vol. 17, pp. 75-116, 1981.

[4] B.G. Baumgart, "Geometric Modeling for Computer Vision," Memo AIM-249, Stanford Artificial Intelligence Laboratory, October 1974.

[5] I. Carlbom and J. Paciorek, "Planar Geometric Projections and Viewing Transformations," *Computing Surveys*, vol. 10, no. 4, pp. 465-502, December 1978.

[6] D. Marr and K.R. Nishihara, "Representation and Recognition of the Spatial Organization of Three-Dimensional Shapes," *Proceedings of the Royal Society of London, Ser. B*, vol. 200, pp. 269-294, 1977.

[7] J. J. Koenderink and A. J. Van Doorn, "The Singularities of the Visual Mapping," *Biological Cybernetics*, vol. 24, pp. 51-59, 1976.

[8] V.I. Arnold, "Indices of Singular Points on 1-forms on a Manifold," *Russian Mathematical Surveys*, vol. 34, no. 2, pp. 1-42, 1976.

[9] J.W. Bruce, "Seeing-The Mathematical Viewpoint," *The Mathematical Intelligencer*, vol. 6, no. 4, 1984.

[10] A.P. Pentland, "Perceptual Organization and Representation of Natural Form," Technical Note 357, SRI, July 15, 1985.

[11] W.M.Newman and R.F.Sproull, *Principles of Interactive Computer Graphics*. New York: Mc Graw Hill, 1979.

[12] D.F. Rogers, *Procedural Elements for Computer Graphics*. New York: Mc Graw Hill, 1985.

[13] S.A. Shafer, *Shadows and Silhouettes in Computer Vision*. Boston: Kluwer Academic Publishers, 1985.

[14] J.G. Verly, P.L. Van Hove, R.L Walton, and D.E. Dudgeon, "Silhouette Understanding System for Laser-Radar Range Imagery," *Proceedings of the Meeting of the IRIS Specialty Group on Active Systems*, Monterey, CA, Nov. 5-7, 1985.

[15] J.G. Verly, P.L. Van Hove, R.L Walton, and D.E. Dudgeon, "Silhouette Understanding System," *Proceedings of the International Conference on Acoustics, Speech and Signal Processing (ICASSP)*, Tokyo, Japan, April 7-11, 1986.

[16] P. Van Hove, "Reconstruction of Axisymmetric Objects from One Silhouette," *Proceedings of the Topical Meeting on Signal Recovery and Synthesis II, sponsored by the Optical Society of America*, Honolulu, Hawaii, April 2-4, 1986.

[17] T. Poggio and V. Torre, "Ill Posed Problems and Regularization in Early Vision," Memo AIM-773, MIT AI Lab, 1982.

[18] W.N. Martin and J.K. Aggarwal, "Volumetric Descriptions of Objects from Multiple Views," *IEEE Transactions on Pattern Analysis and Machine Intelligence*, vol. PAMI-5, no. 2, 1983.

[19] D. Marr, *Vision: A Computational Investigation into the Human Representation and Processing of Visual Information*. San Fransisco: Freeman, 1982.

[20] D.H. Ballard and C.M. Brown, *Computer Vision*. Englewood Cliffs, N.J.: Prentice Hall, 1982.

[21] B.K.P. Horn, *Robot Vision*. Cambridge, MA: MIT Press, 1986.

[22] C.T. Zahn and R.Z. Roskies, "Fourier Descriptors for Plane Closed Curves," *IEEE Transactions on Computers*, vol. C-21, no. 3 , pp. 269-281, March 1972.

[23] P.J. Nahin, "The Theory and Measurement of a Silhouette Descriptor for Image Pre-Processing and Recognition," *Pattern Recognition*, vol. 6, pp. 85-95, 1974.

[24] S.A. Dudani, K.J. Breeding, and R.B. Mc Ghee, "Aircraft Identification by Moment Invariants," *IEEE Transactions on Computers*, vol. C-26, pp. 39-45, 1977.

[25] K.S. Fu, *Syntactic Pattern Recognition and Applications*. Englewood Cliffs, NJ: Prentice Hall, 1982.

[26] M.K. Hu, "Visual Pattern Recognition by Moment Invariants," *IRE Transactions on Information Theory*, vol. 8, pp. 179-187, 1962.

[27] C.W. Richard and H. Hemami, "Identification of Three-Dimensional Objects Using Fourier Descriptors of the Boundary Curve," *IEEE Transactions on Systems, Man and Cybernetics*, vol. SMC-4 , no. 4, pp. 371-378, 1974.

[28] J. Sklansky and G.A. Davison, "Recognizing Three-Dimensional Objects by their Silhouettes," *Journal of the SPIE*, vol. 10, pp. 10-17, Nov./Dec. 1971.

[29] M.R. Teague, "Image Analysis via the General Theory of Moments," *Journal of the Optical Society of America*, vol. 70, no. 8, pp. 920-930, August 1980.

[30] T.P. Wallace and P.A. Wintz, "An Efficient Three-Dimensional Aircraft Recognition Algorithm Using Normalized Fourier Descriptors," *Computer Graphics and Image Processing*, vol. 13, pp. 99-126, 1980.

[31] D. Cyganski and J.A. Orr, "Object Identification and Orientation Estimation from Point Set Tensors," *International Conference on Pattern Recognition*, July 30 - Aug 2, 1984.

[32] W.A. Richards, J.J. Koenderink, and D.D. Hoffman, "Inferring 3D Shapes from 2D Codons," Memo AIM-840, MIT Artificial Intelligence Laboratory, April 1985.

[33] J.J. Koenderink, "The Internal Representation of Solid Shape Based on the Topological Properties of the Apparent Contours," in *Image Understanding 85*, ed. W Richards, 1986.

[34] R.A. Brooks, "Symbolic Reasoning Among 3-D Models and 2-D Images," *Artificial Intelligence*, vol. 17, pp. 285-348, 1981.

[35] C. Goad, "Special Purpose Automatic Programming for 3-D Model-Based Vision," *DARPA Image Understanding Workshop*, pp. 94-104, 1983.

[36] W.E. Grimson and T. Lozano-Perez, "Model-Based Recognition and Localization From Sparse Range or Tactile Data," Memo AIM-738, MIT Artificial Intelligence Laboratory, August 1983.

[37] I.D. Faux and M.J. Pratt, *Computational Geometry for Design and Manufacture*, Chichester, UK: Ellis Horwood, 1979.

[38] M.E. Mortenson, *Geometric Modeling*. New York: J. Wiley and sons, 1985.

[39] P.J. Besl and R.C. Jain, "Three-dimensional Object Recognition," *ACM Computing Surveys*, vol. 17, no. 1, pp. 75-145, 1985.

[40] P.J. Besl and R.C. Jain, "Invariant Surface Characteristics for 3D Object Recognition in Range Images," *Computer Vision, Graphics and Image Processing*, vol. 33, no. 1, pp. 33-80, January 1986.

[41] H. Freeman and J. Chakravarty, "The Use of Characteristic Views in the Recognition of Three-Dimensional Objects," in *Pattern Recognition in Practice*, ed. L.Kanal, North-Holland, 1980.

[42] A.G. Agin and T.O. Binford, "Computer Description of Curved Objects," *Proceedings of the Third International Joint Conference on Artificial Intelligence*, pp. 629-635, August 1983.

[43] J.J. Koenderink, "What does the Occluding Contour tell us about Solid Shape?," *Perception*, vol. 13, pp. 321-330, 1984.

[44] B.K.P. Horn, "Extended Gaussian Images," *Proceedings of the IEEE*, vol. 72, no. 12, December 1984.

[45] J.J. Little, "Recovering Shape and Determining Attitude from Extended Gaussian Images," Technical Report TR-85-2, University of British Columbia, Vancouver, B.C., Canada, April 1985.

[46] K. Ikeuchi, B.K.P. Horn, S. Nagata, T. Callahan, and O. Feingold, "Picking an Object from a Pile of Objects," AI Memo 726, Massachusetts Institute of Technology, May 1983.

[47] M.P. Do Carmo, *Differential Geometry of Curves and Surfaces*. Englewood Cliffs, NJ: Prentice-Hall, 1976.

[48] I. Vaisman, *A First Course in Differential Geometry*. New York : Marcel Dekker, Inc., 1984.

[49] D.M.Y. Somerville, *Analytical Geometry of Three Dimensions*. Cambridge, UK: Cambridge University Press, 1959.

[50] D. Hilbert and S. Cohn-Vossen, *Geometry and The Imagination*. New York: Chelsea, 1952.

[51] G. Fekete and L.S. Davis, "Property Spheres: A new Representation for Object Recognition," *Proceedings of the Workshop on Computer Vision*, pp. 192-201, 1984.

[52] D.J. Struik, *Lectures on Classical Differential Geometry*. Cambridge MA: Addison-Wesley, 1950.

[53] B.K.P. Horn and E.J. Weldon, "Filtering Closed Curves," *Proceedings of the IEEE Conference on Computer Vision and Pattern Recognition*, June 1985.

[54] J.G. Verly and P.L. Van Hove, "Elements of Silhouette Theory for 2-D Convex Objects," Internal report, 1985., M.I.T. Lincoln Laboratory, Lexington, MA, USA.

[55] W.H. Beyer, *CRC Standard Mathematical Tables, 26 th edition*. Roca Baton FL: CRC Press, 1981.

[56] J. Serra, *Image Analysis and Mathematical Morphology*. New York: Academic Press, 1982.

[57] P. Brou, "Finding Objects in Depth Maps," PhD Dissertation, MIT Dep. Elec. Eng. Comput. Sci., September 1983.

[58] A.H. Barr, "Superquadrics and Angle-Preserving Transformations," *Computer Graphics and Applications*, vol. 1, no. 1, pp. 11-23, 1981.

[59] L.A. Lyusternik, *Convex Figures and Polyhedra*. New York: Dover, 1963.

[60] W.E. Grimson and T. Lozano-Perez, "Model-Based Recognition and Localization From Sparse Range or Tactile Data," *International Journal of Robotics Research*, vol. 3, no. 3, Fall 1984.

[61] J.J. Little, *Personal Communication*.

[62] P. Van Hove and J.G. Verly, "A Silhouette-slice Theorem for Opaque 3-D Objects," *Proceedings of the International Conference on Acoustics, Speech and Signal Processing (ICASSP)*, pp. 933-936, Tampa, FL, March 1985.

[63] M. Brady, J. Ponce, A. Yuille, and H. Asada, "Describing Surfaces, to appear as," Memo, MIT Artificial Intelligence Laboratory, 1985.

[64] B. O'Neill, *Elementary Differential Geometry*. New York: Academic Press, 1966.

DISTRIBUTION LIST

	DODAAD Code	
Director Defense Advanced Research Project Agency 1400 Wilson Boulevard Arlington, Virginia 22209 Attn: Program Management	HX1241	(1)
Head Mathematical Sciences Division Office of Naval Research 800 North Quincy Street Arlington, Virginia 22217	N00014	(1)
Administrative Contracting Officer E19-628 Massachusetts Institute of Technology Cambridge, Massachusetts 02139	N66017	(1)
Director Naval Research Laboratory Attn: Code 2627 Washington, D.C. 20375	N00173	(6)
Defense Technical Information Center Bldg 5, Cameron Station Alexandria, Virginia 22314	S47031	(12)
Dr. Judith Daly DARPA / TTO 1400 Wilson Boulevard Arlington, Virginia 22209		(1)

END

2-87

DTIC